**DRIFT AND DETERIORATION OF PETERMANN ICE ISLANDS**

By

© Reza Zeinali Torbati

A Thesis submitted to the

School of Graduate Studies

In partial fulfillment of the requirements for the degree of

**Doctor of Philosophy**

**Faculty of Engineering and Applied Science**

Memorial University of Newfoundland

**February 2024**

St. John's, Newfoundland, Canada

# ABSTRACT

The eastern Canadian waters is an important part of Canadian shipping lanes and subjected to occasional ice island presence, which could pose serious hazards to offshore and shipping activities in this region. It is, therefore, important to better characterize the dynamics of glacial ice features for safe and cost-effective activities in the region. This thesis presents advanced predictive models to provide a better understanding of how atmospheric and oceanic variables influence ice island drift and deterioration.

To understand how ice islands drift under the influence of atmospheric and oceanic forces, a deterministic model was presented, where the relative contribution of various forces governing the drift of four tracked ice islands was quantified. The results showed that in low sea ice concentrations and ice island speeds, ocean current and sea surface tilt forces dominated ice island force balance (63% on average). Wind, however, played a minor role ($< 5\%$), and Coriolis and sea ice forces were significant only at higher ice island speeds and sea ice concentrations, respectively.

Atmospheric and oceanic variables were further studied using a probabilistic Bayesian approach to investigate their relative influences on the fracture events and drift velocities of hundreds of Petermann ice islands tracked in the Canadian Ice Island Drift, Deterioration and Detection database. The presented models identified water temperature and ocean currents as the most important contributor to ice island fracture events and drift velocities, respectively. It was revealed that under severe conditions of wind, current, waves, and air/water temperatures, ice islands are more likely to fracture, with fracture probability reaching as high as 75% in extreme conditions. It was also revealed that under stronger currents, ice islands are most likely to drift at higher speeds and in close proximity to ocean current direction. Models were validated using the 5-fold cross-

validation approach and errors up to 39% and 29% were reported in the fracture and drift probability estimations, respectively.

The presented models have predictive capabilities for future drift and deterioration of Petermann ice islands. However, further training and testing of the developed models is necessary before they can be used as operational forecasting tools.

*I dedicate my thesis to*

*my beloved wife and my wonderful parents*

*for their endless and unconditional support*

*during my graduate studies.*

## ACKNOWLEDGEMENTS

I would like to express my sincere gratitude to my supervisors, Dr. Rocky Taylor and Dr. Ian Turnbull, for their consistent support and guidance throughout my Ph.D. journey and providing me with their valuable feedback and useful insights, without which the completion of this work would not have happened. I am very thankful to my committee member, Dr. Derek Mueller, for his thorough review and constructive criticism of my manuscripts, as well as for his helpful suggestions, instructions, and feedback during my Ph.D. research.

I would like to thank C-CORE for welcoming me to the ice engineering team and letting me to use the facilities. I am also highly indebted to my lecturers at Memorial University during my graduate studies for their exemplary influence.

Last, but not least, I owe my deepest gratitude to my lovely wife and my wonderful parents for their endless support in my studies. I would thank my wife for encouraging me the most to pursue my graduate studies towards a Ph.D. degree, as well as for sharing a great portion of the burden during these years and making it possible for me complete my graduate studies. Special thanks goes to my father who inspired me the most and made me who I am today.

I would also like to thank the School of Graduate Studies at Memorial University of Newfoundland, Hibernia Management and Development Company (HMDC), InnovateNL, and the Mitacs Accelerate Program for their financial support during the course of my Ph.D. study.

**TABLE OF CONTENTS**

## LIST OF TABLES

**LIST OF FIGURES**

**NOMENCLATURE**

**Abbreviations**

CI2D3       Canadian Ice Island Drift, Deterioration and Detection database

PG       Petermann Glacier

IMEI       International Mobile Equipment Identity

CIS       Canadian Ice Service

TIM       Temperature Index Melt

SAR       Synthetic Aperture Radar

CCGS       Canadian Coast Guard Ship

ONRE       Offshore Newfoundland Research Expedition

NW       Northwest

NE       Northeast

SW       Southwest

SSW       South-southwest

S       South

SSE       South-southeast

SE       Southeast

UTC        Universal Time Coordinated

GPS        Global Positioning System

CMEMS        Copernicus Marine Environment Monitoring Service

Res.        Residual

LHM        Lichey and Hellmer's model (2001)

Rng.        Range

M.        Mean

Std.        Standard Deviation

Eqn.        Equation

HMDC        Hibernia Management and Development

OMAE        Ocean, Offshore and Arctic Engineering

WIRL        Water and Ice Research Laboratory

ECMWF        European Centre for Medium-Range Weather Forecasts

NARR        North American Regional Reanalysis

**Symbols and Units**

$T$        Temperature (℃)

| | |
|---|---|
| $km$ | Kilometre |
| $m$ | Metre |
| $s$ | Second |
| $d$ | Day |
| % | Percent |
| $MN$ | Meganewton |
| $\rho_a$ | Air density ($kg\ m^{-3}$) |
| $\vec{v}_a$ | Wind velocity ($m\ s^{-1}$) |
| $\rho_w$ | Water density ($kg\ m^{-3}$) |
| $\vec{v}_w$ | Mean current velocity ($m\ s^{-1}$) |
| $\rho_{si}$ | Sea ice density ($kg\ m^{-3}$) |
| $\rho_i$ | Ice island density ($kg\ m^{-3}$) |
| $\rho_w$ | Water density ($kg\ m^{-3}$) |
| $c_a$ | Air form drag coefficient |
| $c_w$ | Water form drag coefficient |
| $c_{da}$ | Air skin drag coefficient |

| | |
|---|---|
| $c_{dw}$ | Water skin drag coefficient |
| $\Omega$ | Earth's angular speed $(rad\ s^{-1})$ |
| $\phi_i$ | Ice island latitude (°) |
| $c_{si}$ | Sea ice resistance coefficient |
| $A_{ha}$ | Surface area $(m^2)$ |
| $A_{hw}$ | Basal area $(m^2)$ |
| $A_{va}$ | Above water cross sectional area $(m^2)$ |
| $A_{vw}$ | Under water cross sectional area $(m^2)$ |
| $\vec{v}_{si}$ | Sea ice velocity $(m\ s^{-1})$ |
| $\vec{u}$ | Ice island velocity $(m\ s^{-1})$ |
| $\vec{g}$ | Gravitational acceleration $(m\ s^{-2})$ |
| $h_i$ | Ice island thickness $(m)$ |
| $V_{ice}$ | Ice island volume $(m^3)$ |
| $L$ | Ice island length $(m)$ |
| $W$ | Ice island width $(m)$ |
| $h_s$ | Ice island sail height $(m)$ |

$h_k$            Ice island keel depth ($m$)

$M$            Ice island mass ($kg$)

$DDF$            Degree-day factor ($mm\ d^{-1}\ °C^{-1}$)

$PDD$            Positive degree days (°C)

$V_{ba}$            Ice island base thinning rate ($m\ s^{-1}$)

$k$            Bulk heat transfer coefficient ($m^{2/5}\ d^{-1/5}\ °C^{-1}$)

$\vec{v}_w(b)$            Current velocity at the keel depth ($m\ s^{-1}$)

$T_w(b)$            Water temperature at the keel depth (°C)

$T_{mi}$            Melting temperature of ice island (°C)

$T_f$            Water freezing temperature (°C)

$T_\infty$            Water temperature (°C)

$S$            Water salinity ($ppt$)

$T_a$            Air temperature (°C)

$C$            Sea ice concentration

$h_{si}$            Sea ice thickness ($m$)

$P_s$            Sea ice strength threshold ($N\ m^{-1}$)

| | |
|---|---|
| $P$ | Sea ice compressive strength ($N\ m^{-1}$) |
| $P^*$ | Sea ice strength coefficient ($N\ m^{-2}$) |
| $a$ | Sea ice strength coefficient |
| ° | Degree |
| °$N$ | Degree North |
| °$W$ | Degree West |
| °$C$ | Degree Celsius |
| $V_w$ | Wind speed ($m\ s^{-1}$) |
| $\theta_w$ | Wind direction (°) |
| $\theta_{w-c}$ | Relative wind-current direction (°) |
| $V_c$ | Current speed ($m\ s^{-1}$) |
| $\theta_c$ | Current direction (°) |
| $T_w$ | Water temperature (°C) |
| $T_{ss}$ | Sea surface tilt |
| $\theta_{SST}$ | Sea surface tilt direction (°) |
| $\theta_{SST-c}$ | Relative sea surface tilt-current direction (°) |

| | |
|---|---|
| $V_i$ | Ice island speed ($m\ s^{-1}$) |
| $\theta_{i-c}$ | Relative ice island-current direction (°) |
| $E_w$ | Wave energy index ($m^2\ s$) |
| $T_{a\_avg}$ | Lifetime mean air temperature (°C) |
| $T_{w\_avg}$ | Lifetime mean water temperature (°C) |
| $E_{w\_avg}$ | Lifetime mean wave energy index ($m^2\ s$) |
| $t_g$ | Grounding time ($days$) |
| $C_{si}$ | Sea ice concentration |
| $H_{wave}$ | Significant height of combined wind waves and swell ($m$) |
| $T_{wave}$ | Mean wave period ($s$) |
| $\theta_{wave}$ | Wave direction (°) |
| $r$ | Pearson Product-Moment Correlation coefficient |
| $\overline{x}$ | Mean of variable x |
| $\overline{y}$ | Mean of variable y |
| $\tilde{x}$ | Median of variable x |
| $Q_1$ | First quartile |

$Q_3$ Third quartile

$n$ Total number of data points

$x^*$ Defined criteria for variable x

$d, s_1$ State 1 of ice island drift velocity ($m\ s^{-1}$)

$d, s_2$ State 2 of ice island drift velocity ($m\ s^{-1}$)

$d, s_3$ State 3 of ice island drift velocity ($m\ s^{-1}$)

$d, s_4$ State 4 of ice island drift velocity ($m\ s^{-1}$)

$d, s_5$ State 5 of ice island drift velocity ($m\ s^{-1}$)

$d, s_6$ State 6 of ice island drift velocity ($m\ s^{-1}$)

$d, s_7$ State 7 of ice island drift velocity ($m\ s^{-1}$)

$d, s_8$ State 8 of ice island drift velocity ($m\ s^{-1}$)

$P_{frac}$ Fracture event probability (%)

$P_{d,s_1}$ Drift probability in state 1 of ice island drift velocity (%)

$P_{d,s_2}$ Drift probability in state 2 of ice island drift velocity (%)

$P_{d,s_3}$ Drift probability in state 3 of ice island drift velocity (%)

$P_{d,s_4}$ Drift probability in state 4 of ice island drift velocity (%)

$P_{d,s_5}$ Drift probability in state 5 of ice island drift velocity (%)

$P_{d,s_6}$ Drift probability in state 6 of ice island drift velocity (%)

$P_{d,s_7}$ Drift probability in state 7 of ice island drift velocity (%)

$P_{d,s_8}$ Drift probability in state 8 of ice island drift velocity (%)

# 1. INTRODUCTION AND OVERVIEW

## 1.1. Preface

This introductory chapter presents an introduction of ice islands, discusses the knowledge gaps, and provides justifications for the specific objectives of this research and the need for more research concerning ice island drift and deterioration. The chapter also describes how the thesis will unfold and gives a brief description of each chapter.

## 1.2. Introduction

Arctic regions are estimated to contain about 22% of the world's undiscovered petroleum resources (Bird et al., 2008). These regions have unique environmental conditions (*e.g.*, cold temperatures, high sea states, ice-infested waters), which makes it challenging to design offshore and shipping structures that can survive in such extreme conditions. However, the recent increase in atmospheric and oceanic temperatures of Arctic (*e.g.*, Northern Greenlandic coast) has increased surface and basal melting of ice shelves and floating ice tongues (Hill et al., 2017). Additionally, the associated temperature increase has resulted in lower sea ice cover that usually provides a support back pressure on ice shelves and floating ice tongues (Copland et al., 2017). The subsequent lower back pressure has increased the likelihood of calving events, which has led to more frequent observations of glacial ice features such as calved icebergs and ice islands (immense tabular icebergs) in Arctic regions since the onset of major anthropogenic climate change (Copland et al., 2017). Ice islands are a form of tabular icebergs with an undulated surface, a thickness of 30–50 m, and a range of a few thousand square meters to 500 km$^2$ in area (Armstrong et al., 1973). Icebergs and ice islands carry about 30-50 % of the freshwater flux from the Greenland Ice Sheet and play an important role in Greenland freshwater dispersal (Marson et al., 2017; Enderlin et al.,

2018). The resulted meltwater input to local waters can have impacts on marine ecosystems through modifications to biological, chemical, and physical composition of water column structures (Stern et al., 2015), which can provide special habitats for the lower pelagic levels of the marine ecosystem such as phytoplankton, zooplankton, and bacteria (Vernet et al., 2012; Smith et al. 2013), as well as temporary habitats for marine mammals such as seals and polar bears (Halliday et al., 2012).

Warmer atmospheric and oceanic temperatures are likely to increase the number of calving events and further reduce Arctic sea ice. Due to lower sea ice presence in recent years, harsh environment ocean activities in different sectors (*e.g.*, aquaculture, fishery, shipping, offshore renewable and non-renewable energy, seafloor infrastructures, and coastal infrastructures) are becoming more feasible. For example, natural resource extraction and maritime transport in ice environments are becoming more accessible (Buixadé Farré et al., 2014). Recent accessibility in the Arctic has been accompanied by the increasing demand in global trade and natural resources, which makes the eastern Canadian waters an appealing region for shipping activities and exploration and extraction of new energy resources and mineral supplies. For example, recent seismic data shows that offshore Newfoundland and Labrador (*e.g.*, in the Grand Banks area) holds a great potential for new exploration activities due the number of oil and gas basin in the region (Figure 1.1-a). These regions, however, are exposed to glacial ice features such as icebergs and ice islands, which could pose a potential hazard to offshore exploration and maritime activities (Sonnichsen et al., 2005; Newell, 1993). Ice islands, specifically, are massive ice features that can break up to smaller ice island fragments as they drift, which can be of significant risk to natural resource extraction and shipping industries (Fuglem and Jordaan, 2017; Mueller et al., 2013). To ensure a safe and economical operation of the current and future offshore and shipping activities in the eastern

Canadian waters (Figure 1.1), it is therefore important to devise appropriate ice management plans to ensure the risk from glacial ice features can be mitigated. This, however, requires a better understanding and reliable prediction models for drift and deterioration of glacial ice presence in these regions.
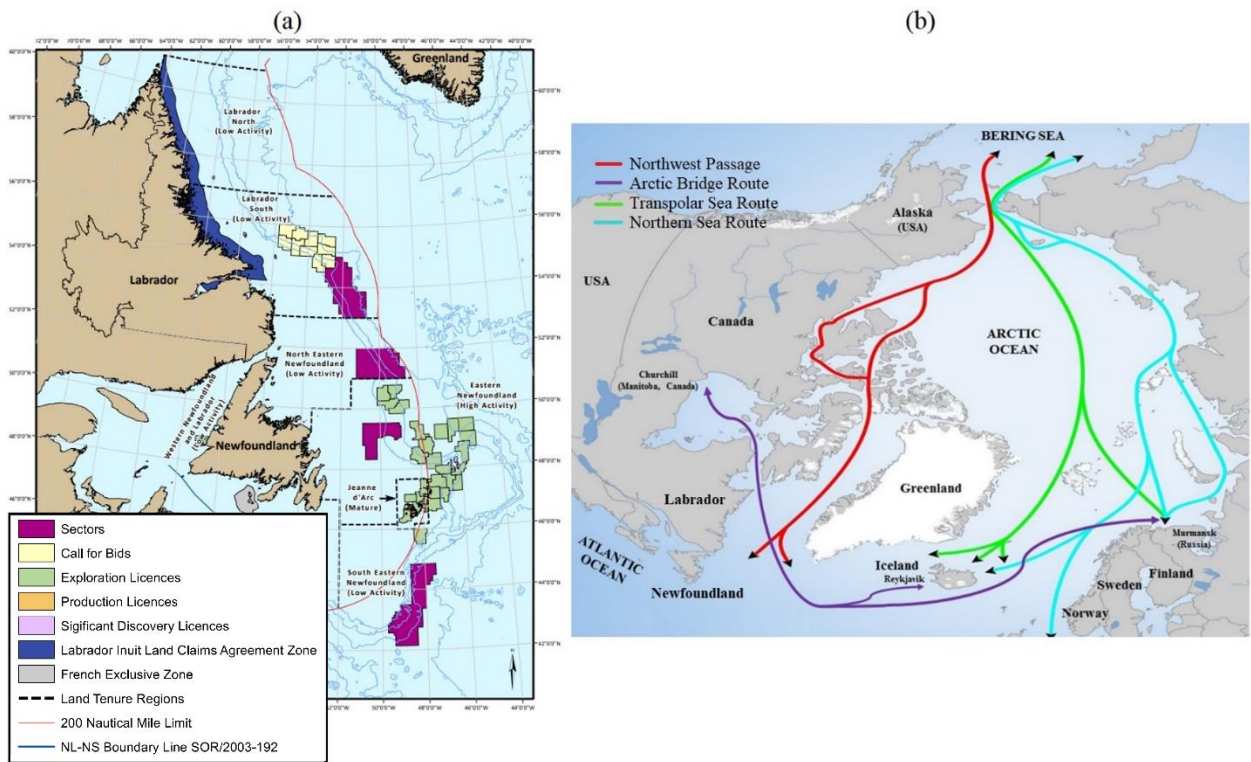


**Figure 1.1.** (a) The oil and gas exploration activities offshore Newfoundland and Labrador (Source: Canada-Newfoundland and Labrador Offshore Petroleum Board, https://www.cnlopb.ca/wp-content/uploads/maps/nlol.pdf) and (b) The Arctic shipping routes (image was extracted from Stadtländer (2020) and modified slightly).

Evaluating the risk to offshore operations involves consideration of both ice occurrence probability in the region and the damage potential from ice features (Ballicater Consulting, 2012; Fuglem and Jordaan, 2017). Iceberg occurrence probability in the waters of eastern Canada has been studied by C-CORE (2005), and it was reported later that Petermann ice islands (*i.e.*, ice islands calved

from the Peterman Glacier in the northwest of Greenland) can be hazardous to the offshore and shipping activities in this region (Saper, 2011; Peterson, 2011).

An important part of an ice risk management strategy is to identify if a hazardous ice feature can be managed (e.g., be avoided or towed), or if the activities in the vicinity of the ice feature should be suspended. These are dependent on the resource availability (*e.g.*, towing vessels, etc.), as well as the kinetic energy of the drifting ice feature, a component that is governed by the mass and velocity of the ice feature as it approaches the hazardous zone. Ice island mass and velocity, however, are dynamic features that are controlled by various atmospheric and oceanic variables (*e.g.*, wind, current, etc.).

The mass and velocity of an ice island are governed by its drift and deterioration (via calving and/or melt), processes that could be influenced by several atmospheric and oceanic factors that need to be accounted for. Therefore, it is important to evaluate the effect of metocean (atmospheric and oceanic) variables on the drift and deterioration of ice islands. Due to the logistical difficulties of collecting in-situ data in remote and harsh environments, there are limited field observations to contribute to modeling and calibrating ice island drift and deterioration (Saper et al., 2015; Wagner et al., 2014; Mueller et al., 2013). It is therefore important to employ remote sensing monitoring techniques to collect the required data for ice island drift and deterioration analysis. Using remote sensing technologies, a database of satellite imagery from hundreds of ice islands was developed at Water and Ice Research Laboratory at Carleton University and named Canadian Ice Island Drift, Deterioration and Detection (CI2D3) database (Desjardins et al., 2018). The database tracked numerous ice islands that were originally calved from Petermann Glacier in 2008, 2010, 2011 and 2012 (Figure 1.2), as well as Ryder, Steensby, C.H. Ostenfeld, and North Greenland ice tongues (Crawford et al., 2018). The CI2D3 database was used for model development in this study as it

provides a framework for long-term tracking of numerous ice islands and their areal reduction as they drift southwards towards Labrador Sea.
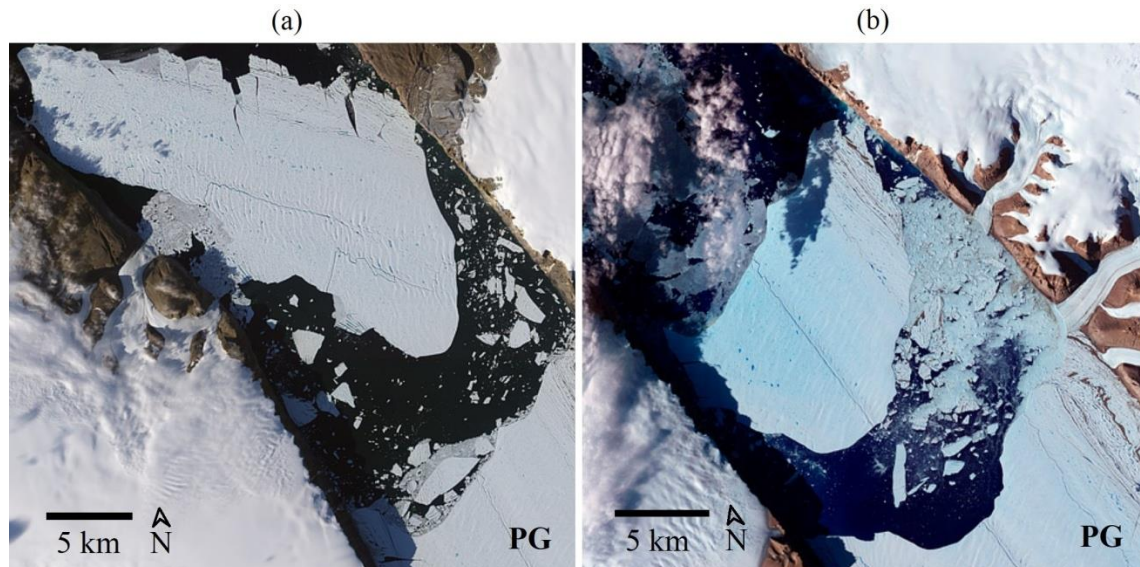


**Figure 1.2.** The massive ice islands that calved from the Petermann Glacier (PG) in 2010 (a) and 2012 (b) in the northwest of Greenland (Source: NASA Earth Observatory, https://earthobservatory.nasa.gov/images/45306/ice-island-calves-off-petermann-glacier, https://earthobservatory.nasa.gov/images/78648/closeup-of-the-ice-island-from-petermann-glacier).

## 1.3.    Research Scope and Objectives

This thesis is primarily focused on the development of drift and deterioration models for Petermann ice islands, which provide better insights into the metocean conditions that govern ice island dynamics and thermodynamics. To identify the metocean forces that govern the drift of ice islands, the thesis first explored the relative influence of various metocean conditions on ice islands' overall force balance, which served as a preliminary research to later investigate the influence of the most salient metocean forces on the drift of ice islands. An advanced probabilistic drift model, however, required a reliable data set of ice islands. So, the thesis used the CI2D3 database that included satellite imagery data (e.g., surface area, positions, etc.) for hundreds of ice

islands as they drifted southwards from the Arctic Ocean to the Atlantic Ocean, which provided a framework for long-term tracking of their drift paths and fracture events. To present an overview of the drift and deterioration of the ice islands in the CI2D3 database, a preliminary analysis of the ice islands' spatial/temporal and arial surface data in the CI2D3 database was presented. For an ice island drift model to have an operational use, it is important to couple it with a deterioration model that is able to predict facture events and size distributions of the ice islands. Similarly, for an ice islands fracture model to have a forecast capability for future ice island fracture events, it needs to be coupled with a drift model that can forecast the positional data. Therefore, the thesis first presented a probabilistic model for the conditional dependence of ice islands' large-scale fracture events on the most salient metocean conditions that they experience over their lives. Then a probabilistic drift model was developed to provide a predictive tool for the drift speeds and directions of ice islands based on the metocean conditions that govern their drifts.

Through evaluation of the ice island drift and deterioration studies, some knowledge gaps were identified, which are summarized below:

- While past ice dynamic forecasting models have mainly focused on the drift of icebergs and ice islands in open water (*e.g.*, Mountain, 1980; Crepon et al., 1988; and Kubat et al., 2005), these deterministic models should also consider how the overall force balance would change under the influence of surrounding sea ice as moderate-to-high presence of sea ice around ice features could influence their drift velocities (Lichey and Hellmer, 2001). Also sea ice plays a critical role in iceberg severity in the eastern Canadian sub-Arctic and the survival of icebergs as they move towards more southern latitudes (Marko et al., 1994). The force exerted by sea ice on icebergs and ice islands has been deterministically studied

through a piecewise concentration-dependent relationship (Lichey and Hellmer, 2001), but this model has never been tested using alternative approaches.

- The past iceberg deterioration models mainly describe formulations for the melt rates (*e.g.*, Savage, 2001) and small-scale fracture events through edge-wasting (*e.g.*, Scambos et al., 2005; Kubat et al., 2007), and generally neglect other deterioration mechanisms such as large-scale fracture events, likely due to the lack of reliable data. Large-scale fracture events, however, were found to play a more major role than melting in the mass loss of large icebergs (Bouhier et al., 2018).

- Previous iceberg drift models are mostly deterministic, where uncertainties in the in the input data such as ocean currents result in error propagation and unknown uncertainty, which could ultimately generate a significant error in the estimated drift speeds and directions (Marko et al., 1988). Also, the available probabilistic models generally account for only a few variables, largely due to the lack of available data for other influencing environmental variables.

- Bayesian Network is a popular approach in probabilistic modelling, which has the ability to quantify the probability of a certain outcome based on the most salient predictive variables (Gutierrez et al., 2011). While Bayesian network has been widely used for evaluating the roles of environmental variables on ship performance and besetting events (*e.g.*, Turnbull et al., 2019; Fu et al., 2016; Montewka et al., 2015; Montewka et al., 2013), this useful approach has not been used in studying how the environmental variables impact ice island drift and deterioration.

### 1.3.1. Novel Contributions

In the context of the knowledge gaps identified above, this research aims to achieve the following main objectives:

- Study the effects of metocean variables on ice islands' overall force balance to better understand the relative influence of the variables that control the drift of ice islands.

- Enhance understanding of the role of sea ice on the overall force balance from metocean variables by testing the piecewise concentration-dependent relationship for sea ice force against a mathematical residual approach.

- Develop a probabilistic model that can use inputs from metocean conditions to model the occurrence of large-scale fracture events of ice islands that result in significant mass reduction.

- Develop a drift model that is able to provide probabilistic estimations of drift speeds and directions for ice islands based on the local atmospheric and oceanic conditions.

- Provide better modeling of physical patterns for ice islands and improve decision support for ice management.

### 1.4. Thesis Organization

The thesis is written in the manuscript format and includes four peer-reviewed publications (three journal papers and one conference paper) that investigated the drift and deterioration of Petermann ice islands, which originated from the Petermann Glacier and drifted southwards towards offshore Newfoundland. Given the manuscript-based nature of the thesis, each chapter includes a detailed review of the related past literature. Therefore, to avoid multiple reviews of the related past studies and to make the chapters more comprehensive, the thesis literature review is not presented as one

consolidated chapter; rather it is distributed among the related chapters and reviewed in the context of the work in each chapter. Also, the statements of co-authorship is presented at the beginning of each chapter. The following four papers came out of this work, which have been presented as the main chapters of this thesis:

- Chapter 2: Zeinali-Torbati, R., Turnbull, I. D., Taylor, R. S., and Mueller, D. (2020). Evaluation of the relative contribution of meteorological and oceanic forces to the drift of ice islands offshore Newfoundland, Journal of Glaciology, 66(256), 203-218, https://doi.org/10.1017/jog.2019.96.

- Chapter 3: Zeinali-Torbati, R., Turnbull, I. D., Taylor, R. S., and Mueller, D. (2019). The calving events of Petermann glacier from 2008 to 2012: ice island drift characteristics, assessment of fracture events, and geographical data analysis, In proceedings of the 38th International Conference on Ocean, Offshore and Arctic Engineering, Glasgow, Scotland, UK, 9-14 June 2019, https://doi.org/10.1115/OMAE2019-96732.

- Chapter 4: Zeinali-Torbati, R., Turnbull, I. D., Taylor, R. S., and Mueller, D. (2021). A probabilistic model for fracture events of Petermann ice islands under the influence of atmospheric and oceanic conditions, The Cryosphere, 15, 5601-5621, https://doi.org/10.5194/tc-15-5601-2021.

- Chapter 5: Zeinali-Torbati, R., Turnbull, I. D., Taylor, R. S., and Mueller, D. (2022). Probabilistic drift prediction of Petermann ice islands under the influence of meteorological and oceanographic variables (Unpublished Manuscript), To be submitted to The Cryosphere.

Chapter 1 provides an introduction of ice islands, addresses the knowledge gaps in the related area, and presents justifications for the objectives of this thesis.

Chapter 2 provides a comprehensive literature review on the past ice island forcing models and presents an evaluation of the relative contributions of atmospheric and oceanic forces to the drift of four ice island fragments tracked at the northeast entrance to the Strait of Belle Isle offshore Newfoundland. The goal of this chapter is to quantify the contribution of metocan forces that govern the drift of ice islands, through deterministic modeling of the ice island masses and the metocean forces. This study also presents a new approach for quantifying the sea ice force on ice islands, which serves as a framework for testing the available deterministic models for sea ice force estimation.

Chapter 3 introduces the Canadian Ice Island Drift, Deterioration and Detection (CI2D3) database and provides a preliminary analysis of drift and deterioration of the Petermann ice islands in the CI2D3 database, which serves as a preliminary study for the fracture and drift models presented in chapters 4 and 5.

Chapter 4 provides a detailed review of the available ice island deterioration models, uses the CI2D3 database, and presents a probabilistic model for forecasting the fracture events of Petermann ice islands, through analyzing the relative influences of atmospheric and oceanic variables. The presented Bayesian model is able to provide estimations of ice island fracture probability under various atmospheric and oceanic conditions.

Chapter 5 provides a review of the past ice island drift models, analyzes the same database that was used in chapter 4, and presents a probabilistic drift forecasting model for drift velocities of Petermann ice islands, through Bayesian analysis of the atmospheric and oceanic conditions that govern their drifts. The presented model provides a framework to estimate the drift speeds and directions of ice islands as they drift under various metoecan conditions.

Chapter 6 provides a summary and conclusions of the thesis, as well as recommendations for future work.

## 1.5. References

Armstrong, T., Roberts, B., and Swithinbank, C. (1973). Illustrated Glossary of Snow and Ice, Scott Polar Research Institute, Special Pub. No. 4, 2$^d$ ed., The Scholar Press Ltd., Menston Yorkshire, UK.

Ballicater Consulting Ltd. (2012). Ice Island and Iceberg Studies 2012, Report prepared for the Canadian Ice Service, Environment Canada, Report 12–01, pp. 51.

Bird, K. J., Charpentier, R. R., Gautier, D. L., Houseknecht, D. W., Klett, T. R., Pitman, J. K., Moore, E. T., Schenk, C. J., Tennyson, M. E., and Wandrey, C. R. (2008). Circum-Arctic resource appraisal: Estimates of undiscovered oil and gas north of the Arctic Circle (No. 2008-3049), US Geological Survey, https://doi.org/10.3133/fs20083049.

Bouhier, N., Tournadre, J., Rémy, F., and Gourves-Cousin, R. (2018). Melting and fragmentation laws from the evolution of two large Southern Ocean icebergs estimated from satellite data, The Cryosphere, 12(7), 2267-228, https://doi.org/10.5194/tc-12-2267-2018.

Buixadé Farré, A., Stephenson, S. R., Chen, L., Czub, M., Dai, Y., Demchev, D., Efimov, Y., Graczyk, P., Grythe, H., Keil, K., Kivekäs, N., Kumar, N., Liu, N., Matelenok, I., Myksvoll, M., O'Leary, D., Olsen, J., Pavithran, S, Petersen, E., Raspotnik, A., Ryzhov, I., Solski, J., Suo, L., Troein, C., Valeeva, V., Rijckevorsel, J., and Wighting, J. (2014). Commercial Arctic shipping through the Northeast Passage: routes, resources, governance,

technology, and infrastructure, Polar Geography, 37(4), 298-324, https://doi.org/10.1080/1088937X.2014.965769.

C-CORE (2005), Characterization of Ice-Free Season for Offshore Newfoundland – Addendum: Calculation of Iceberg Collision Risk during Ice-Free Season, C-CORE Report Number R-04-093-341, Version 2, pp. 51. https://www.cnlopb.ca/wp-content/uploads/news/ccorereportaddendum.pdf.

Copland, L., Mortimer, C. A., White, A., Richer-McCallum, M., and Mueller, D. (2017). Factors contributing to recent ice shelf losses, In Arctic Ice Shelves and Ice Islands, Dordrecht, Netherlands, Springer, 263-286, https://doi.org/10.1007/978-94-024-1101-0_10.

Crawford, A., Crocker, G., Mueller, D., Desjardins, L., Saper, R., and Carrieres, T. (2018). The Canadian Ice Island Drift, Deterioration and Detection (CI2D3) Database, Journal of Glaciology, 1-5. https://doi.org/10.1017/jog.2018.36.

Crepon, M., Houssais, M. N., and Guily, B. S. (1988). The drift of icebergs under wind action, Journal of Geophysical Research: Oceans, 93(C4), 3608-3612, https://doi.org/10.1029/JC093iC04p03608.

Desjardins, L., Crawford, A., Mueller, D., Saper, R., Schaad, C., Stewart-Jones, E., and Shepherd, J. (2018). Canadian ice island drift, deterioration and detection database (CI2D3 database) [v1.1], Canadian Cryospheric Information Network (CCIN), Waterloo, Canada, http://dx.doi.org/10.21963/12678.

Enderlin, E. M., Carrigan, C. J., Kochtitzky, W. H., Cuadros, A., Moon, T., and Hamilton, G. S. (2018). Greenland iceberg melt variability from high-resolution satellite observations. The

Cryosphere, 12(2), 565-575, https://doi.org/10.5194/tc-12-565-2018.

Fu, S., Zhang, D., Montewka, J., Yan, X., and Zio, E. (2016). Towards a probabilistic model for predicting ship besetting in ice in Arctic waters, Reliability Engineering and System Safety, 155, 124-136, https://doi.org/10.1016/j.ress.2016.06.010.

Fuglem, M. and Jordaan, I. (2017). Risk analysis and hazards of ice islands, In Arctic Ice Shelves and Ice Islands, Dordrecht, Netherlands, Springer, 395-415, https://doi.org/10.1007/978-94-024-1101-0_15.

Gutierrez, B. T., Plant, N. G., and Thieler, E. R. (2011). A Bayesian network to predict coastal vulnerability to sea level rise, Journal of Geophysical Research: Earth Surface, 116(F2), https://doi.org/10.1029/2010JF001891.

Halliday, E. J., King, T., Bobby, P., Copland, L., and Mueller, D. (2012). Petermann Ice Island 'A' survey results, offshore Labrador, OTC Arctic Technology Conference, Offshore Technology Conference, https://doi.org/10.4043/23714-MS.

Hill, E. A., Carr, J. R., and Stokes, C. R. (2017). A review of recent changes in major marine-terminating outlet glaciers in Northern Greenland, Frontiers in Earth Science, 4, 111, https://doi.org/10.3389/feart.2016.00111.

Kubat, I., Sayed, M., Savage, S. B., and Carrieres, T. (2005). An operational model of iceberg drift. International Journal of Offshore and Polar Engineering, 15(2), 125-131.

Kubat, I., Sayed, M., Savage, S. B., Carrieres, T., and Crocker, G. (2007). An operational iceberg deterioration model, In Proceedings of the 17th International Offshore and Polar Engineering Conference, Lisbon, Portugal, 1-6 July 2007, 652-657.

Lichey, C. and Hellmer, H. H. (2001). Modeling giant-iceberg drift under the influence of sea ice in the Weddell Sea, Antarctica, Journal of Glaciology, 47(158), 452-460, https://doi.org/10.3189/172756501781832133.

Marko, J. R., Fissel, D. B., and Miller, J. D. (1988). Iceberg movement prediction off the Canadian east coast, In Natural and Man-Made Hazards, Springer, Dordrecht, pp. 435-462, https://doi.org/10.1007/978-94-009-1433-9_31.

Marko, J. R., Fissel, D. B., Wadhams, P., Kelly, P. M., and Brown, R. D. (1994). Iceberg severity of eastern North America: Its relationship to sea ice variability and climate change, Journal of Climate, 7(9), 1335-1351, https://doi.org/10.1175/1520-0442(1994)007%3C1335:ISOENA%3E2.0.CO;2.

Marson, J. M., Myers, P. G., Hu, X., and Le Sommer, J. (2018). Using vertically integrated ocean fields to characterize Greenland icebergs' distribution and lifetime, Geophysical Research Letters, 45(9), 4208-4217, https://doi.org/10.1029/2018GL077676.

Montewka, J., Goerlandt, F., Kujala, P., and Lensu, M. (2015). Towards probabilistic models for the prediction of a ship performance in dynamic ice, Cold Regions Science and Technology, 112, 14-28, https://doi.org/10.1016/j.coldregions.2014.12.009.

Montewka, J., Sinclair, H., Kujala, P., Haapala, J., and Lensu, M. (2013). Modelling ship performance in ice using Bayesian networks, In Proceedings of the 22nd International

Conference on Port and Ocean Engineering under Arctic Conditions, 9-13 June 2013.

Mountain, D. G. (1980). On predicting iceberg drift, Cold Regions Science and Technology, 1, 273-282, https://doi.org/10.1016/0165-232X(80)90055-5.

Mueller, D. R., Crawford, A., Copland, L., and Van Wychen, W. (2013). Ice island and iceberg fluxes from Canadian High Arctic sources, Report to the Northern Transportation Assessment Initiative, Innovation Policy Branch, Transport Canada, Ottawa, Canada. https://www.researchgate.net/publication/340183882_Ice_Island_and_Iceberg_Fluxes_from_Canadian_High_Arctic_Sources_Prepared_for_the_Innovation_Policy_Group_of_Transport_Canada.

Newell, J. P. (1993). Exceptionally large icebergs and ice islands in eastern Canadian waters: a review of sightings from 1900 to present, Arctic, 46(3), 205-211, https://doi.org/10.14430/ARCTIC1345.

Peterson, I. K. (2011). Ice island occurrence on the Canadian East Coast, In Proceedings of the 21st International Conference on Port and Ocean Engineering under Arctic Conditions, Montreal, Canada, 10-14 July 2011.

Saper, R. (2011). Preliminary research plan for glacial ice hazards, Report prepared for the Canadian Ice Service, Marine and Ice Services Division, Environment Canada, Ottawa, Canada, pp. 40. https://wirl.carleton.ca/wp-content/uploads/2017/09/Saper2011.pdf.

Saper, R., Tivy, A., Mueller, D., and Nacke, M. (2015). Report of the Inaugural Meeting of the Glacial Ice Hazards Working Group (GIHWG), Carleton University, Ottawa, Canada, pp. 30. https://wirl.carleton.ca/wp-content/uploads/2016/02/Glacial-Ice-Hazards-Working-

Group15-Feb-2016.pdf.

Savage, S. B. (2001). Aspects of iceberg deterioration and drift, In Geomorphological Fluid Mechanics, Springer, Berlin, Germany, 589, 279-318, https://doi.org/10.1007/3-540-45670-8_12.

Scambos, T., Sergienko, O., Sargent, A., MacAyeal, D., and Fastook, J. (2005). ICESat profiles of tabular iceberg margins and iceberg breakup at low latitudes, Geophysical Research Letters, 32(23), https://doi.org/10.1029/2005GL023802.

Smith Jr, K. L., Sherman, A. D., Shaw, T. J., and Sprintall, J. (2013). Icebergs as unique Lagrangian ecosystems in polar seas, Annual Review of Marine Science, 5(1), 269-287, https://doi.org/10.1146/annurev-marine-121211-172317.

Sonnichsen, G. V., King, T., Jordaan, I., and Li, C. (2005). Probabilistic analysis of iceberg scouring frequency based on repetitive seabed mapping, offshore Newfoundland and Labrador, In Proceedings of the 18th International Conference on Port and Ocean Engineering under Arctic Conditions, Potsdam New York, USA, 26-30 June 2005, 85-94.

Stadtländer, C. T. H. (2020). Book Review: Sustainable Shipping in a Changing Arctic, Frontiers in Marine Science, 6:799, https://doi.org/10.3389/fmars.2019.00799.

Stern, A. A., Johnson, E., Holland, D. M., Wagner, T. J., Wadhams, P., Bates, R., Abrahamsen E. P., Nicholls, K. W., Crawford A., Gagnon, J., and Tremblay, J. E. (2015). Wind-driven upwelling around grounded tabular icebergs, Journal of Geophysical Research: Oceans, 120(8), 5820-5835, https://doi.org/10.1002/2015JC010805.

Turnbull, I. D., Bourbonnais, P., and Taylor, R. S. (2019). Investigation of two pack ice besetting events on the Umiak I and development of a probabilistic prediction model, Ocean Engineering, 179, 76-91, https://doi.org/10.1016/j.oceaneng.2019.03.030.

Vernet, M., Smith Jr, K. L., Cefarelli, A. O., Helly, J. J., Kaufmann, R. S., Lin, H., Long, D. G., Murray, A. E., Robison, B. H., Ruhl, H. A., Shaw, T. J., Sherman, A. D., Sprintall, J., Stephenson Jr, G. R., Stuart, K. M., and Twining, B. S. (2012). Islands of ice: Influence of free-drifting Antarctic icebergs on pelagic marine ecosystems, Oceanography, 25(3), 38-39, https://doi.org/10.5670/oceanog.2012.72.

Wagner, T. J., Wadhams, P., Bates, R., Elosegui, P., Stern, A., Vella, D., Abrahamsen, E. P., Crawford, A., and Nicholls, K. W. (2014). The "footloose" mechanism: Iceberg decay from hydrostatic stresses, Geophysical Research Letters, 41(15), 5522-5529, https://doi.org/10.1002/2014GL060832.

**2.     EVALUATION OF THE RELATIVE CONTRIBUTION OF METEOROLOGICAL AND OCEANIC FORCES TO THE DRIFT OF ICE ISLANDS OFFSHORE NEWFOUNDLAND**

## 2.1.     Preface

This chapter aims to study meteorological and oceanic forces that govern the drift of ice islands to better understand how the drift ice islands is influenced by various metocean forces. The chapter provides a comprehensive literature review on the past ice island forcing models and presents a deterministic model for evaluation of the relative contributions of metocean forces to the drift of four ice island fragments.

This chapter has been published as an original research paper in the Journal of Glaciology. As the primary author of this article, I conducted the literature review, developed the model, performed the analysis, and prepared the manuscript. My co-author, Dr. Ian Turnbull, provided consistent support during the associated data analysis using Matlab. Dr. Ian Turnbull, Dr. Rocky Taylor, and Dr. Derek Mueller provided valuable feedback at different stages of the analysis and preparation of the article, and I subsequently revised the manuscript based on the suggestions from the co-authors and the recommendations from the journal reviewers.

## 2.2.     Abstract

On 29 April 2015, four beacons were deployed onto an ice island in the Strait of Belle Isle to record positional data. The ice island later broke up into many fragments, four of which were tracked by the beacons. The relative influences of wind drag, current drag, Coriolis force, sea surface height gradient, and sea ice force on the drift of the tracked ice island fragments were

analyzed. Using atmospheric and oceanic model outputs, the sea ice force was calculated as the residual of the fragments' net forces and the sum of all other forces. This was compared against the force obtained through ice concentration-dependent relationships when sea ice was present. The sea ice forces calculated from the residual approach and concentration-dependent relationships were significant only when sea ice was present at medium-high concentrations (>70%) in the vicinity of the ice island fragments. The forces from ocean currents and sea surface tilt contributed the most to the drift of the ice island fragments. Wind, however, played a minimal role in the total force governing the drift of the four ice island fragments, and Coriolis force was significant when the fragments were drifting at higher speeds.

Keywords: Atmospheric and oceanic forces; basal ablation; ice island deterioration; ice island drift; sea ice force; surface ablation.

## 2.3. Introduction

Due to the increasing demand in global energy, oil and gas exploration has advanced into ice-prone environments where the occurrence of ice islands (large tabular icebergs) is possible. The occasional presence of ice islands in the eastern Canadian Arctic may pose serious risks to offshore structures and vessels operating in these regions (Mueller et al., 2013). These risks can be reduced by executing appropriate ice avoidance strategies, which require an accurate drift forecasting model. The effectiveness of an ice avoidance strategy rests upon the drift velocity of the ice features, which are governed by the meteorological and oceanic forces on an ice island.

In order to characterize the ice environment and better understand the drift dynamics of icebergs and ice islands in ice-infested waters, it is important to study the influence of atmospheric and oceanic forces on their overall drift. This forces include drag from wind and ocean currents, the

19

Coriolis force, the gravitational pull caused by the sea surface height gradient, and the force imposed by the surrounding sea ice. While there have been several studies on drift forecast modeling of icebergs and ice islands in open water (*e.g.*, Mountain, 1980; Crepon et al., 1988; and Kubat et al., 2005), if sea ice is present, these models would need to be extended to account for the effect of sea ice on the drift of such ice features, as the drift characteristics (*e.g.*, speed and trajectory) are readily influenced by medium-high concentrations of sea ice in the environment (Lichey and Hellmer, 2001). Since a reliable drift model in a sea ice-prone environment can only be developed if appropriate data are available, positional data for the drift of four ice island fragments within the sea ice environment offshore Newfoundland were collected for model development.

This study evaluates the relative contributions of meteorological and oceanic forces caused by wind, current, Coriolis force, sea surface height, and sea ice to the drift of four ice island fragments tracked at the northeast entrance to the Strait of Belle Isle offshore Newfoundland (Figure 2.1). To improve the reliability of estimates for the atmospheric and oceanic forces, the variation in the mass of the ice island fragments was estimated through the dimensional reduction in the horizontal and vertical extents, and then incorporated into the presented force analysis. The forces due to wind, current, Coriolis effect, and sea surface tilt were calculated using reanalysis data and observed fragment drift velocity (from the tracking beacon data). The sea ice force, however, was calculated using the residual approach that was used in Turnbull et al. (2017), where the internal stress gradient force from surrounding ice on the drift of sea ice floes was estimated. In this study, however, we used the residual approach (Turnbull et al., 2017) to estimate the influence of sea ice force on the total force that governs the drift of ice islands, where the force from sea ice was calculated as the difference between the net force and the sum of other meteorological and oceanic

forces on each fragment. The net force was calculated using the mass (estimated as per section 2.6.) and the observed acceleration of the fragments; the latter was estimated from the positional data transmitted by the tracking beacons. This residual-estimated force was then compared and validated against sea ice force estimated from Lichey and Hellmer's iceberg drift model (2001) during the presence of sea ice. Finally, a sensitivity analysis was conducted to present the results over a range of air and water drag coefficients.
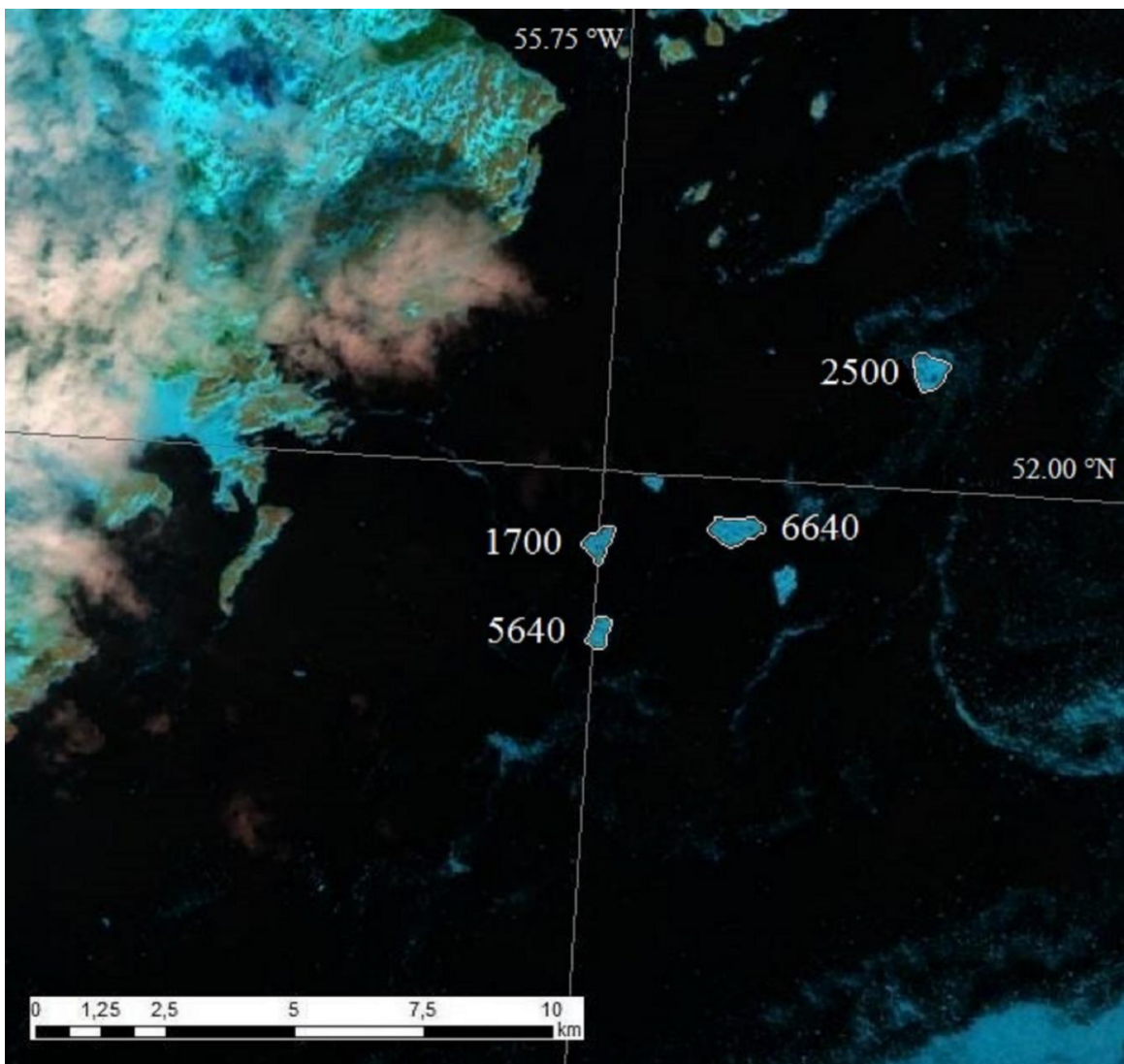


**Figure 2.1.** Landsat 8 image taken on 7 May 2015 over the NE Strait of Belle Isle showing the ice island breaking up into several smaller fragments (image is courtesy of Sigurd Teigen, Equinor

ASA). The numbers next to the fragments indicate the last four digits of the tracking beacon International Mobile Equipment Identity (IMEI) numbers.

### 2.3.1. Previous Studies on Drift and Deterioration of Icebergs and Ice Islands

Operational drift and deterioration models for icebergs have been developed by several agencies such as the Canadian Ice Service (CIS) and International Ice Patrol (White et al., 1980; Kubat et al., 2005, 2007; Murphy and Carrieres, 2010). The accuracy of these models is limited by the complexity in the iceberg geometry due to the occasional calving and rolling events (Kubat et al., 2007), as well as by the uncertainty in atmospheric and oceanic model outputs. Adding to this complexity is the fact that the meteorological and oceanic conditions constantly change over time. Therefore, it is necessary to calibrate these models and combine them with field observations to develop reliable drift and deterioration models.

Several studies have been conducted on the drift of icebergs, both in open water and in the presence of sea ice. One of the initial models was presented by Smith and Banke (1983), in which the iceberg drift was simulated under the influence of winds, ocean currents, and Coriolis deflection. An iceberg drift model was introduced by Lichey and Hellmer (2001) to also account for the force due to sea surface tilt and the surrounding sea ice in their drift model, where the effect of sea ice was analyzed in open water (concentration less than 15%), open pack ice (concentration between 15% and 90%), and closed pack ice (concentration over 90%). Lichey and Hellmer (2001) suggested that incorporation of sea ice force into an iceberg drift model is essential as the presence of dense sea ice over a large area has the ability to entrap icebergs and collect a proportion of the wind and current momentum that is blocked by sea ice. This means that a proportion of wind and current energy is indirectly transferred to iceberg through pack ice given its large surface area, resulting in a more dominant influence of sea ice on the drift of ice islands when sea ice is present at high

concentrations. A new iceberg drift model was developed later by Kubat et al. (2005), which was built on available drift models (*e.g.*, El-Tahan et al., 1983; Banke and Smith, 1984; Murphy and Anderson, 1986), but also included the vertical distribution of ocean currents over the keel depth of the icebergs to present a more realistic influence of currents. Their study also included a sensitivity analysis to examine the effect of various input parameters on the drift trajectory of icebergs, which were also compared against the field observations by Smith and Donaldson (1987). Kubat et al. (2005) stated that while ocean currents and waterline length had the most pronounced effect on iceberg drift velocity, the drift model was most insensitive to the water and air drag coefficients due to the fact that icebergs closely followed the average current velocity over keel depth.

In an observational study, Peterson et al. (2009) studied the drift of a large ice island from the Petermann Glacier using a combination of satellite imagery and tracking beacons. The influence of sea ice cover on the motion of the tracked ice island was found to be significant, given that the ice island was not able to drift into Nares Strait due to blockage or being dominated by the high concentration of sea ice, until a major wind event cleared the sea ice cover letting the ice island escape from Petermann Fjord. Ice island drift was modeled by Crocker et al. (2013) using the North American Ice Service iceberg drift and deterioration model with modified geometry to account for changes in the shape and size of the ice island. While their model resulted in a slightly better drift model than the CIS model, the authors stated that the altered ice island drift model was still poor due to the inaccuracy of estimated ocean currents.

An important component that contributes to the calibration and validation of a drift forecasting model is a reliable estimation of the change in dimensions and mass of the ice feature over its drift time. This can be done through modeling the mechanisms that result in the deterioration of an ice

23

feature. Job (1978) and El-Tahan et al. (1987) identified several processes that contribute to the deterioration of icebergs, including melting due to buoyant vertical convection, melting due to forced convection from air and water, surface ablation due to the solar radiation, wave erosion, and calving of overhanging slabs. While surface ablation is identified as a minor contributor to the overall deterioration of non-tabular icebergs (Savage, 2001), it has a great impact on the total deterioration of ice islands (Crocker et al., 2013). Some of the mechanisms mentioned earlier have been considered in the study by Crawford et al. (2015) where the surface ablation of an ice island was modeled using energy fluxes calculated through the bulk aerodynamic approach and then compared against CIS models and a Temperature Index Melt (TIM) model. The TIM model is a simple empirical model that provides the surface ablation rate as a function of air temperature, a variable that is reasonably easy to forecast (Hock, 2005). While the solar radiation term is ignored in this model, it is able to predict the surface ablation rate relatively well as surface energy fluxes are strongly correlated with the air temperature (Braithwaite and Olesen, 1993; Crawford et al., 2015).

The deterioration of ice islands can also be estimated through observed changes in their dimensions. Due to the harsh conditions and logistical difficulties of data collection in ice-prone environments, there are limited in-situ data on the dimensions, geometry, and thickness of ice islands. Halliday et al. (2012) measured the rate of thinning, as well as the surface and basal ablation rates of an ice island offshore Labrador using ablation stakes and ground penetrating radar. Alternatively, the deterioration of ice islands (*e.g.*, calving events and surface reduction) can be estimated through remote sensing observations using the satellite images when no field data on the dimensions of large ice features are available (Crawford et al., 2018a). Due to the large extent and angular shape of ice islands, these ice features can easily be distinguished from pack ice or open

24

water in satellite images. Although some satellite imagery have a low spatial resolution, the areal reduction in the surface of large ice islands can be monitored through the observed difference between the image acquisitions from various satellite systems such as MODIS and Envisat (Scambos et al., 2005; Peterson et al., 2009). While the amount of daylight and cloud cover may limit the use of these image analysis (optical) methods, spaceborne synthetic aperture radar (SAR) is capable of imaging ice features during times of low light and high cloud cover (Jeffries, 2002).

## 2.4. Methods

### 2.4.1. Study Site

Beacons were deployed from the Canadian Coast Guard Ship (CCGS) Amundsen, a research icebreaker, during the Offshore Newfoundland Research Expedition (ONRE) from 17 April to 4 May 2015. The deployment of the tracking beacons took place on 29 April 2015 offshore northern Newfoundland, where a large ice island (most likely from the Petermann Glacier in NW Greenland) was detected in Landsat imagery at the NE entrance to the Strait of Belle Isle. At this time, the ice island was grounded near the southeastern coast of Labrador and locked in 9+/10ths sea ice concentration. The dimensions of the ice island were estimated to be about 1.6 km in maximum waterline length (with 6% uncertainty) and around 10 m in average freeboard; the latter was estimated using the hydrostatic balance for the parent ice island (Figure 2.2).

**Figure 2.2.** The ice island in this study, shown surrounded by sea ice at the NE end of the Strait of Belle Isle on 29 April 2015.

### 2.4.2. Tracking Beacon Deployments and Characteristics of Ice Island Fragments

Four beacons (Canatec and Associates, Ltd) enclosed in waterproof, plastic cases were deployed by hand via the ship's helicopter on the ice island in a quadrilateral array 500-700 m apart from one another towards the center of ice island (Table 2.1). The beacons were secured to the ice with boards that had beds of nails in them, to prevent the beacons from being blown off the ice island by the wind. The ice tracking beacons transmitted Universal Time Coordinated (UTC) time, internal temperature, and latitude/longitude Global Positioning System (GPS) readings via Iridium satellite to a data management website (with 1.8 m Circular Error Probable). Initially, the four beacons were remotely set to transmit data at six-hour intervals during the time that the ice island

was grounded. The ice island broke up into several fragments (Figure 2.1) on 6 May 2015, which began to drift SW further into the Strait of Belle Isle. The four tracking beacons were then set to transmit hourly data and remained on the ice island fragments until the fragments melted (or experienced calving or rolling) (Table 2.1). The tracking beacons continued to transmit data as surface current drifter buoys, but this study only presents the analysis during the time that the beacons remained on the fragments. To determine whether the beacon was on the ice island or freely drifting in the ocean, diurnal variability in beacon temperatures was analyzed. While on ice, the beacon temperature records consistently displayed large diurnal variations. However, when the beacons fell into water, their temperature records reflected surface water temperature with minor fluctuations.

**Table 2.1.** Summary of ice island tracking beacon deployments (times and locations where the beacons were first deployed) on a large ice island grounded at the NE end of the Strait of Belle Isle.

| Beacon IMEI[a] (Last Four Digits) | Time (UTC[b]) | Latitude (°N) | Longitude (°W) | Time on Ice |
|---|---|---|---|---|
| **6640** | 29 Apr. 2015 21:32 | 52.01536 | 55.66191 | 29 Apr. – 25 Jun. |
| **1700** | 29 Apr. 2015 21:25 | 52.0191 | 55.66693 | 29 Apr. – 25 Jun. |
| **2500** | 29 Apr. 2015 22:14 | 52.02375 | 55.66017 | 29 Apr. – 24 Jun. |
| **5640** | 29 Apr. 2015 21:12 | 52.01904 | 55.65343 | 29 Apr. – 22 Jul. |

[a] International Mobile Equipment Identity
[b] Coordinated Universal Time

### 2.4.3. Reduction in Surface Area

The surface area, length, and width of each ice island fragment in this study were estimated from the available (29 April 2015 – 21 July 2015) SAR images during the fragment drift, using Focus PCI Geomatics software (version 2013). These dimensions were interpolated between satellite observations based on the assumption that their reduction in size was linear. However, it is possible the fragments may have undergone episodic calving between observations.

### 2.4.4. Surface Ablation

The surface ablation of the ice island fragments was estimated using a TIM model, in which the surface melt rate is calculated by (Hock, 2003):

$$V_{sa} = DDF \sum PDD \tag{2.1}$$

where $DDF$ (Table 2.2) represents the degree-day factor, which is a region-specific parameter that the TIM model is sensitive to (Crawford et al., 2015). Reported values of degree-day factors range from 2-11 mm d$^{-1}$ °C$^{-1}$ for glaciers in various sites (Hock, 2003). This study uses an average of 4 mm d$^{-1}$ °C$^{-1}$ for the degree-day factor (Table 2.2), which was estimated based on the assumption that the ice island fragments became completely melted (through surface and basal ablation) at the same time that the beacons fell into water. While the beacons could have fallen into the water due to the break-up or capsize of the fragments, this is unlikely given that the available SAR images did not show any remaining fragments beyond the time we assumed the beacons fell into water. The variable $PDD$ in Eqn. (2.1) represents the positive degree days, which is the sum of the daily mean positive air temperatures ($> 0$°C) during the analyzed period (Hock, 2003).

### 2.4.5. Basal Ablation

The thinning rate through the base of the ice island ($V_{ba}$) was determined using the forced convection basal ablation model that was calibrated with ice island melt rate observations and recorded atmospheric and oceanic data, given by (Crawford, 2018):

$$V_{ba} = k|\vec{v}_w(b) - \vec{u}|^{0.8} \left( \frac{T_w(b) - T_{mi}}{L^{0.2}} \right) \tag{2.2}$$

where $k$ is an empirical coefficient (Table 2.2) given by Crawford (2018), $\vec{v}_w(b)$ is the ocean current velocity at the keel depth, $u$ is the ice island fragment velocity, $T_w(b)$ is the water temperature at the base of the fragment, $T_{mi}$ is the melting temperature of the ice, and $L$ is the length of the ice island fragment. The fragment velocity was calculated between successive beacon position/time records. The calculated values represent the velocity at the midpoint between these positions, so they were linearly interpolated in space and time back to the beacon record positions. The melting temperature of the ice was estimated using an empirical correlation to account for the ice melting point depression due to the interfacial salinity at the base of the ice island fragments (Løset, 1993; Kubat et al., 2007), given by Josberger (1978):

$$T_{mi} = T_f exp\left(-0.19[T_\infty - T_f]\right) \tag{2.3}$$

where $T_\infty$ indicates the ambient water temperature at a distance beyond the influence of the ice island fragment. It should be noted that $T_\infty$ and $T_w(b)$ are effectively the same in our model given that the extracted ocean water temperature from CMEMS has a resolution of 1/12° (~ 9 km). So the ambient water temperature at some distance away from the ice island fragments lies within the same grid point as the ice island where $T_w(b)$ was extracted. $T_f$ is freezing temperature of the water, which was estimated as a function of the water salinity ($S$) given by (Fujino et al., 1974):

$$T_f = -0.036 - 0.0499S - 0.000112S^2 \tag{2.4}$$

The daily water salinity and potential temperature at different depth layers were extracted using Global Ocean Physics Reanalysis Glorys12v1 model from Copernicus Marine Environment Monitoring Service (CMEMS). Potential temperature was then adjusted based on the water pressure and salinity at each depth to calculate the actual water temperature. The velocity of ocean

currents over the depth of ice island fragments was extracted from CMEMS Global Ocean 1/12°

Physics Analysis and Forecast model. The extracted data were all interpolated to the fragments'

observed locations and then integrated into Eqn. (2.2) to allow for the calculation of basal ablation

rates.

To present the total change in the thicknesses of ice island fragments over time, the cumulative

vertical melt was estimated according to the above surface and basal ablation models and

subtracted from the initial thickness. The initial thickness of the original ice island was estimated

using the ice island hydrostatic balance at the time it started to drift. It was assumed that once the

beacons started drifting, the ice island would have a draft slightly less (by 5 m) than the shallowest

water depth under the ice island.

## 2.4.6.  Mass Calculation

The mass of the fragments was calculated by:

$$M = \rho_i V_{ice} \tag{2.5}$$

where $\rho_i$ is the density of the ice island fragments. While the density of pure (bubble-free) ice is

around 917 kg/m$^3$ (Enderlin and Hamilton, 2014), ice islands have lower density. This study uses

the ice density of 873 kg/m$^3$ for the fragments, as measured by Crawford et al. (2018b). The

variable $V_{ice}$ in Eqn. (2.5) represents ice island volume, calculated by:

$$V_{ice} = A_{ha} h_i \tag{2.6}$$

where $A_{ha}$ and $h_i$ represent the ice surface area and thickness of the ice island, respectively. The mass of each fragment was recalculated over time based on the interpolated surface area and modeled thickness.

### 2.4.7. Drift Equation

The equation describing the drift of an ice island fragment is stated as (Lichey and Hellmer, 2001):

$$M\frac{d\vec{u}}{dt} = \vec{F}_a + \vec{F}_w + \vec{F}_c + \vec{F}_{ss} + \vec{F}_{si} \tag{2.7}$$

where $M$ is the mass of the ice island fragment. The five terms on the right side of Eqn. (2.7) represent forces due to air drag, water drag, Coriolis effect, sea surface tilt, and sea ice, respectively. To evaluate these forces when the ice island fragments were not grounded, the atmospheric and oceanic data were extracted from available databases; the 3-hourly values for 10-m wind velocity and 2-m air temperature were extracted from NARR dataset, however, sea surface height and sea ice velocity were extracted from CMEMS Global Ocean 1/12° Physics Analysis and Forecast model. There were time periods in the extracted ocean currents data for the four fragments during which the ocean current velocities were missing. Therefore, the extracted data were linearly interpolated to fill out the gaps in the velocity of ocean currents. While the mass of the ice island was assumed to be constant in some drift models (*e.g.*, Lichey and Hellmer, 2001), it varied in our model (Eqn. (2.7)) to improve the model accuracy.

Air drag and water drag force (Eqn. (2.7)) both on vertical walls and horizontal surfaces of the ice island fragment were calculated by (Smith and Banke, 1983):

$$\vec{F}_a = \left[ \frac{1}{2}(\rho_a c_a A_{va}) + \rho_a c_{da} A_{ha} \right] |\vec{v}_a - \vec{u}|(\vec{v}_a - \vec{u}) \tag{2.8}$$

$$\vec{F}_w = \left[ \frac{1}{2}(\rho_w c_w A_{vw}) + \rho_w c_{dw} A_{hw} \right] |\vec{v}_w - \vec{u}|(\vec{v}_w - \vec{u}) \tag{2.9}$$

where $\rho_a$ is the air density, $c_a$ is the coefficient of resistance (form drag) for air, and $c_{da}$ is the air

drag coefficient (skin drag). In Eqn. (2.8), the vertical and horizontal areas of the ice island

fragment exposed to air flow ($\vec{v}_a$) are denoted by $A_{va}$ and $A_{ha}$, respectively. The parameters and

variables in Eqn. (2.9) are analogous to those in Eqn. (2.8), but are indicated by the subscript $w$

for water. Given the tabular shape of ice islands, the average current velocity ($\vec{v}_w$) in Eqn. (2.9)

was defined as the average of current velocity profile over the fragment draft. $A_{va}$ and $A_{vw}$ were

estimated from the fragment length ($L$), width ($W$), sail height ($h_s$), and draft ($h_k$) by:

$$A_{va} = h_s \frac{(L + W)}{2} \tag{2.10}$$

$$A_{vw} = h_k \frac{(L + W)}{2} \tag{2.11}$$

The resulting force from the Coriolis effect and sea surface tilt are given by (Lichey and Hellmer,

2001):

$$\vec{F}_c = 2M\Omega \sin \Phi_i \, \vec{k} \times \vec{u} \tag{2.12}$$

$$\vec{F}_{ss} = M\vec{g} \sin \alpha \tag{2.13}$$

where $\Omega$ ($7.27 \times 10^{-5} \, rad \, s^{-1}$), $\Phi_i$, and $\vec{k}$ are the Earth's angular speed, the latitude of the ice

island fragment, and the unit vector perpendicular to the surface of Earth, respectively. In Eqn.

(2.13), $g$ is the acceleration due to gravity (9.81 $m\ s^{-2}$) and $\alpha$ represents the sea surface slope.

The sea surface tilt ($\sin \alpha$) was estimated directly from CMEMS satellite altimetry data.

The force due to the surrounding sea ice was calculated using two different approaches: the residual method and Lichey and Hellmer's model (2001). From Eqn. (2.7), the residual force ($\vec{F}_{res}$) in the presence of sea ice was estimated by:

$$\vec{F}_{res} = \vec{F}_{si} + \vec{e}_i = M\frac{d\vec{u}}{dt} - \left(\vec{F}_a + \vec{F}_w + \vec{F}_c + \vec{F}_{ss}\right) \tag{2.14}$$

where $\vec{F}_{si}$ is the sea ice force and $\vec{e}_i$ is the error term that accounts for the error in the input data. In the presented analysis, it was assumed that the error term, $\vec{e}_i$, was sufficiently small, then $\vec{F}_{res} \sim \vec{F}_{si}$. This allowed us to estimate the contributions from sea ice based on the residual force. In the case that there was no sea ice present ($\vec{F}_{si} = 0$), Eqn. (2.14) still holds, but the residual force represents only the error term between the net force and the estimated force components. The residual force in open water is therefore given by:

$$\vec{F}_{res} = \vec{e}_i = M\frac{d\vec{u}}{dt} - \left(\vec{F}_a + \vec{F}_w + \vec{F}_c + \vec{F}_{ss}\right) \tag{2.15}$$

The force due to the surrounding sea ice was calculated by (Lichey and Hellmer, 2001):

$$\vec{F}_{si} = \begin{cases} 0 & C \leq 15\% \\ \frac{1}{2}\rho_{si}c_{si}A_{si}|\vec{v}_{si} - \vec{u}|(\vec{v}_{si} - \vec{u}) & 15\% < C \leq 90\% \\ -\left(\vec{F}_a + \vec{F}_w + \vec{F}_c + \vec{F}_{ss}\right) & C \geq 90\% \ and \ P \geq P_s \end{cases} \tag{2.16}$$

where $\rho_{si}$ is the density of sea ice, $c_{si}$ is the coefficient of resistance for sea ice, assumed to be 1.0 (Lichey and Hellmer, 2001; Bigg et al., 1997), $A_{si}$ is the estimated contact area between sea ice

and the ice island fragment (defined as the product of sea ice thickness and ice island waterline length; Lichey and Hellmer, 2001), $\vec{v}_{si}$ is the sea ice velocity, and $C$ is the concentration of sea ice cover in percent. According to Eqn. (2.16), sea ice with concentrations less than 15% are considered as open water and exert no force on the ice island fragment. However, for sea ice concentrations between 15% and 90% (open drift), sea ice impose additional drag on the ice island. For concentrations over 90% (close pack) where the sea ice compressive strength ($P$) is greater than its threshold value ($P_s$), sea ice envelopes the ice island fragment causing it to drift at the sea ice velocity. The sea ice compressive strength can be estimated from its thickness ($h_{si}$) and concentration by (Hibler, 1979):

$$P = P^* h_{si} e^{-a(1-C)} \tag{2.17}$$

where $P^*$ and $a$ are empirical coefficients with values of 20,000 $N\ m^{-2}$ and 20, respectively (Lichey and Hellmer, 2001). While Eqn. (2.16) presents the sea ice forcing for different sea ice concentrations, only the relationships associated with open water and open drift were used in this study as the concentration of sea ice in the vicinity of ice island fragments during the analyzed period were never beyond 90%. Sea ice concentration and thickness were extracted manually from the CIS daily ice charts and cross-checked against the SAR images at the location of the ice island fragments over their drift period. A summary of all the parameters and variables used in this study, along with their values, is given in Table 2.2.

**Table 2.2.** Description and values of the parameters and variables.

| Parameter /variable | Description | Unit | Value | Reference |
|---|---|---|---|---|
| $\boldsymbol{\rho_a}$ | Air density | $kg\ m^{-3}$ | 1.293 | Lichey and Hellmer (2001) |

| | | | | |
|---|---|---|---|---|
| $\vec{v}_a$ | Wind velocity | $m\,s^{-1}$ | Interpolated from NARR | North American Regional Reanalysis |
| $\rho_w$ | Water density | $kg\,m^{-3}$ | 1025 | Crawford et al. (2018b) |
| $\vec{v}_w$ | Mean current velocity | $m\,s^{-1}$ | Interpolated from CMEMS and averaged over the draft | Copernicus Marine Environment Monitoring Service |
| $\rho_{si}$ | Sea ice density | $kg\,m^{-3}$ | 900 | Turnbull et al. (2017) |
| $c_a$ | Air form drag coefficient | - | 0.4[*] | Lichey and Hellmer (2001) |
| $c_w$ | Water form drag coefficient | - | 0.85 | Lichey and Hellmer (2001) |
| $c_{da}$ | Air skin drag coefficient | - | 0.00025 | Lichey and Hellmer (2001) |
| $c_{dw}$ | Water skin drag coefficient | - | 0.0005 | Lichey and Hellmer (2001) |
| $\Omega$ | Earth's angular speed | $rad\,s^{-1}$ | $7.27\times10^{-5}$ | |
| $\Phi_i$ | Ice island latitude | ° | Recorded by tracking beacons | |
| $c_{si}$ | Sea ice resistance coefficient | - | 1.0 | Lichey and Hellmer (2001) |
| $A_{ha}$ | Surface area | $m^2$ | Estimated from SAR imagery | |
| $A_{hw}$ | Basal area | $m^2$ | Equal to $A_{ha}$ for ice islands | |
| $A_{va}$ | Above water cross sectional area | $m^2$ | Estimated from sail width and height | |
| $A_{vw}$ | Under water cross sectional area | $m^2$ | Estimated from keel width and height | |

| | | | | |
|---|---|---|---|---|
| $\vec{v}_{si}$ | Sea ice velocity | $m\ s^{-1}$ | Interpolated from CMEMS | Copernicus Marine Environment Monitoring Service |
| $\vec{u}$ | Ice island velocity | $m\ s^{-1}$ | Estimated from the ice island observed location | |
| $\vec{g}$ | Gravitational acceleration | $m\ s^{-2}$ | 9.81 | |
| $\rho_i$ | Ice island density | $kg\ m^{-3}$ | 873 | Crawford et al. (2018b) |
| $h_i$ | Ice island thickness | $m$ | Estimated from ice island hydrostatic balance and ablation models | Hock (2003) |
| $V_{ice}$ | Ice island volume | $m^3$ | Estimated from ice island surface area and thickness | |
| $L$ | Ice island length | $m$ | Estimated from SAR imagery | |
| $W$ | Ice island width | $m$ | Estimated from SAR imagery | |
| $h_s$ | Ice island sail height | $m$ | Estimated from the difference between the ice island thickness and keel depth | |
| $h_k$ | Ice island keel depth | $m$ | Estimated from bathymetry data and ice island hydrostatic balance | National Oceanic and Atmospheric Administration |
| $M$ | Ice island mass | $kg$ | Estimated from ice island density and volume | |
| $DDF$ | Degree-day factor | $mm\ d^{-1}\ °C^{-1}$ | 4 | |

| | | | | |
|---|---|---|---|---|
| $PDD$ | Positive degree days | °C | Estimated using NARR data | North American Regional Reanalysis |
| $V_{ba}$ | Ice island base thinning rate | $m\ s^{-1}$ | Estimated from basal ablation model | Crawford (2018) |
| $k$ | Bulk heat transfer coefficient | $m^{2/5}\ S^{-1/5}\ °C^{-1}$ | $1.3 \times 10^{-5}$ | Crawford (2018) |
| $\vec{v}_w(b)$ | Current velocity at the keel depth | $m\ s^{-1}$ | Interpolated from CMEMS | Copernicus Marine Environment Monitoring Service |
| $T_w(b)$ | Water temperature at the keel depth | °C | Interpolated from CMEMS | Copernicus Marine Environment Monitoring Service |
| $T_f$ | Water freezing temperature | °C | Estimated from an empirical correlation | Fujino et al. (1974) |
| $T_\infty$ | Water temperature | °C | Interpolated from CMEMS | Copernicus Marine Environment Monitoring Service |
| $S$ | Water salinity | $ppt$ | Interpolated from CMEMS | Copernicus Marine Environment Monitoring Service |
| $T_a$ | Air temperature | °C | Interpolated from NARR | North American Regional Reanalysis |
| $C$ | Sea ice concentration | - | Extracted from daily ice charts | |
| $h_{si}$ | Sea ice thickness | $m$ | Extracted from daily ice charts | |
| $P_s$ | Sea ice strength threshold | $N\ m^{-1}$ | 660.9 - 14211.6 | Lichey and Hellmer (2001) |
| $P$ | Sea ice compressive strength | $N\ m^{-1}$ | Estimated from Hibler's correlation | Hibler (1979) |
| $P^*$ | Sea ice strength coefficient | $N\ m^{-2}$ | 20,000 | Lichey and Hellmer (2001) |

| $a$ | Sea ice strength coefficient | - | 20 | Lichey and Hellmer (2001) |
|---|---|---|---|---|

[*] A 40% higher value (0.56) was used for $c_a$ to implicitly account for the effect of ocean surface waves (Smith, 1993; Keghouche et al., 2009)

### 2.4.8. Sensitivity Analysis

While commonly used values of skin and form drag coefficients for air and water ($c_{da} = 0.00025$, $c_{dw} = 0.0005$, $c_a = 0.4$, and $c_w = 0.85$) were used in this study (Table 2.2), it is important to examine how sensitive the residual sea ice force results are to a change in these coefficients. Due to the roughness variation in the surfaces, bases, and walls of the ice island fragments, the skin drag coefficients were varied between 0.00025 and 0.008, while the form drag coefficient values ranging from 0.05 to 2 were tested. These values were selected to account for the variation among the reported air/water drag coefficients on icebergs in other studies (*e.g.*, Rackow et al., 2017; Keghouche et al., 2009; Eik, 2009; Kubat et al., 2005; Lichey and Hellmer, 2001), where values in the ranges of 0.00025-0.0025, 0.0005-0.0055, 0.1-2, and 0.05-1.5 were used for the air skin drag, water skin drag, air form drag, and water form drag coefficients, respectively. To examine the individual influence of a varying drag coefficient, the other three coefficients were fixed at the nominal values mentioned earlier. These values were integrated into the residual sea ice force model (Eqn. (2.14)) to examine which of these four drag coefficients the model is most sensitive to.

Due to the uncertainty in the estimated masses and ocean currents, the sensitivity analysis was also performed to study the residual sea ice force results to the variation of ice island fragments' masses, as well as the mean ocean currents speed and direction. Given that the dimensions of the fragments were estimated from satellite imagery data with resolution of 100 m, the propagated error for mass was estimated and integrated into the sensitivity analysis. Also, the mean error in the magnitudes

(speed) and directions of surface currents from CMEMS Global Ocean 1/12° Physics Analysis and Forecast model was reported to be $0.08\ m\ s^{-1}$ and $7.2\degree$, respectively (Lellouche et al., 2018). Assuming the same error for the currents in different layers beneath the water surface, the residual forces (Eqn. (2.7)) were calculated using the estimated average error in speeds ($\pm 0.08\ m\ s^{-1}$; high and low) and directions ($\pm 7.2\degree$; high and low) of the currents to evaluate the model sensitivity to the error in the CMEMS ocean currents.

## 2.5.    Results

This section presents the drift speeds (Figure. 2.3), directions (Figure. 2.4), and statistics Table 2.3) of the four ice island fragments over the time periods that they were tracked by beacons. Diurnal variability in beacon temperatures showed that beacons 6640, 1700, and 2500 remained on the ice island fragments until 24-25 June 2015, however, beacon 5640 tracked the ice island fragment until 22 July 2015 when it broke up (Table 2.1).
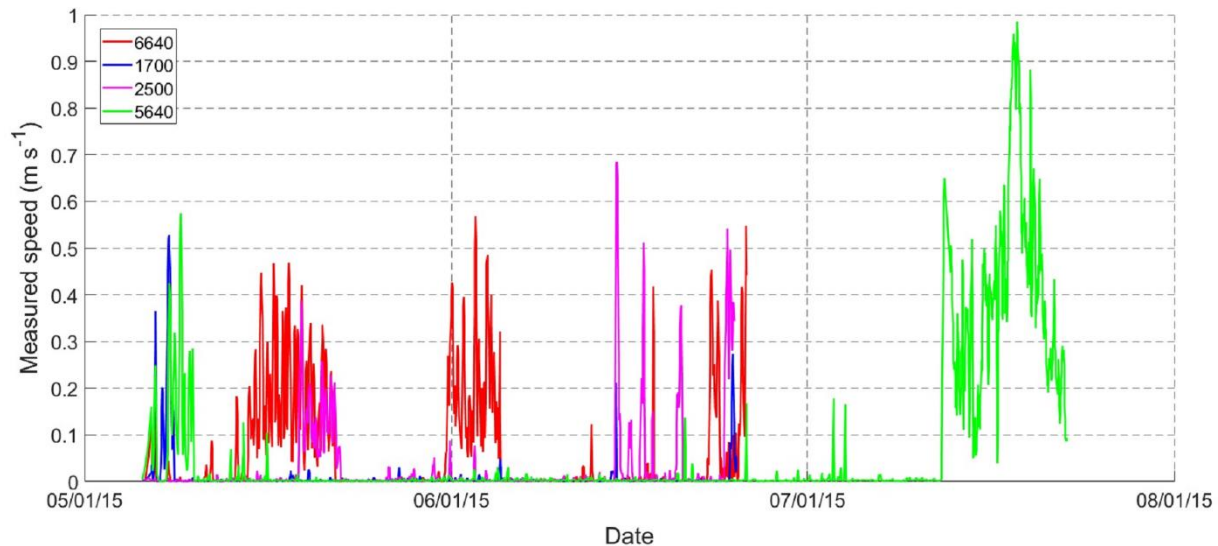


**Figure. 2.3.** Drift speeds of the four ice island fragments over their overall drift periods.
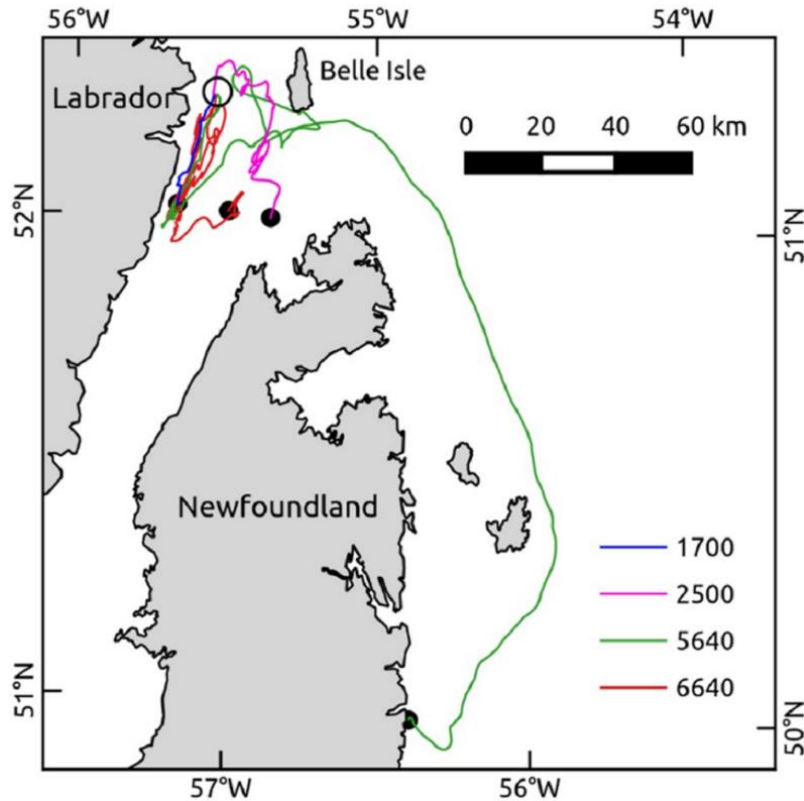
**Figure. 2.4.** Drift trajectories of the four ice island fragments over their drift periods. The open circle and black dots mark the start and ends of the recorded ice fragment trajectories, respectively.

**Table 2.3.** Drift characteristics of the ice island tracking beacons over their drift periods.

| Beacon IMEI[a] | Total Drift Period (UTC[b]) | Mean Drift Speed[*] ($m\ s^{-1}$) | Max. Drift Speed ($m\ s^{-1}$) | Drift Speed Std. Dev. ($m\ s^{-1}$) | Cumulative Drift Distance (km) | Net Drift Distance (km) |
|---|---|---|---|---|---|---|
| 6640 | 29 Apr. – 25 Jun. | 0.18 | 0.57 | 0.12 | 274 | 32 |
| 1700 | 29 Apr. – 25 Jun. | 0.15 | 0.53 | 0.14 | 44 | 30 |
| 2500 | 29 Apr. – 24 Jun. | 0.17 | 0.69 | 0.15 | 124 | 38 |
| 5640 | 29 Apr. – 22 Jul. | 0.36 | 0.99 | 0.22 | 433 | 176 |

[a] International Mobile Equipment Identity
[b] Coordinated Universal Time
[*] The drift speeds were estimated with high accuracy ($\pm 0.001\ m\ s^{-1}$) from the positional and time data transmitted by the tracking beacons

Figure. 2.4 shows the drift trajectories of the ice islands fragments during the drift periods given in

Table **2.3**. The four ice island fragments initially drifted in a looping pattern after break-up, and then one of the ice island fragments (beacon 5640) drifted to the SE side of the Northern Peninsula of Newfoundland. The drift of the ice island fragments back and forth NE-SW in the NE end of the Strait of Belle Isle was attributed to tidal currents by comparing the fluctuations in the drift velocities against the oscillation periods of tidal and inertial currents. Figure. 2.4 along with the ratio of the net drift distance to the total drift distance (

Table **2.3**) revealed that while beacon 6640 experienced the most pronounced looping pattern, beacons 1700 drifted in a fairly straight direction towards the SW of the Strait of Belle Isle. The slight difference in the trajectories of ice island fragments upon break-up is most likely associated with their dimensions and masses which are important variables in the drift equation, Eqn. (2.7). Fragment 5640, which was the smallest of the four fragments, drifted about a month more than the other fragments and the furthest from its original location (Figure. 2.4). The different drift directions of ice island fragments could also be associated with their orientations with respect to ocean current form drag, which is an important contributor to the overall drift of the fragments.

### 2.5.1.  Areal Extent and Thickness Reduction

The initial dimensions of the four ice island fragments after the breakup event of the original ice island are given in Table 2.4. The initial surface areas of the fragments, estimated from the SAR imagery, ranged between 288,675 and 724,628 m$^2$ (Figure. 2.5). SAR imagery resolution is nominally 100 m, and the reported mean error in fragment areas using various methods of digitization ranged between 2.5 % and 5.3 % (Crawford et al., 2018). Using the bathymetry data (extracted from ETOPO1 Global Relief Model, National Oceanic and Atmospheric

41

Administration), the shallowest depth of water at the location of the ice island was 65 m, so the initial draft was assumed to be slightly less, about 60 m, to account for the irregularities in the base of the ice island. Using hydrostatic balance for the parent ice island and assuming sea water density of 1025 kg/m$^3$ and glacial ice density of 873 kg/m$^3$ (Table 2.2), the total thickness of about 70 m was estimated (Figure. 2.6). From the ice island initial thickness and draft, an average initial freeboard of about 10 m was estimated and this appeared reasonable when compared against the photos of the ice island taken during the field expedition. The reduction in the areal extent and thickness of the ice island fragments are presented in Figure. 2.5 and Figure. 2.6, respectively. The thickness melt models revealed that basal ablation was, on average, the main contributor to the overall reduction in the thickness of the ice island fragments, accounting for 52-94% of the total vertical melt rate. This is in agreement with the results of a Petermann ice island deterioration study by Crawford (2018), in which basal ablation was responsible for 73 % of the total melt between November 2015 and September 2016.

**Table 2.4.** The estimated initial dimensions of the ice island fragments from SAR images.

| Beacon IMEI[a] | Analyzed Drift Period (UTC[b]) | Fragment Initial Length (m) | Fragment Initial width (m) | Fragment Initial Surface Area (m$^2$) |
|---|---|---|---|---|
| **6640** | 6 May – 18 May | 1,388 (7%)[*] | 818 (12%) | 724,628 (14%) |
| **1700** | 6 May – 30 May | 925 (11%) | 604 (17%) | 333,300 (20%) |
| **2500** | 6 May – 19 May | 1,294 (8%) | 855 (12%) | 669,586 (14%) |
| **5640** | 6 May – 8 May | 831 (12%) | 532 (19%) | 288,675 (22%) |

[a] International Mobile Equipment Identity
[b] Coordinated Universal Time
[*] The values in brackets indicate the relative uncertainties in the estimated dimensions.
The initial thickness of all fragments was estimated to be about 70 m
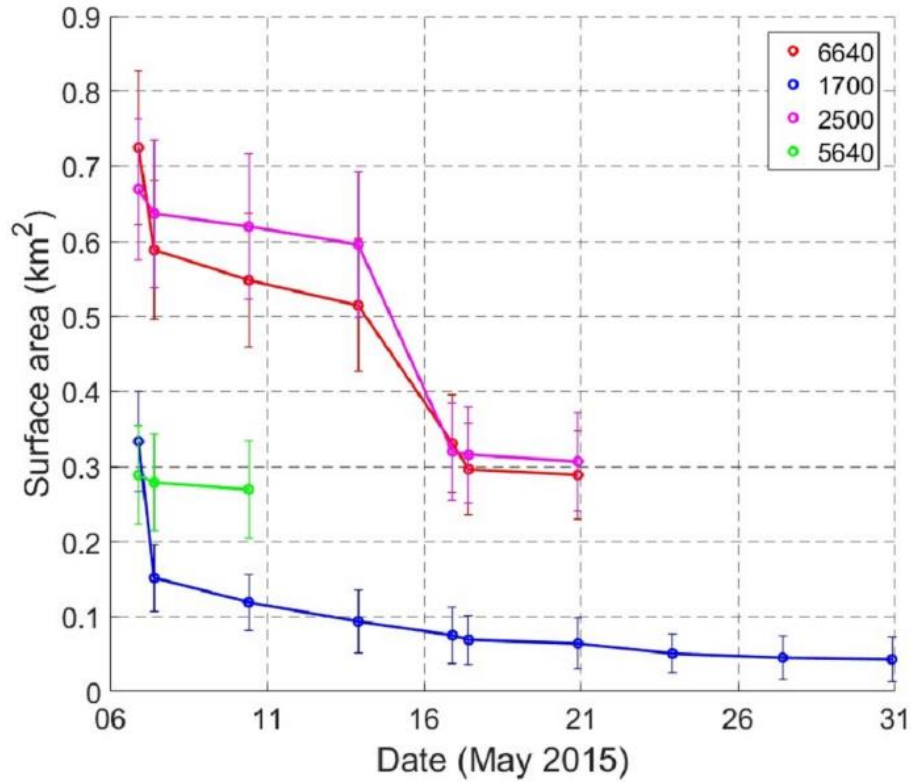
**Figure. 2.5.** The surface areas of the ice island fragments during the analyzed drift period, estimated from the SAR image acquisitions (marked with circles). The vertical bars show the error in the estimated values.
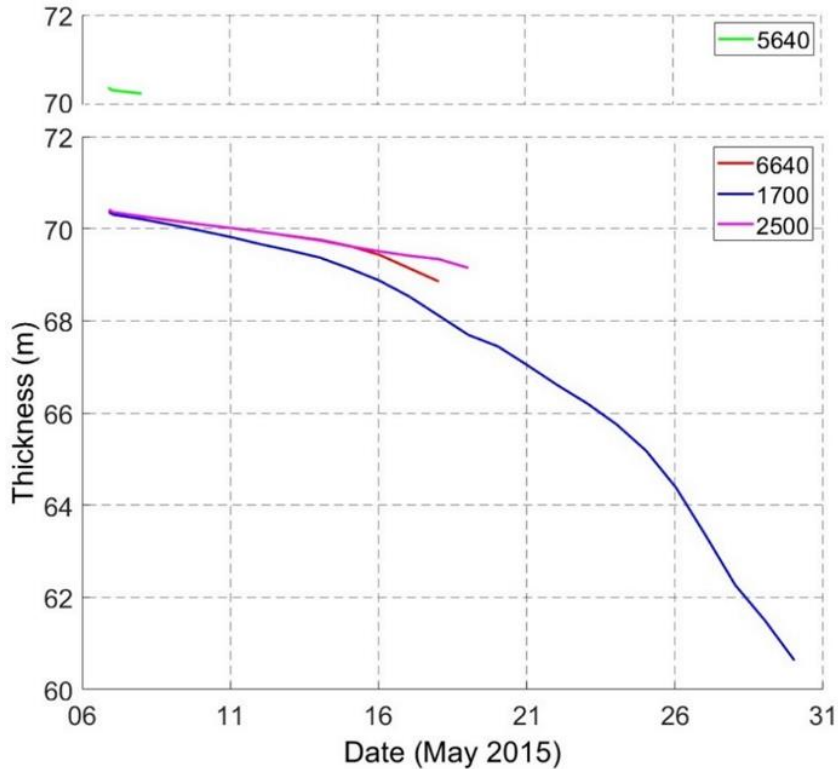
**Figure. 2.6.** The change in the thicknesses of the four ice island fragments during the analyzed drift period, estimated using the surface (TIM) and basal ablation models. The thickness change of fragment 5640 is plotted above the main graph due to the lines overlapping.

### 2.5.2. Atmospheric and Oceanic Forces

The magnitudes and the relative contributions of the forces caused by wind, currents, Coriolis deflection, sea surface tilt, and surrounding sea ice to the overall drift of the ice island fragments are presented in Figure. 2.7 and Figure. 2.8, respectively. While the tracking beacons provided data on the locations of the ice island fragments over a longer period of time, the force analysis was narrowed down to the time periods in which the reanalysis data and satellite images of ice island fragments were simultaneously available (Figure. 2.7, Figure. 2.8, and Figure. 2.10). Also, any grounded periods were removed from subsequent analysis (Figure. 2.8 and Figure. 2.10),

which resulted in removing the whole analysis for fragment 2500 as it was grounded for extended periods of time over the period analyzed in this study (Figure. 2.11).
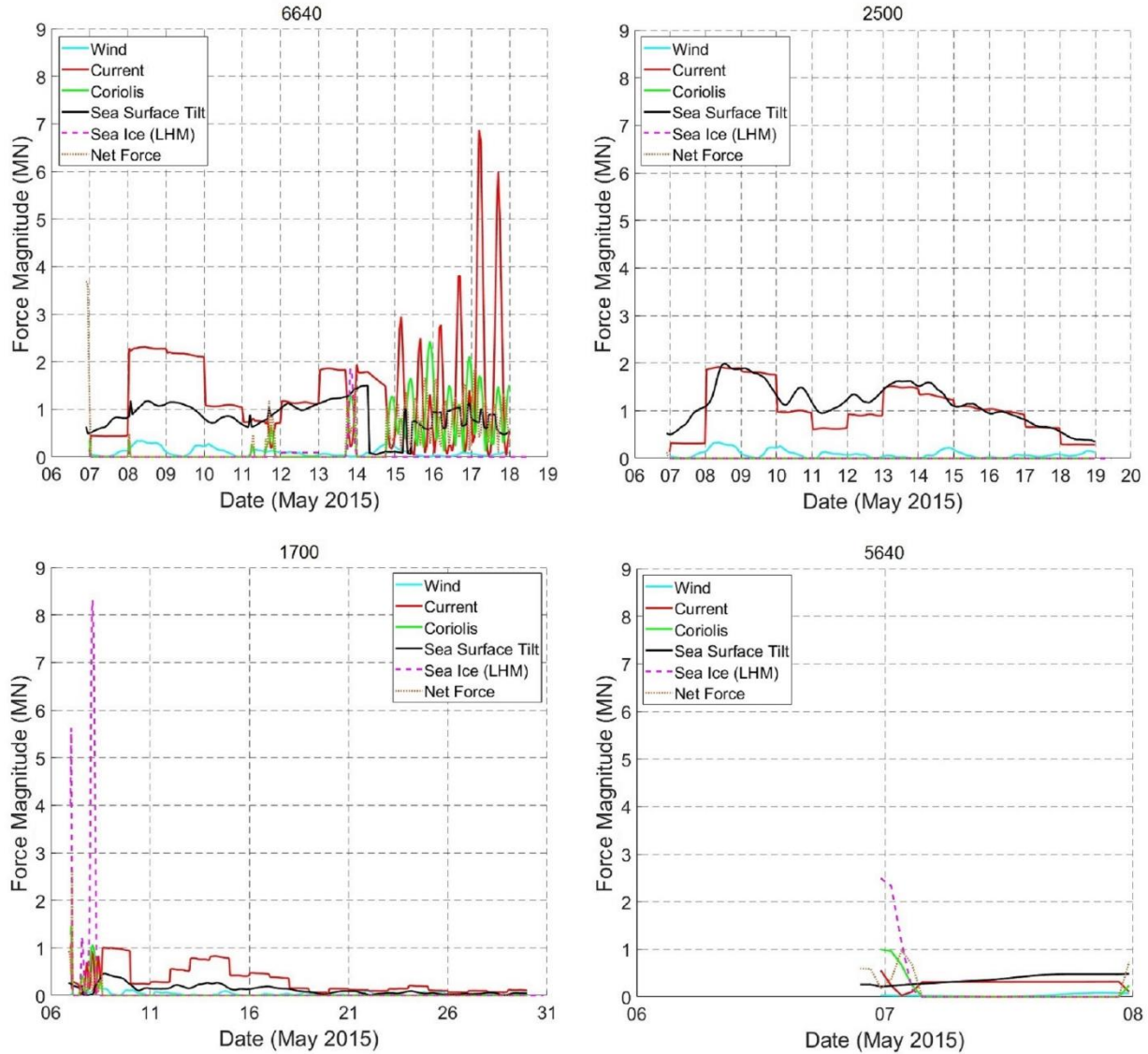


**Figure. 2.7.** The magnitudes of the forces caused by wind, currents, Coriolis deflection, sea surface tilt, and surrounding sea ice on the ice island fragments tracked by beacons 6640, 1700, 2500, and 5640. LHM indicates the estimation using Lichey and Hellmer's model (2001).
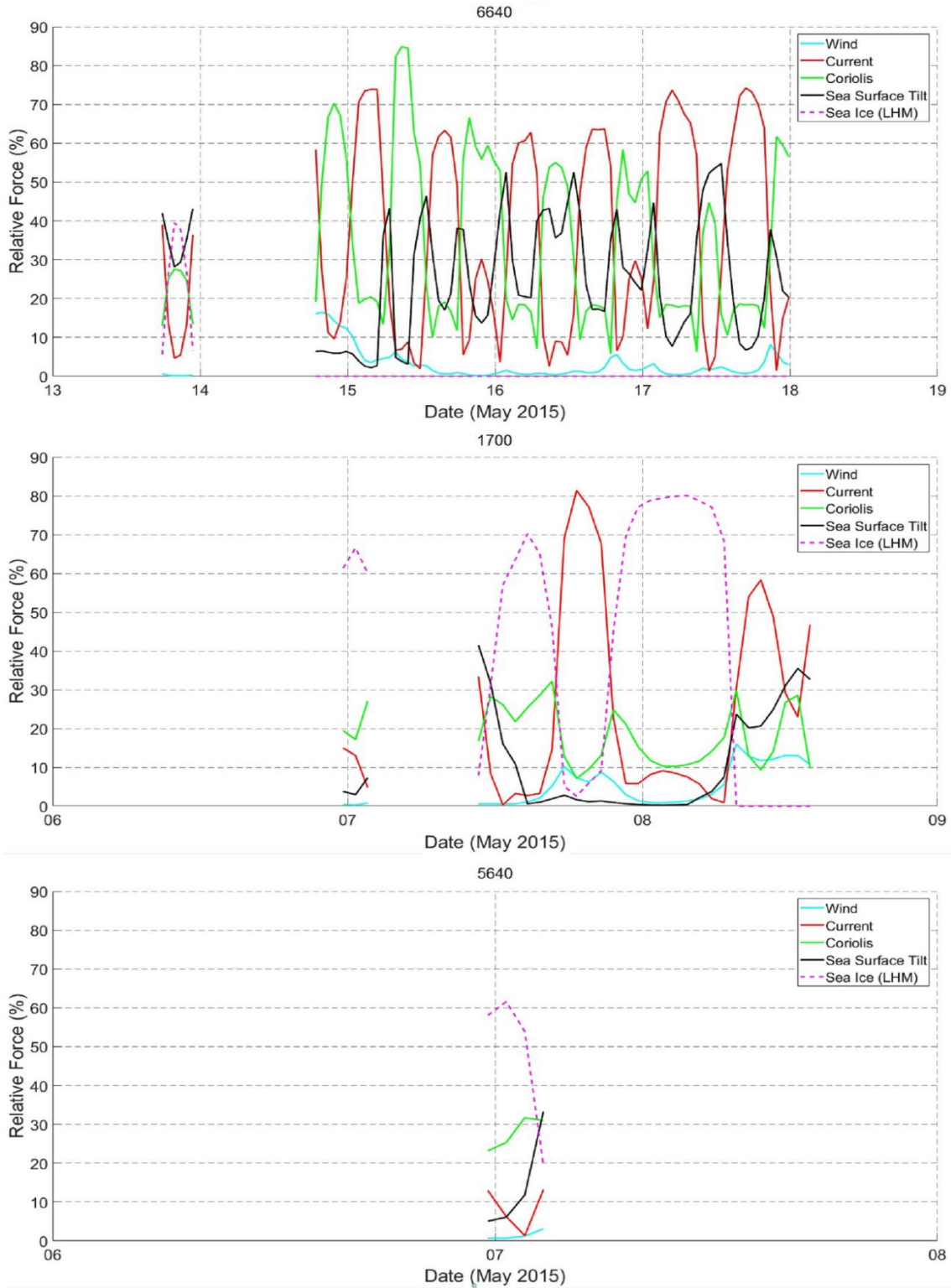
**Figure. 2.8.** The relative contributions of the forces caused by wind, currents, Coriolis deflection, sea surface tilt, and surrounding sea ice to the overall drift of the ice island fragments tracked by beacons 6640, 1700, and 5640 during the time periods that the fragments were drifting.

Figure. 2.7 shows that forces due to ocean currents and sea surface tilt were found to dominate the other forces over the time periods presented in Table 2.4, except when sea ice was present at medium-high concentrations in the proximity of the fragments, or when the fragments drifted at higher speeds. The analysis of the relative contributions of the forces to the drift of the fragments (Figure. 2.8) revealed that when the sea ice exceeded a concentration of 20%, it had the most pronounced effect on the drift of these fragments. The analysis of the relative contribution (Figure. 2.8) and the average magnitude (Table 2.5) of the forces over the analyzed drift periods of the ice island fragments suggest that the force caused by the wind had minimal effects on the overall drift of the four fragments, and that Coriolis force was only significant when drift speeds were high. Given that sea ice was only present during the first few days of each fragment's drift and gave way to open water for much of the remainder of the analyzed drift (Figure. 2.9), the sea ice exerted no force on the ice island fragments for the majority of their observed drift periods (Figure. 2.7). Therefore, the sea ice force analysis was only performed during sea ice cover presence (Figure. 2.10). This analysis shows that the trend over time in the sea ice force calculated from the residual approach (Eqn. (2.14)) were generally similar to the rise and fall of the sea ice force calculated from Lichey and Hellmer's model (2001) (Figure. 2.10). However, the values of sea ice force magnitudes from Lichey and Hellmer's model (2001) were different from the ones obtained from the residual approach.

**Table 2.5.** The statistical analysis of the force magnitudes over the analyzed drift periods of the ice island fragments.

| Beacon IMEI[a] | Wind Force (MN) | | | Current Force (MN) | | | Coriolis Force[b] (MN) | | | Sea Surface Tilt Force (MN) | | | Sea Ice Force[c] (Res.) (MN) | | | Sea Ice Force[c] (LHM[d]) (MN) | | |
|---|---|---|---|---|---|---|---|---|---|---|---|---|---|---|---|---|---|---|
| | Rng.[1] | M.[2] | Std.[3] | Rng. | M. | Std. | Rng. | M. | Std. | Rng. | M. | Std. | Rng. | M. | Std. | Rng. | M. | Std. |
| 6640 | 0.00 0.34 | 0.10 | 0.09 | 0.02 6.87 | 1.39 | 1.06 | 0.11 2.42 | 0.89 | 0.56 | 0.05 1.50 | 0.84 | 0.33 | 1.38 3.85 | 2.59 | 0.83 | 0.07 1.85 | 0.78 | 0.74 |
| 1700 | 0.00 0.17 | 0.03 | 0.03 | 0.00 1.10 | 0.32 | 0.28 | 0.02 1.45 | 0.45 | 0.40 | 0.01 0.46 | 0.12 | 0.10 | 0.20 2.78 | 0.92 | 0.72 | 0.02 8.31 | 2.65 | 2.87 |
| 2500 | 0.00 0.33 | 0.09 | 0.08 | 0.13 1.92 | 1.02 | 0.50 | - - | - | - | 0.35 1.99 | 1.15 | 0.42 | - - | - | - | 0.00 0.00 | 0.00 | 0.00 |
| 5640 | 0.00 0.08 | 0.03 | 0.03 | 0.03 0.56 | 0.29 | 0.10 | 0.24 0.99 | 0.62 | 0.37 | 0.22 0.48 | 0.37 | 0.09 | 0.74 1.45 | 1.08 | 0.28 | 0.16 2.49 | 1.53 | 1.10 |

[a] International Mobile Equipment Identity
[b] Coriolis force was only analyzed during the time periods that the fragments were drifting
[c] Sea ice force was only analyzed during the time periods that the fragments were drifting and sea ice was present in the vicinity of ice island fragments
[d] Lichey and Hellmer's model (2001)
[1] Range
[2] Mean
[3] Standard deviation
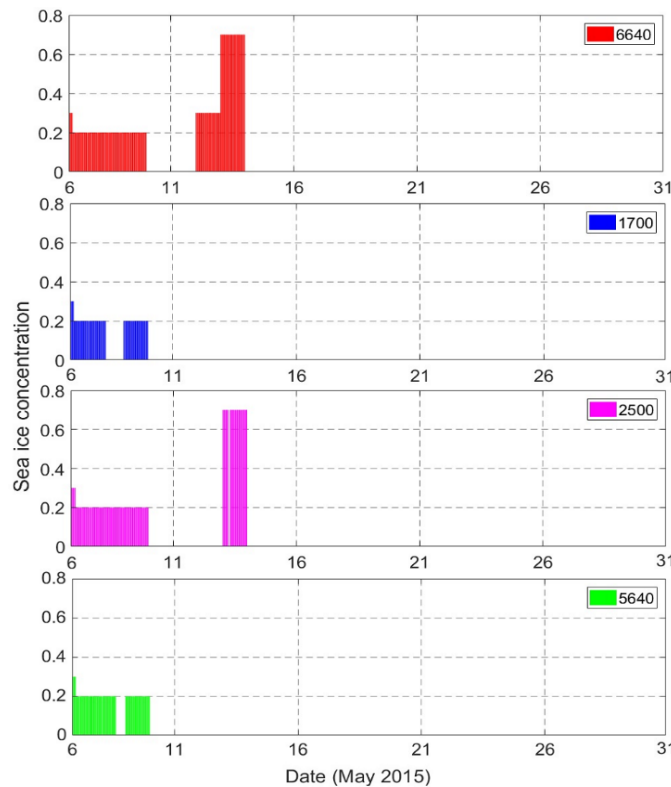


**Figure. 2.9.** The concentration of sea ice surrounding the four ice island fragments during the analyzed drift periods, obtained from CIS daily ice charts.

48
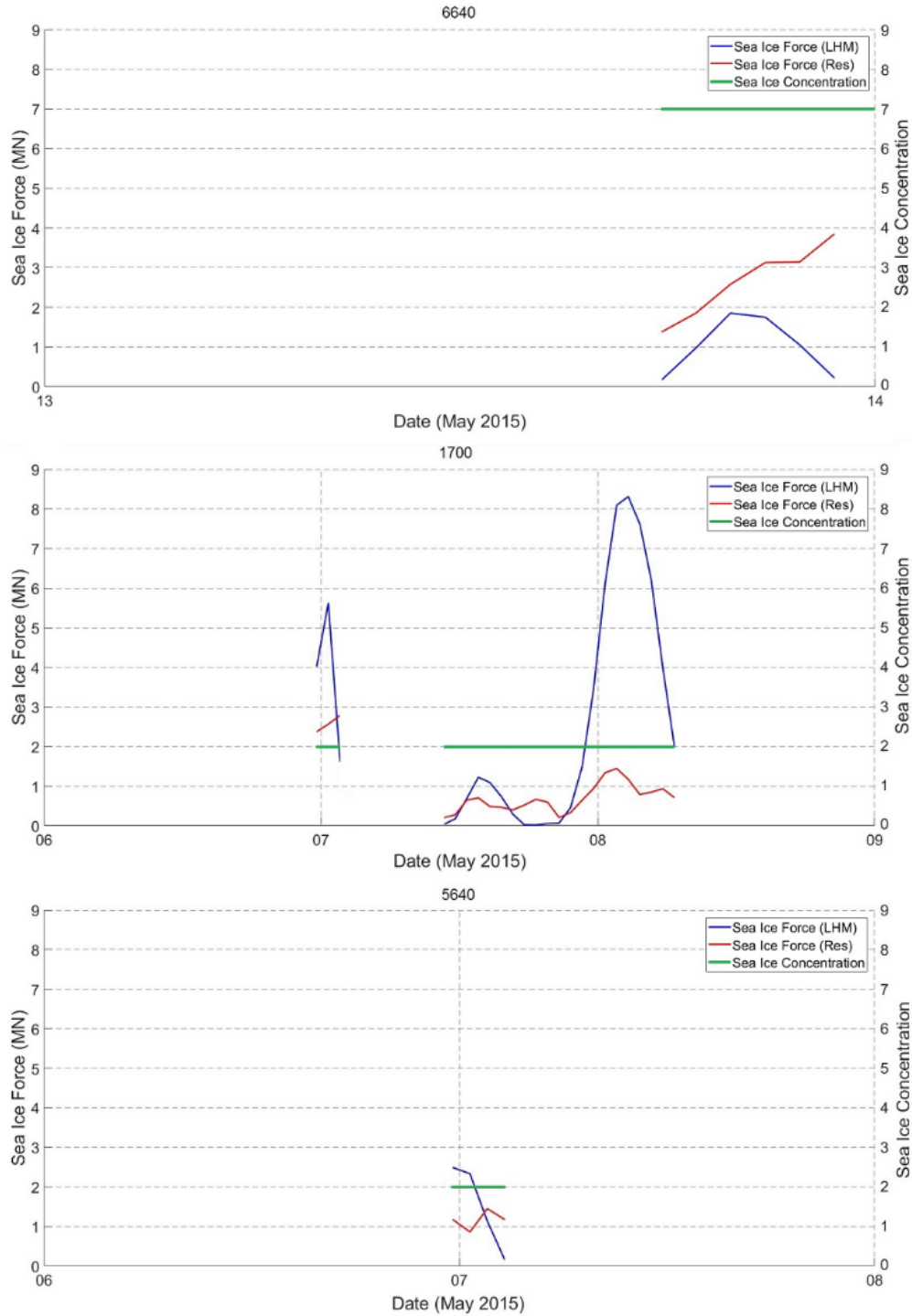
**Figure. 2.10.** Sea ice force magnitudes on the ice island fragments tracked by beacons 6640, 1700, and 5640, calculated using a residual approach (Turnbull et al., 2017) and Lichey and Hellmer's model (2001). The second y-axis (on the right) indicates the sea ice concentration out of ten (green lines) in the vicinity of the ice island fragments. The residual ice force magnitudes were only presented for the drifting periods when sea ice was present.

## 2.6.    Discussion

The fact that ocean currents generally contributed the most to the drift of the ice island fragments is in agreement with other studies (*e.g.*, Keghouche et al., 2009). This is expected given that a large portion of ice island fragments (their keel) is exposed to water currents at different depths. Also, given the significant difference in the density of air and ocean water, it is reasonable that the air drag played a minimal role in the overall drift of the four ice island fragments (Figure. 2.8). A comparison between the force magnitude due to the Coriolis effect (Figure. 2.7) and the drift speeds of the ice island fragments over the analyzed drift periods (Figure. 2.11) revealed that the Coriolis force was significant when the ice island fragments drifted at higher speeds. The significant influence of sea surface tilt force in Figure. 2.7 is most likely attributed to the mean dynamic ocean topography, given that atmospheric pressure gradient is only an important factor in sea surface height for large fragments (Turnbull, 2010), and that the tides are predominantly semidiurnal. While the overall force on the ice island fragments were influenced the most by ocean currents in open water, the ocean currents had a minor contribution in the presence of sea ice (Figure. 2.8). This indicates that sea ice most likely collected a proportion of wind and current momentum (Lichey and Hellmer, 2001) and, when present at high enough concentrations, played a more important role than currents in the drift of the ice island fragments.
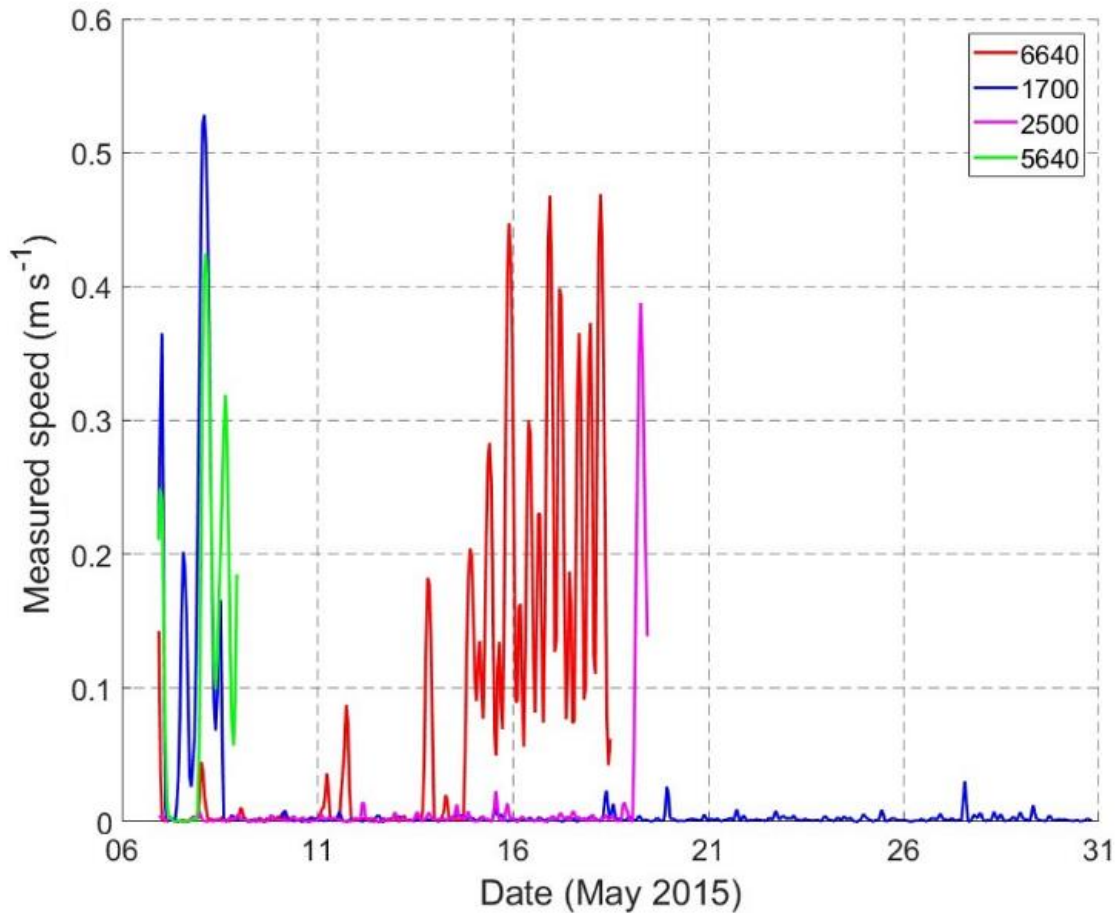
**Figure. 2.11.** Drift speeds of the four ice island fragments over the analyzed drift periods.

The sea ice force on the ice island fragments estimated from the residual approach (Eqn. (2.14))

differed in magnitude from the sea ice force magnitudes that were calculated by Lichey and

Hellmer's model (2001) as evident in Figure. 2.10. The disagreement between the sea ice force

magnitudes from the two models is most likely associated with the errors in the reanalysis data,

specifically the CMEMS ocean currents. This can be observed for fragment 6640 in Figure. 2.12

during the times that sea ice was not present in the vicinity of the ice island fragment. The residual

force during these time periods (Eqn. (2.15)) indicate the existing error in the model, which is most

likely associated with the error in CMEMS ocean currents. The sea ice force from Lichey and

Hellmer's (2001) model in medium sea ice concentrations (Eqn. (2.16)), which is the case for the

drift periods analyzed in this study, is independent of the ocean currents. The accuracy of the residual approach in this study, however, rests upon fairly accurate estimation of ocean currents, given that the other forces are relatively well-constrained. While the ocean surface currents can sometimes be reasonably-estimated from the wind conditions, the currents may vary significantly with depth. Turnbull et al. (2017) used drifter buoys to directly measure the surface currents in the vicinity of the tracked ice floes, but the ocean currents in this study were extracted from CMEMS current data, which generally overestimate the measured current speed and could be wrong by 180 degrees in azimuth (Brickman and Drozdowski, 2012). A small error in the ocean current estimate could make a large difference to the residual sea ice force (Eqn. (2.14)). Therefore, an accurate estimation of ocean currents at different depths is essential to reliably estimate the ocean current force (and consequently residual sea ice force). The different sea ice force records from the two models may also be explained by that fact that Lichey and Hellmer's (2001) model (Eqn. (2.16)) assumes that sea ice force is not dependent on sea ice concentration between concentrations of 15% and 90%. This is likely a limitation of Lichey and Hellmer's model as sea ice concentration is an important factor that influences the sea ice force.
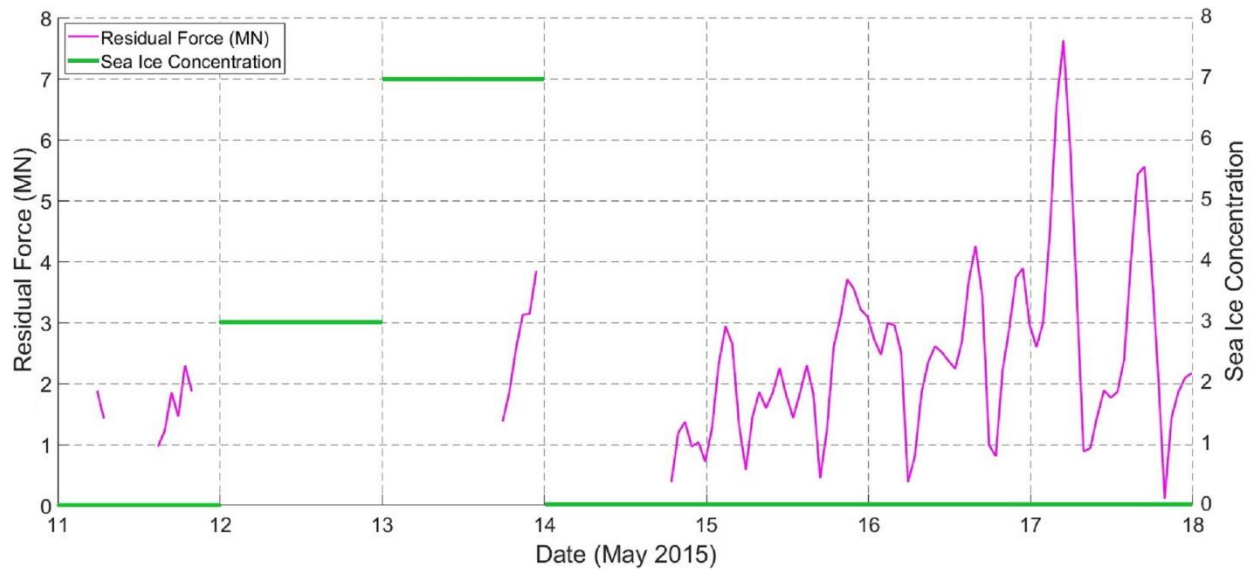
**Figure. 2.12.** Residual force magnitudes on the ice island fragment tracked by beacon 6640 over the analyzed drift periods in open pack ice and open water. The second y-axis (on the right) indicates the sea ice concentration out of ten (green lines) in the vicinity of the ice island fragment.

The residual approach to determine sea ice force on ice island drift (Eqn. (2.14)) is predicated on the assumption that the drift model accurately captures the behaviour of ice island drift when there is no sea ice present. The residuals during periods of open water (Eqn. (2.15)) and Figure. 2.12) indicate that this assumption was not met and therefore, it is likely that a component of the sea ice force reported here is due to the error in the input data. Results should, therefore, be interpreted with caution until the input data can be improved. The presented model did not account for other forces (*e.g.*, due to waves and atmospheric pressure gradient) in the drift equation (Eqn. (2.7)) due to their insignificant influence on the drift of the ice island fragments analyzed in this study. Rackow et al. (2017) stated that while the wave force is damped in high (over 40%) concentration of sea ice, it could generate a more significant force on large ice islands when the concentration of sea ice is less than 40%. In this study, the wave force was not calculated due the uncertainties in its formulation (Rackow et al., 2017), however, the model implicitly accounted for the effect of ocean surface waves by using a 40% higher value for the wind form drag coefficient, since waves

53

are most often in the same direction as wind (Smith, 1993; Keghouche et al., 2009). However, the modeled wind drag force (which also accounted for the effect of waves) had a minor contribution to the overall force on the fragments (Figure. 2.8), so wave force was probably not a significant factor. The force due to the atmospheric pressure gradient was also not likely a significant factor on the ice island fragments in this study as they were too small to cross surface isobars. This force, however, should be considered for significantly larger ice islands (Turnbull, 2010).

### 2.6.1. Sensitivity Analysis

While the sensitivity analysis of the sea ice force model (Eqn. (2.14)) was performed on all of the four ice island fragments, only one fragment (1700) is presented here as the results for the other three fragments were similar. The sensitivity analysis revealed that out of the four drag coefficients, the sea ice force magnitudes on the ice island fragments were most sensitive to the water form drag coefficient, followed by the air form drag coefficient. The force records from the residual approach (Turnbull et al., 2017) also revealed that the sea ice force magnitudes were almost insensitive to varying the skin drag coefficients for both air and water (Figure. 2.13-a,c). These results are expected given that the values of skin drag coefficients are significantly lower than form drag coefficients and that higher proportions of the fragments' walls were exposed to water than air. Therefore, one could expect that varying water drag coefficients would have a greater influence on the total force on the fragments and consequently on the sea ice force magnitudes estimated from the residual approach. The force magnitudes (Figure. 2.13) also revealed that while the sea ice force magnitudes increased as the water drag coefficients were increased, the sea ice force decreased with the air drag coefficients. This indicates that the direction of the water drag force mostly opposed the sea ice force directions. The drag force due to the wind, however, was mainly in the same direction as the sea ice force directions.
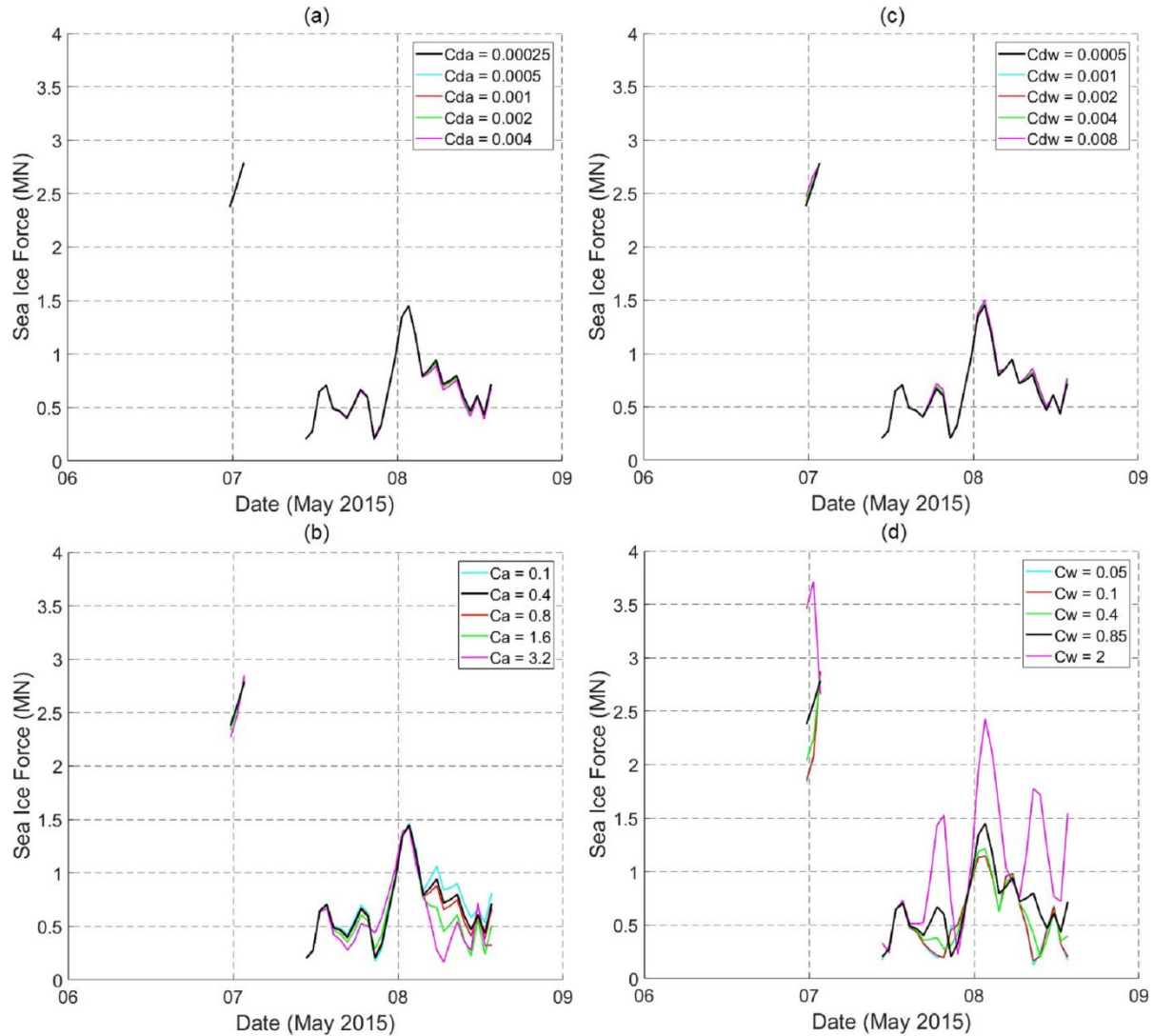
**Figure. 2.13.** The residual sea ice force magnitude on the ice island fragment tracked by beacon 1700, calculated using a residual approach (Turnbull et al., 2017) with varying skin ($c_{da}$ and $c_{dw}$) and form ($c_a$ and $c_w$) drag coefficient values for air (a,b) and water (c,d). Bold lines (in black) indicate the nominal values used in the study. The residual ice force magnitudes were only presented for the drifting periods when sea ice was present.

The sensitivity of the presented residual force model to the mass of the fragments and ocean currents was also studied to examine the importance of the uncertainty in these variables. Given the estimated range for the error in the surface area of the ice island fragments (14-22% as per Table 2.4), and assuming a larger error in the thickness of the fragments (around 25%) due to the fact that they were estimated from empirical/calibrated correlations with several input

parameters/variables (Eqns. (2.1)(2.4)), a propagated uncertainty of about 30% for the mass was estimated and included in the sensitivity analysis (Figure. 2.14). This identified mass of the fragments as an important variable that influences the residual force results. The analysis of the sea ice forces under the influence of varying ocean currents showed that the residual sea ice force results were the most sensitive to error in the ocean current direction (Figure. 2.15-b) and speed (Figure. 2.15-a), when compared to the results for varying drag coefficients (Figure. 2.13). This indicates the importance of an accurate estimation of the ocean current velocity for a reliable sea ice force model (Eqn. (2.14)). When the error in the direction of the extracted ocean currents is taken into account for fragment 1700, it is revealed that the residual sea ice force (red and cyan lines in Figure. 2.15-b) is well in agreement with the sea ice force from Lichey and Hellmer's model (2001) as presented in Figure. 2.10. The sensitivity analysis presented here supports the conclusion that the discrepancy between the sea ice forces from the two models is most likely linked to the error in the extracted ocean currents.
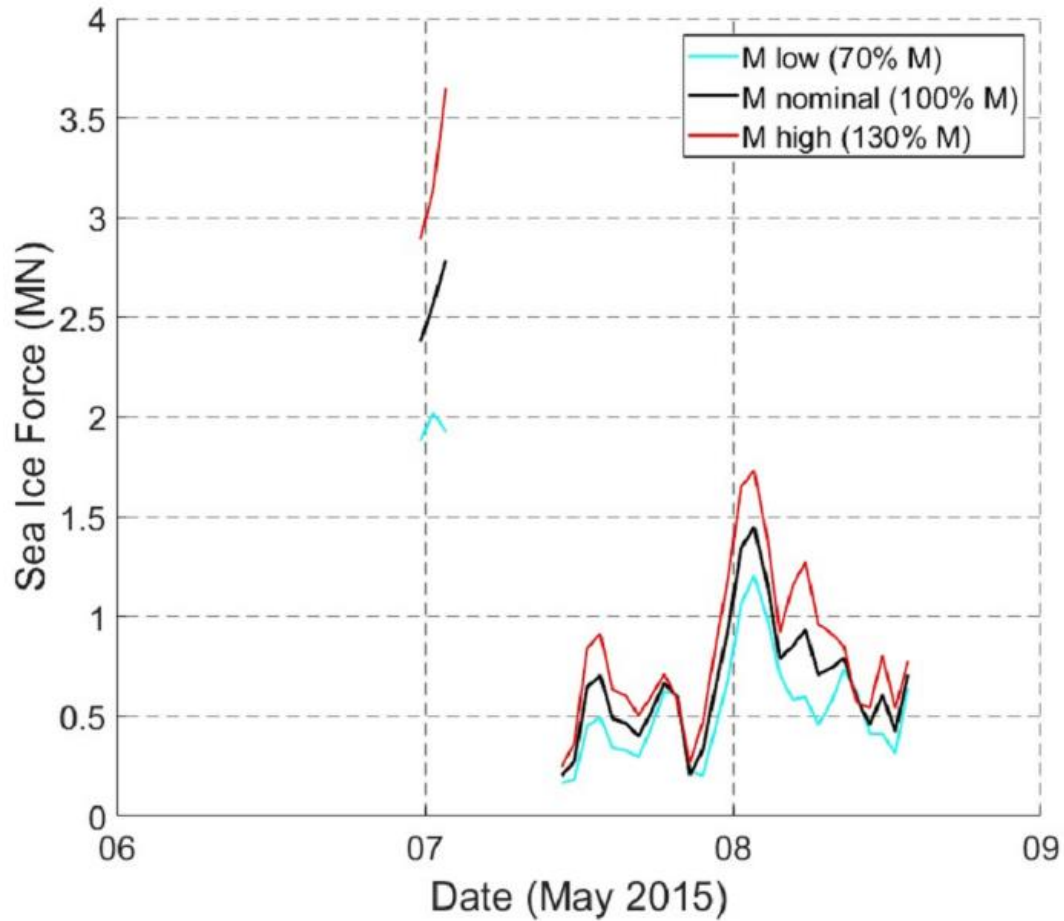
**Figure. 2.14.** The residual sea ice force magnitude on the ice island fragment tracked by beacon 1700, calculated using a residual approach (Turnbull et al., 2017) with varying fragment masses. Bold lines (in black) indicate the nominal values used in the study. The residual ice force magnitudes were only presented for the drifting periods when sea ice was present.
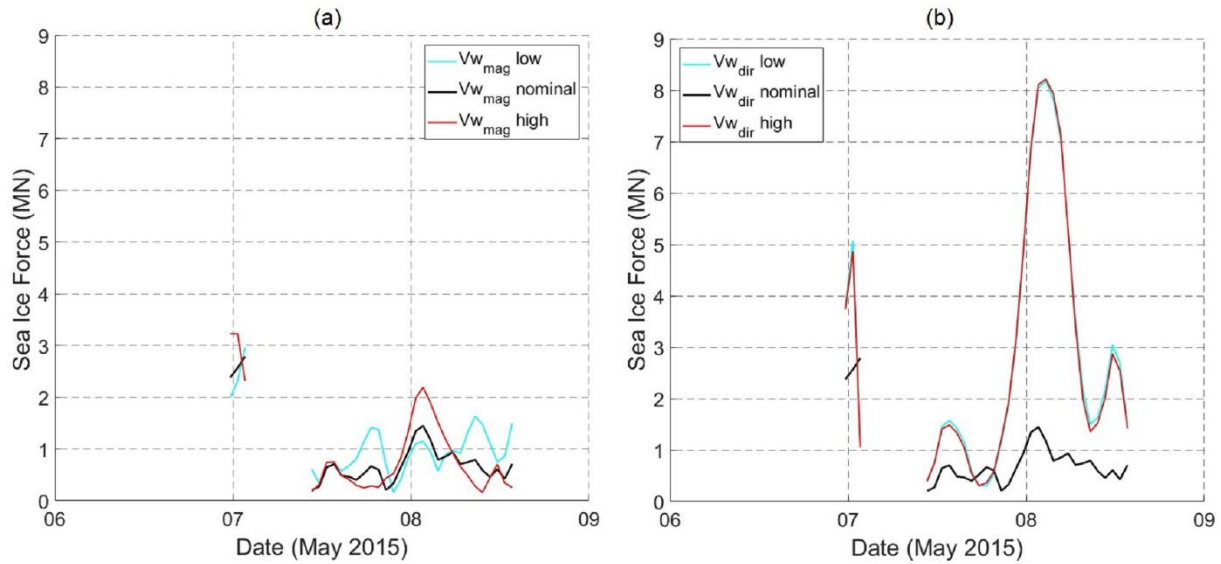
**Figure. 2.15.** The residual sea ice force magnitude on the ice island fragment tracked by beacon 1700, calculated using a residual approach (Turnbull et al., 2017) with varying ocean currents speed (a) and direction (b). Bold lines (in black) indicate the nominal values used in the study. The residual ice force magnitudes were only presented for the drifting periods when sea ice was present.

## 2.7.   Conclusions

This study presented an analysis of the relative influences of atmospheric and oceanic forces on the drift of four ice island fragments tracked offshore Newfoundland during spring/summer of 2015. The four fragments were assumed to drift under the influence of the forces due to wind, ocean currents, Coriolis deflection, sea surface tilt, and sea ice. The variations in the masses of the fragments over their drift periods were calculated from a combination of satellite imagery data, a surface ablation (TIM) model, and a basal ablation model to account for both of the horizontal deterioration and the thickness melt of the ice island fragments over time. Given that the tracking beacons provided accurate positional measurements, through which the drift average velocity and acceleration were calculated, the net force and the Coriolis force on the fragments were relatively well-constrained. The wind and sea surface altimetry data, which were obtained from reanalysis data and satellite measurements, respectively, allowed the forces due to wind and sea surface tilt

58

to be also well-constrained. The ocean current force, however, was not well-constrained due to the uncertainly in the CMEMS currents. The force caused by the surrounding sea ice was calculated as the difference between the net force (*i.e.*, the force that would be required to account for the observed drift) and the sum of force due to wind, ocean currents, Coriolis effect, and sea surface tilt. This was then compared against the sea ice force calculated from the model proposed by Lichey and Hellmer (2001). Constraining the forces due to wind, sea surface tilt, and Coriolis effect, coupled with the net force on the fragments, allowed the reliability of the sea ice force model from the residual approach to rest upon fairly accurate estimation of ocean currents over the periods the fragments were analyzed.

The analysis of the forces on the four fragments revealed that, except the times that sea ice was present at medium-high concentrations and the times that the fragments drifted at higher speeds, the forces due to the ocean currents and sea surface tilt controlled the drift velocity of the fragments, comprising, on average, up to 63% of the total force experienced by the drifting fragments. The sea ice forces estimated from the residual approach differed in magnitude from the ones estimated from Lichey and Hellmer's model (2001), mainly due to the uncertainty in CMEMS current velocities, as shown by the presented sensitivity analysis. The wind contributed the least to the total force experienced by the drifting ice island fragments (1-5% on average). The Coriolis force was only significant during the periods that the fragments drifted at high speed. The present study provides an important step forward in characterizing the drift of ice islands within the sea ice environment offshore Newfoundland under the influence of various driving forces. The results of this study can contribute to the calibration and improvement of the future regional operational ice dynamics models for the east coast of Canada.

## 2.8.    Acknowledgments

## 2.9.    References

Banke, E. G. and Smith, S. D. (1984). A hindcast study of iceberg drift on the Labrador coast, Bedford Institute of Oceanography. https://publications.gc.ca/collections/collection_2015/mpo-dfo/Fs97-18-49-eng.pdf.

Bigg, G. R., Wadley, M. R., Stevens, D. P., and Johnson, J. A. (1997). Modelling the dynamics and thermodynamics of icebergs, Cold Regions Science and Technology, 26(2), 113-135, https://doi.org/10.1016/S0165-232X(97)00012-8.

Braithwaite, R. J. and Olesen, O. B. (1993). Seasonal variation of ice ablation at the margin of the Greenland ice sheet and its sensitivity to climate change, Qamanârssûp sermia, West Greenland, Journal of Glaciology, 39(132), 267-274, https://doi.org/10.3189/S0022143000015938.

Brickman, D. and Drozdowski, A. (2012). Development and validation of a regional shelf model for Maritime Canada based on the NEMO-OPA circulation model, Fisheries and Oceans Canada, Maritimes Region.

Crawford, A., Crocker, G., Mueller, D., Desjardins, L., Saper, R., and Carrieres, T. (2018a). The Canadian Ice Island Drift, Deterioration and Detection (CI2D3) Database, Journal of Glaciology, 1-5. https://doi.org/10.1017/jog.2018.36.

Crawford, A. J. (2018). Ice island deterioration, Ph.D. Dissertation, Department of Geography and Environmental Studies, Carleton University, Ottawa, Canada, https://doi.org/10.22215/etd/2018-13178.

Crawford, A. J., Mueller, D., and Joyal, G. (2018b). Surveying drifting icebergs and ice islands: deterioration detection and mass estimation with aerial photogrammetry and laser scanning, Remote Sensing, 10(4), 575, https://doi.org/10.3390/rs10040575.

Crawford, A. J., Mueller, D. R., Humphreys, E. R., Carrieres, T., and Tran, H. (2015). Surface ablation model evaluation on a drifting ice island in the Canadian Arctic, Cold Regions Science and Technology, 110, 170–182. https://doi.org/10.1016/j.coldregions.2014.11.011.

Crepon, M., Houssais, M. N., and Guily, B. S. (1988). The drift of icebergs under wind action, Journal of Geophysical Research: Oceans, 93(C4), 3608-3612, https://doi.org/10.1029/JC093iC04p03608.

Crocker, G., Carrieres, T., and Tran, H. (2013). Ice island drift and deterioration forecasting in eastern Canada, In Proceedings of the 22nd International Conference on Port and Ocean Engineering Under Arctic Conditions, Espoo, Finland, 9-13 June 2013.

Eik, K. (2009). Iceberg drift modelling and validation of applied metocean hindcast data, Cold Regions Science and Technology, 57(2-3), 67-90, https://doi.org/10.1016/j.coldregions.2009.02.009.

El-Tahan, M., Venkatesh, S., and El-Tahan, H. (1987). Validation and quantitative assessment of the deterioration mechanisms of Arctic icebergs, Journal of Offshore Mechanics and Arctic Engineering, 109(1), 102-108, https://doi.org/10.1115/1.3256983.

El-Tahan, M. S., EI-Tahan, H. W., and Venkatesh, S. (1983). Forecast of iceberg ensemble drift, Offshore Technology Conference, https://doi.org/10.4043/4460-MS.

Enderlin, E. M. and Hamilton, G. S. (2014). Estimates of iceberg submarine melting from high-resolution digital elevation models: application to Sermilik Fjord, East Greenland, Journal of Glaciology, 60(224), 1084-1092, https://doi.org/10.3189/2014JoG14J085.

Fujino, K., Lewis, E. L., and Perkin, R. G. (1974). The freezing point of seawater at pressures up to 100 bars, Journal of Geophysical research, 79(12), 1792-1797, https://doi.org/10.1029/JC079i012p01792.

Halliday, E. J., King, T., Bobby, P., Copland, L., and Mueller, D. (2012). Petermann Ice Island 'A' survey results, offshore Labrador, OTC Arctic Technology Conference, Offshore Technology Conference, https://doi.org/10.4043/23714-MS.

Hibler III, W. D. (1979). A dynamic thermodynamic sea ice model, Journal of Physical Oceanography, 9(4), 815-846, https://doi.org/10.1175/1520-0485(1979)009%3C0815:ADTSIM%3E2.0.CO;2.

Hock, R. (2003). Temperature index melt modeling in mountain areas, Journal of Hydrology, 282, 104–115, https://doi.org/10.1016/S0022-1694(03)00257-9.

Hock, R. (2005). Glacier melt: a review of processes and their modelling, Progress in Physical Geography, 29(3), 362–391, https://doi.org/10.1191%2F0309133305pp453ra.

Jeffries, M. O. (2002). Ellesmere Island ice shelves and ice islands, Satellite Image Atlas of Glaciers of the World: Glaciers of North America - Glaciers of Canada, U.S. Geological Survey Professional Paper 1386-J-1, J147-J164.

Job, J. G. (1978). Numerical modelling of iceberg towing for water supplies—a case study, Journal of Glaciology, 20(84), 533-542, https://doi.org/10.3189/S002214300002092X.

Josberger, E. G. (1978). A laboratory and field study of iceberg deterioration, In Iceberg Utilization, 245-264, https://doi.org/10.1016/B978-0-08-022916-4.50027-3.

Keghouche, I., Bertino. L., and Lisæter, K. A. (2009). Parameterization of an iceberg drift model in the Barents Sea, Journal of Atmospheric and Oceanic Technology, 26(10), 2216-2227, https://doi.org/10.1175/2009JTECHO678.1.

Kubat, I., Sayed, M., Savage, S. B., and Carrieres, T. (2005). An Operational Model of Iceberg Drift, International Journal of Offshore and Polar Engineering, 15(2), 125-131.

Kubat, I., Sayed, M., Savage, S. B., Carrieres, T., and Crocker, G. (2007). An operational iceberg deterioration model, In Proceedings of the 17th International Offshore and Polar Engineering Conference, Lisbon, Portugal, 1-6 July 2007, 652-657.

Lellouche, J. M., Greiner, E., Galloudec, O. L., Garric, G., Regnier, C., Drevillon, M., Benkiran, M., Testut, C. E., Bourdalle-Badie, R., Gasparin, F., and Hernandez, O. (2018). Recent updates to the Copernicus Marine Service global ocean monitoring and forecasting real-time 1/12° high-resolution system, Ocean Science, 14(5), 1093-1126, https://doi.org/10.5194/os-14-1093-2018.

Lichey, C. and Hellmer, H. H. (2001). Modeling giant-iceberg drift under the influence of sea ice in the Weddell Sea, Antarctica, Journal of Glaciology, 47(158), 452-460, https://doi.org/10.3189/172756501781832133.

Løset, S. (1993). Numerical modelling of the temperature distribution in tabular icebergs, Cold Regions Science and Technology, 21(2), 103-115.

Mountain, D. G. (1980). On predicting iceberg drift, Cold Regions Science and Technology, 1, 273-282, https://doi.org/10.1016/0165-232X(80)90055-5.

Mueller, D. R., Crawford, A., Copland, L., and Van Wychen, W. (2013). Ice island and iceberg fluxes from Canadian High Arctic sources, Report to the Northern Transportation Assessment Initiative, Innovation Policy Branch, Transport Canada, Ottawa, Canada. https://www.researchgate.net/publication/340183882_Ice_Island_and_Iceberg_Fluxes_from_Canadian_High_Arctic_Sources_Prepared_for_the_Innovation_Policy_Group_of_Transport_Canada.

Murphy, D. L. and Anderson, L. T. (1986). An Evaluation of the International Ice Patrol Drift Model, in Proceedings of Canadian East Coast Workshop on Sea Ice, Canadian Technical Report of Hydrography and Ocean Sciences, 73, 387-409.

Murphy, D. L. and Carrieres, T. (2010). CIS-IIP iceberg model inter-comparison, Report prepared for the North American Ice Service, pp. 27. ftp://sidads.colorado.edu/pub/projects/noaa/iicwg/business/NAIS_Iceberg_Model_Report_V3_08062010_Final.pdf.

Peterson, I. K., Prinsenberg, S. J., Pittman, M., and Desjardins, L. (2009). The Drift of an Exceptionally-Large Ice Island from the Petermann Glacier in 2008, In Proceedings of the 20th International Conference on Port and Ocean Engineering under Arctic Conditions, Luleå, Sweden, 9-12 June 2009.

Rackow, T., Wesche, C., Timmermann, R., Hellmer, H. H., Juricke, S., and Jung, T. (2017). A simulation of small to giant Antarctic iceberg evolution: Differential impact on climatology estimates, Journal of Geophysical Research: Oceans, 122(4), 3170-3190, https://doi.org/10.1002/2016JC012513.

Savage, S. B. (2001). Aspects of iceberg deterioration and drift, In Geomorphological Fluid Mechanics, N. J. Balmforth & A. Provenzale (Eds.), Lecture Notes in Physics Series, Springer-Verlag, Berlin, 582, 279-318, https://doi.org/10.1007/3-540-45670-8_12.

Scambos, T., Sergienko, O., Sargent, A., MacAyeal, D., and Fastook, J. (2005). ICESat profiles of tabular iceberg margins and iceberg breakup at low latitudes, Geophysical Research Letters, 32(23), https://doi.org/10.1029/2005GL023802.

Smith, S. and Donaldson, N. (1987). Innovations in Dynamic Modelling of Iceberg Drift, In OCEANS'87 IEEE, Halifax, NS, Canada, 28 September - 1 October 1987, 5-10, https://doi.org/10.1109/OCEANS.1987.1160880.

Smith, S. D. (1993). Hindcasting iceberg drift using current profiles and winds, Cold Regions Science and Technology, 22(1), 33-45, https://doi.org/10.1016/0165-232X(93)90044-9.

Smith, S. D. and Banke, E. G. (1983). The influence of winds, currents and towing forces on the drift of icebergs, Cold Regions Science and Technology, 6(3), 241-255, https://doi.org/10.1016/0165-232X(83)90045-9.

Turnbull, I. D. (2010). Drift of large tabular icebergs in response to atmospheric surface pressure gradients, an observational study, Antarctic Science, 22(2), 199-208, https://doi.org/10.1017/S0954102010000027.

Turnbull, I. D., Torbati, R. Z., and Taylor, R. S. (2017). Relative influences of the meteorological and oceanic forcings on the drifting ice pack and estimation of internal ice stress gradients in the Labrador Sea, Journal of Geophysical Research: Oceans, 122(7), 5970-5997, https://doi.org/10.1002/2017JC012805.

White, F. M., Spaulding, M. L., and Gominho, L. (1980). Theoretical Estimates of the Various Mechanisms involved in Iceberg Deterioration in the Open Ocean Environment, U.S. Coast Guard Research and Development Center Report, pp. 126.

# 3. THE CALVING EVENTS OF PETERMANN GLACIER FROM 2008 TO 2012: ICE ISLAND DRIFT CHARACTERISTICS, ASSESSMENT OF FRACTURE EVENTS, AND GEOGRAPHICAL DATA ANALYSIS

## 3.1. Preface

This chapter aims to provide an overview of the drift and deterioration characteristics of Petermann ice islands captured in the Canadian Ice Island Drift, Deterioration and Detection (CI2D3) database. The chapter introduces the CI2D3 database and presents a preliminary analysis of Petermann ice islands' drift and deterioration, which serves as a preliminary study for the probabilistic fracture and drift models presented in chapters 4 and 5.

This chapter has been presented and published as an original conference paper at the 38th International Conference on Ocean, Offshore and Arctic Engineering (OMAE) in Glasgow, Scotland, UK. As the main author of this paper, I conducted the literature review, performed the preliminary analysis of the ice island drift and deterioration using the CI2D3 database, and prepared the manuscript. My co-authors, Dr. Ian Turnbull, Dr. Rocky Taylor, and Dr. Derek Mueller provided consistent support at different stages of the analysis and preparation of the paper. I revised the manuscript based on the co-authors' suggestions and the comments from OMAE's editors.

## 3.2. Abstract

The eastern Canadian Arctic is an ice-prone environment that is a vital part of Canadian Arctic shipping lanes. A better understanding of the ice environment and ice characteristics in this region is essential for supporting safe and economical marine activities. This study presents a first analysis

of the drift of ice islands that originated from the Petermann Glacier calving events in northwest Greenland between 2008 and 2012. These massive calving events generated numerous smaller ice islands and icebergs through subsequent deterioration and break-up events. Surviving ice features drifted further southward into the Baffin Bay and reached as far as offshore Newfoundland (~47 °N) for the case of the 2010 calving event. The drift characteristics of Petermann ice islands are evaluated through the analysis of the recently developed Canadian Ice Island Drift, Deterioration and Detection (CI2D3) database. The average drift distance, speed, and directions of the ice islands that resulted from the 2008, 2010, and 2012 calving events were estimated using successive observations of the monitored ice islands in the CI2D3 database. This study also includes an assessment of fracture events, including the total number of ice island break-up events following each massive calving event and the average number of daughter ice islands resulting from each break-up event. A geographical analysis of the data was also performed to present the location of the fracture events, as well as the time series of latitude change of Petermann ice islands from their origin (northwest Greenland ice tongues) to where until they became too small (<0.25 km$^2$) to be delineated in the CI2D3 database. This information is of particular interest to marine activities in the eastern Canadian Arctic, and oil and gas operations offshore Newfoundland and Labrador.

Keywords: Petermann ice islands, drift characteristics, fracture events, geographical data analysis.

## 3.3. Introduction

For shipping and offshore activities in ice-prone environments such as the eastern Canadian Arctic and offshore Newfoundland and Labrador, glacial ice features are a hazard that must be considered in design and operations. Recently collected seismic data have increased interest in exploration in new, ice-prone frontier oil and gas basins, in addition to current operations on the Grand Banks,

*e.g.*, Hibernia, Terra Nova, White Rose, and Hebron). These new basins hold significant potential for future exploration activities (Figure 3.1). Safe and cost-effective operations require analysis of historical glacial ice characteristics to improve understanding of the ice environment in these regions. Specifically, the intermittent occurrence of ice islands (large tabular icebergs) in more northern regions such as coastal Labrador and the resulting fragments further south such as offshore Newfoundland (Newell, 1993) may present risks to ships and offshore structures that must be considered in design and operations (Mueller et al., 2008; Mueller et al., 2013). To mitigate these risks, it is important to devise appropriate strategies, the reliability of which requires information about the drift and deterioration characteristics of these ice features. Due to the cost and logistical difficulties of collecting data over this vast, remote and harsh marine environment, there are limited field observations and in-situ data to contribute to a better understanding of the drift and deterioration characteristics of ice islands. A database of ice islands originally calved from Petermann Glacier (2008, 2010, 2011, 2012), as well as Ryder, Steensby, C.H. Ostenfeld, and other North Greenland ice tongues was generated from satellite imagery (Crawford et al., 2018b). This study provides an analysis of the drift characteristics (*e.g.*, distance, speed, and direction) and break-up events, as well as the geographical analysis of the fracture events for the ice islands that originated from the massive calving events of the Petermann Glacier (Figure 3.2) in the northwest of Greenland from 2008 to 2012. Given that only a small number of ice islands broke off Petermann Glacier in 2011 (4.3 km$^2$ in total), as well as the ice tongues in Ryder, Steensby, C.H. Ostenfeld, and north Greenland fiords, this study only used the data associated with the calving events in 2008, 2010, and 2012, which correspond to the total loss of about 36 km$^2$, 302 km$^2$, and 145 km$^2$ from Petermann Glacier, respectively (Crawford et al., 2018b). The 2010 calving event

of the Petermann Glacier generated the largest Arctic ice island in the past 50 years (U.S. Geological Survey, 2019) and removed about 25% of the glacier tongue (Nick et al., 2012).
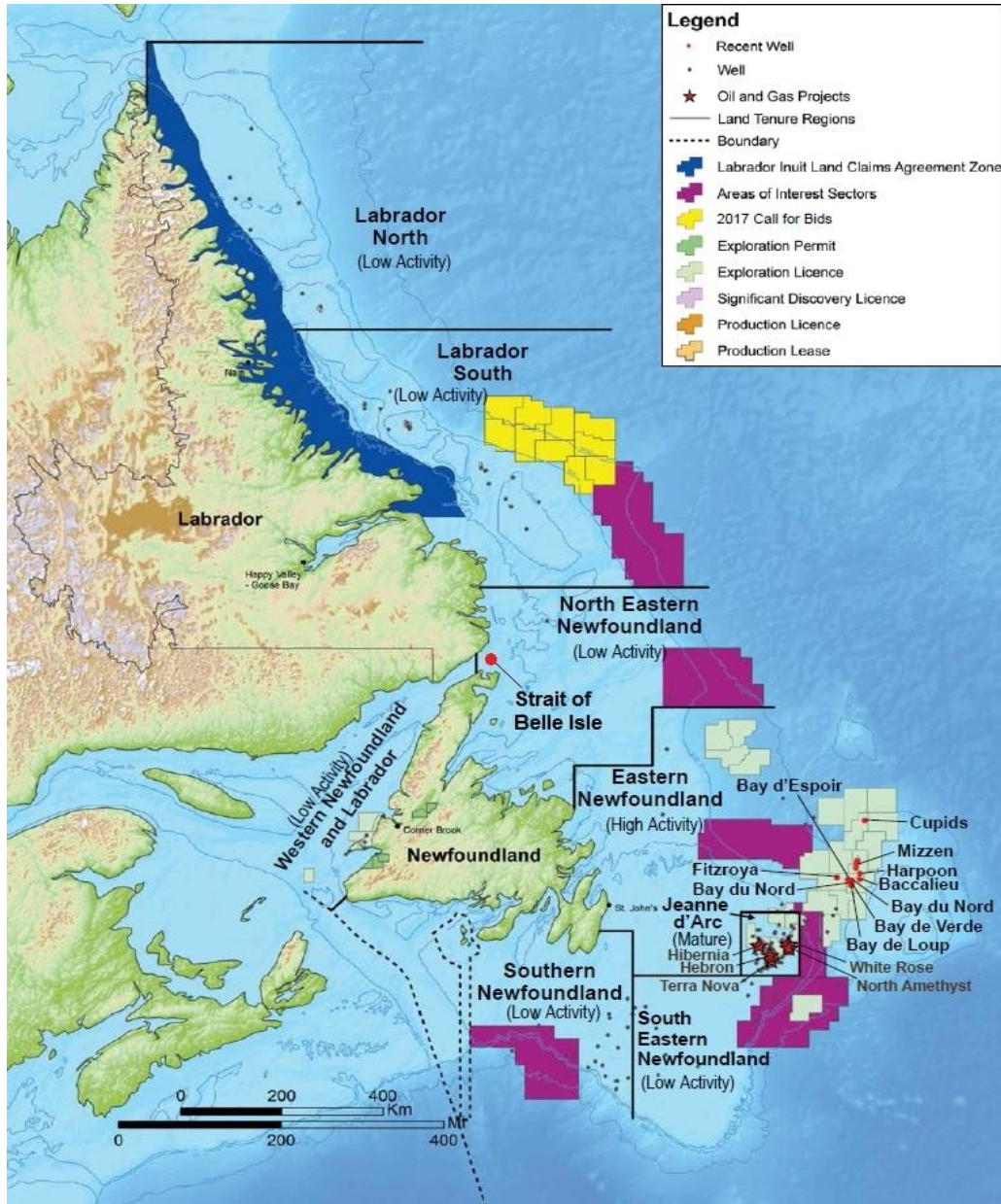


**Figure 3.1.** The oil and gas exploration activities offshore Newfoundland and Labrador (The Economy, 2017).
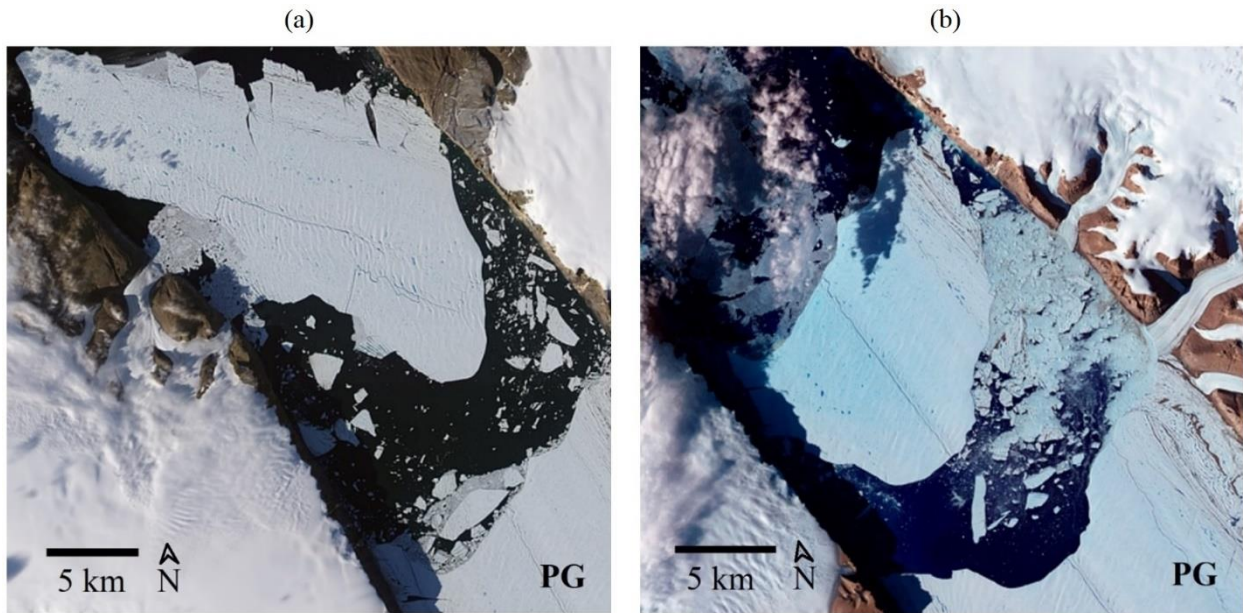
**Figure 3.2.** The 2010 (a) and 2012 (b) Petermann Glacier (PG) calving events in the northwest of Greenland (NASA Earth Observatory, 2019a; NASA Earth Observatory, 2019b).

The drift and deterioration of Petermann ice islands have been studied through remote sensing observations using the satellite imagery (*e.g.*, Halliday et al., 2012; Peterson et al., 2009) due to the challenges in conducting field measurements in ice-prone waters. Given the large dimensions and angular shape of ice islands, they can reliably be identified in pack ice or open water via satellite observations. While some satellite systems have limitation in terms of spatial resolution, there are satellite systems such as MODIS and Envisat that can be used to study the drift characteristics and areal deterioration of large ice islands using successive image acquisitions (Peterson et al., 2009; Scambos et al., 2005). Unlike some satellite systems that have limited ability to capture images in low daylight and high cloud cover, spaceborne synthetic aperture radars (SAR) are capable of providing observations of ice islands even during poor visibility conditions (Jeffries, 2002). The Canadian Ice Island Drift, Deterioration, and Detection (CI2D3) database was developed using satellite imagery in collaboration between the Water and Ice Research Lab (WIRL) at Carleton University and the Canadian Ice Service (CIS) to digitize ice islands arising

71

from the main calving events of ice tongues in northwestern Greenland. The technicians at WIRL used thousands of satellite images from the CIS archive (mainly level 1b RADARSAT 1 and 2 SAR data) and manually generated thousands of polygons of the perimeters of each ice island found between 2008 and 2013 that was larger than 0.25 km$^2$ (Crawford et al., 2018b).

Some aspects of the ice islands in CI2D3 database such as the evolution of size distributions and meltwater dispersal of Petermann ice islands were studied by Crawford et al. (2018a). The authors (Crawford et al., 2018a) stated that while the population of the monitored ice islands was dominated by the small ice islands, a large proportion of total mass and melt water dispersal was associated with large ice islands, a result which was consistent with other studies (Rackow et al., 2017; Stern et al., 2016; Tournadre et al., 2016). For the cases of the 2010 and 2012 calving events, Crawford et al. (2018a) noted that at the end of the monitoring period (December 31$^{st}$, 2013), a total of 2% and 70% of the original ice islands' surface areas remained in the region, respectively, which were not accounted for in CI2D3 database. Crawford et al. (2018a) concluded that fracture played an important role in the deterioration of the Petermann ice islands as their size distributions were well represented by power law models, which was in agreement with the results of size-frequency from other studies (Stern et al., 2016; Tournadre et al., 2016; Enderlin et al., 2016). An analysis of the variation in the mass of the ice islands in CI2D3 database revealed that while the fracture process resulted in higher meltwater dispersal through the increase of the surface area-to-volume ratio, the meltwater flux was not significant enough to adversely impact the Atlantic meridional overturning circulation (Crawford et al, 2018a).

This study aims to build on the work by Crawford et al. (2018a) by characterizing the drift and deterioration behavior of ice islands resulting from 2008, 2010, and 2012 Petermann Glacier calving events. Here it should be noted that we consider the beginning of an ice island to be right

72

after it calved from another ice island (or glacier) and the end of it to be when it calves into two or more fragments. By this definition, the CI2D3 Database contains about 900 ice islands in total; 32, 706, and 176 calved from Petermann Glacier in 2008, 2010, and 2012, respectively. These ice islands were re-observed as they drifted over time, which corresponds to 332, 9,658, and 7,263 ice island observations related to the 2008, 2010, and 2012 calving events, respectively (Crawford et al, 2018a).

## 3.4. Study Site

Calving of Petermann Glacier occurred in 2008, 2010, 2011, 2012, 2013, and 2017 (Crawford et al, 2018a). This study uses data (Desjardins et al., 2018) of three monitored calving events of the Petermann Glacier (2008, 2010, and 2012) in northwest Greenland, a location that in combination with other western parts of Greenland are known as the origin for about 85% of the glacial ice features in the Grand Banks (Ebbesmeyer et al., 1980). These massive calving events generated numerous smaller ice islands and icebergs throughout their deterioration which drifted south into Nares Strait, Baffin Bay and the Labrador Sea, with some ice islands reaching to the coast of Newfoundland that resulted from the 2010 calving event (Crawford et al, 2018b).

## 3.5. Satellite Imagery Data Collection

The satellite imagery data collection for the development of the CI2D3 database was completed by a team of researchers at WIRL (Crawford et al, 2018b). Thousands of archived 100-m resolution, Level 1b RADARSAT-1 and -2 SAR images from July 13th, 2008 to December 31st, 2013 were integrated into GIS software to track ice islands by digitizing their perimeter at a scale of 1:250,000 (Crawford et al, 2018b). A temporal resolution of 14 days between the observations was a minimum requirement; however, much better temporal resolutions were often possible based

on image availability (Crawford et al, 2018b). In order to distinguish the ice islands from open water, WIRL technicians first identified the archived SAR images in the region between northwest Greenland to Newfoundland, and then converted them to be used in ArcGIS (Crawford et al, 2018b). While the polygons relating to the first observation of ice islands were digitized from scratch (with 8.4% error), the subsequent ice island polygons were manually digitized using a copy of the original polygon, which was overlain on the following observation and adjusted with respect to orientation and size (with 6.2% error) (Crawford et al, 2018a). The manual digitization of the polygons allowed for establishing a linkage of the ice islands and their descendants using unique identifiers. A sample map of the generated polygons for some of the 2010 Petermann ice islands is presented in Figure 3.3.

Table 3.1 presents some information about the ice islands which originated from the massive calving events of Petermann Glacier in 2008, 2010, and 2012 (Crawford et al, 2018b).
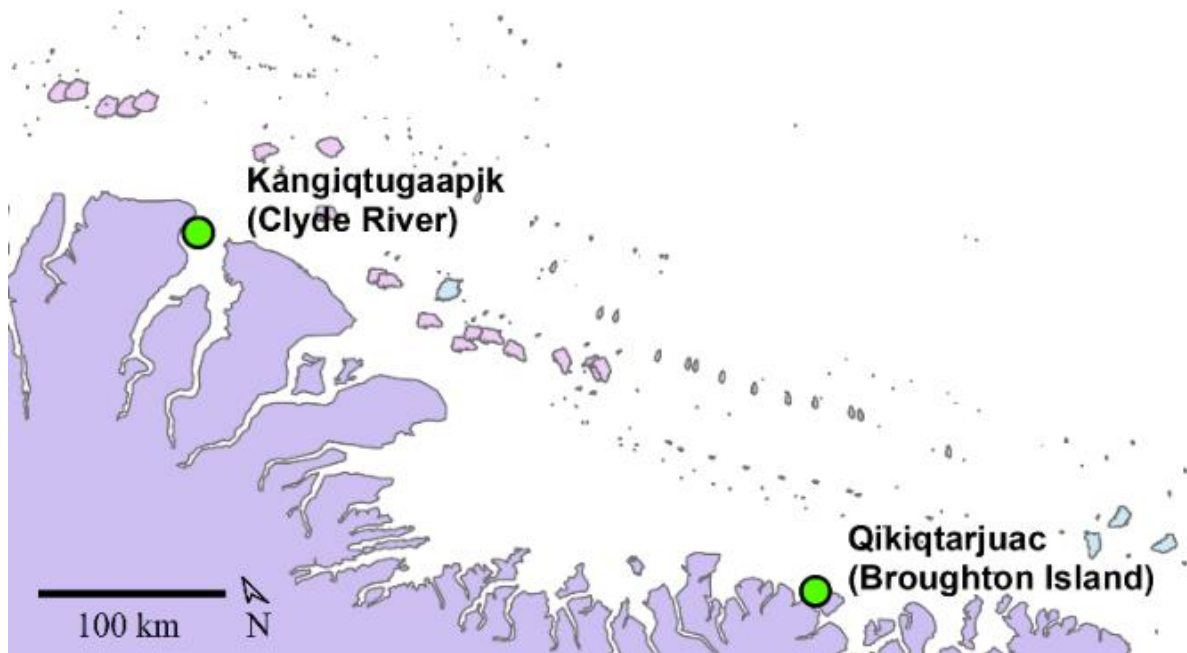
**Figure 3.3.** A sample map of the generated polygons for the 2010 Petermann Glacier calving event, associated with the satellite images from February to April 2011 (Desjardins et al., 2018).

**Table 3.1.** Description of the 2008, 2010, and 2012 Petermann Glacier calving events in the Canadian Ice Island Drift, Deterioration, and Detection database (Crawford et al, 2018b).

| Glacier calving year | Main calving date | Surface area (km²) | Number of digitized polygons |
|---|---|---|---|
| **2008** | July 10th | 36.4 | 332 |
| **2010** | August 5th | 302.4 | 9658 |
| **2012** | July 17th | 144.6 | 7263 |

## 3.6. Drift and Deterioration Analysis

The data structure in the CI2D3 database contains thousands of satellite imagery observations of ice islands from various glaciers. The positional data (latitude, longitude, and scene time) for the 2008, 2010, and 2012 Petermann ice islands were sorted and extracted using MATLAB to allow for the calculation of drift characteristics (distance, speed, and direction) between the observed

75

positions. The deterioration of the Petermann ice islands (areal surface reduction and fracture events) were analyzed using the variation of the surface area values from the successive satellite images associated with each ice island. A geographical analysis of positional data was also performed to identify the locations where the greatest number of calving events occurred.

The Petermann ice islands associated with the 2008, 2010, and 2012 calving events typically drifted in a southward direction through Nares Strait and Baffin Bay. Following the 2010 calving event, some ice islands (as large as 1.3 $km^2$) reached as far as offshore Newfoundland (Figure 3.4). This demonstrates that ice islands can drift for a long period of time (>3 years), which is reasonable given their exceptionally large extents. Ice islands from the 2012 event were not monitored past 2013 and had not reached these southern latitudes.

The change in the latitude of the 2008, 2010 and 2012 Petermann ice islands over time and their drift characteristics in different size categories are presented in Figure 3.5 and Table 3.2, respectively. The average total drift distances of all ice islands originated from the 2008, 2010, and 2012 calving events were 260, 277, and 334 km with a mean net distance of 163, 201, and 196 km towards the mean azimuthal directions of 123, 113, and 120°, respectively. These ice islands drifted southwards an average of 0.46, 1.25, and 1.04° of latitude/month (equivalent to 51, 139, and 115 km/month), some drifting at an extreme southward rate of 2.84° of latitude/week (~45 km/day). The observations showed that large ice islands (>10 $km^2$) drifted longer before experiencing any break-up events. Examples of this is the parent of 2008 Petermann ice islands (2.7×11.2 km) which drifted over 10 months before splitting into two daughter ice islands, and a descendant of the 2010 Petermann Glacier calving event (3.7×8.9 km) that had not fractured for about three years before

76

breaking up into 12 smaller ice islands.
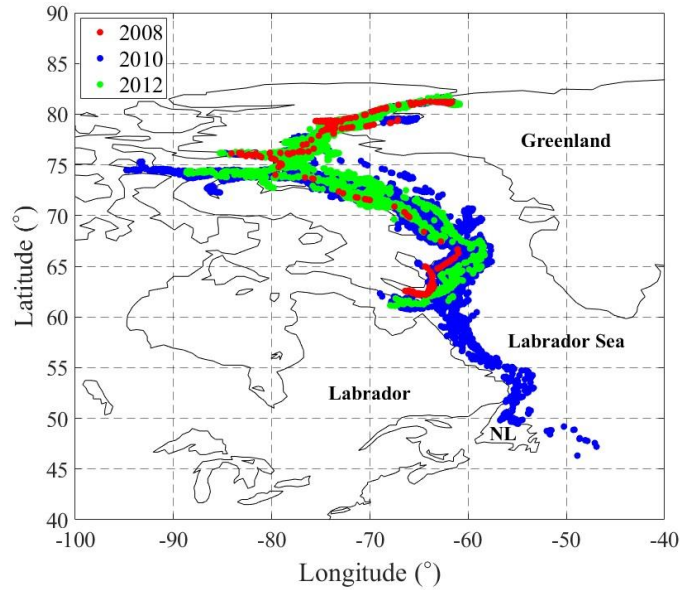


**Figure 3.4.** The drift trajectories of ice islands originated from the massive calving events of the Petermann Glacier in 2008 (red), 2010 (blue), and 2012 (green).
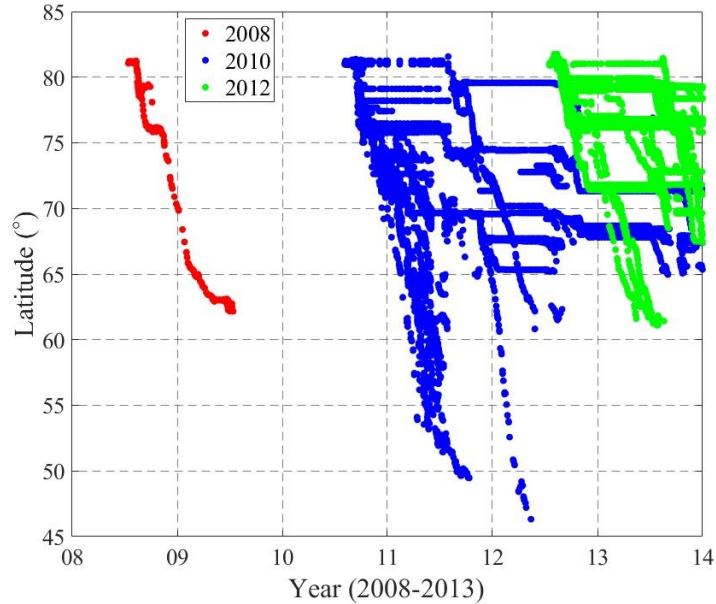


**Figure 3.5.** The latitude over time of the monitored Petermann ice islands in the CI2D3 database originating from the 2008 (red), 2010 (blue), and 2012 (green) calving events.

**Table 3.2.** The drift characteristics of the 2008, 2010, and 2012 Petermann ice islands for different size categories.

| Glacier calving year | Ice island size (km²) | Mean total/net drift distance (km) | Mean drift speed (m/s) | *Mean drift direction (°) |
|---|---|---|---|---|
| | <2 | 84/55 | 0.11 | 127 |
| 2008 | 2-10 | 238/169 | 0.06 | 97 |
| | >10 | 3313/1992 | 0.18 | 123 |
| | <2 | 243/185 | 0.10 | 113 |
| 2010 | 2-10 | 362/266 | 0.12 | 111 |
| | >10 | 1420/704 | 0.08 | 120 |
| | <2 | 327/195 | 0.09 | 116 |
| 2012 | 2-10 | 297/154 | 0.08 | 130 |
| | >10 | 516/312 | 0.09 | 147 |

* Mean directions are expressed as azimuth angle.

The Petermann ice islands lost a significant proportion of their total extent due to lateral deterioration (e.g., sidewall melting, edge wasting, etc.) over the course of their drift. This corresponds to an average of 26, 23, and 13% of their original size per week for the 2008, 2010, and 2012 calving events, respectively, with some ice islands deteriorating at a maximum rate of 57% of their original areal dimensions per day. The lower average melting rate of all ice islands originated from the 2012 calving event is expected given that by the end of the monitoring period (December 2013), a large number ice islands in the small size category (constituting about 70% of the original ice island's surface area) remained in the region (Crawford et al, 2018a), which were not accounted for in this analysis. Table 3.3 reveals that size is an important factor in characterizing the deterioration mechanism of an ice islands. Small ice islands (<2 km$^2$) originated from the 2008, 2010, and 2012 calving events deteriorated significantly through sidewalls (likely via melting due to the higher surface area-to-volume ratio) at a mean rate of 35.3, 23.8, and 16.3% of their initial dimensions (Table 3.3), respectively. Larger ice islands, however, experienced a lower rate of

sidewall deterioration and instead deteriorated through fracturing, which is in agreement with the results of other studies (*e.g.*, Tournadre et al., 2012).

In total, eight, 85, and 64 fracture events occurred over the monitored period of the main Petermann ice islands originating from the 2008, 2010, and 2012 calving events. Large ice islands ($>10 \text{ km}^2$) split into more pieces per fracture event than smaller ice islands (Table 3.3). An example of this is the main Petermann ice island of the 2012 calving event ($\sim$137 km$^2$) which broke up into 17 distinct pieces shortly after its calving from northwest Greenland. Around 69% of all fracture events generated only two daughter ice islands. This corresponds to 74% for the fracture events of the ice islands in small and medium size categories ($<10 \text{ km}^2$) and only 30% for the large size group. The geographical analysis of the 2008 ice islands' fracture events (Figure 3.6) indicated that around 38% of the total number of calving events occurred in the High Arctic ($\sim$80° latitude), while the rest happened around the Labrador Sea entrance ($\sim$62° latitude). It should be noted here that the 2008 calving event generated a small number of ice islands, which explains the low number of fracture events. A substantially higher number of ice islands originated from the 2010 and 2012 calving events, which provided a more robust and consistent analysis of the fracture events of Petermann ice islands (Table 3.3). Similar to the 2008 fracture events, the ice islands originating from the 2010 main calving event of the Petermann Glacier experienced the highest number of fracture events in mainly two locations; offshore Newfoundland ($\sim$50°N, 55°W) and offshore Baffin Island (65<latitude<70°N). This is most likely associated with the fact that a large piece resulting from the 2010 calving event was grounded around Baffin Island for about 1.5 years (Crawford et al., 2016). Unlike the ice islands originating from the 2008 and 2010 calving events, the 2012 Petermann ice island fractured in various locations by the time its descendants reached the Labrador Sea (Figure 3.6). The highest number of fracture events happened in the higher Arctic

around the northwest entrance to Baffin Bay (~75°N, 78°W).

**Table 3.3.** The deterioration characteristics of the 2008, 2010, and 2012 Petermann ice islands for different size categories.

| Glacier Calving year | Ice island size (km$^2$) | Mean areal surface reduction (%/week) | Mean number of calved ice islands |
|---|---|---|---|
| 2008 | <2 | 35.3 | 3 |
| | 2-10 | 6.4 | 5 |
| | >10 | 1.4 | 4 |
| 2010 | <2 | 23.8 | 3 |
| | 2-10 | 19.1 | 3 |
| | >10 | 3.7 | 8 |
| 2012 | <2 | 16.3 | 2 |
| | 2-10 | 1.1 | 2 |
| | >10 | 0.8 | 8 |
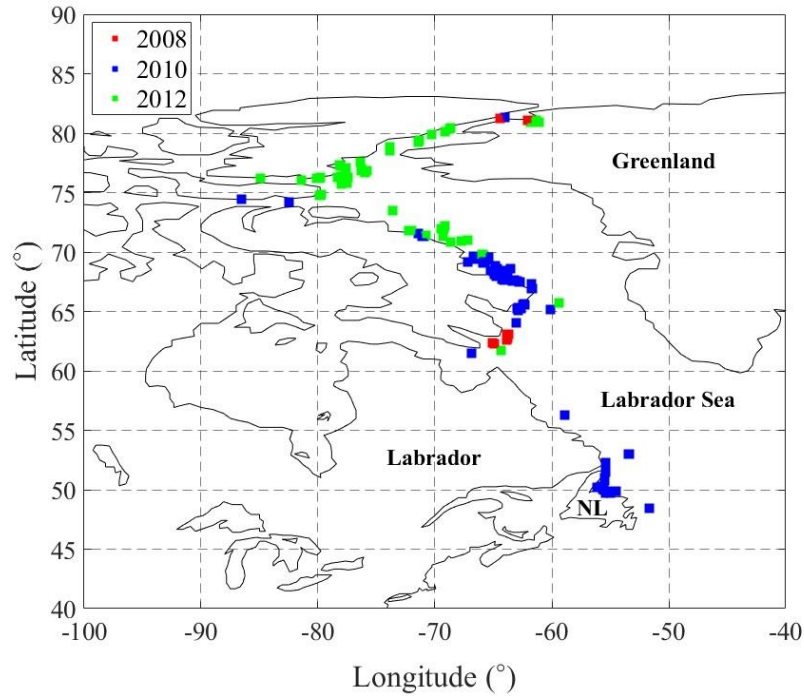
**Figure 3.6.** The location of fracture events for the ice islands originating from the Petermann Glacier calving events in the northwest Greenland in 2008 (red), 2010 (blue), and 2012 (green).

## 3.7.    Importance of the Drift and Deterioration Analysis

The presented descriptive analysis for the drift and deterioration of the Patermann ice islands is of importance to shipping activities in the eastern Canadian Arctic, and the oil and gas operations offshore Newfoundland and Labrador. Given the large dimensions of ice islands, the fracture events could generate numerous smaller ice islands (or icebergs), the presence of which in the Grand Banks of Newfoundland could pose serious risk to the production platforms. The associated risk depends on the ice kinetic energy and frequency, and could influence the exploration schedules (Timco, 2007), as well as the design of offshore structures since the design load is governed by the kinetic energy and collision frequency of the interacting ice feature (Eik and Gudmestad, 2010). The severity of the associated risk can also impact the rate of success when implementing an ice

81

management plan; different actions taken to reduce or avoid the impact from any kind of ice features (Eik, 2008).

The historical drift and deterioration data in the previous section provide important information that could contribute to devising an appropriate ice management strategy when dealing with ice islands. Whether or not a drifting ice feature is manageable or if the activities should be suspended depends on its drift speed and mass when approaching the vicinity of an offshore operations site. The mean drift speeds presented in Table 3.2 provides valuable information on the historical drift characteristics of Petermann ice islands. The mean areal surface reduction and the expected number of calved ice islands (Table 3.3), along with the size distribution of these ice features presented by Crawford et al. (2018a) provide a framework to estimate the mass and frequency of these ice islands. The drift speed and mass of the ice islands are key information to making right decisions regarding the risk assessment of the ice environment as they significantly affect the kinetic energy of ice islands. While smaller ice features could be physically managed by towing through various methods (Rudkin et al., 2005), larger ice islands that have high kinetic energy (due to high mass and/or drift speed) cannot be physically managed, where ice avoiding strategies may need to be implemented (Fuglem and Muggeridge, 1999). While mass and drift speed of ice features provide important information for the execution of a successful ice management plan, it is also important to account for the number of calved ice features that need to be managed simultaneously (McClintock et al., 2002). The ability to estimate the frequency of the ice islands affects the probability of interaction with offshore operations (Crawford et al., 2018b). This could significantly affect the resource planning to mitigate the associated risk of ice island presence (Dugal, 2001), which is crucial to the implementation of the right action plan to physically tow/break the ice islands or avoid these ice features (if possible). The mean direction of the ice

islands is another important characteristic that should be taken into account when devising a plan to tow the ice features. For instance, given the dominant southeast Labrador Current and southwest currents in the Grand Banks (McClintock et al., 2002), it is important for the operators to establish a towing direction (if possible) that could successfully deflect the ice feature based on its drift direction.

The data analysis in this study was performed and presented for three massive calving events of Petermann Glacier (2008-2012) to investigate the annual discrepancy in the drift and deterioration characteristics of the ice islands. While the 2008 calving event was the smallest of the three and generated few descendant ice islands, the 2010 event calved the largest parent ice island that generated numerous descendants that drifted significantly more southwards than the ice islands from the other two events. This represented a heavier ice year that showed different characteristics when compared against other years (Table 3.2 and Table 3.3).

Here it should be noted that while this study presented a preliminary analysis of the drift and deterioration of Petermann ice islands for different size classes observed in the CI2D3 database, the influence of other atmospheric and oceanic variables have not been investigated in this study and is beyond the scope of this study. This is, however, the focus of a forthcoming study that aims to investigate the extent to which various metocean conditions (*e.g.*, sea states, wind and water temperatures/speeds, etc.) influence the drift and deterioration of these ice islands.

## 3.8. Conclusions

The calving events of Petermann Glacier in 2008, 2010, and 2012 generated hundreds of large and small ice islands that drifted southwards towards the Labrador Sea and beyond to the Grand Banks, in some cases. This study provided a preliminary data analysis on the drift and characteristics of

these ice islands by size category using the newly developed CI2D3 Database. The analysis showed that large ice islands (>10 km$^2$), on average, drifted longer before fracturing and generated a larger number of descendants following a fracture event. Size was identified as an important factor in the deterioration of the ice islands. The geographical analysis of the fracture events showed that while the main 2008 and 2010 Petermann ice islands fractured in mainly two locations, the 2012 Petermann ice island broke up in various locations over its drift path. The results of this study provide an important step in characterizing ice island drift and deterioration in the region between the northwest of Greenland and offshore Newfoundland. This could contribute to the field of glacial ice risk mitigation for Baffin Bay and the east coast of Canada.

## 3.9. Acknowledgments

## 3.10. References

Crawford, A. J., Mueller, D., Desjardins, L., and Myers, P. G. (2018a). The aftermath of Petermann glacier calving events (2008–2012): ice island size distributions and meltwater dispersal, Journal of Geophysical Research: Oceans, 123(12), 8812-8827, https://doi.org/10.1029/2018JC014388.

Crawford, A. J., Wadhams, P., Wagner, T. J., Stern, A., Abrahamsen, E. P., Church, I., Bates, R.,

and Nicholls, K. W. (2016). Journey of an Arctic ice island, Oceanography, 29(2), 254-263, https://doi.org/10.5670/oceanog.2016.30.

Crawford, A., Crocker, G., Mueller, D., Desjardins, L., Saper, R., and Carrieres, T. (2018b). The Canadian Ice Island Drift, Deterioration and Detection (CI2D3) Database, Journal of Glaciology, 1-5. https://doi.org/10.1017/jog.2018.36.

Desjardins, L., Crawford, A., Mueller, D., Saper, R., Schaad, C., Stewart-Jones, E., and Shepherd, J. (2018). Canadian ice island drift, deterioration and detection database (CI2D3 database) [v1.1], Canadian Cryospheric Information Network (CCIN), Waterloo, Canada, http://dx.doi.org/10.21963/12678.

Dugal, R. (2001). Ice Detection and Management in support of Canadian east coast oil operations, Offshore Technology Conference, https://doi.org/10.4043/13026-MS.

Ebbesmeyer, C. C., Okubo, A., and Helseth, J. M. (1980). Description of iceberg probability between Baffin Bay and the Grand Banks using a stochastic model, Deep Sea Research Part A, Oceanographic Research Papers, 27(12), 975-986, https://doi.org/10.1016/0198-0149(80)90060-6.

Eik, K. (2008). Review of experiences within ice and iceberg management, The Journal of Navigation, 61(4), 557-572, https://doi.org/10.1017/S0373463308004839.

Eik, K. and Gudmestad, O. T. (2010). Iceberg management and impact on design of offshore structures, Cold Regions Science and Technology, 63(1-2), 15-28, https://doi.org/10.1016/j.coldregions.2010.04.008.

Enderlin, E. M., Hamilton, G. S., Straneo, F., and Sutherland, D. A. (2016). Iceberg meltwater fluxes dominate the freshwater budget in Greenland's iceberg-congested glacial fjords, Geophysical Research Letters, 43(21), 11-287, https://doi.org/10.1002/2016GL070718.

Fuglem, M. and Muggeridge, K. (1999). Design load calculations for iceberg impacts, International Journal of Offshore and Polar Engineering, 9(04), 298-306.

Halliday, E. J., King, T., Bobby, P., Copland, L., and Mueller, D. (2012). Petermann Ice Island 'A' survey results, offshore Labrador, OTC Arctic Technology Conference, Offshore Technology Conference, https://doi.org/10.4043/23714-MS.

Jeffries, M. O. (2002). Ellesmere Island ice shelves and ice islands, Satellite Image Atlas of Glaciers of the World: Glaciers of North America - Glaciers of Canada, U.S. Geological Survey Professional Paper 1386-J-1, J147-J164.

McClintock, J., Bullock, T., McKenna, R., Ralph, F., and Brown, R. (2002). Greenland iceberg management: Implications for Grand Banks management systems, PERD/CHC Report, 20-65.

Mueller, D. R., Copland, L., Hamilton, A., and Stern, D. (2008). Examining Arctic ice shelves prior to the 2008 breakup, Eos, Transactions American Geophysical Union, 89(49), 502-503, https://doi.org/10.1029/2008EO490002.

Mueller, D. R., Crawford, A., Copland, L., and Van Wychen, W. (2013). Ice island and iceberg fluxes from Canadian High Arctic sources, Report to the Northern Transportation Assessment Initiative, Innovation Policy Branch, Transport Canada, Ottawa, Canada. https://www.researchgate.net/publication/340183882_Ice_Island_and_Iceberg_Fluxes_fr

om_Canadian_High_Arctic_Sources_Prepared_for_the_Innovation_Policy_Group_of_Transport_Canada.

NASA Earth Observatory (2019a). Closeup of the Ice Island from Petermann Glacier, Retrieved on January 4, 2019 from https://earthobservatory.nasa.gov/images/78648/closeup-of-the-ice-island-from-petermann-glacier.

NASA Earth Observatory (2019b). Ice Island Calves off Petermann Glacier, Retrieved on January 4, 2019 from https://earthobservatory.nasa.gov/images/45306/ice-island-calves-off-petermann-glacier.

Newell, J. P. (1993). Exceptionally large icebergs and ice islands in eastern Canadian waters: a review of sightings from 1900 to present, Arctic, 46(3), 205-211, https://doi.org/10.14430/ARCTIC1345.

Nick, F. M., Luckman, A., Vieli, A., Van der Veen, C. J., Van As, D., Van De Wal, R. S. W., Pattyn, F., Hubbard, A. L., and Floricioiu, D. (2012). The response of Petermann Glacier, Greenland, to large calving events, and its future stability in the context of atmospheric and oceanic warming, Journal of Glaciology, 58(208), 229-239, https://doi.org/10.3189/2012JoG11J242.

Peterson, I. K., Prinsenberg, S. J., Pittman, M., and Desjardins, L. (2009). The Drift of an Exceptionally-Large Ice Island from the Petermann Glacier in 2008, In Proceedings of the 20th International Conference on Port and Ocean Engineering under Arctic Conditions, Luleå, Sweden, 9-12 June 2009.

Rackow, T., Wesche, C., Timmermann, R., Hellmer, H. H., Juricke, S., and Jung, T. (2017). A

simulation of small to giant Antarctic iceberg evolution: Differential impact on climatology estimates, Journal of Geophysical Research: Oceans, 122(4), 3170-3190, https://doi.org/10.1002/2016JC012513.

Rudkin, P., Boldrick, C., and Barron Jr, P. (2005). PERD Iceberg Management Database, PERD/CHC Report, 20-72.

Scambos, T., Sergienko, O., Sargent, A., MacAyeal, D., and Fastook, J. (2005). ICESat profiles of tabular iceberg margins and iceberg breakup at low latitudes, Geophysical Research Letters, 32(23), https://doi.org/10.1029/2005GL023802.

Stern, A. A., Adcroft, A., and Sergienko, O. (2016). The effects of Antarctic iceberg calving-size distribution in a global climate model, Journal of Geophysical Research: Oceans, 121(8), 5773-5788, https://doi.org/10.1002/2016JC011835.

The Economy (2017). Retrieved on January 5, 2019 from the Department of Finance at Government of Newfoundland and Labrador at https://www.economics.gov.nl.ca/E2017/TheEconomy2017.pdf.

Timco, G. (2007). Grand Banks iceberg management, PERD/CHC Report, 20-84, https://doi.org/10.4224/12328812.

Tournadre, J., Bouhier, N., Girard-Ardhuin, F., and Rémy, F. (2016). Antarctic icebergs distributions 1992–2014, Journal of Geophysical Research: Oceans, 121(1), 327-349, https://doi.org/10.1002/2015JC011178.

Tournadre, J., Girard-Ardhuin, F., and Legrésy, B. (2012). Antarctic icebergs distributions, 2002–

2010, Journal of Geophysical Research: Oceans, 117(C5), https://doi.org/10.1029/2011JC007441.

U.S. Geological Survey (2019). Earthshots: Satellite Images of Environmental Change, Retrieved on January 5, 2019 from https://earthshots.usgs.gov/earthshots/node/70#ad-image-1-0.

# 4. A PROBABILISTIC MODEL FOR FRACTURE EVENTS OF PETERMANN ICE ISLANDS UNDER THE INFLUENCE OF ATMOSPHERIC AND OCEANIC CONDITIONS

## 4.1. Preface

This chapter aims to improve glacial ice deterioration models by building on the preliminary analysis presented in chapter 3, through developing a probabilistic model for the large-scale fracture events of ice islands. The chapter provides a comprehensive review of the ice island deterioration models, employ the CI2D3 database, analyzes the relative influences of atmospheric and oceanic variables on ice island fracture events, and presents a probabilistic Bayesian model that can serve as a forecasting tool for fracture events of Petermann ice islands.

This chapter has been published as an original research article in The Cryosphere. As the primary author of this article, I conducted the literature review, developed the probabilistic model, performed the analysis, and prepared the manuscript. My co-authors, Dr. Ian Turnbull, Dr. Rocky Taylor, and Dr. Derek Mueller identified the research topic and provided valuable feedback at different stages of the analysis and preparation of the article. I subsequently revised the manuscript based on the suggestions from the co-authors and the recommendations from the journal reviewers.

## 4.2. Abstract

Four calving events of Petermann Glacier happened in 2008, 2010, 2011, and 2012, which resulted in the drift and deterioration of numerous ice islands, some reaching as far as offshore Newfoundland. The presence of these ice islands in the eastern Canadian Arctic increases the risk of interaction with offshore operations and shipping activities. This study uses the recently

developed Canadian Ice Island Drift, Deterioration and Detection database to investigate the fracture events that these ice islands experienced, and presents a probabilistic model for the conditional occurrence of such events by analyzing the atmospheric and oceanic conditions that drive the causes behind the ice island fracture events. Variables representing the atmospheric and oceanic conditions that the ice islands were subjected to are extracted from reanalysis datasets and then interpolated to evaluate their distributions for both fracture and non-fracture events. The probability of fracture event occurrence for different combinations of input variable conditions are quantified using Bayes' theorem. Out of the seven variables analyzed in this study, water temperature and ocean current speed are identified as the most and least important contributors, respectively, to the fracture events of the Petermann ice islands. It is also revealed that the ice island fracture probability increases to 75% as the ice islands encounter extreme (very high) atmospheric and oceanic conditions. A validation scheme is presented using cross-validation approach and Pareto principle, and an average error of 13-39% is reported in the fracture probability estimations. The presented probabilistic model has a predictive capability for future fracture events of ice islands and could be of particular interest to offshore and marine ice/risk management in the eastern Canadian Arctic. Future research, however, is necessary for model training and testing to further validate this ice island fracture model.

## 4.3.    Introduction

With the advancement of offshore operations and shipping activities into the harsh environment in the eastern Canadian waters, these activities are being subjected to greater risks from glacial ice features (Saper, 2011). The shipping and resource extraction industries in this region, therefore, require a better understanding of the dynamics and physical properties of these ice features to be able to devise appropriate ice management strategies for safe operations. Specifically, a better

understanding of the drift and deterioration characteristics of icebergs and ice islands (large tabular icebergs) is needed for risk management strategies. However, due to the occasional presence of ice islands in regions with lower latitudes such as offshore Newfoundland and Labrador (Johannessen et al., 2011), there has been limited research on the dynamics of ice islands, when compared to the research concerning annual presence of smaller icebergs in the region. Ice island research studies have been mainly focused on their potential risks to shipping activities and offshore operations (Peterson, 2011; Mueller et al., 2013; Fuglem and Jordaan, 2017), as well as their meltwater input as they deteriorate and melt over large regions (Stern et al., 2015; Merino et al., 2016; Wagner et al., 2017; Crawford et al., 2018d).

For offshore operations, whether or not a drifting ice feature is manageable, or if activities should be suspended, depends on several factors such as its velocity, mass, and the number of ice features approaching the vicinity. Mass and size distribution are both dependent on the deterioration of each ice feature via melting and/or fracturing, processes that are associated with several atmospheric and oceanic variables. Therefore, it is important to evaluate the effect of metocean variables on the deterioration of ice islands. However, the harsh conditions in the eastern Canadian marine environment make it very challenging to collect in-situ metocean data. Also, due to the difficulties involved in tracking a large number of ice islands over their lives (Merino et al., 2016; Rackow et al., 2017; Stern et al., 2016), it has been a challenge to investigate the conditions that lead to ice island deterioration. An alternative way to track a large number of ice islands and monitor their deterioration is using remote sensing observations. Unlike optical methods, Synthetic Aperture Radar (SAR) imagery can produce images of ice islands even when the amount of daylight is low and cloud cover is high (Jeffries, 2002). The recent calving events of Petermann Glacier (2008-2012) and other northern Greenland glaciers have been accompanied by SAR

satellite imagery (July 2008 to December 2013), which allowed tracking the ice islands throughout their periods of drift and deterioration. Through a collaboration between the Canadian Ice Service (CIS) and Water and Ice Research Lab (WIRL) at Carleton University, a large number of SAR images from the CIS archive were analyzed using a geographical information system to develop a geospatial database associated with the ice islands originally calved from Petermann Glacier in 2008-2012, as well as the Ryder, Steensby, C.H. Ostenfeld, and North Greenland ice tongues (Crawford et al., 2018a). The ice islands were delineated and monitored as they deteriorated (via melting and/or fracturing) down to a threshold of 0.25 km$^2$ in surface area (Crawford et al., 2018d), and the information was recorded in the Canadian Ice Island Drift, Deterioration and Detection (CI2D3) database. The calving events of the Petermann Glacier in 2008, 2010, 2011, and 2012 corresponded to the removal of 36, 302, 4, and 145 km$^2$ from the Petermann Ice Tongue, respectively (Crawford et al., 2018a). The calving event that occurred in 2010 was the most significant of all and resulted in the loss of about 25% of the Petermann Glacier ice tongue (Nick et al., 2012). These calving events generated numerous smaller ice islands that drifted southwards toward the Labrador Sea, which were tracked in the CI2D3 database. More information on the CI2D3 database and its documentation can be found in Desjardins et al. (2018) and Crawford et al. (2018b).

### 4.3.1. Past Studies on Iceberg Deterioration

A key component for a reliable ice drift model and risk assessment of icebergs is the ability to estimate their mass (Crawford et al., 2018c), a variable that constantly changes as a result of melting and small/large scale fracturing as it drifts. This can be investigated through melt rate and small-scale physical calving models, field measurements, or remote sensing observations. Iceberg melt rate models predict processes such as forced convection caused by air at the iceberg sail and

water at the keel, solar radiation on the iceberg sail, natural convection on sidewalls, and sidewall erosion at the waterline caused by waves (Job, 1978; El-Tahan et al., 1987; Savage, 2001). The resulting iceberg calving caused by wave erosion has been modeled using empirical models (*e.g.*, White et al., 1980; Savage, 2001) and physical models (*e.g.*, Wagner et al., 2014). Savage (2001) studied the relative contribution of each of these mechanisms to the overall deterioration of three different icebergs. Savage (2001) found that wave erosion at the waterline was the dominant mechanism in contributing to the overall iceberg deterioration (by 50-65%), followed by the resultant wave-induced calving events (by 20-30%). Savage (2001) also found that surface melt played a minor role in the deterioration of icebergs, but it was revealed in another study that the deterioration of ice islands was significantly influenced by the surface melt due to the large surface area of ice islands (Crocker et al., 2013). Kubat et al. (2007) used the deterioration mechanisms described by Savage (2001) to build an operational iceberg forecasting model for the CIS. The sensitivity of the deterioration model to various metocean variables was examined, and it was revealed that the overall deterioration of icebergs was most significantly influenced by wave height (via erosion at the waterline and calving of the overhanging slabs), followed by water temperature (Kubat et al., 2007). The importance of waves and wave-related calving in the overall deterioration of icebergs was also highlighted by Rackow et al. (2017) who investigated the influence of the wave-induced calving, basal melt, and buoyant convection on the deterioration of 6912 icebergs with varying sizes (0.3-4717.6 km$^2$) in the Antarctic. Rackow et al., 2017 highlighted the importance of iceberg size in their thermodynamic characteristics and that while waves played the most important role in the decay of smaller icebergs (<10 km), basal melt was an important contributor to the overall mass loss of giant icebergs (>10 km). In a similar study, Stern et al. (2017) presented a novel framework to simulate drifting tabular icebergs for climate studies. The

authors modeled the melt of tabular icebergs submerged in the ocean in the Antarctic through the three mechanisms that were used in Rackow et al. (2017). Crawford et al. (2015) modeled the energy fluxes at the surface using the bulk aerodynamic approach to estimate the surface melt of an ice island sail, and validated the results against three surface ablation models (from Kubat et al., 2007; Ballicater Consulting Ltd., 2012; Hock, 2003). Bouhier et al. (2018) studied the observed vertical melt of two large Antarctic icebergs through the combined analysis of satellite altimetry and imagery and compared this against melt rate estimates from two different models: a forced convection approach and a thermal turbulent exchange approach. While the former approach was found to underestimate the iceberg melt rates, the latter approach was more reliable in modeling iceberg thickness variations. Zeinali-Torbati et al. (2020) estimated the reduction in the mass of four ice island fragments offshore Newfoundland using a surface ablation model (from Hock, 2003), a basal ablation model (from Crawford, 2018), and the observed areal surface reduction from SAR images. The authors revealed that basal melt had a greater contribution to the overall thickness melt of the ice island fragments, which was in agreement with the results of the thickness melt model in Crawford (2018) and Bouhier et al. (2018). In a field study (Halliday et al., 2012), however, the melt and thinning rate of an ice island offshore Labrador was measured using ablation stakes and ground penetrating radar, and it was revealed that surface ablation contributed more than basal ablation to the overall thinning rate of the ice island. In other fieldwork, Crawford et al. (2020) deployed an ice-penetrating radar on an ice island originated from the 2012 calving event of Petermann Glacier to measure the surface and basal ablation rates over an 11-month period. It was revealed that while basal ablation contributed to 73% of the total thinning rate, it played a minimal role in the ice island overall mass loss when compared to areal surface reduction likely caused by wave erosion, wave-induced calving, and fracture events. The authors, however, stated

that basal ablation significantly influences the thickness of ice islands, which would likely increase the probability of large-scale fracture event occurrence (Crawford et al., 2020).

The deterioration mechanisms mentioned earlier describe formulations for the melt rates and small-scale calving events of icebergs caused by various metocean conditions. However, there are other mechanisms associated with iceberg deterioration such as large-scale fracture caused by internal stress and convection caused by iceberg rolling (Kubat et al., 2007). While fracture mechanisms play a more important role than melting in the overall deterioration of large icebergs (Bouhier et al., 2018), they are not as well studied and are often neglected due to the infrequent occurrence of fracture events (Kubat et al., 2007). It has also been difficult to model these processes using physical models due to the lack of quantitative theories to explain these mechanisms (Savage, 2001). To date, there are only a few deterministic models to describe the large-scale fracture mechanisms for icebergs (*e.g.*, Diemand et al., 1987; Wagner et al., 2014; Bouhier et al., 2018; England et al., 2020). Additionally, the accuracy of deterministic deterioration models for glacial ice will be limited by the uncertainty in the physical parameters that govern the deterioration processes. Iceberg fracture processes have previously been studied using numerical methods to investigate fracture events for different iceberg geometries (Bassis and Jacobs, 2013), due to buoyancy-driven flexure (Sazidy et al., 2019), as well as due to the accumulation of microcracks in the ice structure (Bahr, 1995). Also, a recent study (Smith, 2020) investigated the fracture events of ice islands when a large protuberance develops on their keels, where a finite element analysis was used to estimate the buoyancy-driven bending stress and predict the associated fractures. However, these numerical models did not account for the relative role of metocean conditions in the fracture processes. Probabilistic methods, however, have the ability to account for the relative contribution of meteorological and oceanographic conditions to the

fracture events of glacial ice features. Bouhier et al. (2018) investigated the fracture-related decay of two large Antarctic icebergs through analyzing the correlation between their relative volume loss and environmental variables (sea surface temperature, current speed, difference of iceberg and current velocities, significant wave height, wave peak frequency, and wave energy at the bobbing period). The authors found that while wave-related quantities had no significant impact on the relative volume loss, sea surface temperature and iceberg velocity showed the highest correlation with the observed volume loss. Based on these two salient variables, Bouhier et al. (2018) characterized fracture events using a probability distribution and presented a deterministic bulk fracture model, which performed successfully in the estimation of iceberg relative volume loss. However, they noted that given the stochastic nature of fracturing process, individual fracture events cannot be predicted. England et al. (2020) presented an approach for modelling the fracture events of large tabular icebergs by incorporating a stochastic representation of the "footloose mechanism" (Wagner et al., 2014) into the analytical iceberg drift by Wagner et al. (2017). The authors showed that coupling their fracture model with an analytical drift model significantly impacted the iceberg meltwater distribution and resulted in improved simulated iceberg trajectories. England et al. (2020), however, noted that the fracture mechanism in their model is simplified based on several assumptions, a key one being the probability of a child iceberg fracturing from the parent iceberg is set as constant in time. However, this parameter should be, in fact, dependent on the environmental variables such as sea surface temperature.

The fracture models noted above are not able to quantify the probability of fracture events under different atmospheric and oceanic conditions, a quantity that can be estimated using Bayesian approach. To date, no previous research has adopted Bayesian approach to predict the probability of ice island fracture events under the influence of the metocean conditions that control these

events, likely due to the lack of reliable data. However, several studies have adopted a probabilistic approach using a Bayesian belief network and hydro-meteorological variables for navigational risk assessment of ships (Zhang et al., 2013) or to estimate the conditional probability of ship besetting in sea ice covered waters (Turnbull et al., 2019; Fu et al., 2016; Montewka et al., 2015; Montewka et al., 2013). This study uses the CI2D3 database and adopts a similar methodology to that used in these besetting studies to present a probabilistic fracture model for ice islands as a function of the metocean conditions.

The CI2D3 database was previously used by Crawford et al. (2018d) to investigate the size distributions and meltwater flux of Petermann ice islands. The analysis of size distribution revealed that small ice islands constituted a significant proportion of ice island population, but large ice islands contributed the most to the total mass and melt water flux (Crawford et al., 2018d). The authors also revealed that fracture processes significantly contributed to the overall deterioration of Petermann ice islands as the ice island size distribution followed a power law model, which corroborated the results of Stern et al. (2016), Tournadre et al., (2016), Enderlin et al. (2016), Bouhier et al. (2018), and Barbat et al. (2019).

This study uses the CI2D3 database to study fracture events of the ice islands which originated from the calving events of Petermann Glacier in 2008-2012. Various atmospheric and oceanic variables are analyzed to probabilistically determine the set of conditions that lead to the highest chance of fracture event occurrence. This study first presents a description of the data structure in the CI2D3 database. Then, an overview of the results from a preliminary data analysis on the deterioration of Petermann ice islands is presented, followed by the results of the probabilistic fracture model. Finally, a validation scheme is presented to quantify the accuracy of the probabilistic fracture model.

98

## 4.4.    Methodology

### 4.4.1.  Data Extraction from CI2D3 Database

The CI2D3 database (version 1.1) contains data extracted from around 25,000 satellite imagery observations of ice islands from various glaciers, including the Petermann, Ryder, Steensby, C.H. Ostenfeld, and North Greenland glaciers. The data contains a geospatial polygon and 28 attribute fields for each observation. An algorithm was developed in MATLAB (version R2017b) to extract the data subsets associated with the 2008, 2010, 2011, and 2012 Petermann ice islands (17,755 observations). For each observation, the spatial and temporal data (latitude, longitude, and time) were extracted. Here it should be noted that the "birth" or beginning of a given ice island is considered to be immediately after it calved from another ice island (or glacier), and the "death" or end of that feature is taken as when it calves into two or more fragments. By this definition, 328 fracture events and 845 ice islands were identified. The ice islands were tracked in the CI2D3 database, and the parent-child relationship between the ice islands was captured as fracture events happened. To identify the parent-child relationship, the unique identifier for each ice island observation was extracted and matched with the *lineage* and *mother* fields (*i.e.*, fields in the database structure that tie subsequent observations together and relate the ice islands to their parents). This permits identification of the previous observations of each ice island back to the time it was born, which were later used for estimating the cumulative effect of variables (*e.g.*, air and water temperatures, and waves) that each ice island experienced over its lifespan. The algorithm also used the *ddinfo* field to identify if the ice island was grounded or drifting at the time of observation. This was used to estimate the grounding time over the lifespan of each ice island.

99

### 4.4.2. Atmospheric and Oceanic Data Extraction

A series of atmospheric and oceanic data were collected from reanalysis databases in the region of interest between northwest Greenland and offshore Newfoundland (46-83 °N, 45-95 °W) from July 2008 to December 2013. Daily average values (0.3° spatial resolution) for zonal-meridional components of 10-m wind velocity ($m\ s^{-1}$) and 2-m air temperature (℃) were extracted from the North American Regional Reanalysis (NARR); daily average values (1/12°) for zonal-meridional components of ocean current velocity ($m\ s^{-1}$) and potential water temperature (℃) in 25 depth layers (down to 156 m) from the Global Ocean Physics Reanalysis model in Copernicus Marine Environment Monitoring Service (CMEMS); six-hourly values (1/8°) for significant height of combined wind waves and swell ($m$) and mean wave period ($s$) from the European Centre for Medium-Range Weather Forecasts (ECMWF) ERA-Interim Reanalysis; and sea ice concentration (%) from the CIS digital daily ice charts. The extracted metocean data were linearly interpolated in space and time to the positions and times of the ice island centroids recorded in the CI2D3 database to represent the distribution of atmospheric and oceanic conditions over the drift tracks of the ice islands.

The temporal resolution of the satellite observations in the CI2D3 database were not consistent for all ice islands over their drift periods. The reanalysis variables used in this study were usually available sub-daily (hourly, three-hourly, or six-hourly), but the temporal resolution of the images used to create the CI2D3 database range periodically from sub-daily to bi-weekly. Therefore, all atmospheric and oceanic data were extracted or averaged as daily values and then interpolated in space and time to the positions and times of the ice island observations.

### 4.4.3. Probabilistic Model Development

To evaluate the conditional dependence of ice island fracture events on atmospheric and oceanic variables, a Bayesian approach was employed. Bayesian analysis is a well-used method in probabilistic studies to evaluate the probability of a certain outcome using the most salient predictive variables (Gutierrez et al., 2011). This method is recognized by its strong reasoning ability in uncertain situations and its ability to combine and analyze data from various datasets (Fu et al., 2016). Using the Bayesian method, the dependency and independency of a set of variables (Figure 4.1-a) were analyzed via a directed acyclic graph (Figure 4.1-b). Initially, the distribution of 10 atmospheric and oceanic variables were studied. These included wind speed ($V_w$), air temperature ($T_a$), ocean current speed ($V_c$), water temperature ($T_w$), wave energy index ($E_w$), lifetime mean air temperature ($T_{a\_avg}$), lifetime mean water temperature ($T_{a\_avg}$), lifetime mean wave energy index ($E_{w\_avg}$), grounding time ($t_g$), and sea ice concentration ($C$). Wind and current speeds were estimated as the magnitude of the extracted zonal-meridional components for wind and ocean currents, respectively. Water temperature was estimated as the average of water temperatures at all layers from the water surface down to a depth of 50 m. Given that wave energy flux is proportional to mean wave period and significant wave height squared (Christakos et al., 2020; Akpınar et al., 2019; Waters, 2008; Falnes, 2007), the wave energy index was defined as:

$$E_w = (H_{wave})^2 (T_{wave}),$$
$\qquad\qquad\qquad\qquad\qquad\qquad\qquad\qquad\qquad\qquad\qquad$ (4.1)

where $H_{wave}$ represents the significant height of combined wind waves and swell ($m$) and $T_{wave}$ represents the mean wave period ($s$). Time since previous calving was also explored as a variable, but this had very little predictive power and was excluded from subsequent analyses. However, in order to capture the cumulative effect of temperature and waves over the lifespan of the ice island,

we first identified all previous observations of each ice island back to the time and location that it was born. Then, the air and water temperatures, and wave energy index were interpolated spatially and temporally to all previous observations. To exclude the effect of observation frequency, these variables were interpolated in space and time to a daily interval. These daily-average values were then averaged over the number of days the ice island drifted to effectively compute the lifetime mean wave energy index, as well as the mean air and water temperatures over the lifespan of the ice island, which differ from positive degree day calculations that are often used in ice melt rate models (*e.g.*, Hock, 2003). To better capture the short-lived extreme conditions in air and water temperatures prior to fracture events, the two-week mean values for air and water temperatures were also tested, but they did not make significant difference in the outcome and brought no improvement to the model performance, so they were subsequently excluded from the model inputs. Grounding time was estimated by adding the number of days that an ice island was grounded over its lifespan. The distribution of these variables around fractured ice islands and all ice island observations were investigated and compared. However, further analysis of $E_{w\_avg}$ and $t_g$ distributions for fracture events and all observations identified no correlation between these variables and the occurrence of fracture events, so they were excluded from the Bayesian fracture model development. Also, studying the sea ice cover around the ice island observations showed that sea ice concentrations were less than 3/10ths for about 99% of the observations, so it was discarded from further analysis as a model input variable. Sea ice, however, may play a role in fracture events of ice islands in other regions (*e.g.*, England et al., 2020), so the presented model would need to be extended for application in such regions.
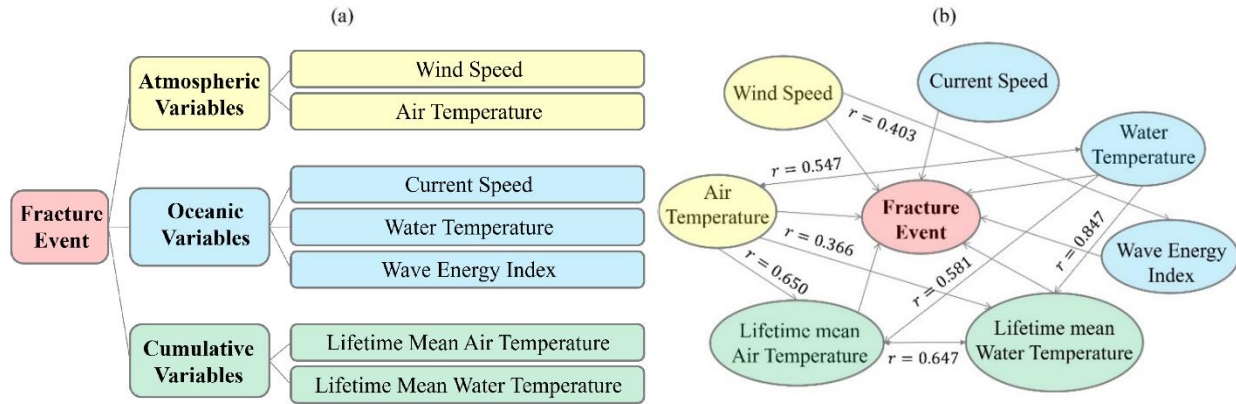
**Figure 4.1.** The classification of variables for the Bayesian fracture network (a), and the associated directed acyclic graph that shows the inter-relationship between the variables with the arrowheads showing the causality and the r values showing the associated correlation coefficients (b).

The distribution of the metocean variables presented in Figure 4.1 were studied for all ice island observations and compared against the variable distributions at the time of fracture events. However, the extracted reanalysis data revealed different number of data points available for the analysis of the seven variables presented. For example, for wind speed and air temperature, 17735 data points were available for all observations of Petermann ice islands. For current speed and water temperature, 16791 and 16784 data points were available for all observations of Petermann ice islands, respectively. These points covered most of the spatial and temporal records from the CI2D3 database. However, for wave energy index, only 3985 data points from all observations were available during the same time period. Similarly, different number of data points were available for each variable during the fracture events. The different numbers of data points for each variable are likely due to the fact that the ice islands drifted near the coastlines at times, and these data were extracted from reanalysis models that have insufficient spatial resolution to model data close to the coastlines. Therefore, the distributions of the studied variables from all observations and fractured subset are represented by relative frequencies to allow for consistent comparison of these distributions.

103

The correlation between a pair of variables was investigated using the Pearson Product-Moment Correlation coefficient ($r$), given by (Freedman et al., 2010):

$$r = \frac{\sum_i^n (x_i - \overline{x})(y_i - \overline{y})}{\sqrt{\sum_i^n (x_i - \overline{x})^2}\sqrt{\sum_i^n (y_i - \overline{y})^2}},$$ (4.2)

where $x_i$, $y_i$ are a pair of variables for the $i^{\text{th}}$ set of data and $\overline{x}$, $\overline{y}$ are the means of variables $x$, $y$ from all observations ($n$). The full set of data was used to perform the correlation analysis, and the inter-relationships between the variables is presented in Figure 4.1-b. Directed arrows were drawn from each variable to all of the variables that showed a correlation coefficient greater than 0.35.

The probability of fracture event occurrence in extreme metocean conditions (*i.e.*, conditions where the values of the model variables were extremely high) was investigated using a full set of model criteria with the high state ($> x^*$) of each variable. *States* here refer to the variable intervals defined based on a threshold. The selected criteria ($x^*$) for the extreme condition of each variable was identified by varying each criterion over the range of each variable from the fracture subset to maximize the fracture event probability. The distribution of conditional posterior probability was calculated through Bayes' Theorem, given by Stuart and Ord (1994):

$$P(X|Y) = \frac{P(X) \times P(Y|X)}{P(Y)},$$ (4.3)

where $P(X)$ is the prior probability of fracture event occurrence, $P_{frac}$; $P(Y|X)$ is the likelihood of a specific criteria set occurrence during fracture events, $P(V_w, T_a, V_c, T_w, E_w, T_{a\_avg}, T_{w\_avg}|Frac)$; and $P(Y)$ is the evidence of the criteria set occurrence for all observations, $P(V_w, T_a, V_c, T_w, E_w, T_{a\_avg}, T_{w\_avg})$. The probabilities in Eqn. (4.3) should be recalculated when new evidence become available, a process that reduces the dependence of the

posterior probability on the original estimated prior probability (Eleye-Datubo et al., 2006). Given the large size of the CI2D3 database, the value of $P(X)$ was estimated as the frequency of fracture events (*i.e.*, the number of fracture events divided by the total number of observations) before any criteria set based on metocean conditions was considered. The values of $P(Y|X)$ and $P(Y)$ were determined using the relative frequency of the set of states in fracture events and all observations, respectively. The relative frequency is given by Bonafede and Giudici (2007):

$$P(S_i) = \frac{n_i}{n}, \tag{4.4}$$

where $S_i$ represents a set of the variables' states, $n_i$ represents the count of the observed set of the states in fracture events (or all observations), and $n$ represents the total number of fracture events (or all observations) in the dataset.

To calculate the probability of fracture events in different metocean conditions, the ranges of atmospheric and oceanic variables at the time of fracture events were first divided into two states using the variable distribution medians from the fracture subset (Table 4.1). The conditional fracture probabilities were then estimated using a similar Bayesian approach (Eqn. (4.3)) through analyzing concurrent atmospheric and oceanic conditions at the time of fracture events that were extracted from the entire record for all ice island observations. Due to the limited number of fracture events (328), the number of state combinations in the presented model needed to be reduced to avoid model saturation and increase the model reliability. Among the atmospheric and oceanic variables analyzed in this study, current speed played an insignificant role in the fracture events of the ice islands, so it was not considered for further analysis.

**Table 4.1.** Various states of atmospheric and oceanic variables for the Bayesian fracture model.

| Variables | Median [1] | Unit | State 1 | State 2 |
|---|---|---|---|---|
| Wind Speed $(V_w)$ | 2.8 | $m\ s^{-1}$ | $\leq 2.8$ | $> 2.8$ |
| Air Temperature $(T_a)$ | $-2.1$ | °C | $\leq -2.1$ | $> -2.1$ |
| Water Temperature $(T_w)$ | $-0.3$ | °C | $\leq -0.3$ | $> -0.3$ |
| Wave Energy Index $(E_w)$ | 5.1 | $m^2\ s$ | $\leq 5.1$ | $> 5.1$ |
| Lifetime Mean Air Temperature $(T_{a\_avg})$ | $-3.5$ | °C | $\leq -3.5$ | $> -3.5$ |
| Lifetime Mean Water Temperature $(T_{w\_avg})$ | $-0.7$ | °C | $\leq -0.7$ | $> -0.7$ |

[1] Median values in the distributions of the given variables from the fracture subset

The developed probabilistic model was validated using a resampling approach based on the Pareto principle (Macek, 2008), which suggests 80% of the data be used for model training and development, and 20% be reserved for testing the developed model (Suthaharan, 2016). To reduce the effect of variation in the subset selection and have a more robust evaluation of the developed model, a k-fold cross-validation approach (Ozdemir, 2016) was used (k=5). So, input variables associated with the fracture and non-fracture data were randomly partitioned into five disjoint subsets of approximately equal size, where each time one of these subsets served for model testing, and the rest were used to train the model. This corresponded to the selection of training subsets with approximately 14204 data points (262 fracture events and 13942 non-fracture events) and test subsets with approximately 3551 data points (66 fracture events and 3485 non-fracture events). The conditional fracture probabilities of ice islands for the given criteria sets were calculated using the atmospheric and oceanic conditions for each test subset and then cross-validated against the predicted values associated with its corresponding training set.

## 4.5.    Results and Discussion

### 4.5.1.   Preliminary Analysis of Ice Island Fracture Events

The descendants of ice islands resulting from the calving events of Petermann Glacier in 2008, 2010, 2011, and 2012 generally drifted in a southward direction toward the Labrador Sea (Figure 4.2-a). These ice islands experienced 328 fracture events (Figure 4.2-b), which resulted in 845 ice islands. The 2010 event calved the largest ice island (

Table **4.2**), which generated 637 ice islands through its fractures (242 times), some of which drifted as far as offshore Newfoundland (Figure 4.2-a). The second largest calving event happened in 2012 which generated 169 ice islands through 73 fracture events, but the resulting ice islands were only recorded as far as offshore Iqaluit, given that the monitoring period in the CI2D3 database ended in December 2013. The other two calving events (2008 and 2011) generated 29 and 10 ice islands, which resulted from nine and four calving events, respectively. The size distribution of ice islands showed that large ice islands ($>10$ km$^2$) drifted longer before undergoing a fracture event and split into greater numbers of pieces per fracture event. Examples of this are two large ice islands (~137 km$^2$ and 60 km$^2$) originating from the 2010 calving event, which generated nine distinct pieces upon fracturing. However, around 70% of all fracture events generated only two children ice islands. A more detailed drift and deterioration analysis of the Petermann ice islands is presented in Zeinali-Torbati et al. (2019).
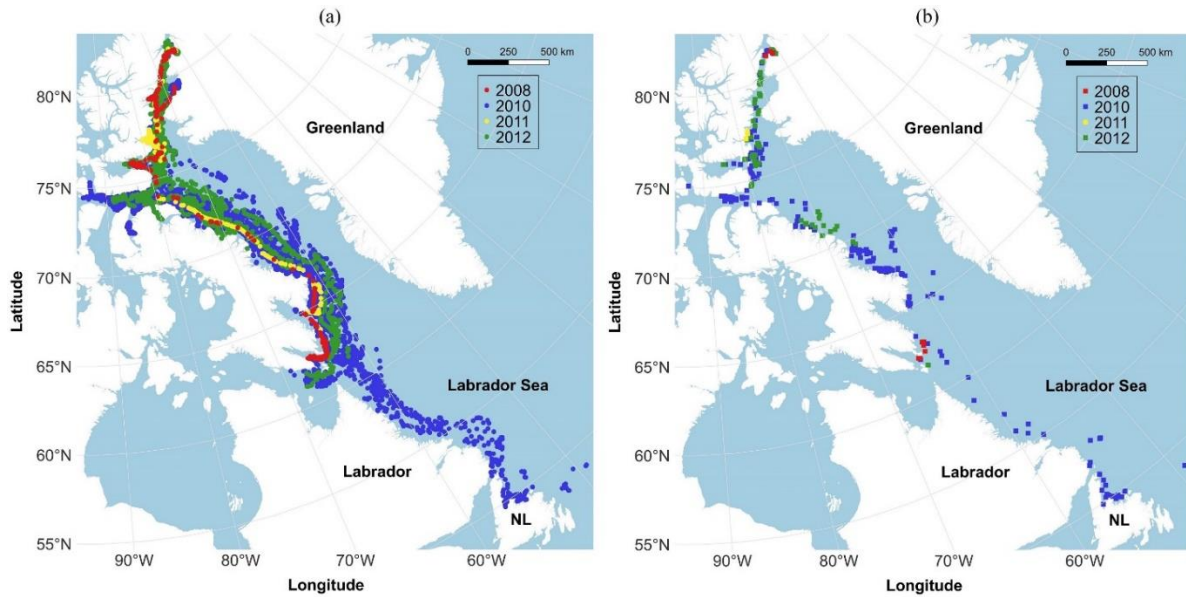
**Figure 4.2.** The drift trajectories (a) and the locations of fracture events (b) for the ice islands originating from the calving events of the Petermann Glacier in 2008 (red), 2010 (blue), 2011 (yellow), and 2012 (green).

**Table 4.2.** Description of the ice islands originating from the massive calving events of Petermann Glacier in 2008, 2010, 2011, and 2012.

| Calving year | Surface area (km$^2$) | Number of digitized polygons | Number of fracture events | Number of ice islands |
|---|---|---|---|---|
| **2008** | 36.4 | 332 | 29 | 9 |
| **2010** | 302.4 | 9658 | 637 | 242 |
| **2011** | 4.3 | 502 | 10 | 4 |
| **2012** | 144.6 | 7263 | 169 | 73 |

### 4.5.2. Distributions of Atmospheric and Oceanic Variables

The atmospheric, oceanic, and lifetime mean variables shown in Figure 4.1 were examined at the time of ice island fracture events, and then compared with the metocean conditions for all ice island observations using the methodology described earlier. Figure 4.3 through Figure 4.5 show the summary statistics and histogram plots of the relative frequency of regional metocean variables

108

surrounding the Petermann ice islands from all observations (blue), as well as from the fracture events (red).

Figure 4.3-a shows that the mean water temperature surrounding all Petermann ice islands was negative (-0.8 ℃) indicating that they mainly drifted within cold waters; however, the water temperature values reached up to 10.4 ℃. The statistics for lifetime mean water temperature from all observations (Figure 4.3-c) were almost the same as water temperature: a negative mean value of -0.8 ℃ and a range of -1.8 ℃ to 10.4 ℃. Comparing the distribution of water temperatures in Figure 4.3-a,b reveals that fracture events happened at higher water temperatures; while only 20% of ice islands from the entire dataset were surrounded by water temperatures above 0 ℃, 42% of fractured ice islands were subjected to positive water temperatures. In a similar way, it was revealed from long-term water temperature distributions that only 13% of the ice islands from all observations drifted in positive lifetime mean water temperatures (Figure 4.3-c). This, however, corresponded to about 34% of the ice islands in the fracture subset (Figure 4.3-d). The summary statistics presented in Figure 4.3 reveal that water temperature and lifetime mean water temperature played significant roles in the fracture events of Petermann ice islands; compared to the temperature records for all ice island observations, the ice islands at the time of fracture events experienced, on average, 1.2 ℃  and 0.8 ℃ greater values of water temperature and lifetime mean water temperature, respectively. This indicates the important contribution of warm waters to faster deterioration of glacial ice features (as stated by Kubat et al., 2007), likely due to higher internal stress caused by the increased heat transfer from water to the ice feature. The significant contribution of water temperature to fracturing process was corroborated by Bouhier et al. (2018), where a significant correlation between iceberg relative volume loss and sea surface temperature was found. Warm surface waters also plays an important role in the initiation of fractures on large

tabular Antarctic icebergs (England et al., 2020) through edge-wasting (*c.f.*, Scambos et al., 2005).
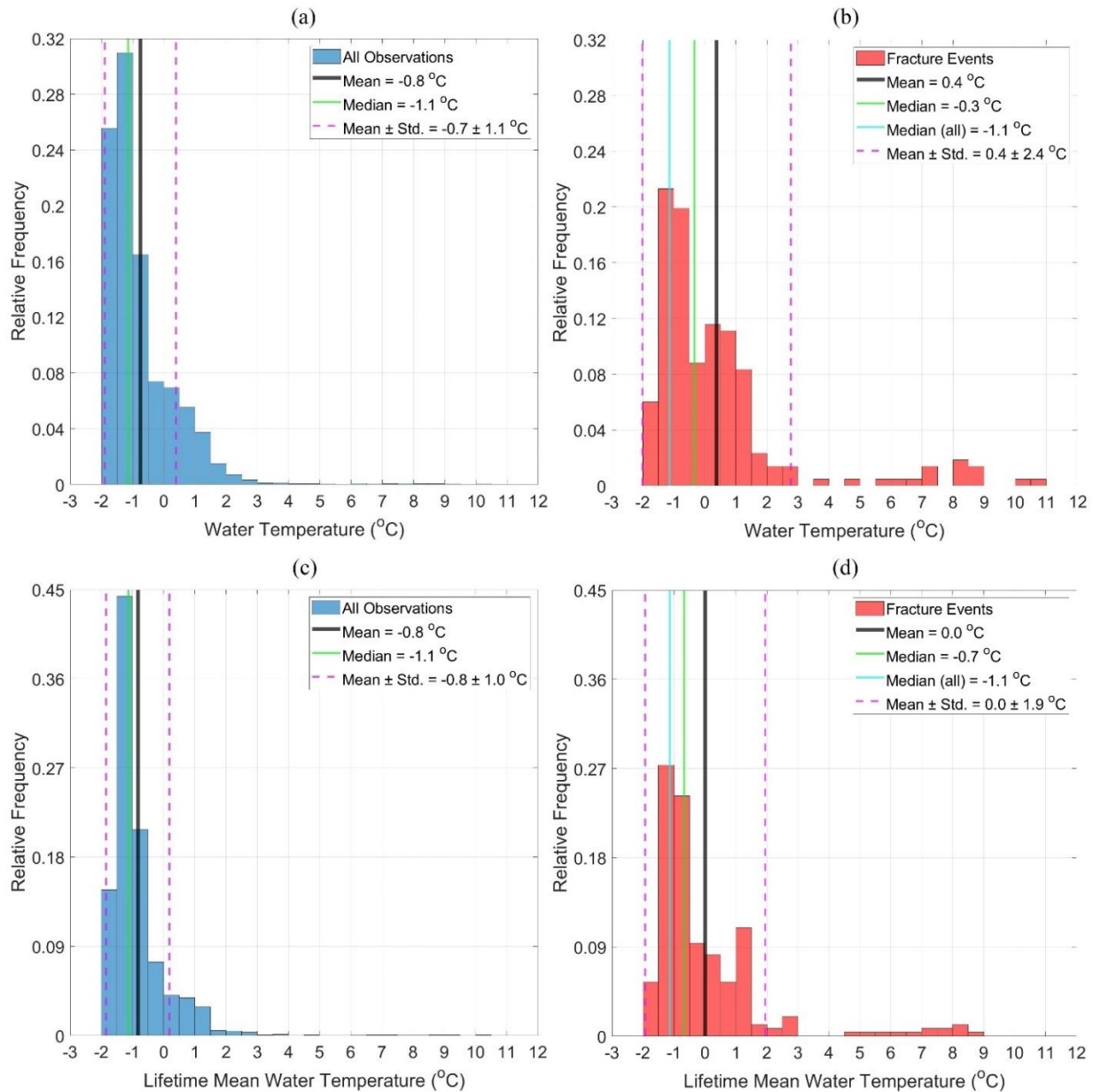


**Figure 4.3.** Relative frequency histogram plots of water temperature (a; n=16784, b; n=298) and lifetime mean water temperature (c; n=13537, d; n=256) surrounding Petermann ice islands for all observations (a,c), and for the fracture events (b,d).

Figure 4.4-a shows that the air temperatures to which the ice islands were subjected ranged from -35.6 ℃ to 17.9 ℃ for all observations, but the mean air temperature of -9.4 ℃ reveals that the ice

islands drifted a significant amount of time in cold air temperatures. Similarly, the Petermann ice islands were mainly subjected to negative lifetime mean air temperatures with an average of -11.6 ℃ ranging from -33.7 ℃ to 17.9 ℃ (Figure 4.4-c). Investigation of air temperature and its long-term effect at the time of fracture events (Figure 4.4-b,d) revealed that, on average, the ice islands were subjected to much higher values of these variables. The average air temperature at the time of fracture events was -5.2 ℃, which was 4.2 ℃ higher than the mean air temperature surrounding all ice islands. In a similar way, the ice islands from the fracture subset were, on average, subjected to 5.7 ℃ higher lifetime mean air temperature than the ice islands from all observations. The air temperature distributions (Figure 4.4-a,b) show that while the air temperatures associated with all ice island observations were most frequent around 0 ℃, the values associated with the fracture events were most frequent between 0 ℃ and 4 ℃. This, along with a 4.2 ℃ higher mean air temperature value from the fracture subset indicate that higher air temperature values are likely linked with the occurrence of fracture events. The analysis of lifetime mean air temperature distributions over the lifespan of each ice island (Figure 4.4-c,d) revealed that while only 14% of all ice island observations experienced lifetime mean air temperatures greater than 0 ℃, about 35% of the ice islands from the fracture subset were subjected to positive lifetime mean air temperatures. This indicates that the long exposure of ice islands to relatively warm air temperatures was likely an important factor in the occurrence of the fracture events.
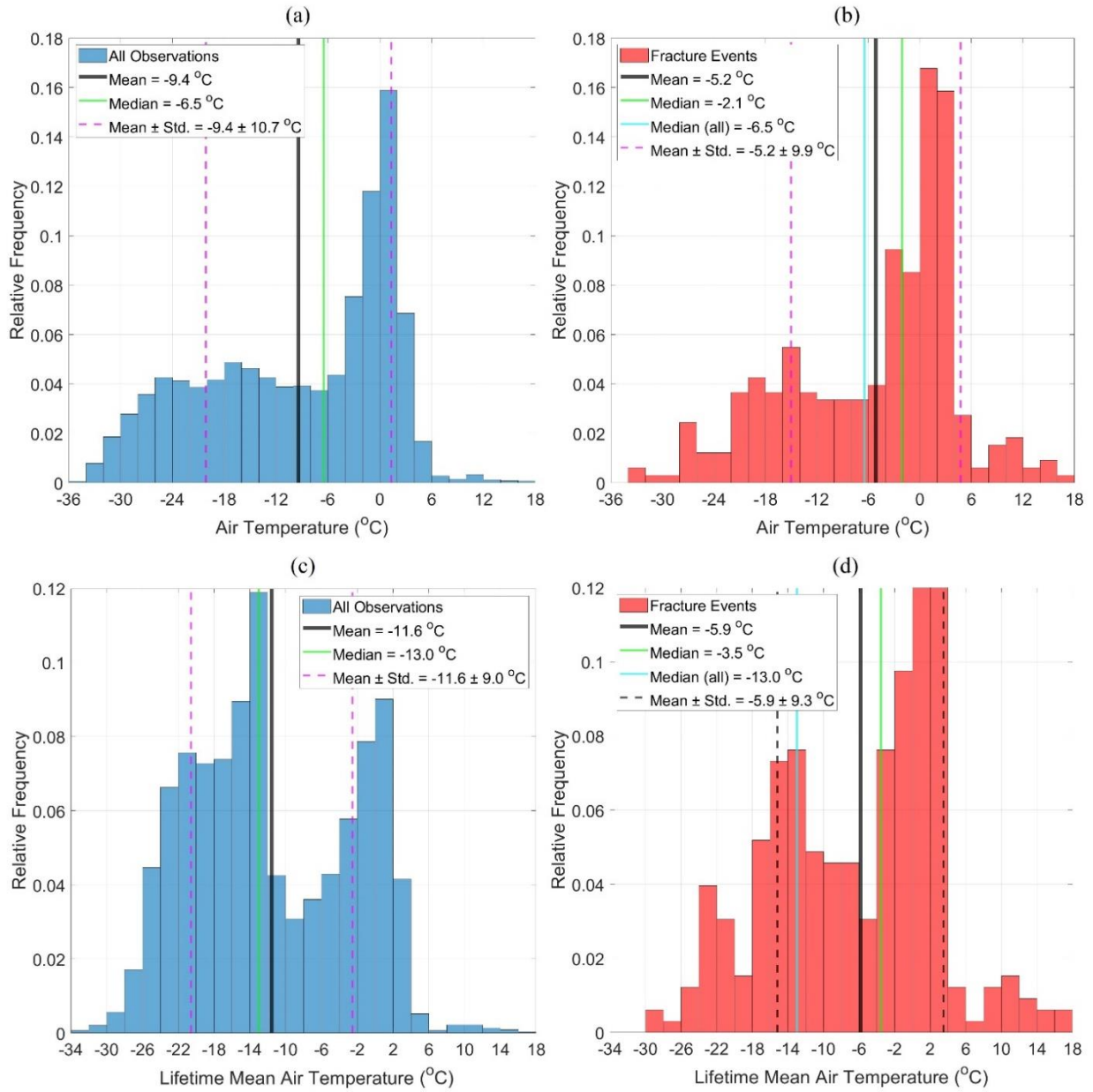
**Figure 4.4.** Relative frequency histogram plots of air temperature (a; n=17735, b; n=328) and lifetime mean air temperature (c; n=17755, d; n=328) surrounding Petermann ice islands for all observations (a,c), and for the fracture events (b,d).

The results associated with all observations of waves (Figure 4.5-a) show that while the wave energy index values varied from 0.1 $m^2 s$ to 62.1 $m^2 s$, the ice islands were mainly subjected to relatively low wave energy index with an average value of 5.3 $m^2 s$. Similarly, the regional wind and current speeds surrounding the ice islands from all observations were often relatively low,

with a mean value of 2.9 $m\ s^{-1}$ and 0.08 $m\ s^{-1}$, respectively (Figure 4.5-c,e). The summary statistics of the records from the fracture events (Figure 4.5-b,d,f) revealed that the regional mean wave energy index, wind speed, and current speed around the ice islands at the time of fracture events were statistically higher (by 38%, 17%, and 38%, respectively) when compared to the associated values for all ice islands observations. The analysis of wave energy index distributions around the Petermann ice islands presented in Figure 4.5-a,b show that only 30% of Petermann ice islands encountered wave energy index values greater than 6 $m^2\ s$. The fracture events, however, occurred at greater wave energy index values, where 46% of ice island observations experienced wave energy index values greater than 6 $m^2\ s$. The analysis also shows that while relatively high values of wave energy index, coupled with other metocean variables, most likely contribute to the occurrence of ice island fracture events, this variable by itself does not lead to a high fracture probability of Petermann ice islands. This is consistent with the results of the iceberg deterioration study by Bouhier et al. (2018) where the authors found no significant link between the relative volume loss of two large Antarctic icebergs and the wave-related variables. Investigation of wind speeds over the ice islands (Figure 4.5-c,d) showed that the ice islands from all observations were subjected most frequently to weak winds (~1-3 $m\ s^{-1}$). Similarly, at the time of fracture events, the ice islands were most frequently subjected to weak winds (~2-4 $m\ s^{-1}$). The fact that there is little difference in these distributions suggests that wind speed by itself was not a significant variable in the fracture of ice islands. The comparison of ocean current speed records around the studied ice islands (Figure 4.5-e,f) revealed that the current speed values from the fracture subset were statistically greater than the full observational records. However, similar to all records, the fractured ice islands were mainly subjected to weak regional current speeds, which suggests minor contribution of current speed to the fracture event occurrence.
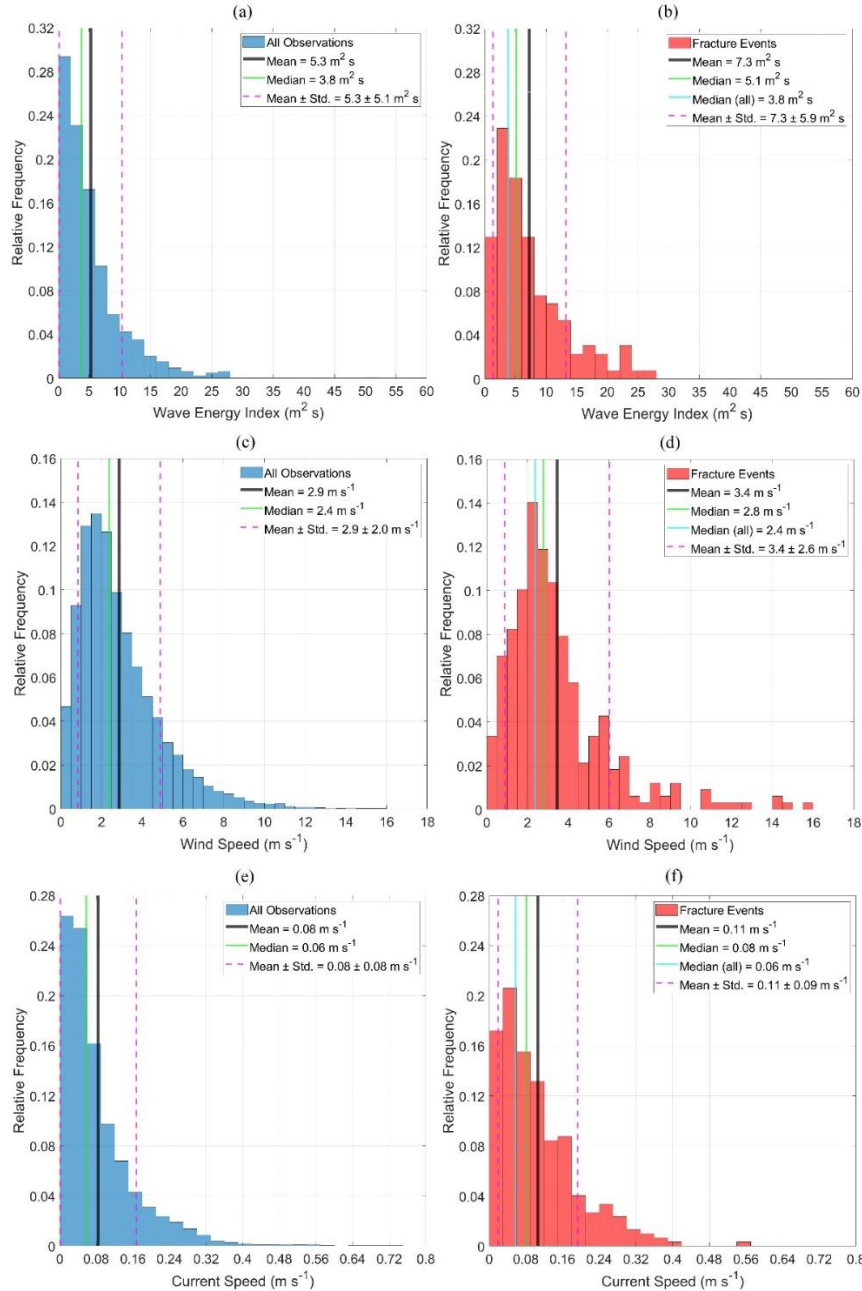
**Figure 4.5.** Relative frequency histogram plots of wave energy index (a; n=3985, b; n=131), wind speed (c; n=17735, d; n=328), and current speed (e; n=16791, f; n=296) surrounding Petermann ice islands for all observations (a,c,e), and for the fracture events (b,d,f).

The enhancement of fracture events under the conditions where the ice islands experienced higher values of metocean variables was investigated through ratios of the relative frequency for fracture events and all observations over the range of variables presented in Figure 4.3-Figure 4.5. These

114

results are presented in Appendix A (Figure 4A.1-Figure 4A.3), where values close to one imply that fracture events are as likely to occur as the frequency of observations. Values large compared to one indicate that fracture events are more likely to occur than the frequency of observations. Values less than one imply that fracture events are less likely to occur relative to the frequency of observations. The results in Figure 4A.1-Figure 4A.3 reveal that the ratio of the relative frequency for fracture events and all observations generally increases with the values of metocean variables, which clearly indicate a tendency for fracture events to occur under more extreme conditions.

The pairwise correlation between the metocean variables revealed that water temperature was positively correlated with the air temperature, a finding that was stated in a number of other studies (*e.g.*, Morrill et al., 2001; Erickson and Stefan, 2000). Table 4.3 also revealed a correlation between the wind speed and wave energy index, which was expected as the wave energy index is dependent on the significant wave height (Eqn. (4.1)). The positive correlation between wind speed and wave height was also stated in Fu et al. (2016). Other inter-relationships between the variables include the correlations between the daily-average air/water temperatures and the lifetime mean air/water temperatures. These correlations are expected given that the lifetime mean variables were defined as the time-average of daily-average variables over the life of each ice island.

**Table 4.3.** Pearson product-moment correlation coefficients of the metocean variables in the developed fracture model. The variables included water temperature ($T_w$), wind speed ($V_w$), air temperature ($T_a$), current speed ($V_c$), wave energy index ($E_w$), lifetime mean air temperature ($T_{a\_avg}$), and lifetime mean water temperature ($T_{w\_avg}$).

| Variable | $V_w$ | $T_a$ | $V_c$ | $T_w$ | $E_w$ | $T_{a\_avg}$ | $T_{w\_avg}$ |
|---|---|---|---|---|---|---|---|
| $V_w$ | 1 | | | | | | |
| $T_a$ | 0.132 | 1 | | | | | |
| $V_c$ | 0.097 | 0.079 | 1 | | | | |
| $T_w$ | 0.236 | 0.547 | 0.076 | 1 | | | |
| $E_w$ | 0.403 | 0.046 | 0.066 | 0.232 | 1 | | |
| $T_{a\_avg}$ | 0.216 | 0.650 | 0.145 | 0.581 | 0.097 | 1 | |
| $T_{w\_avg}$ | 0.265 | 0.366 | 0.153 | 0.847 | 0.297 | 0.647 | 1 |

The associated p-values for all correlations show significance at the level of 0.00005 (p-value<0.00005).

It should be noted here that correlation does not imply causation, but there is clearly an element of causation within the correlations noted above. Given the positive correlation between the temperature variables ($T_a, T_w, T_{a\_ave}, T_{w\_ave}$), it is expected that ice islands exposed to warm water temperatures also experience warm air temperatures and lifetime mean air and water temperatures, conditions that contribute to ice melting. The resulting ablation could lead to ice island gravitational change and trigger fracture events. Similarly, the positive correlation between $V_w$ and $E_w$ implies a high chance for simultaneously high states of wind speed and wave energy index. These variables are linked to the external forces acting on ice islands. While, strong winds increase the associated wind drag forces, large values of wave energy index result in higher forces from waves. These forces together contribute to the accumulation of stress in the ice island, which could ultimately exceed the local threshold of fracture energy and result in fracture events. Wave actions also play a role via the "footloose mechanism" (Wagner et al., 2014), which could result in the instability of the ice geometry and potentially lead to ice island fracture events.

### 4.5.3. Metocean Conditional Criteria Sets and Fracture Event Frequency

To examine the probability of fracture event occurrence in very high states of metocean conditions, a full set of model criteria associated with the atmospheric and oceanic conditions at the time of fracture events was obtained and presented as criteria set i=6 (Table 4.4), using the methodology described earlier. The same approach was employed to investigate the influence of simplifying the fracture model using fewer number of variables, and the results were presented by criteria sets i=1-5 in Table 4.4.

**Table 4.4.** Fracture model conditional criteria sets and the associated conditional probability ($P_{frac}$) for extreme conditions. The variables included water temperature ($T_w$), wind speed ($V_w$), air temperature ($T_a$), current speed ($V_c$), wave energy index ($E_w$), lifetime mean air temperature ($T_{a\_avg}$), and lifetime mean water temperature ($T_{w\_avg}$).

| Criteria Set i | $T_w$ (°C) | $V_w$ ($m\ s^{-1}$) | $T_a$ (°C) | $V_c$ ($m\ s^{-1}$) | $E_w$ ($m^2\ s$) | $T_{a\_avg}$ (°C) | $T_{w\_avg}$ (°C) | $P_{frac}$ (%) |
|---|---|---|---|---|---|---|---|---|
| 1 | >4 | | | | | | | 16 |
| 2 | >4 | >6 | | | | | | 28 |
| 3 | >4 | >6 | >7 | | | | | 45 |
| 4 | >4 | >6 | >7 | >0.1 | | | | 60 |
| 5 | >4 | >6 | >7 | >0.1 | >5 | | | 75 |
| 6 | >4 | >6 | >7 | >0.1 | >5 | >0 | >0 | 75 |

Table 4.4 has a predictive capability for the occurrence of fracture events for the Petermann ice islands under different extreme atmospheric and oceanic conditional criteria sets. For example, if the conditions associated with the criteria set i=2 hold (*i.e.*, water temperatures greater than 4 °C and wind speeds greater than 6 $m\ s^{-1}$), there is a 28% chance that these conditions lead the ice islands to fracture. To elaborate, criteria set i=2 accounts for only water temperature and wind speed, where there are five events from the fracture subset (328 events) and 18 events from all observations (17755 events) that meet the given criteria. Therefore, a conditional fracture

probability of 0.28 was obtained for this criteria set, as follows:

$$P(Frac|T_w > 4\,°C, V_w > 6\ m\ s^{-1}) = \frac{P_{frac} \times P(T_w > 4\,°C, V_w > 6\ m\ s^{-1}|Frac)}{P(T_w > 4\,°C, V_w > 6\ m\ s^{-1})}$$

$$= \frac{\frac{328}{17755} \times \frac{5}{328}}{\frac{18}{17755}} \approx 0.28\ , \tag{4.5}$$

Some features of the criteria sets presented in Table 4.4 and their associated fracture event probability are noteworthy. An important implication of the results in Table 4.4 is the predominant link between the daily-average variables (*i.e.*, $T_w$, $V_w$, $T_a$, $V_c$, and $E_w$) with the fracture event occurrence. When only the criteria for the air and water temperatures, wind and current speeds, and wave energy index are considered without accounting for the lifetime mean variables (criteria set i=5), 75% of all events meeting these criteria occurred for the ice islands from the fracture subset. However, when only the high states of one or two variables are considered, the fracture probability drops to less than 30%, which indicates the strong effect of concurrent atmospheric and oceanic conditions on the occurrence of ice island fracture events. Also, the criteria set i=6 in Table 4.4 reveals that, the addition of the lifetime mean variables did not increase the fracture probability above 75%. This is due to the fact that the criteria set i=5 narrowed down the atmospheric and oceanic conditions to a condition that already meets the criteria added in criteria set i=6, implying that the conditions presented in criteria set i=5 are enough to predict a fracture event probability up to 75%. It is worth noting that the criteria sets represented in Table 4.4 implicitly account for the inter-relationship between the variables. For example, the criteria set i=3, which considers high winds and high air/water temperatures, accounts for the correlation between air and water temperatures (Table 4.3), indicating that there is a high chance for the

coincident occurrence of high air and water temperatures. It is also important to note that Table 4.4 only shows the criteria sets associated with the fracture events of ice islands originating from the calving events of the Petermann Glacier in 2008, 2010, 2011, and 2012. If more data become available from other fracture events of the Petermann ice islands, where the fracture events occur under different combinational criteria sets of atmospheric and oceanic conditions, then the variable ranges, the number of criteria sets, and the fracture probabilities presented in Table 4.4 would need to be updated. Under such conditions, the model variables themselves could also be modified if additional variables (*e.g.*, sea ice concentration) were deemed to be important.

The atmospheric and oceanic conditional criteria sets presented in Table 4.4 only show some specific criteria sets for extreme conditions and clearly do not represent all possible combinations of the conditions. These criteria sets were selected by the progressive addition of one or two conditions to the previous criteria set, so that the associated conditional fracture probability would increase. However, to account for all possible conditions of the variables, the ranges for the atmospheric and oceanic variables were divided into two states using the methodology described earlier in Table 4.1. The elimination of current speed variable (as explained in the Sect. 2.3) reduced the number of state combinations from 128 to 64, which allowed for a greater number of occurrences for each combination of the states, with bin edges previously described in Table 4.1. Through an iterative process, the conditional fracture probability for each combination of the states was then calculated using Bayes' Theorem (Eqn. (4.3)). Due to the large number of elements (64 values) in the conditional probability table, it is not possible to illustrate all combinations of the variable states (Table 4.1) and their associated probability. So, the model description is limited to its qualitative part.

The results obtained from the presented Bayesian approach provide a framework to

probabilistically forecast the future fracture events of ice islands originally calved from the Petermann Glacier. This probabilistic model can provide supplementary information to the available deterministic ice dynamic prediction models by quantifying the probability of ice island fracture event occurrence under various sets of concurrent atmospheric and oceanic conditions. To use this model, one needs to first identify the spatial and temporal coordinates of a given ice island and then extract or forecast the six daily-average and lifetime mean variables discussed earlier. Then, the obtained set of conditions is identified in the developed conditional probability table to quantify the associated probability of fracture event occurrence under the given set of atmospheric and oceanic conditions.

### 4.5.4. Case Study

To better describe the utility of the developed fracture model, a case study was conducted on a descendant of ice islands resulting from the calving event of Petermann Glacier in 2010. This ice island was selected for a case study due to its drift characteristics. The ice island drifted for a long period (26 November 2010 – 5 July 2011; >7 months) and experienced a significant change in latitude (>15º). The spatial and temporal data for consecutive observations of this ice island were identified using the CI2D3 database. The atmospheric and oceanic variables were extracted from reanalysis databases and then interpolated to the positions and times of the given observations. The lifetime mean variables were also estimated using the methodology explained earlier, and the variables were all used as input to the presented fracture model to study the conditional fracture probabilities of the ice island over its drift path (Figure 4.6-a). To investigate the effect of different atmospheric and oceanic conditions on the fracture events of the same ice island, metocean data from 2017-2018 were extracted and interpolated to the same positions as the case study ice island. Here it was assumed that the same drift trajectory applies, however, this would not likely be the

case given that iceberg drift models are largely governed by the real-time metocean conditions (Lichey and Hellmer, 2001; Kubat et al., 2005; Eik, 2009; Keghouche et al., 2009; Rackow et al., 2017; Zeinali-Torbati et al., 2020). This would be, however, an area for future work, where a drift model needs to be integrated into the proposed fracture model to have a reliable estimation of ice island positional data. The interpolated metocean data for the 2017-2018 case were then used in the presented fracture model to investigate how the fracture probability map would change under the influence of different atmospheric and oceanic conditions (Figure 4.6-b). The fracture probability map for the 2010-2011 case (Figure 4.6-a) reveals that the ice island drifted some time (~14 days) in the medium-high fracture probability zone (shown by the orange and red colors around Labrador coast) before breaking up into two pieces. This, however, was not the case for the 2017-2018 ice island during the same time period (Figure 4.6-b) as this ice island only spent some time (~14 days) in the small-medium fracture probability zone (shown by the green and orange colors) towards the end of its hypothetical drift off Labrador coast, which could thus likely have been longer than the 2010-2011 drift. The hypothetical 2017-2018 ice island, in fact, never experienced the metocean conditions that lead to a probability of fracture <4%. This is likely due to the fact that the 2017-2018 ice island was generally exposed to lower water temperature (~0.3 °C on average) over its drift. This result is expected given that water temperature was identified as the most important contributor to the fracture events of Petermann ice islands analyzed in this study.
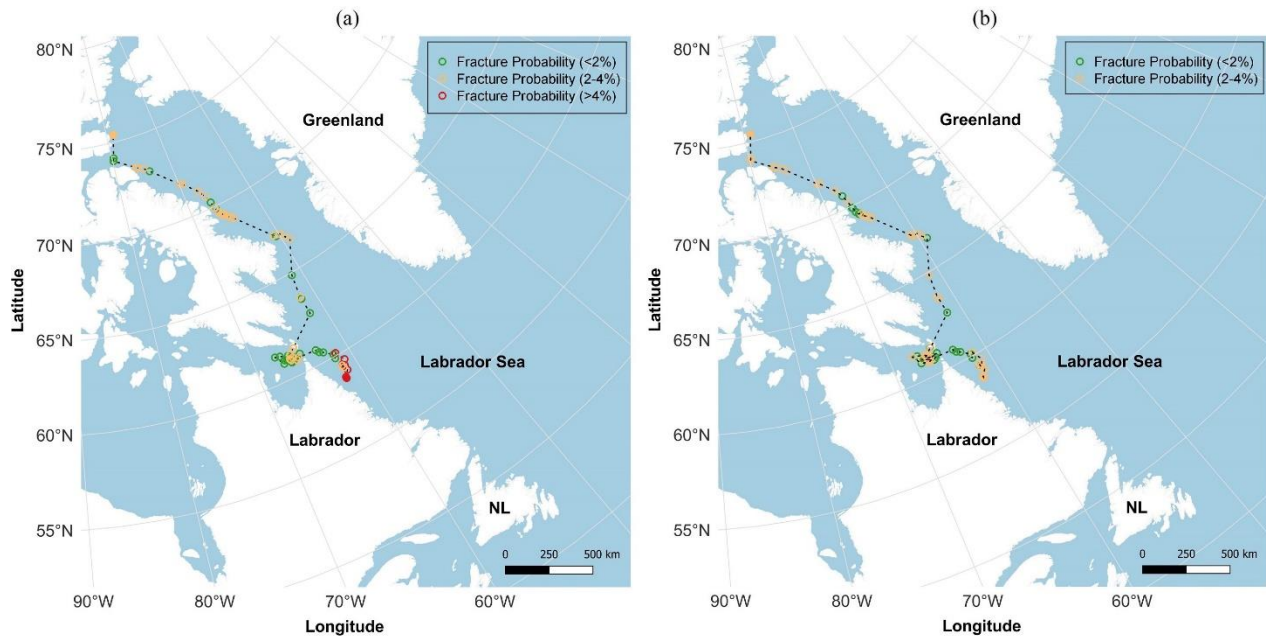
**Figure 4.6.** The fracture probability map for a descendant of the Petermann ice island from the 2010 calving event (a), compared against the projected fracture probabilities for the same ice island in 2017-2018 (b). The filled dots show the positions of the ice island at the time it was born and the time it fractured.

While a Bayesian network has never been employed for forecasting ice island fracture events, the probabilistic model presented in this paper was developed based on the methodology used in Turnbull et al. (2019) and Fu et al. (2016), where the Bayesian approach was used to predict vessel besetting events in pack ice. The study by Fu et al. (2016) used a Bayesian network to investigate the inter-relationship between nine variables (*i.e.*, ship speed, engine power, wind speed, air temperature, low visibility, sea temperature, ice concentration, ice thickness, and wave height), as well as their influence on the probability of a ship getting stuck in ice while navigating through the Northern Sea Route. Using a similar Bayesian approach, Turnbull et al. (2019) studied two pack ice besetting events of the Umiak I and developed a probabilistic forecast model for future besetting events experienced by Umiak I under the influence of nine ice and metocean variables (*i.e.*, ice concentration, ice thickness, floe size, minimum coast distance, wind-coast direction, wind speed, current-coast direction, current speed, and wind divergence). While this approach has

122

not been used in a past iceberg fracture model, there are some deterioration models such as the one by Kubat et al. (2007) that account for the influence of metocean variables (*e.g.*, wind speed, current speed, water temperature, wave height, and wave period) on the calving events of the overhanging slabs resulting from the repeated action of waves. Kubat et al. (2007) revealed that wave height and water temperature dominate effects on iceberg deterioration through melt and small-scale wave-induced calving events. However, the probabilistic model presented here accounts for the large-scale fracture events in ice islands under the influence of various metocean conditions that govern the occurrence of these events. To date, there has been limited research (*e.g.*, Bouhier et al., 2018) investigating the atmospheric and oceanic conditions that lead to the highest probability of large-scale iceberg fracture event occurrence. While the bulk volume loss model by Bouhier et al. (2018) can provide a representation of iceberg relative volume loss variation with sea surface temperature and iceberg velocity, it is not able to estimate iceberg fracture probability under the influence of environmental variables presented here. Therefore, it is difficult to provide a validation scheme that can appropriately compare the results of the presented Bayesian fracture model with an existing physical ice island fracture model. Hence, the presented model was validated using a well-known scheme in probabilistic data analysis studies, which was described in Sect. 4.4.3.

## 4.6. Probabilistic Model Validation

The developed fracture model was validated using k-fold cross-validation approach described in Sect. 4.4.3, and the results were presented in Table 4.5. The model validation analysis for the selected criteria sets in Table 4.5 reveal that the mean fracture probabilities estimated from the test subsets are in agreement with the mean estimations from the training subsets as the ranges for the fracture probability values overlap. Investigation of the errors between the pairwise (test vs.

training) fracture probability values show that the test sets selected using the 5-fold cross-validation approach are able to provide estimations that are, on average, within 13-39% of the values forecasted using the training sets. It was also revealed from the standard deviation values that the presented model is more reliable when a fewer number of variables or state combinations are considered (*e.g.*, criteria set i=1). This is because, as the number of variables or state combinations increases, there are fewer fracture events and the ranges of atmospheric and oceanic conditions become more constrained, so the number of events meeting these given criteria decreases. With fewer observations, there will be more variability and consequently a higher error in the predicted fracture probability values. If more fracture data in each criteria set become available, the model will become more robust and the error in fracture probability estimations is expected to reduce.

**Table 4.5.** Model validation for some of the criteria sets in the model (*e.g.,* criteria set i=5 shows one of the 64 state combinations of the six variables; criteria set i=4 represents one of the 16 state combinations of the four variables). The variables included water temperature ($T_w$), wind speed ($V_w$), air temperature ($T_a$), wave energy index ($E_w$), lifetime mean air temperature ($T_{a\_avg}$), and lifetime mean water temperature ($T_{w\_avg}$). Model error is derived through statistical comparison of fracture probability estimations from training sets and test sets, obtained using 5-fold cross-validation method.

| Criteria Set i | $T_w$ (°C) | $V_w$ ($m\,s^{-1}$) | $T_a$ (°C) | $E_w$ ($m^2\,s$) | $T_{a\_avg}$ (°C) | $T_{w\_avg}$ (°C) | $P_{frac\_training}$[1] (%) Mean | Std.[3] | $P_{frac\_test}$[1] (%) Mean | Std.[3] | *Pairwise* % *Error*[2] Test vs. Training | $P_{frac\_all}$[1] (%) |
|---|---|---|---|---|---|---|---|---|---|---|---|---|
| 1 | >-0.3 | | | | | | 3.3 | 0.1 | 3.4 | 0.4 | 13 | 3.3 |
| 2 | >-0.3 | >2.8 | | | | | 3.4 | 0.2 | 3.5 | 0.9 | 20 | 3.5 |
| 3 | >-0.3 | >2.8 | >-2.1 | | | | 3.8 | 0.3 | 3.8 | 1.2 | 24 | 3.8 |
| 4 | >-0.3 | >2.8 | >-2.1 | >5.1 | | | 6.1 | 0.6 | 6.0 | 2.4 | 33 | 6.2 |
| 5 | >-0.3 | >2.8 | >-2.1 | >5.1 | >-3.5 | >-0.7 | 6.5 | 0.9 | 6.6 | 3.4 | 39 | 6.7 |

[1] $P_{frac\_training}$, $P_{frac\_test}$, and $P_{frac\_all}$ represent the fracture probability estimations from the training subsets, test subsets, and all data points, respectively
[2] Relative error between the fracture probability estimations from the training and test subsets
[3] Standard deviation

The 5-fold cross-validation analysis presented in Table 4.5 only shows some of the possible combinations of variable states that were defined based on the median values of the model variables from the fracture subset (presented in Table 4.1). This corresponds to 1/2 one-variable combinations (i=1), 1/4 two-variable combinations (i=2), 1/8 three-variable combinations (i=3), 1/16 four-variable combinations (i=4), and 1/64 six-variable combinations (i=6). However, the model skill was also analyzed for the remaining combinations, and it was revealed that the model does not perform well under implausible combinations of the atmospheric and oceanic conditions, which are not likely to be encountered and do not hinder the model most of the time. As an example, the condition where $T_w > -0.3\,°C$, $V_w > 2.8\,m\,s^{-1}$, $T_a \leq -2.1\,°C$ ), $E_w > 5.1\,m^2\,s$, $T_{a\_avg} > -3.5\,°C$, and $T_{w\_avg} \leq -0.7\,°C$ was a very unlikely combination that only occurred once among all ice island observations, and no fracture event occurred under such conditions. Based on the extracted/interpolated metocean data for the full model with all six variables, 36 combinations (out of 64) never occurred, so the fracture probabilities under such conditions are unknown. However, the remaining 28 combinations that were met revealed a larger error (~100-200%) between the probability estimations from the training and test subsets, when the associated combination was unlikely to occur (<1%). For instance, due to the very few data points existing for these improbable combinations, there were some cases that were not observed in the test subsets but were observed only a few times in the training subsets, which inflated an error of 100%. However, our model showed higher reliability under plausible combination of metocean conditions, such as the criteria sets i=1-5 in Table 4.5 (13-39% error), or when fewer number of variables were used in the model that generated lower error between the probability estimations from the test and training subsets (*e.g.*, 11-97% for 1-4 variables).

## 4.7. Conclusions and Future Work

This study presented a probabilistic forecast model for the fracture events of ice islands through the analysis of the relative influences of atmospheric and oceanic forces. The recurrent deterioration of the ice islands originating from four recent calving events of Petermann Glacier were studied using the data in the CI2D3 database to probabilistically investigate the conditions that lead to fracture event occurrence of the ice islands. It was revealed in Figure 4.3 through Figure 4.5 that while fracture events generally occurred when the ice islands were subjected to more severe atmospheric and oceanic conditions (*e.g.*, high wind and current speed, air and water temperature, wave energy index, and lifetime mean air and water temperature), warm water temperature played the most important role in the large-scale fracture events of Petermann ice islands. The results also showed that ice islands subjected to high values of daily-average metocean variables (as specified in Table 4.4), are expected to have a 75% chance of fracturing. The model validation was performed using k-fold cross-validation approach based on the Pareto principle, and it was found that the error between the estimated fracture probabilities from training and test sets ranged from 13% when only water temperature criterion is considered, to 39% for the full set of criteria.

The results of this study provide an important step toward the development of a probabilistic forecast model for fracture events of ice islands. The model presented here was built on the fracture event data associated with the ice islands that originated from Petermann Glacier, and therefore applies only to specific ice islands which share similar ice strength properties. Ice islands from other glaciers may have higher or lower ice strength characteristics and could experience fracture events under narrower or wider ranges of metocean conditions than presented in this study. The atmospheric and oceanic conditions, and their corresponding fracture event probabilities presented

126

in Table 4.4 and Table 4.5 need to be updated if more deterioration data become available to improve the model accuracy. The atmospheric and oceanic conditions in the presented model were extracted from reanalysis datasets; however, for the presented model to have an operational forecast use, the metocean conditions and fracture event probabilities should be estimated using the inputs from deterministic models that have the ability to provide short-term forecasts. The results of this study can be used with a limited number of variables. For example, in case only daily-average wind and air/water temperature data for the ice islands are available, the model should be restricted to criteria sets i=1–3. Once more data become available (*e.g.*, wave and lifetime mean variables), then the probabilistic fracture event estimations may take into account the expanded criteria sets (*e.g.*, i=4-5).

Future work should focus on improving this model through expanding the deterioration database of Petermann ice islands, as well as evaluating the fracture event data associated with other ice islands. The presented model was developed based on the data from 328 fracture events; however, more data are needed to train and test this model. The probabilistic model presented here only considered two states for each variable to avoid model saturation given the limited number of data points. If more data become available, one can improve the model resolution by using a greater number of variable states (*e.g.*, three or four). While this study used seven input variables to develop a probabilistic fracture model, future research can also investigate the role of other variables such as sea ice concentration/thickness and ice island size on fracture events of ice islands. Also, the incorporation of in-situ measured metocean data can contribute significantly to further validation of the presented ice island fracture model. Finally, for this model to have a forecast capability for future ice island fracture events, the presented fracture model needs to be coupled with a drift model able to reliably forecast the positional data. The output of the presented

fracture model can generate fracture probability distributions over the forecast drift trajectory from an ice island drift model, which could serve as a framework to predict the most likely locations/times for fracture event occurrence. This would need to be coupled with a size distribution model to estimate the resulting mass of the ice island fragment (s) following a fracture event. The mass estimation would then need to be incorporated into a drift forecasting model until a fracture event is predicted, when the scheme iterates again. A probabilistic drift model for the Petermann ice islands in the CI2D3 database is currently under development by the same authors, which will then be integrated into the presented fracture model to ultimately present a coupled ice island drift and deterioration forecast model.

The research presented here fills some of the critical knowledge gaps in glacial ice deterioration forecasts. The results of this study provide an important step in characterizing the atmospheric and oceanic conditions that govern the large-scale fracture events of ice islands, which are important for improving the calibration of operational ice dynamics models. The increase in the air and water temperatures due to the climate change is expected to drive more frequent massive calving events of Petermann Glacier in the future (Münchow et al., 2016), which could lead to the generation of numerous drifting ice islands off the east coast of Canada. The ability to predict fracture events of these ice islands could contribute to the development of more reliable strategies to mitigate the risks associated with the presence of glacial ice features, which is necessary for supporting safe offshore operations and marine activities in the ice-prone waters off the east coast of Canada.

## 4.8.    Appendix A
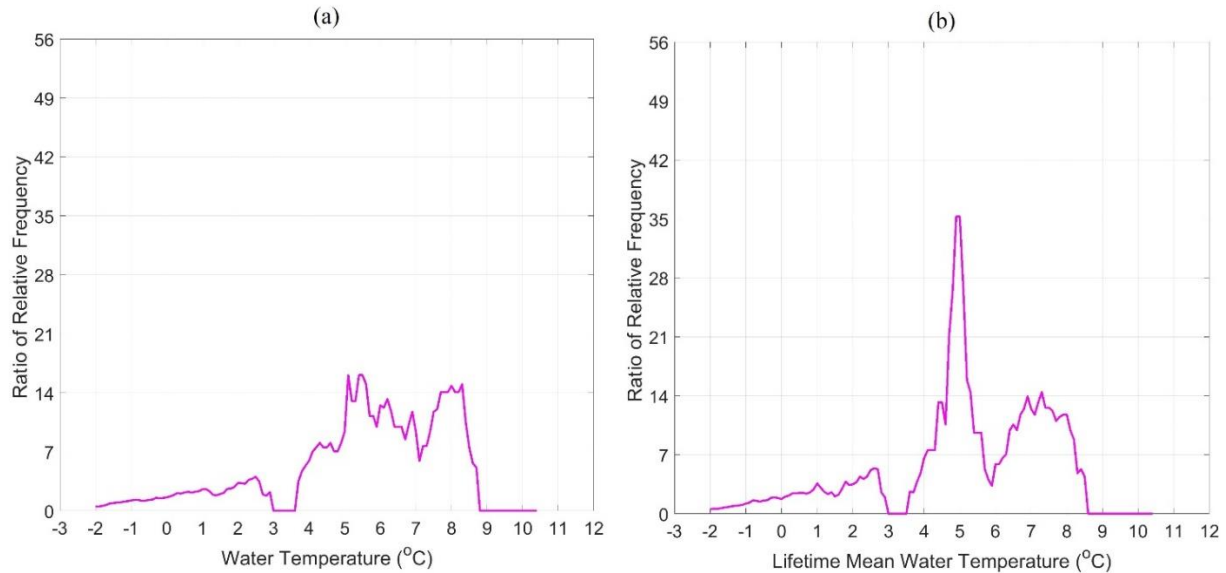


**Figure 4A.1.** The ratio of the relative frequency for fracture events and all observations over the range of water temperature (a) and lifetime mean water temperature (b) that surrounded Petermann ice islands. Values close to one implies that fracture events are as likely to occur as the frequency of observations. Values large compared to one indicates that fracture events are more likely to occur than the frequency of observations. Values less than one implies that fracture events are less likely to occur relative to the frequency of observations.
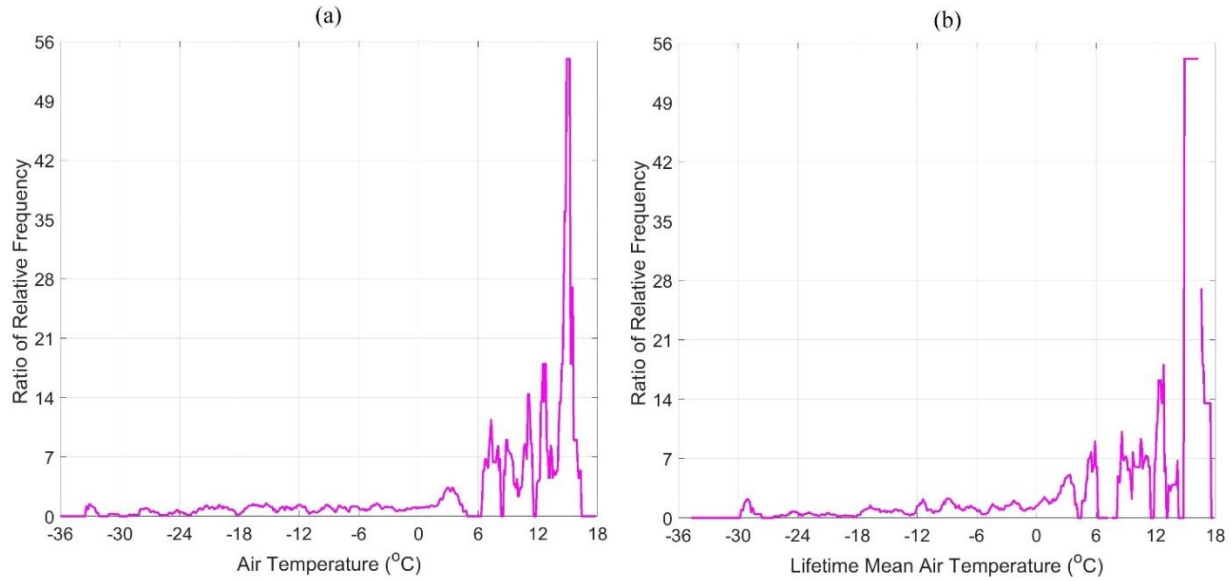
**Figure 4A.2.** The ratio of the relative frequency for fracture events and all observations over the range of air temperature (a) and lifetime mean air temperature (b) that surrounded Petermann ice islands. Values close to one implies that fracture events are as likely to occur as the frequency of observations. Values large compared to one indicates that fracture events are more likely to occur than the frequency of observations. Values less than one implies that fracture events are less likely to occur relative to the frequency of observations.
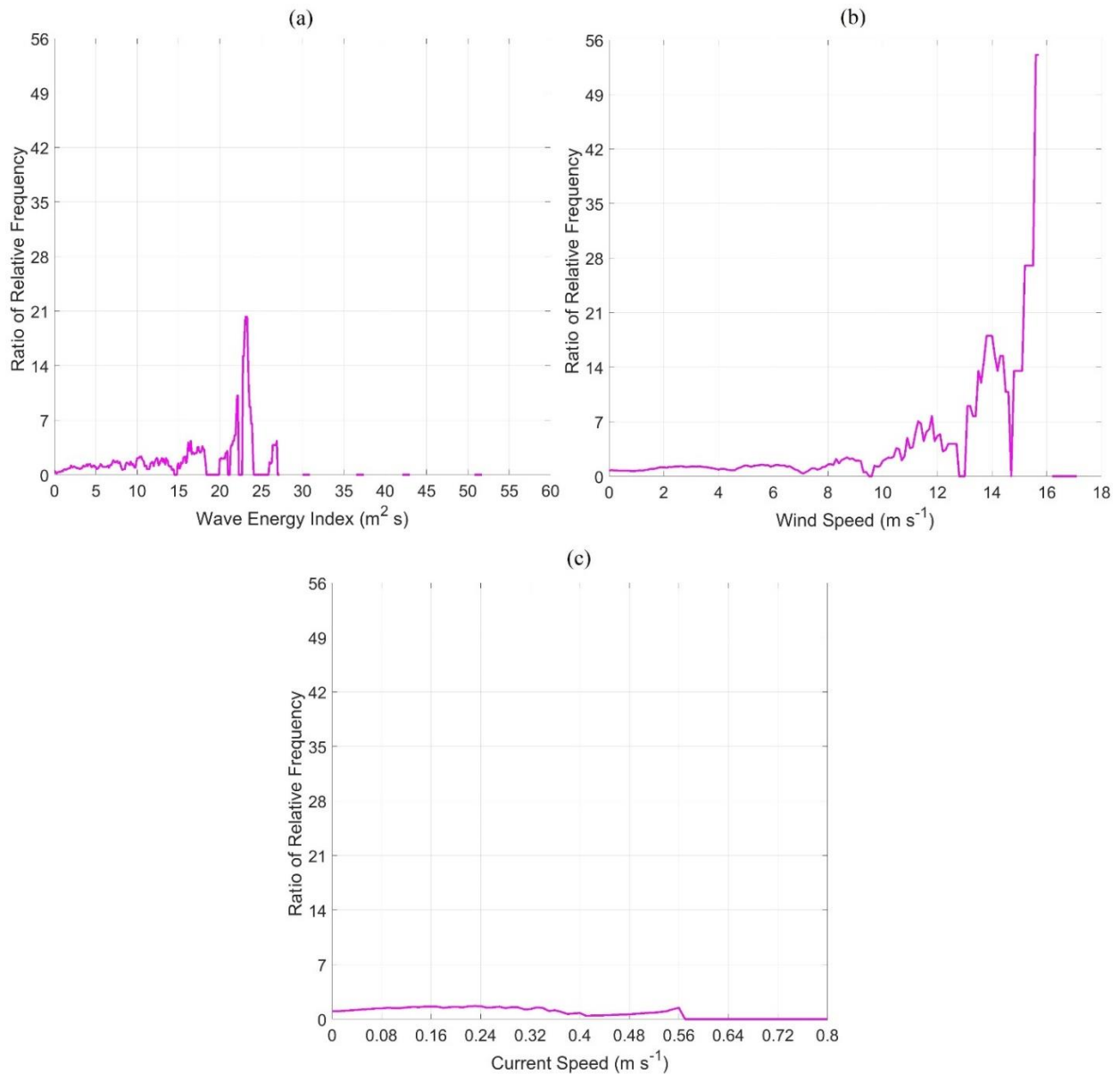
**Figure 4A.3.** The ratio of the relative frequency for fracture events and all observations over the range of wave energy index (a), wind speed (b), and current speed (c) that surrounded Petermann ice islands. Values close to one implies that fracture events are as likely to occur as the frequency of observations. Values large compared to one indicates that fracture events are more likely to occur than the frequency of observations. Values less than one implies that fracture events are less likely to occur relative to the frequency of observations.

***Data availability.*** The CI2D3 database and its documentation can be accessed at

http://dx.doi.org/10.21963/12678.

## 4.9.    References

Akpınar, A., Jafali, H., and Rusu, E. (2019). Temporal variation of the wave energy flux in hotspot areas of the black sea, Sustainability, 11(3), 562, https://doi.org/10.3390/su11030562.

Bahr, D. B. (1995). Simulating iceberg calving with a percolation model, Journal of Geophysical Research: Solid Earth, 100(B4), 6225-6232, https://doi.org/10.1029/94JB03133.

Ballicater Consulting Ltd. (2012). Ice Island and Iceberg Studies 2012, Report prepared for the Canadian Ice Service, Environment Canada, Report 12–01, pp. 51.

Barbat, M. M., Rackow, T., Hellmer, H. H., Wesche, C., and Mata, M. M. (2019). Three years of near-coastal Antarctic iceberg distribution from a machine learning approach applied to SAR imagery, Journal of Geophysical Research: Oceans, 124(9), 6658-6672, https://doi.org/10.1029/2019JC015205.

Bassis, J. N. and Jacobs, S. (2013). Diverse calving patterns linked to glacier geometry, Nature Geoscience, 6(10), 833-836, https://doi.org/10.1038/ngeo1887.

Bonafede, C. E. and Giudici, P. (2007). Bayesian networks for enterprise risk assessment, Physica A, 382(1), 22-28, https://doi.org/10.1016/j.physa.2007.02.065.

Bouhier, N., Tournadre, J., Rémy, F., and Gourves-Cousin, R. (2018). Melting and fragmentation laws from the evolution of two large Southern Ocean icebergs estimated from satellite data, The Cryosphere, 12(7), 2267-228, https://doi.org/10.5194/tc-12-2267-2018.

Christakos, K., Varlas, G., Cheliotis, I., Spyrou, C., Aarnes, O. J., and Furevik, B. R. (2020). Characterization of wind-sea-and swell-induced wave energy along the Norwegian coast, Atmosphere, 11(2), 166, https://doi.org/10.3390/atmos11020166.

Crawford, A. J. (2018). Ice island deterioration, PhD Dissertation, Department of Geography and Environmental Studies, Carleton University, Ottawa, Canada, https://doi.org/10.22215/etd/2018-13178.

Crawford, A. J., Mueller, D. R., Humphreys, E. R., Carrieres, T., and Tran, H. (2015). Surface ablation model evaluation on a drifting ice island in the Canadian Arctic, Cold Regions Science and Technology, 110, 170-182, https://doi.org/10.1016/j.coldregions.2014.11.011.

Crawford, A. J., Wadhams, P., Wagner, T. J., Stern, A., Abrahamsen, E. P., Church, I., Bates, R., and Nicholls, K. W. (2016). Journey of an Arctic ice island, Oceanography, 29(2), 254-263, https://doi.org/10.5670/oceanog.2016.30.

Crawford, A. J., Crocker, G., Mueller, D., Desjardins, L., Saper, R., and Carrieres, T. (2018a). The Canadian ice island drift, deterioration and detection (CI2D3) database, Journal of Glaciology, 1-5, https://doi.org/10.1017/jog.2018.36.

Crawford, A. J., Desjardins, L., Saper, R., Mueller, D., Stewart-Jones, E. (2018b). Canadian ice island drift, deterioration and detection (CI2D3) database documentation [v1.1], Water and Ice Research Laboratory, Carleton University, Ottawa, pp 19.

Crawford, A. J., Mueller, D., and Joyal, G. (2018c). Surveying drifting icebergs and ice islands: deterioration detection and mass estimation with aerial photogrammetry and laser scanning, Remote Sensing, 10(4), 575, https://doi.org/10.3390/rs10040575.

Crawford, A. J., Mueller, D., Desjardins, L., and Myers, P. G. (2018d). The aftermath of Petermann glacier calving events (2008–2012): ice island size distributions and meltwater dispersal, Journal of Geophysical Research: Oceans, 123(12), 8812-8827, https://doi.org/10.1029/2018JC014388.

Crawford, A. J., Mueller, D., Crocker, G., Mingo, L., Desjardins, L., Dumont, D., and Babin, M. (2020). Ice island thinning: rates and model calibration with in-situ observations from Baffin Bay, Nunavut, The Cryosphere, 14, 1067-1081, https://tc.copernicus.org/articles/14/1067/2020.

Crocker, G., Carrieres, T., and Tran, H. (2013). Ice island drift and deterioration forecasting in

eastern Canada. In Proceedings of the 22nd International Conference on Port and Ocean Engineering Under Arctic Conditions, Espoo, Finland, 9-13 June 2013.

Desjardins, L., Crawford, A., Mueller, D., Saper, R., Schaad, C., Stewart-Jones, E., and Shepherd, J. (2018). Canadian ice island drift, deterioration and detection database (CI2D3 database) [v1.1], Canadian Cryospheric Information Network (CCIN), Waterloo, Canada, http://dx.doi.org/10.21963/12678.

Diemand D., Nixon W. A., and Lever J. H. (1987). On the splitting of icebergs - natural and induced, In proceedings of the 6th International Conference on Ocean, Offshore and Arctic Engineering, Houston, Texas, USA.

Eik, K. (2009). Iceberg drift modelling and validation of applied metocean hindcast data. Cold Regions Science and Technology, 57(2-3), 67-90, https://doi.org/10.1016/j.coldregions.2009.02.009.

Eleye-Datubo, A. G., Wall, A., Saajedi, A., and Wang, J. (2006). Enabling a powerful marine and offshore decision-support solution through Bayesian network technique, Risk Analysis, 26(3), 695-721, https://doi.org/10.1111/j.1539-6924.2006.00775.x.

El-Tahan, M., Venkatesh, S., and El-Tahan, H. (1987). Validation and quantitative assessment of the deterioration mechanisms of Arctic icebergs, Journal of Offshore Mechanics and Arctic Engineering, 109(1), 102-108, https://doi.org/10.1115/1.3256983.

Enderlin, E. M., Hamilton, G. S., Straneo, F., and Sutherland, D. A. (2016). Iceberg meltwater fluxes dominate the freshwater budget in Greenland's iceberg-congested glacial fjords, Geophysical Research Letters, 43(21), 11-287, https://doi.org/10.1002/2016GL070718.

England, M. R., Wagner, T. J., and Eisenman, I. (2020). Modeling the breakup of tabular icebergs, Science Advances, 6(51), eabd1273, https://doi.org/10.1126/sciadv.abd1273.

Erickson, T. R. and Stefan, H. G. (2000). Linear air/water temperature correlations for streams during open water periods, Journal of Hydrologic Engineering, 5(3), 317-321, http://dx.doi.org/10.1061/(ASCE)1084-0699(2000)5:3(317).

Falnes, J. (2007). A review of wave-energy extraction, Marine Structures, 20(4), 185-201, https://doi.org/10.1016/j.marstruc.2007.09.001.

Freedman, D. A. (2010). Statistical models and causal inference: a dialogue with the social sciences, Cambridge University Press, https://doi.org/10.1017/CBO9780511815874.

Fu, S., Zhang, D., Montewka, J., Yan, X., and Zio, E. (2016). Towards a probabilistic model for predicting ship besetting in ice in Arctic waters, Reliability Engineering and System Safety, 155, 124-136, https://doi.org/10.1016/j.ress.2016.06.010.

Fuglem M., Jordaan I. (2017). Risk analysis and hazards of ice islands, In: Copland L., Mueller D. (eds) Arctic Ice Shelves and Ice Islands, Springer Polar Sciences, Springer, Dordrecht, https://doi.org/10.1007/978-94-024-1101-0_15.

Gutierrez, B. T., Plant, N. G., and Thieler, E. R. (2011). A Bayesian network to predict coastal vulnerability to sea level rise, Journal of Geophysical Research: Earth Surface, 116(F2), https://doi.org/10.1029/2010JF001891.

Halliday, E. J., King, T., Bobby, P., Copland, L., and Mueller, D. R. (2012). Petermann ice island 'A' survey results, offshore Labrador, In Proceedings of the Arctic Technology

Conference, Houston, Texas, USA, 3-5 December 2012, OTC 23714, https://doi.org/10.4043/23714-MS.

Hock, R. (2003). Temperature index melt modeling in mountain areas, Journal of Hydrology, 282, 104–115, https://doi.org/10.1016/S0022-1694(03)00257-9.

Jeffries, M. O. (2002). Ellesmere Island ice shelves and ice islands, Satellite Image Atlas of Glaciers of the World: Glaciers of North America - Glaciers of Canada, U.S. Geological Survey Professional Paper 1386-J-1, J147-J164.

Job, J. G. (1978). Numerical modelling of iceberg towing for water supplies—A case study, Journal of Glaciology, 20(84), 533-542, https://doi.org/10.3189/S002214300002092X.

Johannessen, O. M., Babiker, M., and Miles, M. W. (2011). Petermann Glacier, North Greenland: massive calving in 2010 and the past half century, The Cryosphere Discussions, 5(1), 169-181, https://doi.org/10.5194/tcd-5-169-2011.

Keghouche, I., Bertino, L., and Lisæter, K. A. (2009). Parameterization of an iceberg drift model in the Barents Sea, J. Atmos. Oceanic Technol., 26(10), 2216-2227, https://doi.org/10.1175/2009JTECHO678.1.

Kubat, I., Sayed, M., Savage, S. B., and Carrieres, T. (2005). An operational model of iceberg drift, International Journal of Offshore and Polar Engineering, 15(2), 125-131.

Kubat, I., Sayed, M., Savage, S.B., Carrieres, T., and Crocker, G. (2007). An operational iceberg deterioration model, In Proceedings of the 17th International Offshore and Polar Engineering Conference, Lisbon, Portugal, 1-6 July 2007, 652-657.

Lichey, C. and Hellmer, H. H. (2001). Modeling giant-iceberg drift under the influence of sea ice in the Weddell Sea, Antarctica, Journal of Glaciology, 47(158), 452-460, https://doi.org/10.3189/172756501781832133.

Macek, K. (2008). Pareto principle in datamining: an above-average fencing algorithm, Acta Polytechnica, 48(6), 55-59, https://doi.org/10.14311/1075.

Merino, N., Le Sommer, J., Durand, G., Jourdain, N. C., Madec, G., Mathiot, P., and Tournadre, J. (2016). Antarctic icebergs melt over the Southern Ocean: Climatology and impact on sea ice, Ocean Modelling, 104, 99-110, https://doi.org/10.1016/j.ocemod.2016.05.001.

Montewka, J., Sinclair, H., Kujala, P., Haapala, J., and Lensu, M. (2013). Modelling ship performance in ice using Bayesian networks, In Proceedings of the 22<sup>nd</sup> International Conference on Port and Ocean Engineering under Arctic Conditions, 9-13 June 2013.

Montewka, J., Goerlandt, F., Kujala, P., and Lensu, M. (2015). Towards probabilistic models for the prediction of a ship performance in dynamic ice, Cold Regions Science and Technology, 112, 14-28, https://doi.org/10.1016/j.coldregions.2014.12.009.

Morrill, J. C., Bales, R. C., and Conklin, M. H. (2001). The relationship between air temperature and stream temperature, In AGU Spring Meeting Abstracts, 2001, H42A-09.

Mueller, D. R., Crawford, A., Copland, L., and Van Wychen, W. (2013). Ice island and iceberg fluxes from Canadian High Arctic sources, Report to the Northern Transportation Assessment Initiative, Innovation Policy Branch, Transport Canada, Ottawa, Canada. https://www.researchgate.net/publication/340183882_Ice_Island_and_Iceberg_Fluxes_from_Canadian_High_Arctic_Sources_Prepared_for_the_Innovation_Policy_Group_of_Tr

ansport_Canada.

Münchow, A., Padman, L., Washam, P., and Nicholls, K. W. (2016). The ice shelf of Petermann
Gletscher, North Greenland, and its connection to the Arctic and Atlantic Oceans,
Oceanography, 29(4), 84–95, https://doi.org/10.5670/oceanog.2016.101.

Nick, F. M., Luckman, A., Vieli, A., Van der Veen, C. J., Van As, D., Van De Wal, R. S. W.,
Pattyn, F., Hubbard, A. L., and Floricioiu, D. (2012). The response of Petermann Glacier,
Greenland, to large calving events, and its future stability in the context of atmospheric and
oceanic warming, Journal of Glaciology, 58(208), 229-239,
https://doi.org/10.3189/2012JoG11J242.

Ozdemir, S. (2016). Principles of Data Science (1st ed.), Packt Publishing.

Peterson, I. K. (2011). Ice island occurrence on the Canadian East Coast, In Proceedings of the
21st International Conference on Port and Ocean Engineering under Arctic Conditions,
Montreal, Canada, 10-14 July 2011.

Rackow, T., Wesche, C., Timmermann, R., Hellmer, H. H., Juricke, S., and Jung, T. (2017). A
simulation of small to giant Antarctic iceberg evolution: Differential impact on climatology
estimates, Journal of Geophysical Research: Oceans, 122(4), 3170-3190,
https://doi.org/10.1002/2016JC012513.

Saper, R. (2011). Preliminary research plan for glacial ice hazards, Report prepared for the
Canadian Ice Service, Marine and Ice Services Division, Environment Canada, Ottawa,
Canada, pp. 40. https://wirl.carleton.ca/wp-content/uploads/2017/09/Saper2011.pdf.

Savage, S. B. (2001). Aspects of iceberg deterioration and drift, In Geomorphological Fluid Mechanics, Springer, Berlin, Germany, 589, 279-318, https://doi.org/10.1007/3-540-45670-8_12.

Sazidy, M., Crocker, G., and Mueller, D. (2019). A 3D numerical model of ice island calving due to buoyancy-driven flexure, In Proceedings of the 25th International Conference on Port and Ocean Engineering under Arctic Conditions, Delft, The Netherlands, 9-13 June 2019.

Scambos, T., Sergienko, O., Sargent, A., MacAyeal, D., and Fastook, J. (2005). ICESat profiles of tabular iceberg margins and iceberg breakup at low latitudes, Geophysical Research Letters, 32(23), https://doi.org/10.1029/2005GL023802.

Smith, J. (2020). Modelling ice island calving events with Finite Element Analysis, Master's Thesis, Department of Geography and Environmental Studies, Carleton University, Ottawa, Canada, https://doi.org/10.22215/etd/2020-13905.

Stern, A. A., Johnson, E., Holland, D. M., Wagner, T. J., Wadhams, P., Bates, R., Abrahamsen E. P., Nicholls, K. W., Crawford A., Gagnon, J., and Tremblay, J. E. (2015). Wind-driven upwelling around grounded tabular icebergs, Journal of Geophysical Research: Oceans, 120(8), 5820-5835, https://doi.org/10.1002/2015JC010805.

Stern, A. A., Adcroft, A., and Sergienko, O. (2016). The effects of Antarctic iceberg calving-size distribution in a global climate model, Journal of Geophysical Research: Oceans, 121(8), 5773-5788, https://doi.org/10.1002/2016JC011835.

Stern, A. A., Adcroft, A., Sergienko, O., and Marques, G. (2017). Modeling tabular icebergs submerged in the ocean, Journal of Advances in Modeling Earth Systems, 9(4), 1948-1972,

https://doi.org/10.1002/2017MS001002.

Stuart, A. and Ord, K. (1994). Kendall's Advanced Theory of Statistics, Volume 1: Distribution Theory, 6th Edition, Edward Arnold, London.

Suthaharan, S. (2016). Machine learning models and algorithms for big data classification, Integrated Series in Information Systems, 36, 1-12, https://doi.org/10.1007/978-1-4899-7641-3.

Tournadre, J., Bouhier, N., Girard-Ardhuin, F., and Rémy, F. (2016). Antarctic icebergs distributions 1992–2014, Journal of Geophysical Research: Oceans, 121(1), 327-349, https://doi.org/10.1002/2015JC011178.

Turnbull, I. D., Bourbonnais, P., and Taylor, R. S. (2019). Investigation of two pack ice besetting events on the Umiak I and development of a probabilistic prediction model, Ocean Engineering, 179, 76-91, https://doi.org/10.1016/j.oceaneng.2019.03.030.

Wagner, T. J., Wadhams, P., Bates, R., Elosegui, P., Stern, A., Vella, D., Abrahamsen, E. P., Crawford, A., and Nicholls, K. W. (2014). The "footloose" mechanism: Iceberg decay from hydrostatic stresses, Geophysical Research Letters, 41(15), 5522-5529, https://doi.org/10.1002/2014GL060832.

Wagner, T. J., Dell, R. W., and Eisenman, I. (2017). An analytical model of iceberg drift, Journal of Physical Oceanography, 47(7), 1605-1616, https://doi.org/10.1175/JPO-D-16-0262.1.

Waters, R. (2008). Energy from ocean waves: full scale experimental verification of a wave energy converter, Doctoral Dissertation, Uppsala University, Sweden.

White, F. M., Spaulding, M. L., and Gominho, L. (1980). Theoretical estimates of the various mechanisms involved in iceberg deterioration in the open ocean environment, U.S. Coast Guard Research and Development Center Report, pp. 126.

Zeinali-Torbati, R., Turnbull, I. D., Taylor, R. S., and Mueller, D. (2019). The calving events of Petermann glacier from 2008 to 2012: ice island drift characteristics, assessment of fracture events, and geographical data analysis. In Proceedings of the 38th International Conference on Ocean, Offshore and Arctic Engineering, Glasgow, Scotland, UK, https://doi.org/10.1115/OMAE2019-96732, 9-14 June 2019.

Zeinali-Torbati, R., Turnbull, I. D., Taylor, R. S., and Mueller, D. (2020). Evaluation of the relative contribution of meteorological and oceanic forces to the drift of ice islands offshore Newfoundland, Journal of Glaciology, 66(256), 203-218, https://doi.org/10.1017/jog.2019.96.

Zhang, D., Yan, X. P., Yang, Z. L., Wall, A., and Wang, J. (2013). Incorporation of formal safety assessment and Bayesian network in navigational risk estimation of the Yangtze River, Reliability Engineering and System Safety, 118, 93-105, https://doi.org/10.1016/j.ress.2013.04.006.

# 5. PROBABILISTIC DRIFT PREDICTION OF PETERMANN ICE ISLANDS UNDER THE INFLUENCE OF METEOROLOGICAL AND OCEANOGRAPHIC VARIABLES

## 5.1. Preface

This chapter aims to improve glacial ice dynamics models by building on the ice island deterioration model presented in chapter 4, through developing a probabilistic model for the drift velocity of ice islands. The chapter provides a review of the available ice island drift models, uses the CI2D3 database, analyzes the relative influence of atmospheric and oceanic conditions on the drift of ice islands, and presents a probabilistic Bayesian drift forecasting model that can estimate probabilities for the drift speeds and directions of Petermann ice islands as they drift under various metoecan conditions.

This chapter will be submitted as an original research paper to a scientific journal. As the main author of this article, I carried out the literature review, developed the drift probabilistic model, conducted the analysis, and wrote the manuscript. My co-authors, Dr. Ian Turnbull, Dr. Rocky Taylor, and Dr. Derek Mueller contributed to the identification of the research topic and provided consistent guidance and suggestions at different stages of the model development and preparation of the paper. I revised the manuscript based on their suggestions, accordingly, but it may undergo another minor revision before submission to a journal.

## 5.2. Abstract

Economic activities such as shipping, offshore renewable and non-renewable energy developments, fishing, and other activities in the ice environment in the eastern Canadian waters

must contend with the risk from the icebergs and ice islands in the region. The associated risk may be mitigated by applying appropriate operational ice management strategies, which require improved drift-forecasting models that are able to provide reliable estimates of iceberg velocities as they drift under the influence of meteorological and oceanographic forces. Improved knowledge of ice island drift and deterioration may also reduce risks through informing policy and strategic frameworks for regulating shipping and energy developments. This study presents a novel Bayesian approach to provide probabilistic ice island drift-forecasting models via studying the conditional dependence of ice island drift speeds and directions on the atmospheric and oceanic conditions that govern their drifts. The Canadian Ice Island Drift, Deterioration and Detection (CI2D3) database was used to extract the positional and temporal data and estimate the drift velocities for the ice islands that originated from the calving events of the Petermann Glacier in 2008-2012. The variables that influence ice island drifts were extracted from reanalysis databases and interpolated spatially and temporally to the positions and times of the observed ice islands in the CI2D3 database to study their distributions for various ice islands with different drift velocities (states). The drift probability in each state of the ice island drift velocity was estimated using the Bayes' theorem. From this analysis, it was revealed that when currents are strong, ice islands mainly tend to drift at speeds >0.1 $m\ s^{-1}$ and within close proximity to the direction of the ocean currents. The approach used in the model development was validated using the k-fold cross-validation scheme and based on the Pareto principle, and a mean error of less than 30% was revealed for most of the drift probability estimations. The predictive capability of the developed drift model makes it a promising tool for probabilistic estimation of future ice island drift velocities. Further validation of the presented model is recommended to operationalize the drift-forecasting model of ice risk in support of offshore and marine activities.

## 5.3. Introduction

The presence glacial ice features in the Arctic and Atlantic oceans can impact ocean economy through disruption of activities related to aquaculture, fishery, shipping, offshore renewable and non-renewable energy, and coastal infrastructures. Such activities in ice environments need to contend with the risk of ice interaction. One type of such ice features in eastern and northeastern Canadian waters is the presence of ice islands (large tabular icebergs), which poses challenges to the design of vessels and structures (Fuglem and Jordaan, 2017; Mueller et al., 2013; Newell, 1993). Also, these glacial ice features sometimes ground on shallow areas such as the continental shelf of Baffin Island (Wagner et al., 2014), which can influence the ecosystems of benthic zones (Dowdeswell and Bamber, 2007), damage subsea cables and other seafloor infrastructure (Sackinger et al., 1988), and alter the composition of local water due to the freshwater influx caused by ice melting (Jansen et al., 2007). These regions, therefore, require improved ice prediction capability to enable safe and cost-effective operations. Such models should account for key physical inputs that influence the drift characteristics and dynamics of icebergs and ice islands.

Glacial ice drift models, in general, can be categorized into short-term (<12 hours), intermediate-term (1-5 days), and long-term (3-6 months) forecasts, which can be used for ice management within 30 km of an offshore activity, prediction of regional iceberg distribution, and advanced forecasts of iceberg severity for resource planning, respectively (Marko et al., 1988). The drift of glacial ice has been widely modelled using theoretical approaches in which the forcing due to various atmospheric and oceanic variables are integrated into Newton's second law equation to estimate the ice velocity (Keghouche et al., 2009; Allison et al., 2014; Turnbull et al., 2015). To solve these Newtonian equations, past studies (*e.g.*, Lichey and Hellmer, 2001; Kubat et al., 2005) used numerical approaches that require the ice prior velocity, or analytical solutions (Wagner et

al., 2017). The reliability of such theoretical models is generally limited due to the irregularities in the geometry of glacial ice features, usually resulted from fracture or rolling events (Kubat et al., 2007), as well as inherent variability in natural processes and driving forces. These models are strongly limited by their reliance on accurate input forcing data, resulting in the propagation of errors in modeled iceberg drift trajectory when input variables are inaccurate (Baadshaug, 2018). Probabilistic drift models, however, can present the output as a range of possible drift velocities based on the given input variables. It is, therefore, important to calibrate and combine these deterministic approaches with probabilistic methods to improve understanding of dominant driving forces, sensitivity to input uncertainties, and assessment of the reliability of drift models. To this end, in this chapter the aim is to present a probabilistic forecast model for the drift of ice islands using inputs from various atmospheric and oceanic variables.

### 5.3.1.  Past Iceberg Drift Studies

One of the initial models for iceberg drift was developed by Sodhi and El-Tahan (1980), where the authors presented a numerical model for the drift trajectories of five icebergs using inputs from the local winds and currents only. Another early study (Smith and Banke, 1983) presented an iceberg drift model governed by three variables; wind, ocean current, and Coriolis effect. Later in 1997, an improved deterministic iceberg model was presented which accounted for the effect of more forces (*e.g.*, wave radiation, sea ice drag, pressure gradient due to iceberg displacement) on the drift trajectories of icebergs in North Atlantic and Arctic Ocean (Bigg et al., 1997). In a similar deterministic model, Lichey and Hellmer (2001) investigated the relative influence of various environmental forces including sea surface tilt and sea ice on the drift of a giant iceberg in Antarctica, where the exerted force by sea ice was modelled using a piecewise concentration-dependent relationship. An operational drift model for icebergs was presented by Kubat et al.

146

(2005), which incorporated a more accurate input from water drag force by accounting for the distribution of the currents over the iceberg keel. Kubat et al. (2005) also performed a sensitivity study and revealed that ocean currents significantly impact the drift trajectory of icebergs. The important contribution of ocean currents to iceberg drift was observed in another study (Eik, 2009), where a numerical drift model was presented to investigate the drift of icebergs in Barents Sea using data from tracking beacons, as well as the measured inputs from winds, currents, waves. In a similar study but with modelled inputs, Keghouche et al. (2009) evaluated the drift of icebergs in Barents Sea under the influence of different metocean forces, and identified the pronounced influence of wind, current, and Coriolis forces on iceberg drift. Crocker et al. (2013) studied the drift of a large Petermann ice island using a satellite tracking buoy and presented a deterministic drift model similar to the operational model presented by Kubat et al. (2005), but with modified geometry and minor adjustments to model physics. The authors stated that their hindcast model resulted in a slight improvement, but its performance for short-term forecasts was still poor and the model underpredicted the ice island drift speeds when the ocean currents were weak. An operational drift model was presented by Turnbull et al. (2015), who developed a short-term trajectory forecast model for 73 icebergs in Baffin Bay based on the in-situ measured inputs. The authors observed that the model performed well when the regional ocean currents were strong and identified ocean currents as the dominant variable for obtaining a reliable forecast model (Turnbull et al., 2015). Rackow et al. (2017) simulated the drift of tabular Antarctic icebergs in three size (length) categories (small, ≤2.2 km; medium, ≤10 km; large, >10 km) using theoretical models, and revealed that while small iceberg trajectories are mostly influenced by winds and currents, large icebergs are mainly driven by sea surface tilt. The drift of tabular Antarctic icebergs was also studied by Stern et al. (2017), where, unlike the previous studies that considered icebergs as point

particles, the icebergs were modelled by numerical bonds between smaller elements. The authors accounted for metocean forces as well as the interaction force from other elements and noted that iceberg drift velocities were mainly determined by wind velocities (Stern et al. 2017). Zeinali-Torbati et al. (2020) used tracking beacon data and investigated the drift of four ice island fragments offshore Newfoundland to quantify the relative contribution of atmospheric and oceanic forces to the drift of ice islands. It was revealed in Zeinali-Torbati et al. (2020) that while wind played a minor role, ocean currents and sea surface tilt contributed the most to the drift of the studied ice islands.

Most of the previous studies have used tracking beacon data for estimation of iceberg drift velocity, but the logistical challenges of in-situ positional and temporal data collection in ice-covered waters make it difficult to develop a large database for a probabilistic drift analysis. An alternative way for estimations of the drift velocity for icebergs and ice islands is using satellite images that can provide positional data for successive observations of such ice features. Ice islands, specifically, are large in extent and can be easily identified in remote sensing observations. Spaceborne synthetic aperture radar (SAR) imaging has enabled researchers to track ice features in various atmospheric conditions (Jeffries, 2002). Recently, researchers at Carleton University; Water and Ice Research Laboratory (WIRL) analyzed thousands of archived SAR images from Canadian Ice Service (CIS) and developed the Canadian Ice Island Drift, Deterioration, and Detection (CI2D3) database (Desjardins et al., 2018) to capture the drift trajectories and fracture events of the ice islands that resulted from the calving events of Petermann Glacier in 2008, 2010, 2011, and 2012 and other glaciers such as Ryder, Steensby, C.H. Ostenfeld, and north Greenland. Numerous ice islands resulted from the calving events of Petermann Glacier during 2008-2012, which drifted through Nares Strait, Baffin Bay, Davis Strait, and the Labrador Sea. Ice islands >0.25 km$^2$ were

tracked from summer 2008 to the end of 2013, which allowed for analyzing most of the descendants from 2008, 2010, and 2011 calving events. For the case of the 2012 ice islands, however, the CI2D3 database included the descendants that constituted only 30% of the total original calved ice island surface area (Crawford et al., 2018a). This database was previously used by Crawford et al. (2018a) to study the size distributions and meltwater contributions of the Petermann ice islands, and fracture events were identified to have a predominant influence on the overall deterioration of the monitored ice islands. While smaller Petermann ice islands comprised most of the ice island population, larger ice islands contributed the most to the overall mass and meltwater (Crawford et al., 2018a). The CI2D3 database was also employed in Zeinali-Torbati et al. (2021) to develop a probabilistic fracture forecast model that can quantify the probability of ice island fracture events under the influence of various metocean conditions, where water temperature was identified as the most predominant variable behind the large-scale fracture events of Petermann ice islands. The present study exploits the available data in the CI2D3 database to build on the work by Zeinali-Torbati et al. (2021) to develop an ice island drift forecast model. A probabilistic model has been developed using a Bayesian approach to predict the drift speeds and directions of ice islands under the influence of the most salient physical processes that govern their motions.

## 5.4. Methodology

### 5.4.1. Extraction of Spatial/Temporal Data and Ice Island Velocities

The CI2D3 database was originally developed by the Water and Ice Research Laboratory (WIRL) at Carleton University with collaboration from the Canadian Ice Service (CIS). The most recent version of the database (v1.1) is available at

149

, which includes various types of polygon and geospatial data (*e.g.*, area, length, latitude, longitude, time, etc.) on 25,364 ice island observations originated from various glaciers (*e.g.*, Ryder, Steensby, C.H. Ostenfeld, and north Greenland). However, the data associated with the Peterman ice islands constituted about 70% of all observations and are the dominant source in the database. In this study, only ice islands that resulted from calving events of the Petermann Glacier are considered (2008-2012), which accounted for a total loss of about 487 km$^2$ from the glacier (Crawford et al., 2018b). The CI2D3 database shapefile was exported to Matlab version R2019a to extract the positional and temporal data for 17,755 polygons related to the ice islands originated from the Petermann Glacier in 2008-2012. A Matlab script was developed to estimate the ice island velocities using the extracted latitudes, longitudes, and times for consecutive ice island observations. The estimated velocities were filtered using a threshold value of 0.02 $m\ s^{-1}$ to exclude grounded features. Also, velocities that were estimated based on a large time gap (beyond two days) between successive ice island observations were excluded from further analysis to allow for more reliable ice velocity estimations. It is worth noting that ice island drift period in this study was defined as the interval between two successive break-up events that are recorded in the database. Based on this definition, the drift of 845 Petermann ice islands created as a result of 328 fracture events have been considered in this study. As fracture events occurred, the mother-daughter relationship and previous observations of each ice island were identified using hierarchical attribute fields in the CI2D3 database that tie subsequent observations together and relate the ice islands to their parents. This allowed for estimations of the total drift distance and net displacement for each ice island.

### 5.4.2. Metocean Data Extraction

Various types of reanalysis datasets have been used to extract the variables required for this study.

The atmospheric and oceanic data extraction was limited to the locations and times that the Petermann ice islands drifted (47-82 °N; 46-94 °W; July 2008-December 2013). The North American Regional Reanalysis (NARR) dataset was used to obtain the daily-average zonal and meridional components of 10-m wind velocity with 0.3° resolution. The Global Ocean Physics Reanalysis model from the Copernicus Marine Environment Monitoring Service (CMEMS) was used to extract the daily-average zonal and meridional components of ocean current velocity with 0.083° resolution in 20 layers down to the depth of 66 m from the water surface. The same dataset from CMEMS was used to obtain 0.083° daily-average sea surface heights. The ERA-Interim Reanalysis dataset from the European Centre for Medium-Range Weather Forecasts (ECMWF) was used to extract the daily-average significant wave heights and mean wave directions with 0.125° spatial resolution. These reanalysis data were all interpolated spatially and temporally to the drift locations and times of the Petermann ice islands. It should be noted here that while the reanalysis atmospheric and oceanic data were available in sub-daily resolutions, the time interval between the ice island observations were inconsistent and had ranged from hourly to 48-hourly, with a mean and median value of about one day. On this basis, the extraction of daily-average values for the reanalysis variables was judged to be reasonable to capture the data resolution consistent with that of the CI2D3 database.

### 5.4.3. Drift Model Development

The conditional drift velocities of the Petermann ice islands were estimated using the Bayesian method, which is a widely used approach for probabilistic estimations of an event occurance under the influence of multiple governing variables (Gutierrez et al., 2011). For this Bayesian drift model, the relationship between the model variables (Figure 5.1-a) has been presented using a directed acyclic graph (Figure 5.1-b). The initial model accounted for nine variables, including

wind speed ($V_w$), wind direction ($\theta_w$), current speed ($V_c$), current direction ($\theta_c$), sea surface tilt ($T_{ss}$), sea surface tilt direction ($\theta_{SST}$), ice island latitude ($\Phi_i$), significant wave height ($H_{wave}$), and mean wave direction ($\theta_{wave}$). Wind speed was calculated as the magnitude of the resultant for the daily-average zonal and meridional components of wind for each ice island observation. Similarly, wind direction was estimated as the angle that the resultant of daily-average zonal and meridional components of wind for each ice island observation made with the horizontal. The daily-average zonal and meridional components for ocean currents were estimated as the weighted average of the components at all layers between the water surface and the depth of 50 m. To do this, the ocean current components that were extracted from 20 layers (from water surface down to the depth of 66 m) were linearly interpolated to 11 layers at 5-m intervals (from water surface down to the depth of 50 m) and then averaged to represent a weighted average. Current speed and direction were estimated using the resultant of the zonal and meridional components of the weighted average ocean current for each ice island observation, using a similar approach to what was used for estimating wind speed and direction. The zonal and meridional components of the sea surface tilt were estimated based on the horizontal and vertical gradients calculated from the extracted/interpolated satellite altimetry data. These components were used to estimate the sea surface tilt and its direction at each ice island observation using the approach explained earlier for wind and currents. Ice latitude for each observation was directly extracted from the ice island centroid data in the CI2D3 database. The significant wave height (combined wind waves and swell) and mean wave direction were directly extracted from ECMWF ERA Interim, but the interpolated data revealed limited available data points to use in the model; out of the 6747 data observations used for developing the drift model, only 1854 wave data points were available, since the ice islands were very close to the shore. Also, wave-driven drift for large glacial ice features

such as the Petermann ice islands in this study is generally insignificant (Lu et al., 2021), likely

due to the small ratio of significant wave height to ice island thickness for such large ice features.

The limited number of wave data points represented little predictive power, so significant wave

height and mean wave direction were excluded from further analysis for the Bayesian drift model

development.
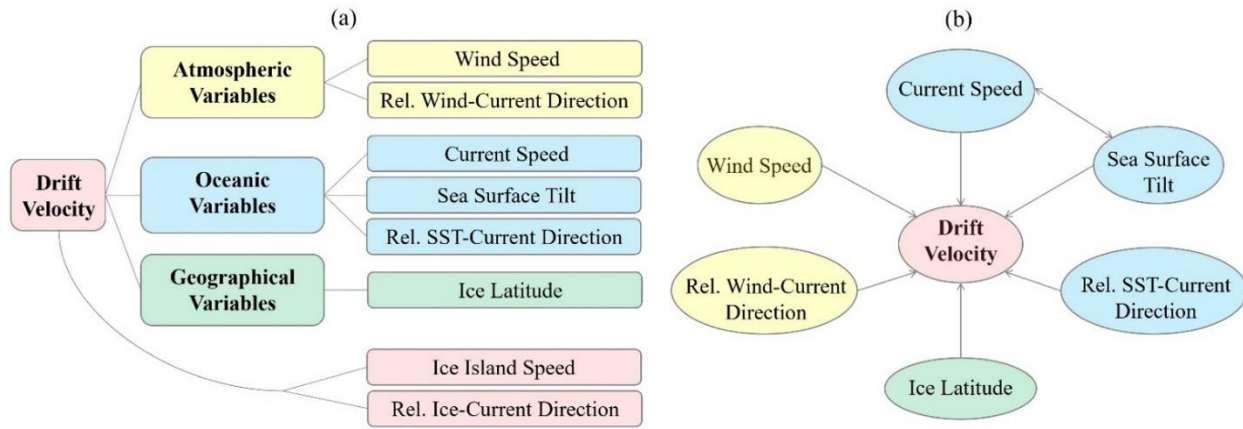


**Figure 5.1.** The classifications of input variables (yellow, blue, and green) and output variables (pink) for the Bayesian drift model (a), and the directed acyclic graph for the drift model (b) where the arrowheads depict the causality as determined by a pairwise correlation analysis.

The directional variables (wind and sea surface tilt directions) were all adjusted relative to ocean

current direction as ocean currents was found as the most important contributor to the drift of

icebergs and ice islands (Kubat et al., 2005; Eik, 2009; Keghouche et al., 2009; Zeinali-Torbati et

al., 2020). This eliminated ocean current direction as an explicit variable for the drift model,

however, it is implicitly accounted for as all directional variables were represented relative to the

direction of ocean currents. Therefore, the number of model input variables reduced to six,

including wind speed ($V_w$), relative wind-current direction ($\theta_{w-c}$), current speed ($V_c$), sea surface

tilt ($T_{ss}$), relative sea surface tilt-current direction ($\theta_{SST-c}$), and ice island latitude ($\Phi_i$). These input

variables were used to predict the ice island speed ($V_i$) and its direction relative to the ocean

currents ($\theta_{i-c}$), as shown in Figure 5.2.
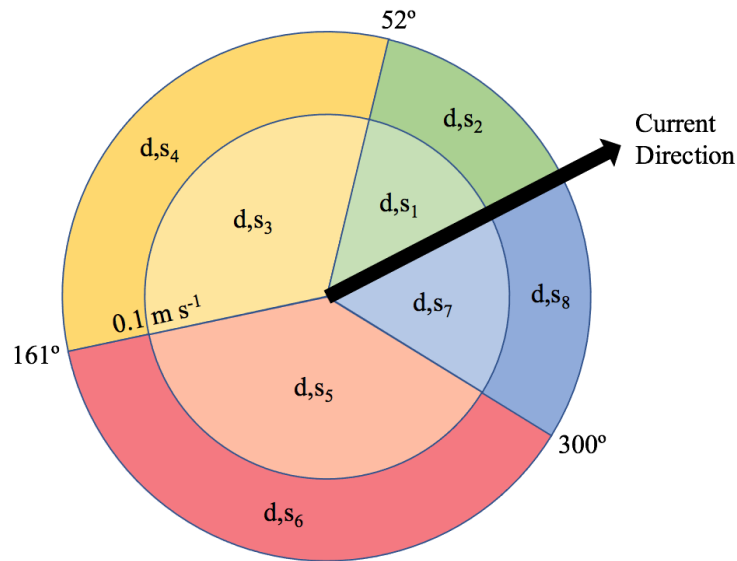


**Figure 5.2.** The eight states of ice island velocity ($d, s_1 - d, s_8$), defined based on the median value for ice island speed ($0.1 \ m \ s^{-1}$) and quartile values for ice island direction relative to ocean currents (52°, 161°, 300°).

First, the distributions of the input variables for the ice island observations in each state of ice island velocity were studied and compared against the associated distributions for all ice island observations. The number of data points available for the six interpolated input variables associated with all ice island observations were inconsistent, likely due to the ice islands' occasional presence close to coastlines where the reanalysis models have poor resolution. Investigating the interpolated variables revealed that for wind speed and relative wind-current direction, respectively, 6744 and 6382 data points were available, but for current speed 6385 data point existed. While the lowest number of data points were available for sea surface tilt and relative sea surface tilt-current direction (6210), the highest number of the points were available for ice latitude (6747). In a similar way, the availability of the input data in each state of the ice island drift velocity were inconsistent. To ensure meaningful comparisons of the variable distributions

154

for each state of ice island velocity and all ice island observations, all data distributions have been presented as relative frequencies.

To study the relationship between the input variables (Figure 5.1-b), two approaches were employed using the full set of data points for all ice island observations. The pairwise linear correlation was analyzed by the Pearson correlation coefficient (Freedman et al., 2010), as follows:

$$r = \frac{\sum_i^n (x_i - \bar{x})(y_i - \bar{y})}{\sqrt{\sum_i^n (x_i - \bar{x})^2} \sqrt{\sum_i^n (y_i - \bar{y})^2}} \tag{5.1}$$

where $r$ is the correlation coefficient; $x_i$ and $y_i$ represent a set from all data points ($n$) for a pair of input variables; and $\bar{x}$ and $\bar{y}$ indicate the mean values of all data points for the given pair of variables. The nonlinear correlation between the variables was also investigated using the pairwise scatter plots of the input variables. Directed arrows were drawn between the variables if the associated linear or nonlinear correlation was found to be significant.

To predict the drift velocity of ice islands under various atmospheric and oceanic conditions, the ranges of the input variables presented in Figure 5.1-a were categorized into two or four states (Table 5.1) according to their medians ($\tilde{x}$) or quartiles ($Q_1$ and $Q_3$). Due to the limited number of data points available for model training and to avoid model saturation, only four states were used for the directional variables ($\theta_{w-c}$ and $\theta_{SST-c}$) and only two states were used for the other variables ($V_w$, $V_c$, $T_{ss}$, and $\Phi_i$). This represented $4^2 \times 2^4$ or 256 state combinations of the input variables, each representing a criteria set for the full model with all six variables. In a similar way, the output ice island drift velocity (speed, $V_i$; direction, $\theta_{i-c}$) was categorized into eight states using four directional states for $\theta_{i-c}$ and two states for $V_i$. The conditional probability of ice island drifting in each state of output drift velocity (Table 5.1) was predicted by Bayes' theorem using the full set

of model criteria, given by:

$$P(A|B) = \frac{P(A) \times P(B|A)}{P(B)} \tag{5.2}$$

where $P(A)$ represents the probability of ice island's drift in each state of drift velocity without any given conditions, $P(V_i, \theta_{i-c})$; $P(B|A)$ is the conditional probability of a given criteria set occurrence in each state of the ice island drift velocity, $P(V_w, \theta_{w-c}, V_c, T_{ss}, \theta_{SST-c}, \Phi_i | V_i, \theta_{i-c})$; and $P(B)$ is the probability of a given criteria set occurrence for all ice island observations, $P(V_w, \theta_{w-c}, V_c, T_{ss}, \theta_{SST-c}, \Phi_i)$. The probability $P(B|A)$ in Eqn. (5.2) was estimated as the relative frequency of the given criteria set in each state of the ice island drift velocity, calculated by (Bonafede and Giudici, 2007):

$$P(crs = j) = \frac{n_j}{n} \tag{5.3}$$

where $crs = j$ indicates the $j^{\text{th}}$ set of the variables' state combinations, $n_j$ is the frequency of the given criteria set in each state of drift velocity, and $n$ indicates the total number of data points in each state of ice island drift velocity. Similarly, $P(B)$ was calculated by the same approach (Eqn. (5.3)), but using the criteria set frequency associated with all ice island observations.

**Table 5.1.** The states of atmospheric and oceanic variables for the Bayesian drift model. The input variables include wind speed ($V_w$), relative wind-current direction ($\theta_{w-c}$), current speed ($V_c$), sea surface tilt ($T_{ss}$), relative SST-current direction ($\theta_{SST-c}$), and ice island latitude ($\Phi_i$). The output variable includes ice island velocity ($V_i, \theta_{i-c}$), where $V_i$ and $\theta_{i-c}$ represent ice island speed and relative ice-current direction, respectively.

| INPUT VARIABLES | State 1 | State 2 | State 3 | State 4 |
|---|---|---|---|---|
| $V_w$ ($m\ s^{-1}$) | $\leq V_{w,\tilde{x}}$ | $> V_{w,\tilde{x}}$ | - | - |
| $\theta_{w-c}$ (°) | $\leq \theta_{w-c,Q_1}$ | $(\theta_{w-c,Q_1}, \theta_{w-c,\tilde{x}}]$ | $(\theta_{w-c,\tilde{x}}, \theta_{w-c,Q_3}]$ | $> \theta_{w-c,Q_3}$ |
| $V_c$ ($m\ s^{-1}$) | $\leq V_{c,\tilde{x}}$ | $> V_{c,\tilde{x}}$ | - | - |
| $T_{ss}$ (−) | $\leq T_{ss,\tilde{x}}$ | $> T_{ss,\tilde{x}}$ | - | - |
| $\theta_{SST-c}$ (°) | $\leq \theta_{SST-c,Q_1}$ | $(\theta_{SST-c,Q_1}, \theta_{SST-c,\tilde{x}}]$ | $(\theta_{SST-c,\tilde{x}}, \theta_{SST-c,Q_3}]$ | $> \theta_{SST-c,Q_3}$ |
| $\Phi_i$ (°) | $\leq \Phi_{i,\tilde{x}}$ | $> \Phi_{i,\tilde{x}}$ | - | - |

| OUTPUT VARIABLE | State 1 | State 2 | State 3 | State 4 | State 5 | State 6 | State 7 | State 8 |
|---|---|---|---|---|---|---|---|---|
| $V_i, \theta_{i-c}$ ($m\ s^{-1}$, °) | $\leq V_{i,\tilde{x}}$, $\leq \theta_{i-c,Q_1}$ | $> V_{i,\tilde{x}}$, $\leq \theta_{i-c,Q_1}$ | $\leq V_{i,\tilde{x}}$, $(\theta_{i-c,Q_1}, \theta_{i-c,\tilde{x}}]$ | $> V_{i,\tilde{x}}$, $(\theta_{i-c,Q_1}, \theta_{i-c,\tilde{x}}]$ | $\leq V_{i,\tilde{x}}$, $(\theta_{i-c,\tilde{x}}, \theta_{i-c,Q_3}]$ | $> V_{i,\tilde{x}}$, $(\theta_{i-c,\tilde{x}}, \theta_{i-c,Q_3}]$ | $\leq V_{i,\tilde{x}}$, $> \theta_{i-c,Q_3}$ | $> V_{i,\tilde{x}}$, $> \theta_{i-c,Q_3}$ |

$\tilde{x}$ represents the median value in the distribution of the given variable
$Q_1$ and $Q_3$ represent the first and third quartiles in the distribution of the given variable, respectively

The validation of the developed drift model was performed using the k-fold (k=5) cross-validation method (Ozdemir, 2016) to reduce the sensitivity of the model validation to the subset selection process. To define the folds, the 80%-20% pareto principle was used, meaning that 80% of data were used for training the model and the rest (20%) served as testing subsets (Macek, 2008; Suthaharan, 2016). In other words, the model variables associated with each state of ice island drift velocity were randomly divided into five equal-size disjoint subsets. Each time, four subsets were used for model development and one subset was reserved for testing the trained model. For all model criteria sets, the Bayesian drift probabilities (Eqn. (5.3)) in each state of ice island velocity was estimated using the input variables from each test subset and compared against the estimated

drift probability from the associated training subset, a framework that allowed for statistical analysis of our model performance.

## 5.5.    Results and Discussion

### 5.5.1.   Preliminary Analysis of Ice Island Drift Velocities

Investigating the drift speeds of the ice islands (Figure 5.3-a) revealed that out of the 17755 observations, about 46% of the drift speeds were below a threshold of $0.02 \ m \ s^{-1}$, so they were assumed to be grounded and subsequently excluded from the analysis (

**Table 5.2). Also, about 26% of the cases had observation intervals above a threshold of two days, which were deemed to be too large timesteps for reliable drift speed estimations. Excluding the cases that were grounded or had large timestep from the previous observations resulted in 6747 valid ice island observations, which generally drifted in a southeastward direction (Figure 5.3-b) with a circular mean and median azimuthal direction of 118° and 129°, respectively. These ice islands had an average drift distance of 415 km and an average net displacement of 262 km before experiencing a break-up event and drifted with an average speed of 0.14 $m \ s^{-1}$ and a median value of 0.10 $m \ s^{-1}$, some reached as far as the Grand Banks of Newfoundland (Figure 5.3-b). The description of the Petermann ice islands and preliminary analysis of the drift velocities in each year are presented in**

Table 5.2. More detailed information on the drift characteristics of Petermann ice islands can be found in Zeinali-Torbati et al. (2019).
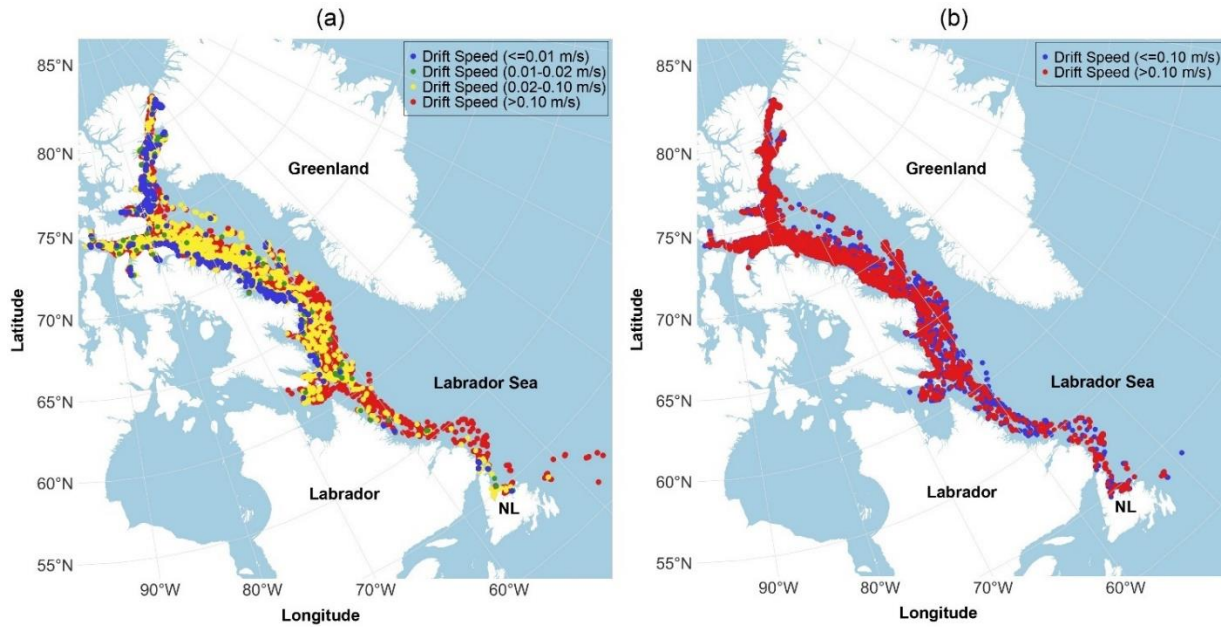
**Figure 5.3.** The drift speeds for all ice island observations (a) and the drift speeds used in the model after grounded ice islands (ice speed<0.02 $m\ s^{-1}$) and large gap sizes between successive observations (>2 days) were excluded (b).

**Table 5.2.** Preliminary analysis of the Petermann ice islands and their drift velocities by the years that the calving events occurred.

| Petermann Glacier Calving Year | Number of Ice Islands | Number of Ice Island Observations | Number of Grounded Observations | [*]Mean Drift Speed ($m\ s^{-1}$) | [*]Mean Drift Direction (°) |
|---|---|---|---|---|---|
| **2008** | 29 | 332 | 44 | 0.15 | 120 |
| **2010** | 637 | 9658 | 4198 | 0.16 | 116 |
| **2011** | 10 | 502 | 146 | 0.12 | 103 |
| **2012** | 169 | 7263 | 3812 | 0.13 | 121 |
| **All** | 845 | 17755 | 8200 | 0.14 | 118 |

[*] Mean drift speed and direction represent the mean values associated with the data from the remaining ice island observations after grounded ice islands (ice speed<0.02 $m\ s^{-1}$) and large gap sizes between successive observations (>2 days) were excluded

### 5.5.2. Distributions of Metocean Variables

The distributions and summary statistics of the input variables in each state of the ice island drift velocity were studied and compared against the associated distributions and statistics for all ice island observations. While this was performed for all six variables (Figure 5.4 and Figure 5.5;

Figure 5A.1-Figure 5A.10), here only the distributions and summary statistics for current speed are presented as it was identified to play the most dominant role in the drift of large ice features such as icebergs and ice islands (Kubat et al., 2005; Eik, 2009; Keghouche et al., 2009; Zeinali-Torbati et al., 2020). Figure 5.4 represents the relative frequency histogram plot of regional current speeds for all ice island observations, and Figure 5.5 shows the associated current speed distributions in each of the eight states of the drift velocity (a-h). It was revealed in Figure 5.4 that the while Petermann ice islands were subjected to the mean current speed of $0.10 \ m \ s^{-1}$, some encountered current speeds as high as $0.78 \ m \ s^{-1}$. The presented summary statistics in Figure 5.4 also show that the current speeds surrounding the ice islands were relatively weak and most frequent around $0.02$-$0.06 \ m \ s^{-1}$. Comparing the distributions in Figure 5.4 and Figure 5.5 revealed that ice islands that drifted at speeds above $0.1 \ m \ s^{-1}$ and within 0-52 ° or 300-360 ° from ocean current direction (b, h) were subjected to 57% higher median current speeds than the value associated with all observations ($0.07 \ m \ s^{-1}$). On the other hand, the ice islands that drifted at low speeds ($\leq 0.1 \ m \ s^{-1}$) and within 161-300 ° from the direction of the ocean current (e) experienced the lowest median current speed ($0.04 \ m \ s^{-1}$) of all states (a-h). These indicate that while stronger currents led to the ice islands moving with higher speeds in directions aligned with ocean currents (b, h), weaker currents resulted in ice island drift with lower speeds in directions farther from the directions of the ocean currents (e). This suggests that low-velocity currents are less able to overcome the momentum of the drifting ice island, while tend to keep it on its trajectory independent of the current speed. As currents become stronger, they are able to overcome momentum and align the ice island drift direction more with the current direction. This highlights the relative influence of ocean currents on the drift velocity of ice islands, which is in agreement with the results of the deterministic iceberg and ice island drift studies (*e.g.,* Kubat et al., 2005;

Zeinali-Torbati et al., 2020).
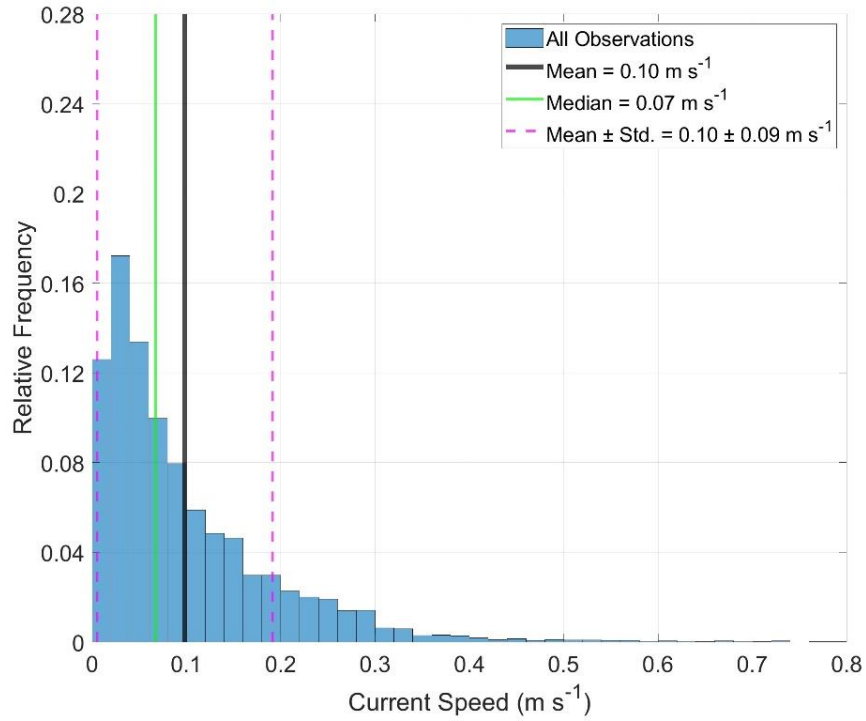


**Figure 5.4.** Relative frequency histogram plot of current speed surrounding Petermann ice islands for all observations (n=6747).
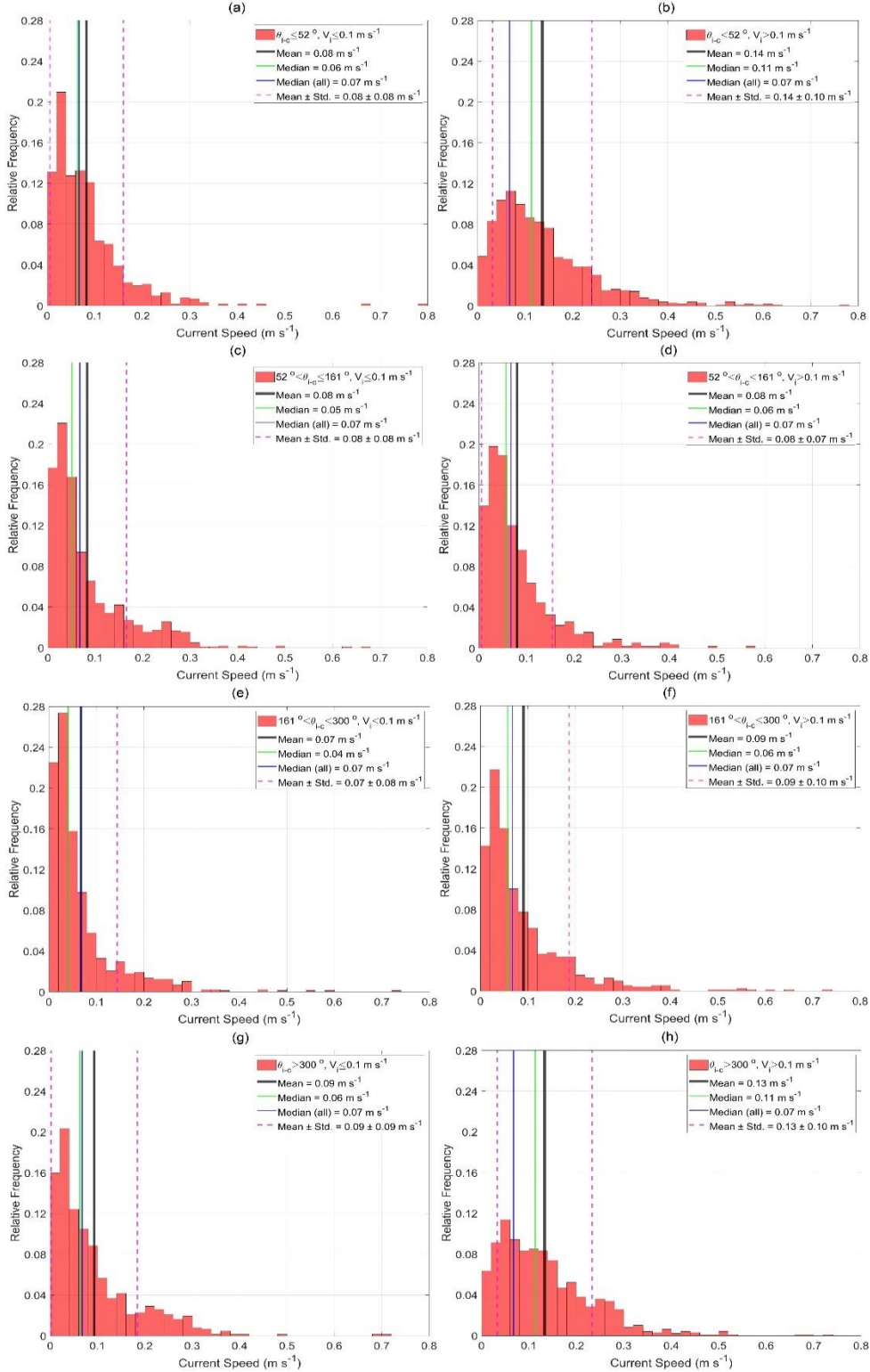
**Figure 5.5.** Relative frequency histogram plots of current speed surrounding Petermann ice islands for each state of ice island velocity (a; n=611, b; n=983, c; n=1025, d; n=581, e; n=881, f; n=708, g; n=620, h; n=976).

The distribution of the directional variables ($\theta_{i-c}$, $\theta_{w-c}$, and $\theta_{SST-c}$) were also analyzed and presented using rose plots (Figure 5.6) to better depict the general directions of ocean currents (Figure 5.6-a), as well as the relative directions of ice island drifts (Figure 5.6-b), winds (Figure 5.6-c), and sea surface tilts (Figure 5.6-d) for all ice island observations. The circular format of the rose plots in Figure 5.6 indicates the 16 cardinal directions of the variables, with the length of the spokes around the circle indicating the frequency of the associated directions and the different colors representing the associated current speeds. As an example, the rose plot of ocean currents (Figure 5.6-a) shows that current directions were most frequent in directions close to southwards (*e.g.*, SW, SSW, S, SSE, and SE) and that stronger currents (represented by light blue and green) were mostly observed in such directions. The rose plot in Figure 5.6-b reveals that the ice islands drifted mainly in close proximity of the ocean current directions, given that the relative directions were most frequent around 0°. Similarly, the ice islands were subjected to winds that mainly had directions close to their associated ocean currents. The rose plot for the relative sea surface tilt-current direction (Figure 5.6-c), however, shows that the sea surface tilt directions were mainly about 90° to the right (clockwise) of the current directions (Figure 5.6-a), a result that is expected given that the geostrophic current is the result of a force balance between the water pressure gradient and the Coriolis force (Colling, 2001). This implies that there is very limited variation in the distribution of the sea surface tilt directions relative to ocean current directions. Therefore, a 90° clockwise direction for the sea surface tilt relative to the currents was assumed, and this variable was excluded from further analysis for the Bayesian drift model development, which reduced the number of model variables to five.
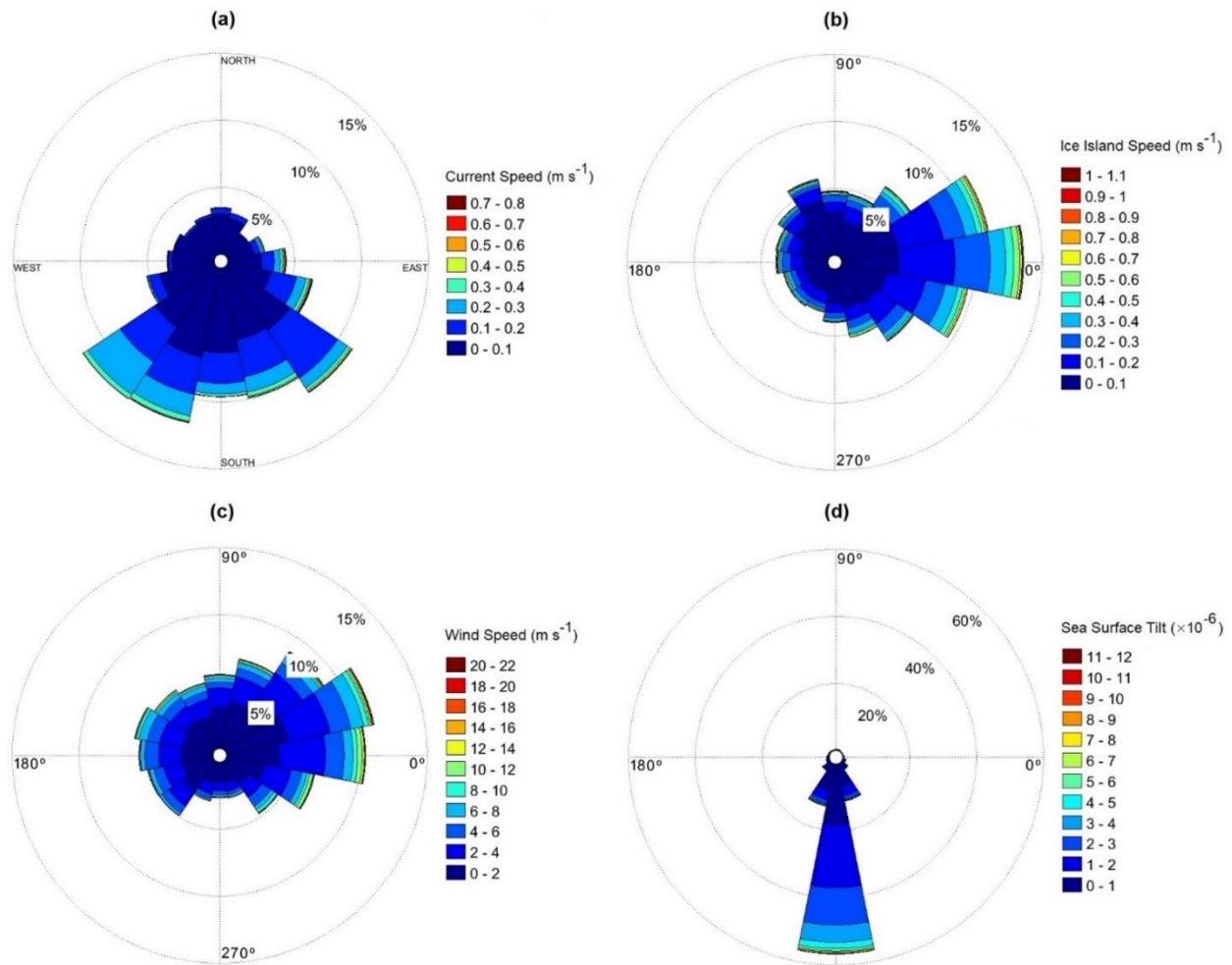
**Figure 5.6.** Rose plots of (a) current speed and direction; (b) ice island speed and direction relative to current direction; (c) wind speed and direction relative to current direction; and (d) sea surface tilt and direction relative to current direction that the Petermann ice islands experienced over their lifetimes.

The analysis of the correlation between the input variables revealed a significant positive linear correlation between current speed and sea surface tilt (Table 5.3). This significant correlation is expected given that sea surface tilt is estimated based on the differences in ocean surface level, a component that is driven by ocean currents (Misra, 2020). The analysis of the correlations among the other input variables presented in Table 5.3 revealed no other significant linear correlations. Also, the pairwise scatter plots of the input variables were investigated for possible nonlinear inter-relationship among them, but no nonlinear associations between the variables were found.

164

**Table 5.3.** Pearson product-moment correlation coefficients of the drift model variables, including wind speed ($V_w$), relative wind-current direction ($\theta_{w-c}$), current speed ($V_c$), sea surface tilt ($T_{ss}$), relative SST-current direction ($\theta_{SST-c}$), and ice island latitude ($\Phi_i$).

| Variable | $V_w$ | $\theta_{w-c}$ | $V_c$ | $T_{ss}$ | $\theta_{SST-c}$ | $\Phi_i$ |
|---|---|---|---|---|---|---|
| $V_w$ | 1 | <0.001 | 0.354 | 0.271 | <0.001 | <0.001 |
| $\theta_{w-c}$ | -0.079 | 1 | <0.001 | <0.001 | <0.001 | <0.001 |
| $V_c$ | -0.012 | -0.131 | 1 | <0.001 | 0.036 | <0.001 |
| $T_{ss}$ | 0.014 | -0.163 | 0.929 | 1 | 0.040 | <0.001 |
| $\theta_{SST-c}$ | -0.046 | 0.106 | -0.027 | -0.026 | 1 | 0.001 |
| $\Phi_i$ | 0.049 | -0.077 | -0.102 | -0.131 | 0.041 | 1 |

The values in the grey cells show the p-values for the associated correlations.

### 5.5.3. Metocean Conditional Criteria Sets and Drift Velocity Frequency

Using the Bayesian approach described in the Model Development section, the conditional probability of drift speeds and directions ($P_{d,s_1}$-$P_{d,s_8}$) under various states of the input variables were quantified, and selected examples of the results were presented in Table 5.4. The full model with all five variables was presented as criteria set j=5, but given the model's utility with fewer variables, simplified models (criteria set j=1-4) were also investigated to predict ice island drift velocities in case some of the variables were unavailable. For each criteria set, Eqn. (5.2) was used to estimate the drift velocity probabilities $P_{d,s_1}$-$P_{d,s_8}$ using probabilities $P(A)$, $P(B|A)$ and $P(B)$. $P(A)$ was calculated as the division of the number of data points in each state of drift velocity by the total number of data points. The relative frequencies $P(B|A)$ and $P(B)$ were calculated based on the number of data points in each state of the drift velocity and all observations that meet the given conditions. For instance, criteria set j=3, which represents a three-variable model, was developed based on current speed, relative wind-current direction, and ice island latitude. This criteria set was met by 161 cases among the observations in the second state of the drift velocity (983 events) and 557 cases among all ice island observations (6747 events). So, the conditional

probability of ice island drifting in the second state ($\theta_{i-c} \leq 52\,°, V_i > 0.1\ m\ s^{-1}$) was estimated by:

$$P_{d,s_2}(j = 3) = P(s_2|j = 3) = P(j = 3|s_2) \times \frac{P(s_2)}{P(j = 3)}$$

$$= P(V_c > 0.07\ m\ s^{-1}, \theta_{w-c} \leq 51\,°, \Phi_i \leq 75\,°|\theta_{i-c} \leq 52\,°, V_i > 0.1\ m\ s^{-1})$$

$$\times \frac{P(\theta_{i-c} \leq 52\,°, V_i > 0.1\ m\ s^{-1})}{P(V_c > 0.07\ m\ s^{-1}, \theta_{w-c} \leq 51\,°, \Phi_i \leq 75\,°)}$$

$$= \frac{161}{983} \times \frac{\frac{983}{6747}}{\frac{557}{6747}} \approx 0.29\ or\ 29\% \tag{5.4}$$

This implies that under the conditions specified by criteria set j=3, there is a 29% probability that the ice islands drift at speeds beyond 0.1 $m\ s^{-1}$ and within 52 ° from the ocean current direction. Using the same approach, the probability of ice islands drifting in other states of the ice island velocity ($P_{d,s_1}, P_{d,s_3} - P_{d,s_8}$) was estimated and presented. This revealed that if the conditions represented by criteria set j=3 hold, the ice islands will most likely (29%+28%=57% chance) move with high speeds (>0.1 $m\ s^{-1}$) and within 52 ° or -60 ° (300-360 °) from the direction of the ocean currents. Under the same conditions, it will be most unlikely (4% chance) for the ice islands to drift at high speeds (>0.1 $m\ s^{-1}$) in directions that are far (within 52-161 °) from the direction of the ocean currents. For each criteria set and drift velocity state represented in Table 5.4, Eqn. (5.2) was used to estimate the drift speeds and directions of ice islands under different atmospheric, oceanic, and geographical conditions.

**Table 5.4.** Selected drift model conditional criteria sets and the associated conditional probability for each state of ice island drift velocity ($P_{d,s_1}$-$P_{d,s_8}$). The variables include wind speed ($V_w$), relative wind-current direction ($\theta_{w-c}$), current speed ($V_c$), sea surface tilt ($T_{ss}$), and ice island latitude ($\Phi_i$).

| Criteria Set j | $V_c$ ($m\ s^{-1}$) | $\theta_{w-c}$ (°) | $\Phi_i$ (°) | $V_w$ ($m\ s^{-1}$) | $T_{ss}$ (−) | [a]$P_{d,s_1}$ (%) | [b]$P_{d,s_2}$ (%) | [c]$P_{d,s_3}$ (%) | [d]$P_{d,s_4}$ (%) | [e]$P_{d,s_5}$ (%) | [f]$P_{d,s_6}$ (%) | [g]$P_{d,s_7}$ (%) | [h]$P_{d,s_8}$ (%) |
|---|---|---|---|---|---|---|---|---|---|---|---|---|---|
| 1 | >0.07 | | | | | 9 | **22** | 13 | 8 | 8 | 10 | 9 | 21 |
| 2 | >0.07 | ≤51 | | | | 8 | **26** | 14 | 3 | 7 | 8 | 9 | 25 |
| 3 | >0.07 | ≤51 | ≤75 | | | 11 | **29** | 5 | 4 | 5 | 11 | 7 | 28 |
| 4 | >0.07 | ≤51 | ≤75 | >2.2 | | 8 | **38** | 6 | 3 | 2 | 11 | 7 | 25 |
| 5 | >0.07 | ≤51 | ≤75 | >2.2 | >1.1×10⁻⁶ | 6 | **39** | 5 | 3 | 2 | 11 | 7 | 27 |

[a] The probability of ice island drifting at speed $V_i \leq 0.1\ m\ s^{-1}$ and direction $\theta_{i-c} \leq 52\,°$
[b] The probability of ice island drifting at speed $V_i > 0.1\ m\ s^{-1}$ and direction $\theta_{i-c} \leq 52\,°$
[c] The probability of ice island drifting at speed $V_i \leq 0.1\ m\ s^{-1}$ and direction $52\,° < \theta_{i-c} \leq 161\,°$
[d] The probability of ice island drifting at speed $V_i > 0.1\ m\ s^{-1}$ and direction $52\,° < \theta_{i-c} \leq 161\,°$
[e] The probability of ice island drifting at speed $V_i \leq 0.1\ m\ s^{-1}$ and direction $161\,° < \theta_{i-c} \leq 300\,°$
[f] The probability of ice island moving at speed $V_i > 0.1\ m\ s^{-1}$ and direction $161\,° < \theta_{i-c} \leq 300\,°$
[g] The probability of ice island drifting at speed $V_i \leq 0.1\ m\ s^{-1}$ and direction $\theta_{i-c} > 300\,°$
[h] The probability of ice island drifting at speed $V_i > 0.1\ m\ s^{-1}$ and direction $\theta_{i-c} > 300\,°$

The selected results in Table 5.4 provide a framework for prediction of the drift speeds and directions of the Petermann ice islands under different metocean conditions represented by each criteria set. Table 5.4 reveals a dominant influence of ocean current speed on the drift directions of ice islands. Criteria set j=1, which indicates the one-variable model with currents only, indicates that when current speeds were greater than $0.07\ m\ s^{-1}$, 22% and 21% of the ice islands drifted with high speeds within 52 ° and 300-360 ° from ocean currents, respectively. This implies that under strong currents and without accounting for the other variables, there is 61% probability (9%+22%+9%+21%) that an ice island moves in close proximity (within 52 ° or 300-360 °) of the ocean current direction. This probability increases to 68% (8%+26%+9%+25%) with the addition of a new condition in which the winds are blowing within 51 ° from the ocean currents (criteria set j=2). Another noticeable implication of the drift probabilities presented in Table 5.4 is that higher current speeds generally result in higher ice island drift speeds. Criteria set j=1 indicates

that under current speeds beyond 0.07 $m\ s^{-1}$, there is 61% chance (22%+8%+10%+21%) that ice islands move at speeds beyond 0.1 $m\ s^{-1}$. The addition of other constraints such as low latitudes (≤75 °) and high wind speeds (>2.2 $m\ s^{-1}$) increases the likelihood of the ice islands to drift with high speeds in close directions relative to ocean currents (*e.g.*, criteria set j=4). This is likely due to the fact that the Coriolis force would cause less deflection on the drift velocities in lower latitudes (Phillips, 2000; Persson, 2005), and that stronger winds would assist the ice islands to drift towards ocean currents, given that surface currents closely follow wind directions (Brown, 1991). Under the conditions represented by criteria set j=5, which is associated with the full model with all five variables, 66% of ice islands (39%+27%) are expected to drift at high speeds (> 0.1 $m\ s^{-1}$) and towards their regional ocean current directions (within 52 ° or 300-360 °). Under such conditions, the model predicts a very high probability (6%+39%+7%+27%=79%) for the ice islands to move within 52 ° or 300-360 ° from ocean currents, and it is highly likely (39%+3%+11%+27%=80%) for them to drift with high speeds (>0.1 $m\ s^{-1}$).

The presented model implicitly accounts for the correlations among the input variables. For instance, Table 5.3 revealed a strong positive correlation between current speed and sea surface tilt that implies a high probability for concurrent occurrence of strong currents and large sea surface tilts, which was taken into account for the events represented by criteria set j=5 in Table 5.4.

The presented conditional criteria sets in Table 5.4 only represent five selected combinations of the input variables for the models with 1-5 variables. Criteria sets j=1-5 were selected through an iterative process of adding a new criterion to the previous one to represent the conditions that would increase the probability of ice islands' drifts at speeds $V_i > 0.1\ m\ s^{-1}$ and directions $\theta_{i-c} \leq$ 52 ° ($P_{d,s_2}$ in Table 5.4). For the full model with all five variables (criteria set j=5), only one of the

64 state combinations and its associated probability were presented. While the drift velocity probabilities were estimated for each combination of variable states, it was impractical to present the results of all criteria sets, so only selected results were presented in Table 5.4.

Using this Bayesian drift model, it is possible to produce probabilistic predictions of the drift speeds and directions for future ice islands subjected to different atmospheric and oceanic conditions. To do this, the atmospheric and oceanic variables in Figure 5.1 should be forecast at the centroids of the given ice island to identify its associated criteria set and drift probability. The full model with all five variables (*e.g.*, criteria set j=5 in Table 5.4) needs inputs from all five variables. However, in the absence of one or more variables, simplified models with fewer variables (*e.g.*, criteria sets j=1-4) should be used. It should be noted here that the criteria sets and drift probabilities for the presented drift model were developed based on the descendants of the ice islands originally calved from the Petermann Glacier in 2008-2012. However, the estimated drift probabilities from Eqn. (5.2) should be updated when more drift data (new evidence) becomes available, a process that make the posterior drift probabilities less dependent on the prior drift probabilities (Eleye-Datubo et al., 2006). In other words, the presented model should be updated if new data from other ice islands becomes available as the addition of more data will likely cause a change in the criteria sets and their associated drift probabilities, which should be updated in the model.

### 5.5.4. Ice Island Case Study

A case study is presented to demonstrate how the developed drift model can be applied to predict the drift trajectories for a descendant of the Petermann ice island offshore Labrador (~ 58.28 ºN, 60.07 ºW) that originated from the massive calving event of the Petermann Glacier in 2010. The

1.9 km² ice island of interest was calved on 25 March 2011, drifted for about three months (~ 5 °
latitude change), and fractured on 20 June 2011. The CI2D3 database was used to track and identify
the respective observed positions (spatial and temporal) of the ice island, which were then used to
estimate the corresponding metocean variables shown in Figure 5.1-b using the methods presented
in the methodology section. These variables were fed into the drift model to forecast the associated
probabilities for the drift speeds and directions of the ice island. Based on the estimated
probabilities in each state of the output ice island velocity, a number of random drift speeds and
directions were selected from the observed drift speeds and directions in the given state, which
were then used to identify the associated drift trajectories and positions after one day, as shown in
Figure 5.7. The drift trajectories presented in Figure 5.7 reveal that, based on the metocean
conditions for the ice island of interest in this case study, the drift paths specified by black and
orange colours (states 2 and 8) were the most probable trajectories. In other words, the ice island
was most likely to drift at speeds beyond $0.1\ m\ s^{-1}$ and within close proximity of the ocean current
direction. This indicates the predominant influence of ocean currents on the drift of icebergs and
ice islands, as noted in previous studies (*e.g.*, Kubat et al., 2005; Eik, 2009; Keghouche et al.,
2009; Turnbull et al., 2015; Zeinali-Torbati et al., 2020). Figure 5.7 also shows the mean predicted
trajectory (black line) and the observed trajectory (red line) of the ice island, which reveals that
while the mean predicted drift trajectory of the ice island was in agreement with the observed drift
direction, the forecast mean drift speed was almost half of the observed speed. The investigation
of other cases of Petermann ice island observations revealed that the presented model generally
provides better forecast direction quality for faster ice islands, a finding that corroborated the
results of the iceberg drift forecasting model by Yulmetov (2021). This is in part because faster
moving ice islands have greater momentum and higher directional stability with drift direction less

influenced by changes to metocean conditions. It was also revealed that our drift predictions were, on average, more reliable under stronger local ocean currents. This was in agreement with the results of the previous deterministic drift models (Turnbull et al., 2015; Crocker et al., 2013), where the forecast model underestimated drift speeds and provided more erratic drift directions in the regions where ocean currents were not dominant.
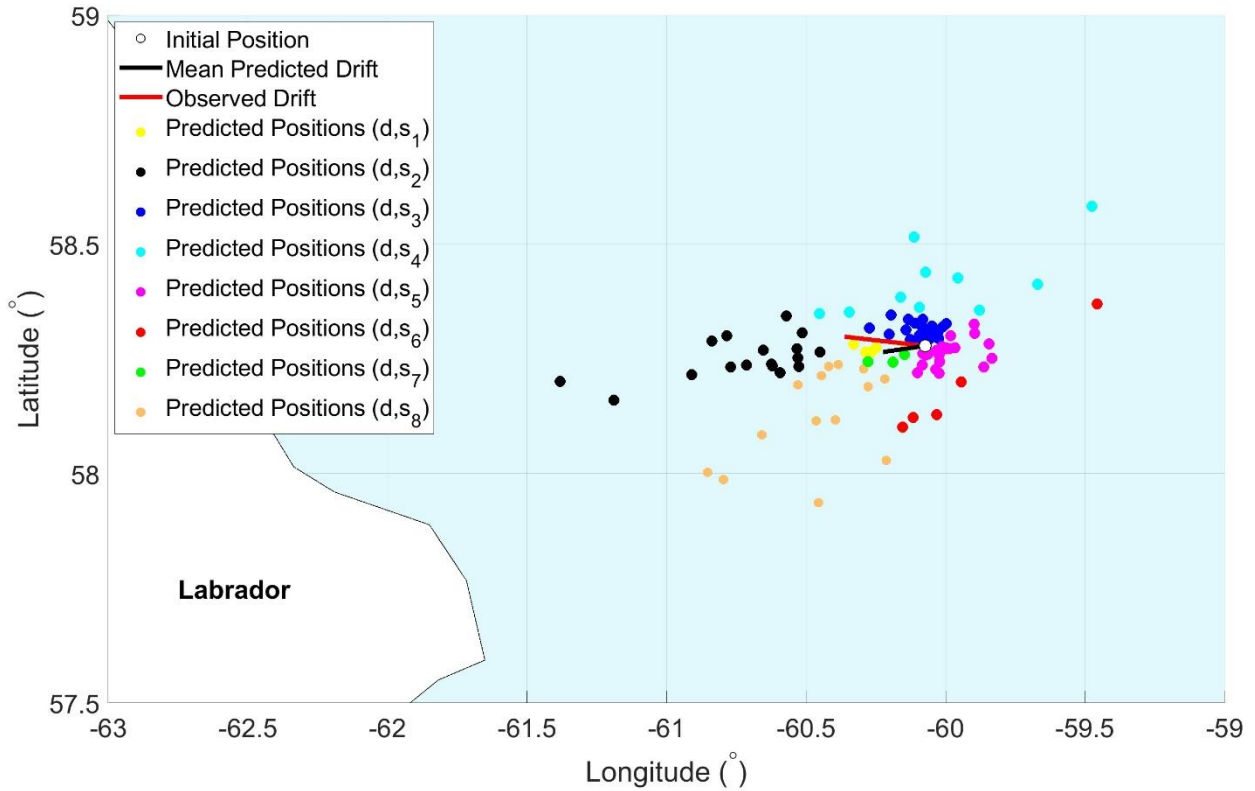


**Figure 5.7.** The observed and mean predicted drift trajectories (solid lines) and predicted drift positions (solid dots) for a descendant of the Petermann ice island from the 2010 calving event. The predicted positions specified by $d, s_1 - d, s_8$ represent probabilistic locations of ice island's drifting at $V_i \leq 0.1\ m\ s^{-1}$, $\theta_{i-c} \leq 52\degree$; $V_i > 0.1\ m\ s^{-1}$, $\theta_{i-c} \leq 52\degree$; $V_i \leq 0.1\ m\ s^{-1}$, $52\degree < \theta_{i-c} \leq 161\degree$; $V_i > 0.1\ m\ s^{-1}$, $52\degree < \theta_{i-c} \leq 161\degree$; $V_i \leq 0.1\ m\ s^{-1}$, $161\degree < \theta_{i-c} \leq 300\degree$; $V_i > 0.1\ m\ s^{-1}$, $161\degree < \theta_{i-c} \leq 300\degree$; $V_i \leq 0.1\ m\ s^{-1}$, $\theta_{i-c} > 300\degree$; and $V_i > 0.1\ m\ s^{-1}$, $\theta_{i-c} > 300\degree$, respectively.

## 5.6. Model Validation

The Bayesian drift model was validated based on the 5-fold cross-validation method explained in

the methodology section. Since it is not feasible to display model validation for all criteria sets and all states of the drift velocity, Table 5.5 shows the validation results for only one of the eight states of the drift velocity (state 2) and for some of the criteria sets in the model specified by j=1-5. The validation results (Table 5.5) shows an agreement between the mean drift probability estimates from the training and test subsets (bold-faced values in the middle columns), given the overlap between the probability ranges. The standard deviations for the training and test subsets show that the amount of variation of the drift probability estimations increases with the number of variables considered in the criteria sets. This indicates that the developed model is more robust for the simplified models with fewer variables, such as criteria sets j=1-2. This result is expected given that criteria sets that consider more variables (*e.g.*, j=4-5) represent more constrained conditions where fewer number of events meet the given criteria, leading to more sensitivity and variability in the estimated drift probabilities. However, the variability in the drift probability predictions should reduce if more drift data are fed into the Bayesian drift model. The analysis of the pairwise errors between the results from the training and test subsets reveals that the drift probability forecasts from the test subsets are, on average, within 2.5-29.0 % of the estimates obtained from the training subsets.

**Table 5.5.** Model validation for some of the criteria sets in the model (*e.g.,* criteria set j=5 shows one of the 64 state combinations of the five variables; criteria set j=4 represents one of the 32 state combinations of the four variables). The validation is presented for only one of the eight states of the drift velocity, $P_{d,s_2}$ (*i.e.*, the probability of ice island drifting at speed $V_i > 0.1\ m\ s^{-1}$ and direction $\theta_{i-c} \leq 52\,°$). The variables include wind speed ($V_w$), relative wind-current direction ($\theta_{w-c}$), current speed ($V_c$), sea surface tilt ($T_{ss}$), and ice island latitude ($\Phi_i$). Model error is derived through statistical comparison of drift probability estimations from training sets and test sets, obtained using 5-fold cross-validation method.

| Criteria Set j | $V_c$ $(m\ s^{-1})$ | $\theta_{w-c}$ (°) | $\Phi_i$ (°) | $V_w$ $(m\ s^{-1})$ | $T_{ss}$ (−) | $P_{d,s_2\_training}$[1] (%) Mean | Std.[3] | $P_{d,s_2\_test}$[1] (%) Mean | Std.[3] | *Pairwise* % *Error*[2] Test vs. Training | $P_{d,s_2\_all}$[1] (%) |
|---|---|---|---|---|---|---|---|---|---|---|---|
| 1 | >0.07 | | | | | **22.1** | 0.2 | **22.1** | 0.6 | 2.5 | **22.1** |
| 2 | >0.07 | ≤51 | | | | **25.6** | 0.8 | **25.7** | 3.3 | 9.6 | **25.6** |
| 3 | >0.07 | ≤51 | ≤75 | | | **28.9** | 1.3 | **29.1** | 5.5 | 18.2 | **28.9** |
| 4 | >0.07 | ≤51 | ≤75 | >2.2 | | **38.0** | 2.2 | **37.5** | 9.0 | 24.5 | **38.1** |
| 5 | >0.07 | ≤51 | ≤75 | >2.2 | >1.1×10⁻⁶ | **39.2** | 2.7 | **38.5** | 11.3 | 29.0 | **39.2** |

[1] $P_{d,s_2\_training}$, $P_{d,s_2\_test}$, and $P_{d,s_2\_all}$ represent the drift probability estimations from the training subsets, test subsets, and all data points, respectively
[2] Absolute error between the drift probability estimations from the training and test subsets
[3] Standard deviation

The model validation results presented in Table 5.5 only show five of the 122 state combinations for the set of variables represented by criteria sets j=1-5, which were defined using the medians and quartiles of the variable distributions as presented in Table 5.1. In other words, criteria sets j=1, 2, 3, 4, and 5 represent 1/2, 1/8, 1/16, 1/32, and 1/64 state combinations of the variables, respectively. The model performance under the other combinations of variable states were analyzed, but not presented here. The corresponding analysis for the remaining combinations reveals that the developed model has lower certainty in predicting the drift velocities for less likely combinations of the variable states. These lower likelihood conditions are unlikely to occur and therefore do not frequently affect the model. For instance, the combination of $V_c \leq 0.07\ m\ s^{-1}$, $142\,° < \theta_{w-c} \leq 242\,°$, $\Phi_i \leq 75\,°$, $V_w > 2.2\ m\ s^{-1}$, $T_{ss} > 1.1 \times 10^{-6}$ was highly unlikely (<0.1%) and only occurred five times (out of the 6747 events). Under these conditions, no drift was observed in states 1, 3, 4, 5, 8 (see Table 5.1). However, 1, 3, and 1 cases among all

observations drifted in states 2, 6, 7, respectively. The analysis of the full model (five variables) revealed that out of the 64 variable state combinations, 32 combinations were very unlikely to occur (<1%). Under such infrequent and unlikely conditions, the drift probability values from the test subsets, on average, ranged within 118-226 % of the estimations from the training subsets. For example, some state combinations were so unlikely that were met only a few times in the training subsets but were never observed in the test subsets, which therefore generated 100% error between the estimations from the test and training subsets. The model, however, performed well for the most frequent combinations of variable states, such as criteria sets j=1-5 in Table 5.5 (with error ranging from 2.5 % to 29.0 %), or when simplified models with one-four variables were used (4-72 % error).

## 5.7.    Conclusions and Future Work

The analysis presented in this chapter was based on the positional and temporal data from to numerous ice islands that originated from the calving events of the Petermann Glacier in 2008, 2010, 2011, and 2012. These data were used to develop a probabilistic Bayesian model to quantify the drift velocities of ice islands under the effects of atmospheric and oceanic conditions that govern their dynamics. Results obtained using the developed drift model revealed ocean currents (speed and direction) as the most important contributor to the drift velocities of ice islands, given that the Petermann ice islands in this study generally drifted in directions close to the local ocean currents direction, particularly for higher speed ocean currents. This effect becomes more pronounced with the addition of other criteria sets. For example, under strong currents, along with higher sea surface tilts, lower latitudes, and stronger winds that are directed in close proximity of ocean current direction, ice islands become much more likely (66%) to drift at higher speeds and in directions that are close to the direction of local ocean currents. Model validation revealed that

the estimated drift probabilities from the test subsets were within 29% of the values from the training subsets. The probability estimations of the ice island drift velocities, however, became less precise as the conditional criteria sets became more restricted.

An advantage of the presented Bayesian model is that it can provide drift probability predictions even with limited metocean data at hand. For instance, with the availability of only ocean current speeds, the model represented by criteria set j=1 can be applied, but the model can be updated and expanded to the one represented by criteria set j=4 when wind and latitude data become available. It is also noteworthy to mention that our probabilistic drift model was developed using the data from the CI2D3 database that were associated with the Petermann ice islands (which originated from the Petermann Glacier). To check the robustness of the model, it should be implemented for other ice islands in the database that have similar characteristics and properties.

In order to improve the model accuracy and apply it to other ice islands (*e.g.*, Antarctic ice islands), future work should use drift data inputs from such ice islands and update the results in Table 5.4 and Table 5.5, accordingly. Here we only used the spatial and temporal data from the CI2D3 database, but more drift data from other ice islands are required to better train and further validate the model. With the limited available data and to ensure the model is not saturated, only four states were considered for the directional variables and two states for the other variables. The model resolution, however, can be improved by using more drift data (once accumulated), which would allow for consideration of a greater number of states for each variable. The model was built on the metocean data extracted from reanalysis databases, where the data are derived from models. The model accuracy can be further improved by using higher-accuracy inputs from in-situ measured data or deterministic models that can provide more accurate short-term forecasts. Our study here accounted for nine variables in the initial model development, however, future research can

improve the presented drift model by studying the influence of additional variables such as ice island mass on the drift probability estimations. Future work should further validate the presented model through direct comparison of the model outputs against independent observed data or estimated drift velocities from other drift models. Also, for the presented drift model to have broader operational use, it is important to be coupled with a deterioration model and a grounding model able to predict size (mass) distributions of the ice islands.

Finally, it is worth noting that ongoing climate change is expected to increase the number of ice islands that calve from the Petermann Glacier (Münchow et al., 2016), which may result in more frequent presence of icebergs and ice islands in the waters on the east coast of Canada, although how far south they drift will be highly informed by deterioration rate. The results of this study improve our ability to probabilistically estimate the future ice island drift velocities based on the atmospheric and oceanic conditions that govern the drift of ice islands. This provides an important step in reducing uncertainty and improving the risk management strategies for safe offshore and marine operations in environments affected by ice islands.

## 5.8.    Appendix A
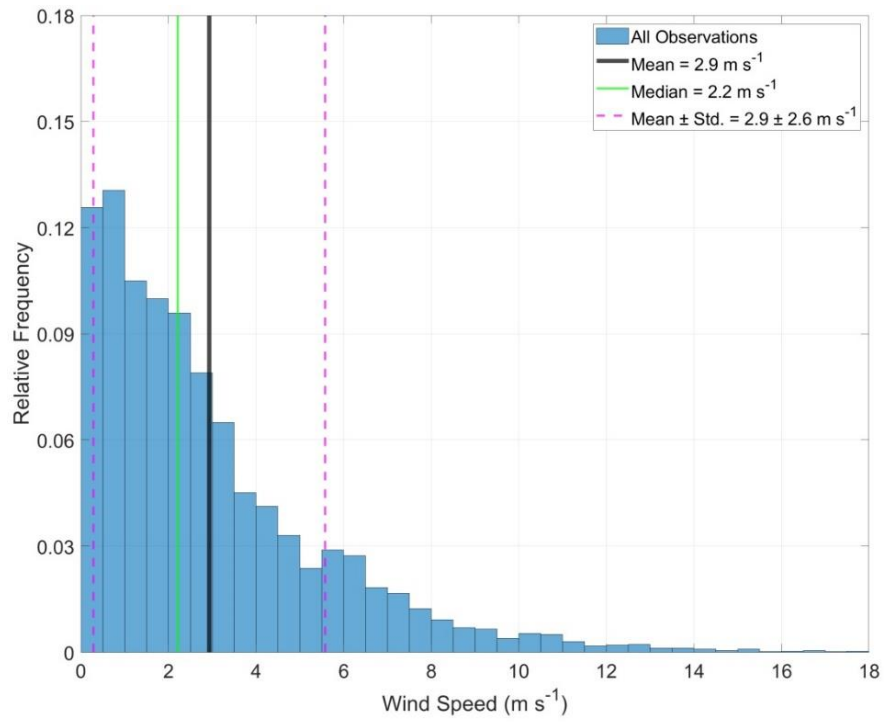


**Figure 5A.1.** Relative frequency histogram plot of wind speed surrounding Petermann ice islands for all observations (n=6747).
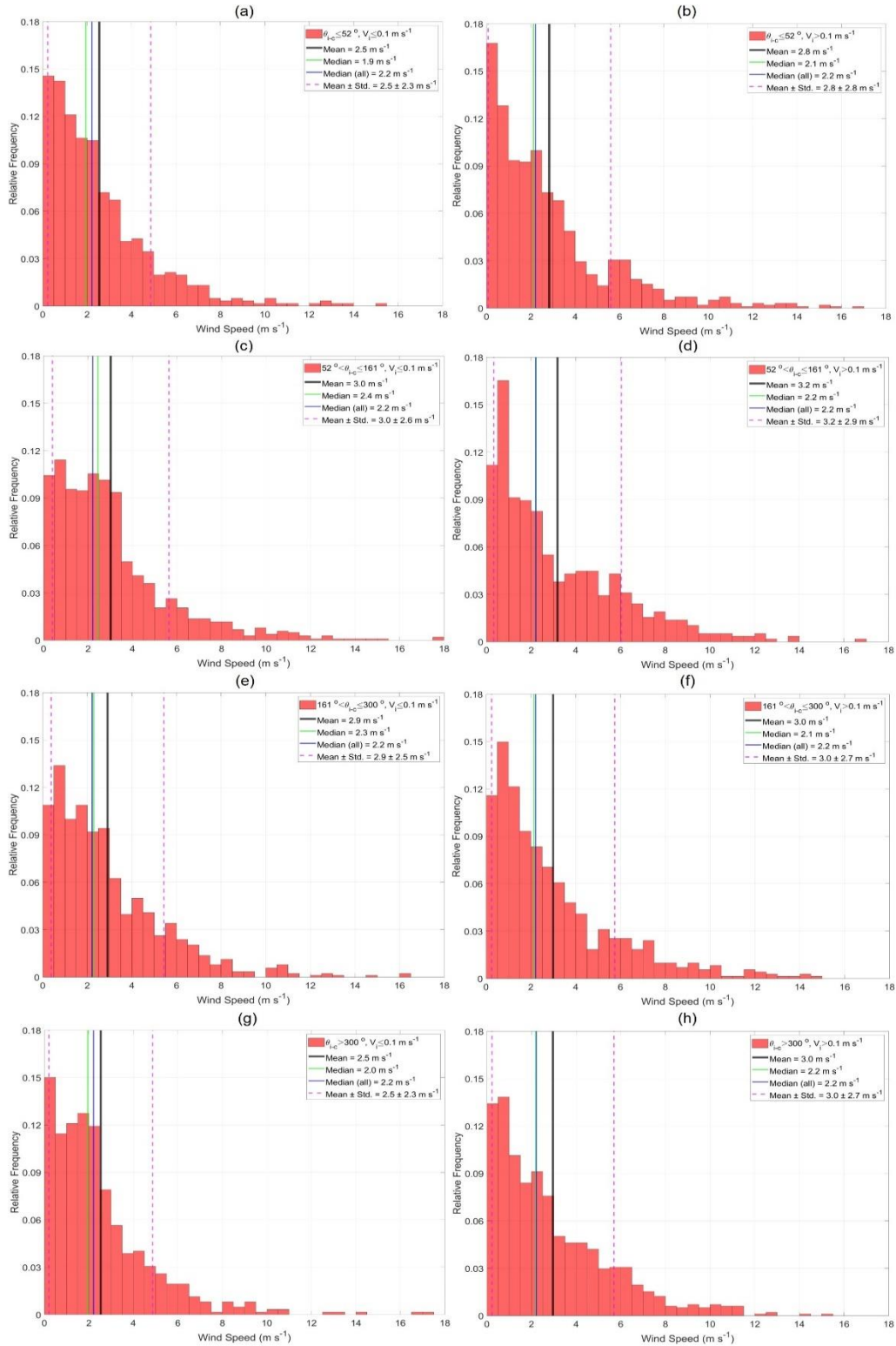
**Figure 5A.2.** Relative frequency histogram plots of wind speed surrounding Petermann ice islands for each state of ice island velocity (a; n=611, b; n=983, c; n=1025, d; n=581, e; n=881, f; n=708, g; n=620, h; n=976).

**Figure 5A.3.** Relative frequency histogram plot of relative wind-current direction surrounding Petermann ice islands for all observations (n=6747).

**Figure 5A.4.** Relative frequency histogram plots of relative wind-current direction surrounding Petermann ice islands for each state of ice island velocity (a; n=611, b; n=983, c; n=1025, d; n=581, e; n=881, f; n=708, g; n=620, h; n=976).
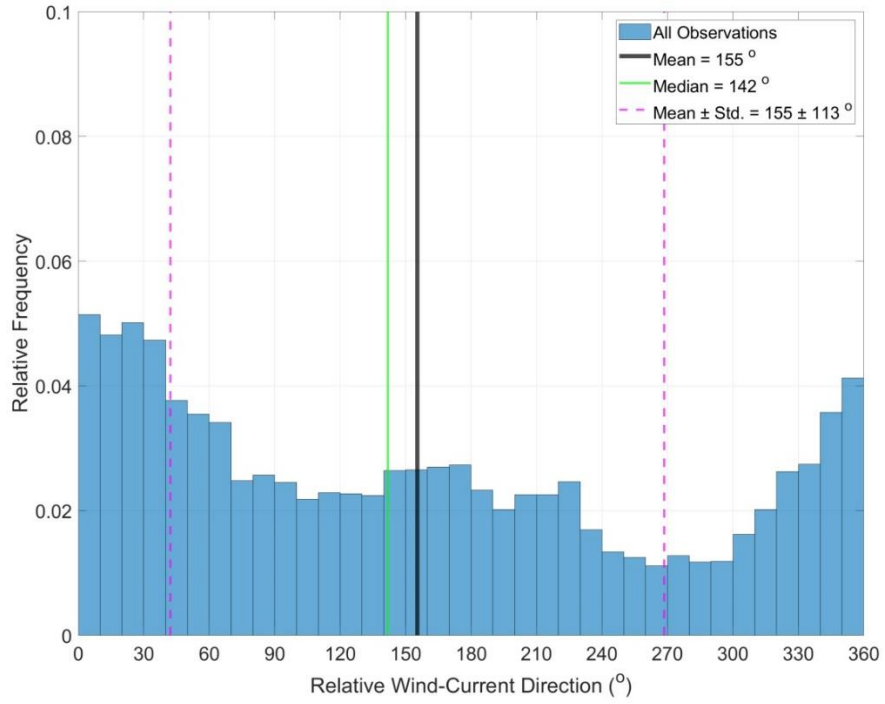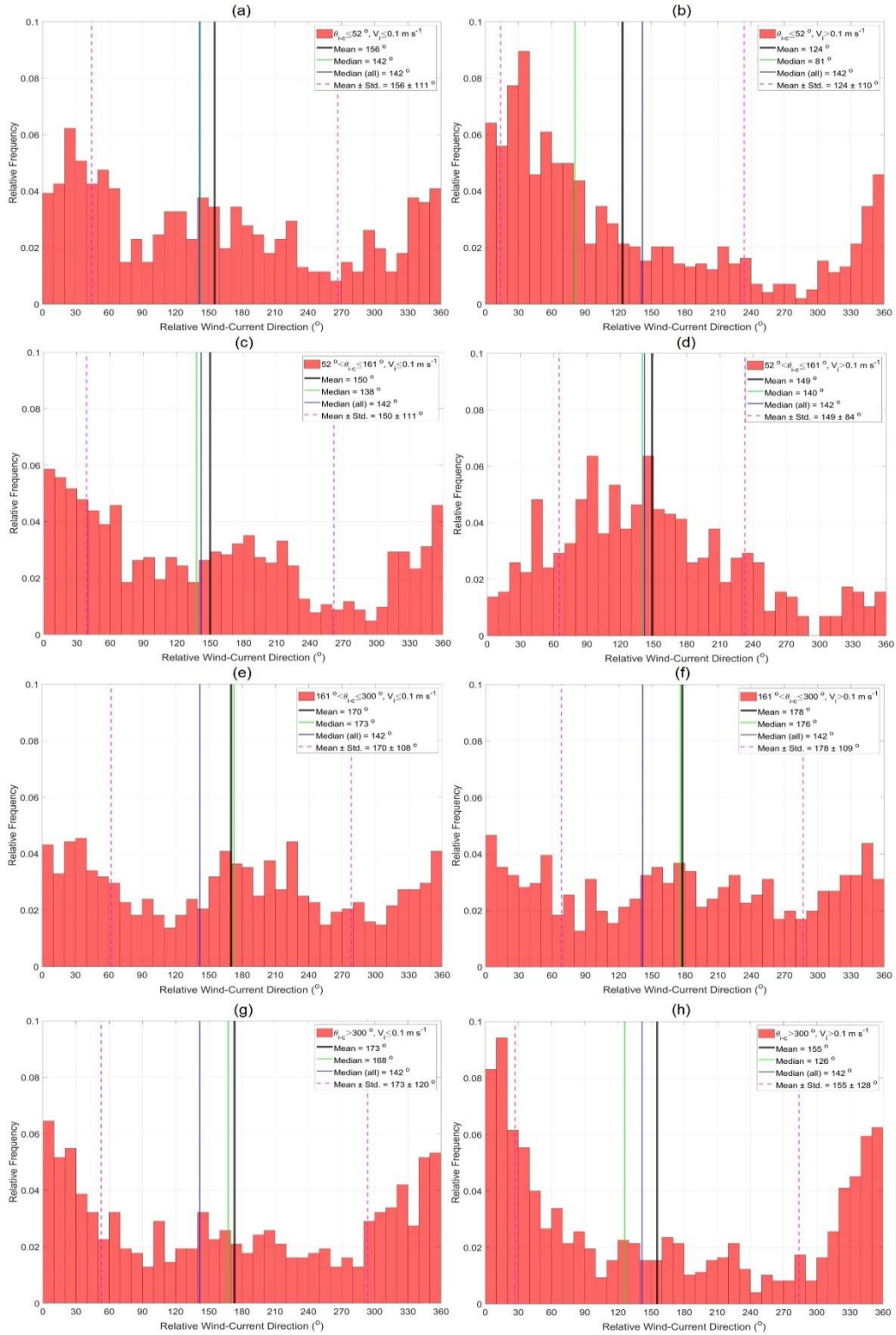
**Figure 5A.5.** Relative frequency histogram plot of sea surface tilt surrounding Petermann ice islands for all observations (n=6747).

**Figure 5A.6.** Relative frequency histogram plots of sea surface tilt surrounding Petermann ice islands for each state of ice island velocity (a; n=611, b; n=983, c; n=1025, d; n=581, e; n=881, f; n=708, g; n=620, h; n=976).
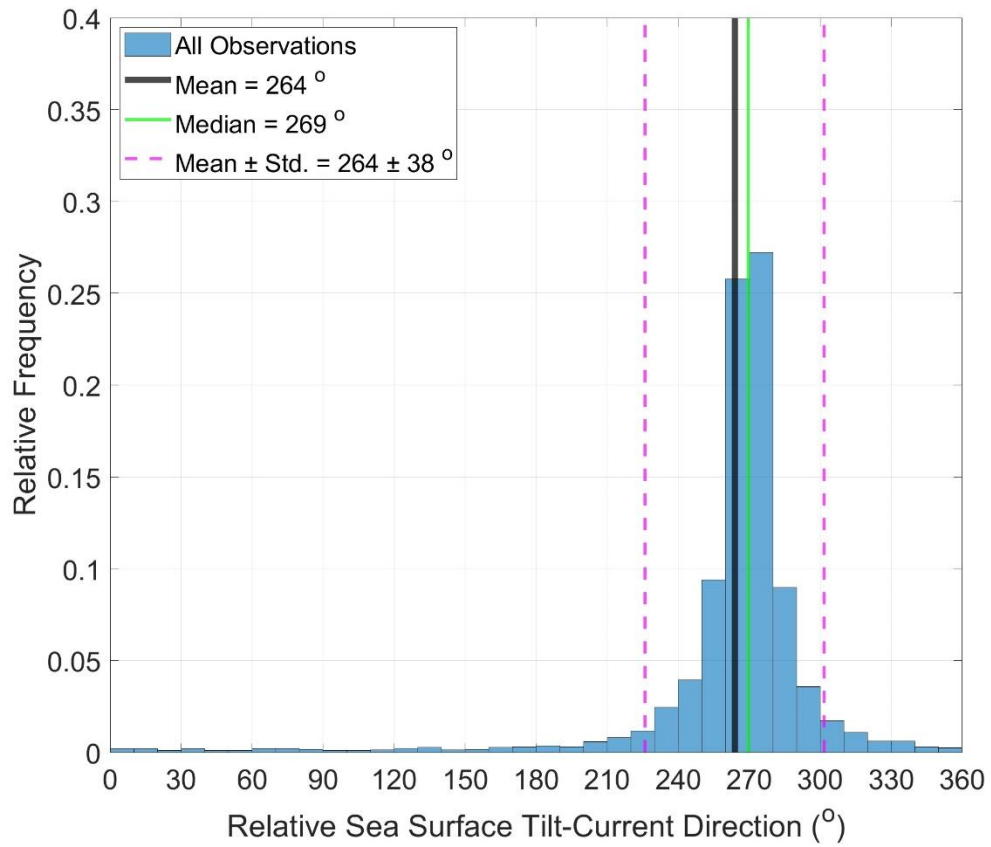
**Figure 5A.7.** Relative frequency histogram plot of relative sea surface tilt-current direction surrounding Petermann ice islands for all observations (n=6747).
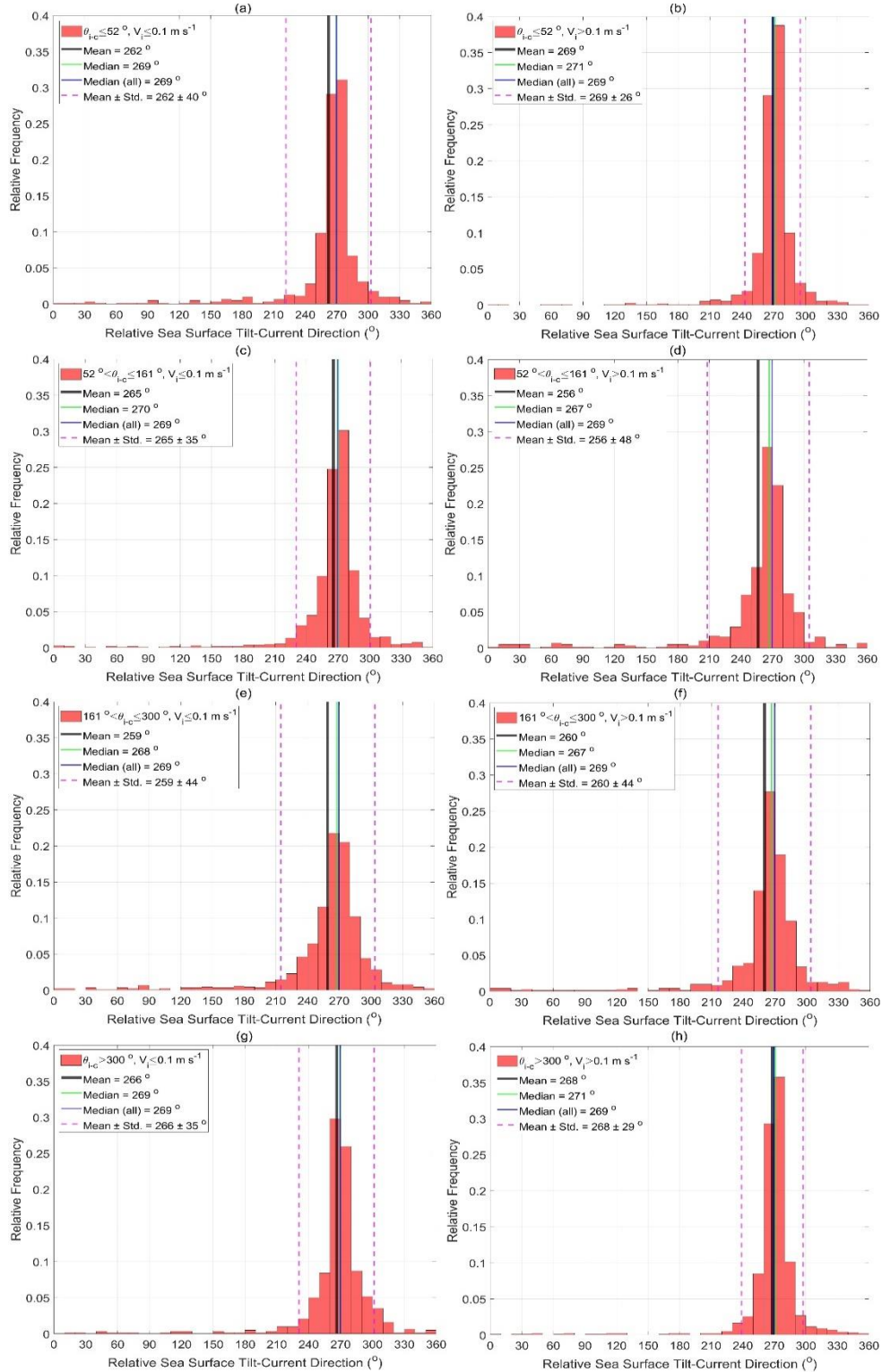
**Figure 5A.8.** Relative frequency histogram plots of relative sea surface tilt-current direction surrounding Petermann ice islands for each state of ice island velocity (a; n=611, b; n=983, c; n=1025, d; n=581, e; n=881, f; n=708, g; n=620, h; n=976).
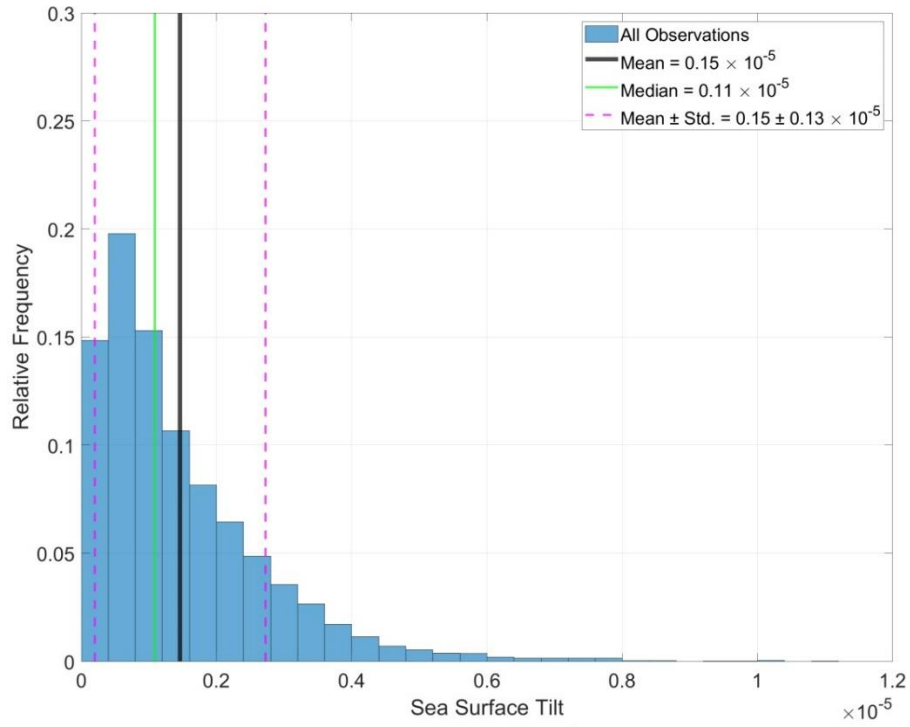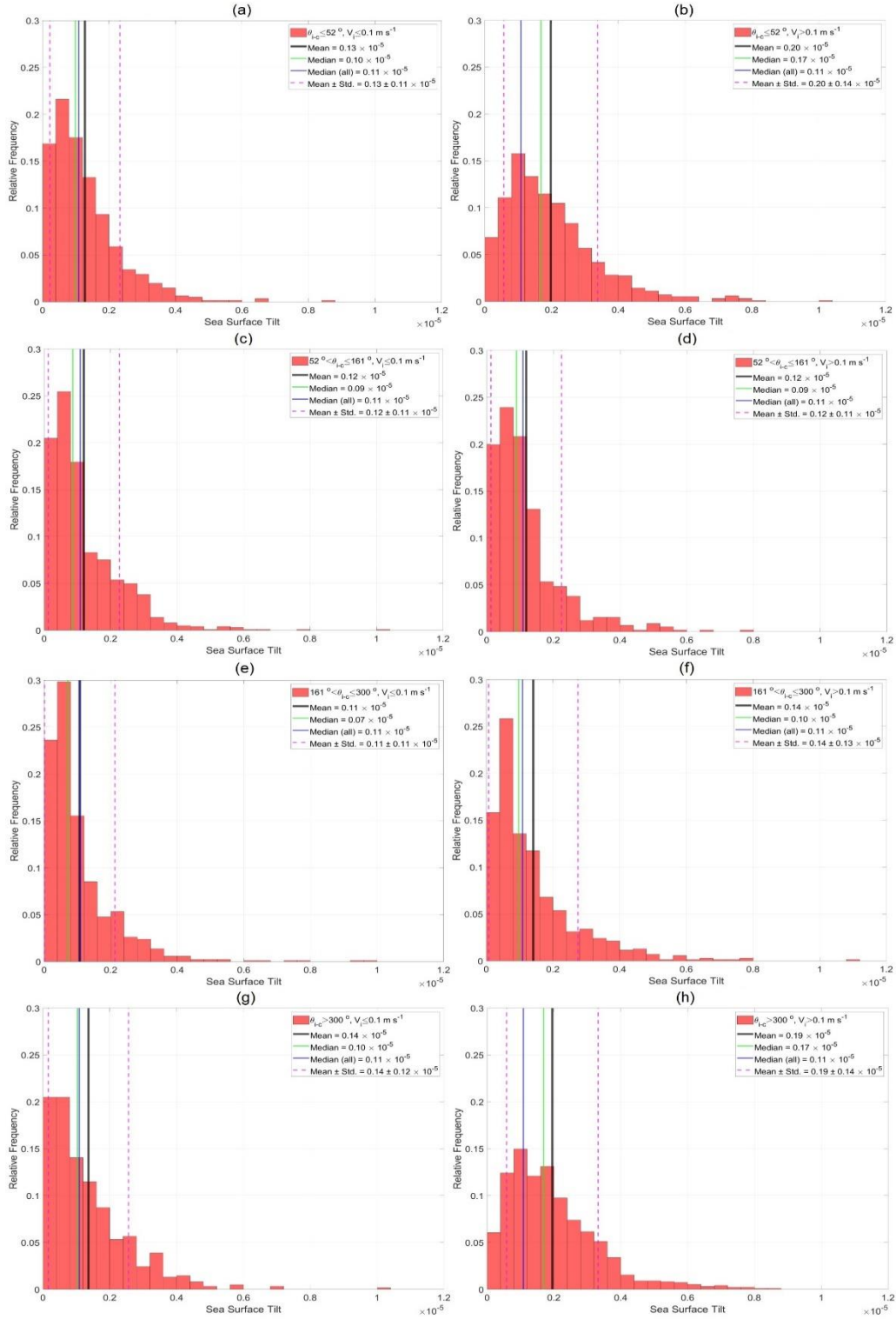
184

**Figure 5A.9.** Relative frequency histogram plot of latitude for all observations of the Petermann ice islands (n=6747).

**Figure 5A.10.** Relative frequency histogram plots of latitude for Petermann ice islands in each state of ice island velocity (a; n=611, b; n=983, c; n=1025, d; n=581, e; n=881, f; n=708, g; n=620, h; n=976).
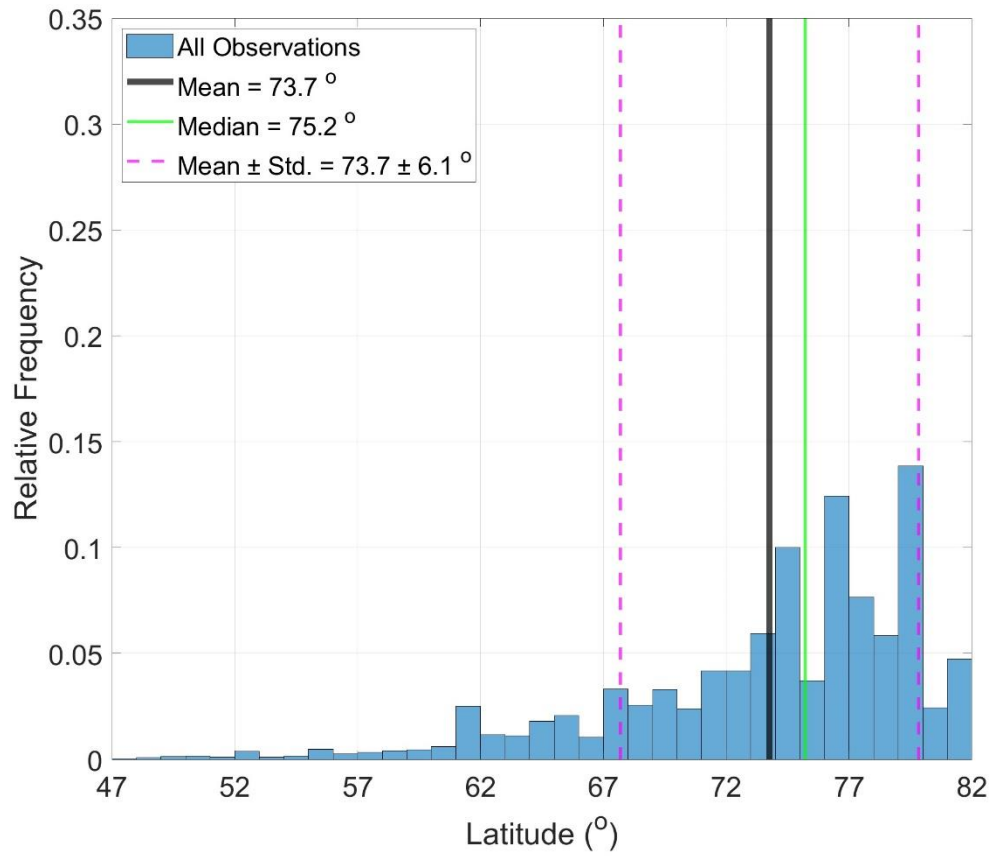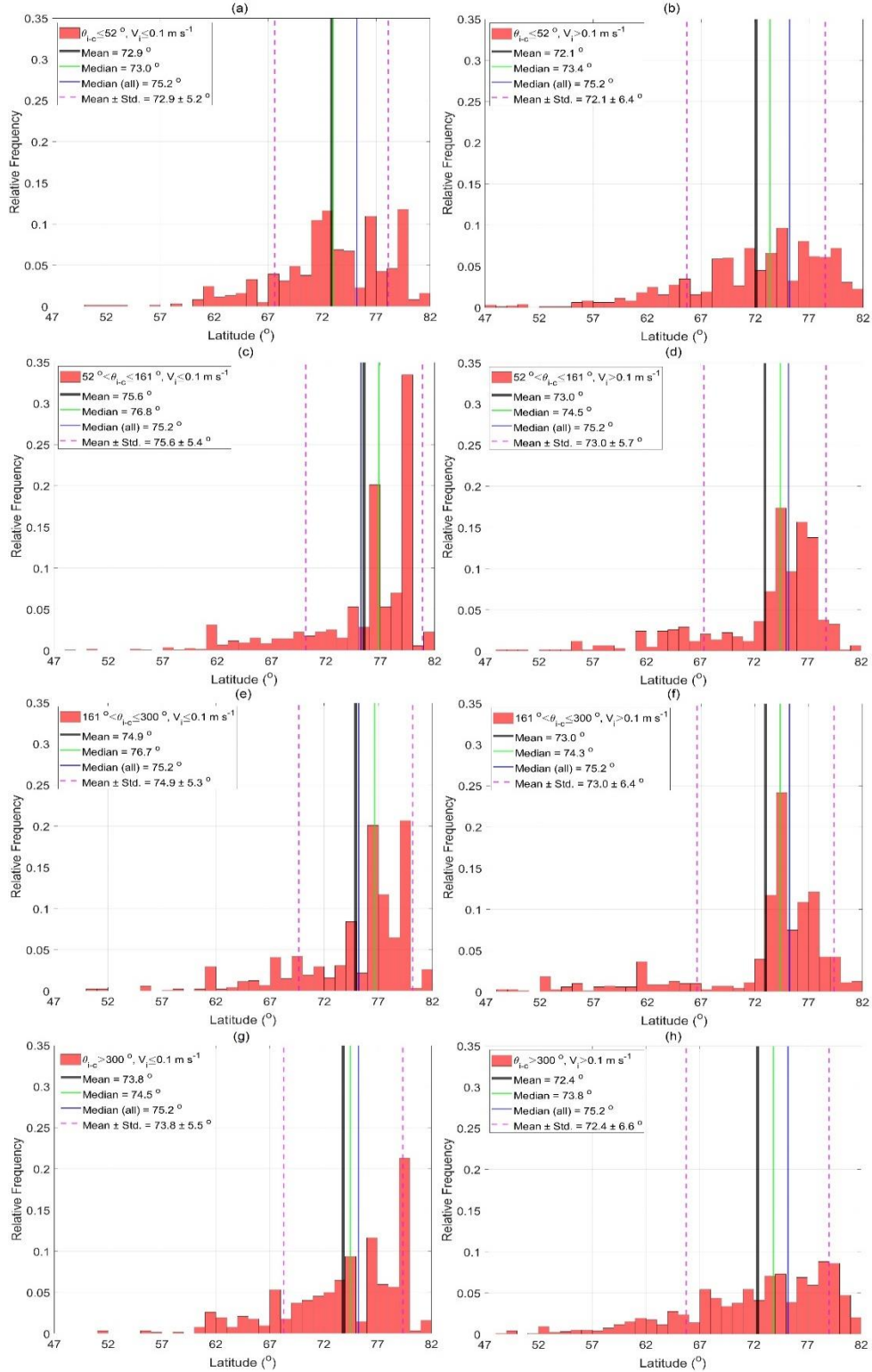
## 5.9.    References

Allison, K., Crocker, G., Tran, H., and Carrieres, T. (2014). An ensemble forecast model of iceberg drift, Cold Regions Science and Technology, 108, 1-9, https://doi.org/10.1016/j.coldregions.2014.08.007.

Baadshaug, O. (2018). Iceberg drift-trajectory modelling and probability distributions of the predictions, Master's Thesis, Department of Physics and Technology, UiT The Arctic University of Norway, Tromsø, Norway.

Bigg, G. R., Wadley, M. R., Stevens, D. P., and Johnson, J. A. (1997). Modelling the dynamics and thermodynamics of icebergs, Cold Regions Science and Technology, 26(2), 113-135, https://doi.org/10.1016/S0165-232X(97)00012-8.

Bonafede, C. E. and Giudici, P. (2007). Bayesian networks for enterprise risk assessment, Physica A: Statistical Mechanics and its Applications, 382, 22-28, https://doi.org/10.1016/j.physa.2007.02.065.

Brown, J. (1991). The final voyage of Rapaiti: A measure of sea-surface drift velocity in relation to the surface wind, Marine Pollution Bulletin, 22(1), 37-40, https://doi.org/10.1016/0025-326X(91)90443-V.

Colling, A. (2001). Ocean circulation, Vol. 3, second edition, Butterworth-Heinemann.

Crawford, A. J., Mueller, D., and Joyal, G. (2018a). Surveying drifting icebergs and ice islands: deterioration detection and mass estimation with aerial photogrammetry and laser scanning, Remote Sensing, 10(4), 575, https://doi.org/10.3390/rs10040575.

Crawford, A., Crocker, G., Mueller, D., Desjardins, L., Saper, R., and Carrieres, T. (2018b). The Canadian Ice Island Drift, Deterioration and Detection (CI2D3) Database, Journal of Glaciology, 1-5. https://doi.org/10.1017/jog.2018.36.

Crocker, G., Carrieres, T., and Tran, H. (2013). Ice island drift and deterioration forecasting in eastern Canada. In Proceedings of the 22nd International Conference on Port and Ocean Engineering Under Arctic Conditions, Espoo, Finland, 9-13 June 2013.

Desjardins, L., Crawford, A., Mueller, D., Saper, R., Schaad, C., Stewart-Jones, E., and Shepherd, J. (2018). Canadian ice island drift, deterioration and detection database (CI2D3 database) [v1.1], Canadian Cryospheric Information Network (CCIN), Waterloo, Canada, http://dx.doi.org/10.21963/12678.

Dowdeswell, J. A. and Bamber, J. L. (2007). Keel depths of modern Antarctic icebergs and implications for sea-floor scouring in the geological record, Marine Geology, 243(1-4): 120-131, doi:10.1016/j.margeo.2007.04.008.

Eik, K. (2009). Iceberg drift modelling and validation of applied metocean hindcast data, Cold Regions Science and Technology, 57(2-3), 67-90, https://doi.org/10.1016/j.coldregions.2009.02.009.

Eleye-Datubo, A. G., Wall, A., Saajedi, A., and Wang, J. (2006). Enabling a powerful marine and offshore decision-support solution through Bayesian network technique, Risk Analysis, 26, 695–721, https://doi.org/10.1111/j.1539-6924.2006.00775.x.

Freedman, D. A. (2010). Statistical models and causal inference: a dialogue with the social sciences, Cambridge University Press, University of California, Berkeley, CA, United States, https://doi.org/10.1017/CBO9780511815874.

Fuglem M., Jordaan I. (2017). Risk analysis and hazards of ice islands, In: Copland L., Mueller D. (eds) Arctic Ice Shelves and Ice Islands, Springer Polar Sciences, Springer, Dordrecht, https://doi.org/10.1007/978-94-024-1101-0_15.

Gutierrez, B. T., Plant, N. G., and Thieler, E. R. (2011). A Bayesian network to predict coastal vulnerability to sea level rise, Journal of Geophysical Research: Earth Surface, 116(F2), https://doi.org/10.1029/2010JF001891.

Jansen, D., Schodlok, M., and Rack, W. (2007). Basal melting of A-38B: A physical model constrained by satellite observations, Remote Sensing of Environment, 111(2-3), 195-203, doi:10.1016/j.rse.2007.03.022.

Jeffries, M. O. (2002). Ellesmere Island ice shelves and ice islands, Satellite Image Atlas of Glaciers of the World: Glaciers of North America - Glaciers of Canada, U.S. Geological Survey Professional Paper 1386-J-1, J147-J164.

Keghouche, I., Bertino, L., and Lisæter, K. A. (2009). Parameterization of an iceberg drift model in the Barents Sea, Journal of Atmospheric and Oceanic Technology, 26(10), 2216-2227, https://doi.org/10.1175/2009JTECHO678.1.

Kubat, I., Sayed, M., Savage, S. B., and Carrieres, T. (2005). An operational model of iceberg drift. International Journal of Offshore and Polar Engineering, 15(2), 125-131.

Kubat, I., Sayed, M., Savage, S. B., Carrieres, T., and Crocker, G. (2007). An operational iceberg deterioration model, In Proceedings of the 17th International Offshore and Polar Engineering Conference, Lisbon, Portugal, 1-6 July 2007, 652-657.

Lichey, C. and Hellmer, H. H. (2001). Modeling giant-iceberg drift under the influence of sea ice in the Weddell Sea, Antarctica, Journal of Glaciology, 47 (158), 452-460, https://doi.org/10.3189/172756501781832133.

Lu, W., Amdahl, J., Lubbad, R., Yu, Z., and Løset, S. (2021). Glacial ice impacts: Part I: Wave-driven motion and small glacial ice feature impacts. Marine Structures, 75, 102850, https://doi.org/10.1016/j.marstruc.2020.102850.

Macek, K. (2008). Pareto principle in datamining: an above-average fencing algorithm, Acta Polytechnica, 48(6), 55-59, https://doi.org/10.14311/1075.

Marko, J. R., Fissel, D. B., and Miller, J. D. (1988). Iceberg movement prediction off the Canadian east coast, In Natural and Man-Made Hazards, Springer, Dordrecht, pp. 435-462, https://doi.org/10.1007/978-94-009-1433-9_31.

Misra, V. (2020). Regionalizing global climate variations: a study of the southeastern US regional climate, Elsevier.

Mueller, D. R., Crawford, A., Copland, L., and Van Wychen, W. (2013). Ice island and iceberg fluxes from Canadian High Arctic sources, Report to the Northern Transportation Assessment Initiative, Innovation Policy Branch, Transport Canada, Ottawa, Canada. https://www.researchgate.net/publication/340183882_Ice_Island_and_Iceberg_Fluxes_from_Canadian_High_Arctic_Sources_Prepared_for_the_Innovation_Policy_Group_of_Tr

ansport_Canada.

Münchow, A., Padman, L., Washam, P., and Nicholls, K. W. (2016). The ice shelf of Petermann Gletscher, North Greenland, and its connection to the Arctic and Atlantic Oceans, Oceanography, 29, 84-95, https://doi.org/10.5670/oceanog.2016.101.

Newell, J. P. (1993). Exceptionally large icebergs and ice islands in eastern Canadian waters: a review of sightings from 1900 to present, Arctic, 46(3), 205-211, https://doi.org/10.14430/ARCTIC1345.

Persson, A. (2005). The Coriolis Effect, History of Meteorology, 2, 1-24.

Phillips, N. A. (2000). An explication of the Coriolis effect, Bulletin of the American Meteorological Society, 81(2), 299-304, https://doi.org/10.1175/1520-0477(2000)081<0299:AEOTCE>2.3.CO;2.

Rackow, T., Wesche, C., Timmermann, R., Hellmer, H. H., Juricke, S., and Jung, T. (2017). A simulation of small to giant Antarctic iceberg evolution: Differential impact on climatology estimates, Journal of Geophysical Research: Oceans, 122(4), 3170-3190, https://doi.org/10.1002/2016JC012513.

Sackinger, W. M., Jeffries, M. O., Lu, M. C., and Li, F. C. (1988). Arctic Ice Islands, Final report for the U.S. Department of Energy, University of Alaska Fairbanks, United States, pp. 291.

Smith, S. D. and Banke, E. G. (1983). The influence of winds, currents and towing forces on the drift of icebergs, Cold Regions Science and Technology, 6(3), 241-255, https://doi.org/10.1016/0165-232X(83)90045-9.

Sodhi, D. S. and El-Tahan, M. (1980). Prediction of an iceberg drift trajectory during a storm, Annals of Glaciology, 1, 77-82, https://doi.org/10.3189/S0260305500017018.

Stern, A. A., Adcroft, A., Sergienko, O., and Marques, G. (2017). Modeling tabular icebergs submerged in the ocean, Journal of Advances in Modeling Earth Systems, 9(4), 1948-1972, https://doi.org/10.1002/2017MS001002.

Suthaharan, S. (2016). Machine learning models and algorithms for big data classification, Integrated Series in Information Systems, 36, 1-12, https://doi.org/10.1007/978-1-4899-7641-3.

Turnbull, I. D., Fournier, N., Stolwijk, M., Fosnaes, T., and McGonigal, D. (2015). Operational iceberg drift forecasting in Northwest Greenland, Cold Regions Science and Technology, 110, 1-18, https://doi.org/10.1016/j.coldregions.2014.10.006.

Wagner, T. J., Dell, R. W., and Eisenman, I. (2017). An analytical model of iceberg drift, Journal of Physical Oceanography, 47(7), 1605-1616, https://doi.org/10.1175/JPO-D-16-0262.1.

Wagner, T. J., Wadhams, P., Bates, R., Elosegui, P., Stern, A., Vella, D., Abrahamsen, E. P., Crawford, A., and Nicholls, K. W. (2014). The "footloose" mechanism: Iceberg decay from hydrostatic stresses, Geophysical Research Letters, 41(15), 5522-5529, https://doi.org/10.1002/2014GL060832.

Yulmetov, R. (2021). Iceberg Drift Forecasting Using Machine Learning, In Proceedings of the 26th International Conference on Port and Ocean Engineering under Arctic Conditions, Moscow, Russia, 14-18 June 2021.

Zeinali-Torbati, R., Turnbull, I. D., Taylor, R. S., and Mueller, D. (2019). The calving events of Petermann glacier from 2008 to 2012: ice island drift characteristics, assessment of fracture events, and geographical data analysis, In proceedings of the 38th International Conference on Ocean, Offshore and Arctic Engineering, Glasgow, Scotland, UK, 9-14 June 2019, https://doi.org/10.1115/OMAE2019-96732.

Zeinali-Torbati, R., Turnbull, I. D., Taylor, R. S., and Mueller, D. (2020). Evaluation of the relative contribution of meteorological and oceanic forces to the drift of ice islands offshore Newfoundland, Journal of Glaciology, 66(256), 203-218, https://doi.org/10.1017/jog.2019.96.

Zeinali-Torbati, R., Turnbull, I. D., Taylor, R. S., and Mueller, D. (2021). A probabilistic model for fracture events of Petermann ice islands under the influence of atmospheric and oceanic conditions, The Cryosphere, 15, 5601-5621, https://doi.org/10.5194/tc-15-5601-2021.

# 6. CONCLUSIONS AND RECOMMENDATIONS FOR FUTURE WORK

## 6.1. Summary and Conclusions

This study aimed to fill some important knowledge gaps in the field of glacial ice dynamics forecast models to provide better understanding of glacial ice behavior in the eastern Canadian waters, which are important locations for ocean activities such as shipping, offshore renewable, and non-renewable energy. The thesis focused on development of advanced models that provide a deeper understanding of the drift and deterioration of ice islands originally calved from Petermann Glacier during 2008-2012 in the northwest of Greenland, but it is expected that these models are applicable to other regions.

To identify the most salient metocean forces that control the drift of ice islands, a deterministic forcing model was developed in chapter 2, which served as a preliminary study for the development of the presented probabilistic drift forecasting model. The forcing model detailed an analysis of the relative influences of various metocean forces on the drift of four ice island fragments in the eastern entrance to Strait of Belle Isle off the southeast coast of Labrador during spring and summer of 2015. The ice island fragments' drifts were governed by forces due to wind, ocean currents, Coriolis deflection, sea surface slope, and sea ice. The deterioration of the ice island fragments during their drifts were estimated using satellite imagery data, combined with a surface ablation (TIM) model and a basal ablation model. This allowed for accounting for the melt rates and the change in the mass of the ice island fragments, which served as an input to the forcing model. The tracking beacons provided accurate positional and temporal data needed for estimating the average drift velocity and acceleration. The wind, current, and sea surface altimetry data were extracted from reanalysis data and satellite measurements. The forcing exposed by the surrounding

sea ice was calculated using a mathematical method, as the difference between each ice island's net force and the sum of forcings (*i.e.*, due to wind, ocean currents, Coriolis effect, and sea surface tilt), which was then compared against the sea ice forcing estimation from the concentration-dependent relationship (from Lichey and Hellmer, 2001) for validation. The forcing model's sensitivity to the ice island fragments' masses, ocean currents, and water/air drag coefficients was analyzed to study the possible sources of error for the developed forcing model. The results of the presented forcing model showed that the estimated sea ice forces from the presented residual approach and concentration-dependent relationship were only significant when the surrounding sea ice concentrations were medium or high. It was also revealed that ocean currents and sea surface tilt played a major role in the drift of the ice island fragments. On the other hand, wind contributed the least to ice island drift, and Coriolis deflection was only significant when the ice islands drifted at higher speeds.

For an ice island drift forecasting model to have an operational use, it is important that it receives inputs from a deterioration model that can predict fracture events of ice islands as they drift under the influence of metocean forces. Therefore, the research first developed a predicting model for ice island fracture events through analyzing the CI2D3 database that included satellite imagery tracking data for numerous ice islands from the moment they were calved from the Petermann Glacier until they became too small ($<0.25$ km$^2$) to be reliably delineated. To better understand the dynamics and characteristics of the ice islands of interest in the CI2D3 database, a preliminary data analysis was conducted in chapter 3 to present some statistics on their drift and deterioration (driven by fracture and melt). Then advanced probabilistic analysis of the CI2D3 database were presented in chapter 4 to study the causes behind the large-scale fracture events of the Petermann ice islands. To do this, the governing variables (*i.e.*, wind speed, air temperature, ocean current

speed, water temperature, wave energy index, lifetime mean air temperature, lifetime mean water temperature, lifetime mean wave energy index, grounding time, and sea ice concentration) were extracted from reanalysis databases and interpolated to the locations where the break-up events were identified from the satellite imagery database. A probabilistic fracture model was developed based on the conditional dependence of the break-up events on the most salient metocean variables. This was done through a Bayesian network, in which the distributions of local wind speed, air temperature, ocean current speed, water temperature, lifetime mean air temperature, and lifetime mean water temperature were used as input to the model and the probability of fracture event occurrence for all combinations of the input variables were calculated using Bayes' theorem. To assess the robustness of the developed fracture model, the conditional probability model was validated using the cross-validation approach. The model results showed that while warmer water temperature was the most important contributor to the fracture events of the ice islands, current speed played a minimal role. It is also revealed that under extreme conditions of atmospheric and oceanic variables, the probability of ice island fracture event occurrence increases to 75%. The model validation showed that the error in the fracture probability estimations ranged from 13% for a single-variable model to 39% for the full model.

Finally, using the knowledge based from the developed models in chapters 2 and 4, a probabilistic drift forecasting tool was presented in chapter 5 to evaluate the drift behaviour of the ice islands under the influence of the most salient atmospheric and oceanic conditions. This was done by adopting a Bayesian network similar to what was used for the fracture model, but with different metocean variables that govern the drift of ice islands, including wind speed, wind direction, current speed, current direction, sea surface tilt, sea surface tilt direction, ice island latitude, significant wave height, and mean wave direction. These governing metocean and ice conditions

196

were extracted from reanalysis databases, as well as from CI2D3 database, and then interpolated spatially and temporally to the observed locations and times of the ice islands from the selected dataset. The interpolated data were integrated into a Bayesian network to develop a probabilistic model where the output presented the distributions of ice islands' drift speeds and directions over their drift periods. To evaluate the reliability of the proposed model, the metocean data associated with drift of all Petermann ice islands were split into five subsets using the Pareto Principle to validate the developed probabilistic drift model based on the k-fold resampling approach. The drift velocity estimations from the Bayes' theorem revealed that ocean current speed and direction were the most controlling variables in the drift speed and direction of ice islands, and that ice islands are most likely to drift at high speeds ($>0.1 \ m \ s^{-1}$) and in close proximity of the local ocean current direction. The model validation using the cross-validation approach revealed that the mean error in the drift probability estimations ranged from 2.5% for the model with one variable only to 29% for the full model with all the variables.

The models presented in this thesis have a predictive capability for fracture events and drift velocities of the Petermann ice islands and provide an important step forward in characterizing the drift and deterioration of ice islands within the ice-prone environment in the eastern Canadian Arctic under the influence of various atmospheric and oceanic variables. This thesis filled critical knowledge gaps in the development of ice dynamics models through novel contributions to the field of research, including, 1) using a deterministic approach to quantify the relative contribution of the atmospheric and oceanic forces that govern the dynamics of ice islands, 2) using a probabilistic method to develop a predicting tool for ice island large-scale fracture events, and 3) developing a probabilistic model that can forecast the drift velocities of ice islands based on metocean conditions that they encounter. This work contributed to the field of glacial ice hazard

mitigation through development of a new probabilistic method for ice island drift and deterioration using a newly developed database. Past deterministic drift and deterioration models are limited by the uncertainty in the physical parameters that govern the drift and break-up events of ice islands, but the probabilistic models developed here can model levels of uncertainty for a range of possible outcomes for ice island fracture events and drift velocities based on the atmospheric and oceanic conditions that surround the ice islands. While deterministic models are promising for short-term forecasts, these probabilistic predicting models can be used for resource planning through long-term forecasts of future ice island fracture event frequency and drift paths for a range of atmospheric and oceanic conditions that they may encounter. These forecasts provide important information for mitigating the risk of glacial ice interaction with offshore activities and are therefore crucial to implementation of a successful ice management strategy (McClintock et al., 2002; Crawford et al., 2018). The developed models here are better suited for strategic applications such as seasonal forecasts of ice island encounter severity or to support strategic inputs to planning offshore operations in specific regions of the Canadian East Coast. Use of the developed models as operational forecasting tools for short-term purposed requires future research to further train and test the developed drift and deterioration models. The reliable estimation of fracture events and drift velocities are key information to the calibration and improvement of the future operational ice dynamics models, as well as to the development of appropriate ice management strategies to mitigate the risk of ice island presence in ocean environments such as the east coast of Canada.

## 6.2. Recommendations for Future Work

The research presented here focused on the drift and deterioration models of only the ice islands that calved from the Petermann Glacier. Therefore, the amount of data used to train the drift and deterioration models was limited. For example, the developed fracture model was trained and

tested based on only 328 fracture events. Additionally, due to the limited data, the presented Bayesian models were developed based on binary states of the input variables, except for directional variables. This limited the resolution of the developed drift and deterioration models, otherwise the models would have been saturated. Future research should therefore expand the database and consider data from ice islands calved from other glaciers to further train/validate the Bayesian models and improve their resolutions by employing more states of the input variables. The presented ice island dynamics models can also be improved if future research uses input data from in-situ measurements rather than modelled data from the reanalysis datasets that were used in this research. Future studies should also investigate the roles of other variables on ice islands' drift and deterioration. For example, sea ice presence in high concentrations in the vicinity of ice islands may influence the drift velocities of ice islands (Lichey and Hellmer, 2001). Future work should be extended to investigating the effects of landfast ice forming around ice islands in shallower water that can stop the motion of the ice islands (Marko et al., 1982), and the role of high concentrations of sea ice in reducing waterline deterioration due to the suppression of waves and lowering water temperatures. Also, the research presented here did not detail the process of ice island grounding events, including the onset, duration and cessation of these events. The process of the onset of grounding, the duration of these grounding events, and the physical conditions at the time of the release from grounding are very important to full understandings of the dynamics of ice island fragments, including the limits to the lifetime and spatial extents of the potential hazards from ice islands. The mass of ice islands may also be an influencing factor in the drift (Zeinali-Torbati et al., 2020) and deterioration of ice islands, which should be accounted for if more data become available. Finally, this thesis presented separate predictive models for ice

island drift and deterioration, which should ultimately be coupled to support future operational ice dynamics forecast modeling.

## 6.3.    References

Crawford, A., Crocker, G., Mueller, D., Desjardins, L., Saper, R., and Carrieres, T. (2018). The Canadian Ice Island Drift, Deterioration and Detection (CI2D3) Database, Journal of Glaciology, 1-5. https://doi.org/10.1017/jog.2018.36.

Lichey, C. and Hellmer, H. H. (2001). Modeling giant-iceberg drift under the influence of sea ice in the Weddell Sea, Antarctica, Journal of Glaciology, 47 (158), 452-460, https://doi.org/10.3189/172756501781832133.

Marko, J. R., Birch, J. R., and Wilson, M. A. (1982). A study of long-term satellite-tracked iceberg drifts in Baffin Bay and Davis Strait, Arctic, 35(1), 234-240, http://dx.doi.org/10.14430/arctic2322.

McClintock, J., Bullock, T., McKenna, R., Ralph, F., and Brown, R. (2002). Greenland iceberg management: Implications for Grand Banks management systems, PERD/CHC Report, 20-65.

Zeinali-Torbati, R., Turnbull, I. D., Taylor, R. S., and Mueller, D. (2020). Evaluation of the relative contribution of meteorological and oceanic forces to the drift of ice islands offshore Newfoundland, Journal of Glaciology, 66(256), 203-218, https://doi.org/10.1017/jog.2019.96.